National Library
of Canada

Acquisitions and
Bibliographic Services Branch

395 Wellington Street
Ottawa, Ontario
K1A 0N4

Bibliothèque nationale
du Canada

Direction des acquisitions et
des services bibliographiques

395, rue Wellington
Ottawa (Ontario)
K1A 0N4

Your file Votre référence

Our file Notre référence

NOTICE

The quality of this microform is heavily dependent upon the quality of the original thesis submitted for microfilming. Every effort has been made to ensure the highest quality of reproduction possible.

If pages are missing, contact the university which granted the degree.

Some pages may have indistinct print especially if the original pages were typed with a poor typewriter ribbon or if the university sent us an inferior photocopy.

Reproduction in full or in part of this microform is governed by the Canadian Copyright Act, R.S.C. 1970, c. C-30, and subsequent amendments.

AVIS

La qualité de cette microforme dépend grandement de la qualité de la thèse soumise au microfilmage. Nous avons tout fait pour assurer une qualité supérieure de reproduction.

S'il manque des pages, veuillez communiquer avec l'université qui a conféré le grade.

La qualité d'impression de certaines pages peut laisser à désirer, surtout si les pages originales ont été dactylographiées à l'aide d'un ruban usé ou si l'université nous a fait parvenir une photocopie de qualité inférieure.

La reproduction, même partielle, de cette microforme est soumise à la Loi canadienne sur le droit d'auteur, SRC 1970, c. C-30, et ses amendements subséquents.

Canada

UNIVERSITY OF ALBERTA

A Finite Element Analysis of the Instability Mechanisms in Non - Axisymmetric Rotor Systems

by

Anthony G. Taylor

A thesis submitted to the Faculty of Graduate Studies and Research in partial fulfilment of the requirements for the degree of Doctor of Philosophy.

Department of Mechanical Engineering

Edmonton, Alberta
Spring 1993

National Library
of Canada

Acquisitions and
Bibliographic Services Branch

395 Wellington Street
Ottawa, Ontario
K1A 0N4

Bibliothèque nationale
du Canada

Direction des acquisitions et
des services bibliographiques

395, rue Wellington
Ottawa (Ontario)
K1A 0N4

Your file Votre référence

Our file Notre référence

The author has granted an irrevocable non-exclusive licence allowing the National Library of Canada to reproduce, loan, distribute or sell copies of his/her thesis by any means and in any form or format, making this thesis available to interested persons.

L'auteur a accordé une licence irrévocable et non exclusive permettant à la Bibliothèque nationale du Canada de reproduire, prêter, distribuer ou vendre des copies de sa thèse de quelque manière et sous quelque forme que ce soit pour mettre des exemplaires de cette thèse à la disposition des personnes intéressées.

The author retains ownership of the copyright in his/her thesis. Neither the thesis nor substantial extracts from it may be printed or otherwise reproduced without his/her permission.

L'auteur conserve la propriété du droit d'auteur qui protège sa thèse. Ni la thèse ni des extraits substantiels de celle-ci ne doivent être imprimés ou autrement reproduits sans son autorisation.

ISBN 0-315-82178-7

Canada

UNIVERSITY OF ALBERTA

RELEASE FORM

NAME OF AUTHOR:	**Anthony G. Taylor**
TITLE OF THESIS:	**A Finite Element Analysis of the Instability Mechanisms in Non - Axisymmetric Rotor Systems**
DEGREE:	Doctor of Philosophy
YEAR THIS DEGREE GRANTED:	1993

Permission is hereby granted to The University of Alberta Library to reproduce single copies of this thesis and to lend or sell such copies for private, scholarly, or scientific research purposes only.

The author reserves all other publication and other rights in association with the copyright in the thesis, and except as herinbefore provided neither the thesis nor any substantial portion thereof may be printed or otherwise reproduced in any material form whatever without the author's prior written permission.

A. G. Taylor

Anthony G. Taylor
3911-118 St.
Edmonton
Alberta
Canada T6J-1X2

Date : April 26th. 1993

UNIVERSITY OF ALBERTA

FACULTY OF GRADUATE STUDIES AND RESEARCH

The undersigned certify that they have read, and recommend to the Faculty of Graduate Studies and Research for acceptance, a thesis entitled **A Finite Element Analysis of the Instability Mechanisms in Non - Axisymmetric Rotor Systems** submitted by **Anthony G. Taylor** in partial fulfilment of the requirements for the degree of Doctor of Philosophy.

.....
Dr. A. Craggs

.....
Dr. D.J. Steigmann

.....
Dr. A.W. Lipsett

.....
Dr. T.M. Hrudey

.....
Dr. J. Kirkhope

Date : 19 April 1993

Abstract

The stability of rotating machinery has been studied since the early decades of this century. However, even at the present day, instability problems are not uncommon in large high speed turbomachinery, either at the commissioning stage or during normal service. The consequences of such problems can be extremely costly and sometimes dangerous. The analysis of the behaviour of turbomachinery by commissioning engineers and 'trouble-shooting' specialists in rotor-dynamics has been, to a large extent experiential. However, the prediction and analysis of some of these problems at the design stage has proven very difficult in spite of the great many academic and industrial papers written since the beginning of the century.

In this thesis a finite element model is developed for a flexible rotor - shaft system supported on bearings which have distributed stiffness and damping coefficients. The equations of motion are set up with respect to a rotating frame of reference fixed within the rotor so that asymmetries of diametral mass and area moments of inertia can be accommodated. Shear deflection was also included in the model. By this means, cyclically varying coefficients are avoided for the rotor. The analyses carried out with this model establish instability mechanisms, involving backward - precessing modes. These results agree with the behaviour of other systems for which the mathematics are similar and the presence of shear deflection is shown to be necessary for these instabilities.

Finite element models of the hydro-dynamic lubrication problem for plain and tilting - pad bearings are also presented and the data derived from these were used in the flexible rotor models, thus examining the effect of damping on the instability mechanisms. The effects of internal damping on the stability of a symmetric rotor is also briefly examined.

Acknowledgements

I would like to thank my thesis advisor, Dr. A. Craggs and the other members of my committee, Drs. D.J. Steigmann and A.W. Lipsett for their advice and guidance. The pains - taking work of my external examiners, Dr. J. Kirkhope and Dr. T.M. Hrudey is also greatfully acknowledged. I would also like to thank the former Department chairman Dr. M.G. Faulkner for his encouragement in undertaking this Ph.D. programme and Dr. J.D. Dale, the present chairman, for his continuing encouragement. The research was partially supported by an operating grant from the Natural Sciences and Engineering Research Council held by Dr. A. Craggs and financial support was also given through a Province of Alberta Graduate Fellowship and the R.R. Gilpin Memorial Scholarship. This support is gratefully acknowledged.

I would also like to thank Messrs. A. Wilson and A. Hay for their assistance in innumerable matters concerning computers and software and the other graduate students who accepted me as one of them in spite of the considerable difference in our ages. In particular I would mention Dr. W. (Bill) Eckert with whom I was able to share many ideas and solve many problems of mutual interest.

Finally I wish to acknowledge the support and encouragement of my wife Diane whom I encouraged to do a Ph.D. some years ago and who has now returned the complement. I would not have been able to attempt this programme without her.

Contents

Acknowledgements iv

Chapter 1
Introduction 1

Chapter 2
Literature Review 5

2.1 Scope of Review 5
2.2 Instabilities and Bearing Coefficients 5
2.3 Derivation of Bearing Coefficients - Laminar Flow 10
2.4 Tilting - Pad Bearings 15
2.5 Finite Element Analysis for Bearings 19
2.6 Turbulent Flow Bearing Coefficients 23
2.7 Internal Friction 31
2.8 Space Shuttle Turbo - Pumps 36
2.9 Discussion 39

Chapter 3
Rigid Rotor Analysis 40

3.1 Rotating Coordinate Frame 41
3.1.1 Rate of Change of Momentum 41
3.1.2 Stiffness and Damping Forces / Moments 50
3.2 The Eigenvalue Problem 60

3.3 Non-Axisymmetric Rotor Without Damping. 61
3.4 Inertial Coordinate Formulation 67
3.4.1 Bearing Coefficients due to Fluid Swirl 68
3.4.2 Modal Frequencies and Stability vs. Speed 72
3.4.3 Modal Orbits 80

Chapter 4
Flexible Shaft - Rotor **100**
4.1 Flexible Shaft - Rotor Element Development 101
4.1.1 Kinetic Energy 101
4.1.2 Strain Energy 106
4.1.3 Distributed Bearing Stiffness 107
4.1.4 Hamilton's Principle 108
4.2 Results 110
4.2.1 Distributed Bearing Stiffness 110
4.2.2 Stability Analysis 111
4.3 Uniform Flexible Non-Axisymmetric Rotor, Exact Solution 114
4.4 Discussion 116

Chapter 5
Dynamics of a Plain Journal Bearing **131**
5.1 Finite Element Approximation to Reynolds Equation - Steady State . 131
5.1.1 Bearing Element Development 133
5.1.2 Boundary Conditions 136
5.2 General (Dynamic) Case 139
5.3 Stiffness and Damping Coefficients 141

Chapter 6
Tilting - Pad Bearings **153**
6.1 Load Capability and Dynamic Coefficients 156
6.2 Analysis of a Four - Pad Tilting - Pad Bearing 158
6.3 Discussion 160

Chapter 7
Flexible Shaft - Rotor with Internal and External Damping. 171

7.1 Derivation of Damping Terms. 171

7.2 Speed Dependent Bearing Coefficients 175

7.3 Results and Discussion - External Damping 176

7.4 Internal Damping 178

Chapter 8
Conclusions and Suggestions for Further Research 183

References 187

Appendix A
Analytical Methods 194

A.1 Complex Eigenvalues and Eigenvectors 194

A.1.1 Eigenvalues 194

A.1.2 Eigenvectors 195

A.2 Direction of Precession and Orbit Shape 197

A.2.1 Precession 197

A.2.2 Orbits 199

Appendix B
Finite Element Analysis - Coefficient Matrices 202

B.1 Mass Terms 202

B.2 Strain Energy 219

Appendix C
Plain Bearing Stiffness and Damping Coefficients 223

List of Tables

5.1 Comparison of Steady - State Data Produced in Present Study and that of Pinkus and Sternlicht 151

5.2 Comparison of Dynamic Data Produced in Present Study and that of Pinkus and Sternlicht, (who used $\pi\dot{\varepsilon}'$ as the non - dimensionalized squeeze - film velocity). 152

List of Figures

2.1 Equations of Motion of Centre of Mass of Simple Rotor - Equation of Motion in y Dir. $-K_2y - c\dot{y} - D_2x = m\ddot{y}$, Equation of Motion in x Dir. $-K_1x - c\dot{x} + D_1y = m\ddot{x}$. 6

2.2 Slipper Bearing 11

2.3 Journal Precessing in Bearing Annulus: The journal has components of precessional velocity $\dot{x}_j$, $\dot{z}_j$ and constant angular velocity ω. O_j and O_b are the journal and bearing centres. 30

2.4 Simple Rotor with Internal Friction 32

2.5 Static Deflection Under Gravity and Friction Loading 35

3.1 Inertial and Body - Fixed Coordinate Systems. The $Oxyz$ axes are inertial and the axes $O'\xi\eta\zeta$ are fixed in the rotating body. The angles ϕ_x, ϕ_y and ωt are the standard 'Euler' angles. $O\zeta$ is the the axis of rotation of the rotor and the C.G. is at O'. 42

3.2 Dynamic Imbalance. The two equal concentrated masses equidistant, both axially and radially from the C.G. will produce a rotating moment in the plane of the rotor when rotating but be balanced when stationary, i.e. about a diameter. 49

3.3 Stiffness Coefficients due to Unit x Deflection 52

3.4 Stiffness Coefficients due to Unit y Deflection 52

3.5 Stiffness Coefficients due to Unit ϕ_x Deflection 53

3.6 Stiffness Coefficients due to Unit ϕ_y Deflection 53

3.7 Creation of a Region of Instability due to Asymmetry of Diametral Moments of Inertia for a Rigid Rotor with Zero Damping. $\delta = (J_{\xi\xi} - J_{\eta\eta})/(J_{\xi\xi} + J_{\eta\eta})$ and $\lambda = 2J_{\zeta\zeta}/(J_{\xi\xi} + J_{\eta\eta})$. 63

3.8 Modal Frequencies Relative to Rotating Coordinate Frame of Reference, Corresponding to the Case of $\delta = 0.1$ and $\lambda = 0.3$. The plots with the same symbols correspond to complex conjugate eigenvalues. 64

3.9 Modal Frequencies Relative to Rotating Coordinate Frame of Reference, Corresponding to the Case of $\delta = 0.2$ and $\lambda = 0.5$. 65

3.10 Variation of Stability Boundaries with Rotor C.G. Position: at the mid point; half way between mid point and one bearing, and at one bearing. The regions between plots with the same symbol are unstable, e.g. the dotted and cross - hatched regions. 66

3.11 Model for Equation of Motion for Swirling Fluid Masses Within Bearings Relative to a Frame of Reference Rotating with the Fluid at Angular Velocity ω_s 69

3.12 Whirl Frequency vs. Speed for No Damping, No Swirl but with Asymmetric Support and Gyroscopic Effects. 74

3.13 Real and Imaginary Parts of Eigenvalue vs. Non - Dimensionalized Speed - No Swirl 75

3.14 Real and Imaginary Parts of Eigenvalue vs. Non - Dimensionalized Speed - Damping Ratio = 0.2 76

3.15 Real and Imaginary Parts of Eigenvalue vs. Non - Dimensionalized Speed - Damping Ratio = 0.4 77

3.16 Real and Imaginary Parts of Eigenvalue vs. Non - Dimensionalized Speed - Damping Ratio = 0.6 78

3.17 Real and Imaginary Parts of Eigenvalue vs. Non - Dimensionalized Speed: C.G. Mid - Way Between Centre and One Bearing - Damping Ratio = 0.4 79

3.18 Modal Orbits at Forward End - S=0.2 No Damping, Angular Modes Only, Asymmetrical Support Stiffness 82

3.19 Modal Orbits at Forward End - S=0.4 No Damping, Angular Modes Only 83

3.20 Modal Orbits at Forward End - S=0.6 No Damping, Angular Modes Only 84

3.21 Modal Orbits at Forward End - S=0.8 No Damping, Angular Modes Only 85

3.22 Modal Orbits at Forward End - S=1.0 No Damping, Angular Modes Only 86

3.23 Modal Orbits at Forward End - S=2.0 No Damping, Angular Modes Only 87

3.24 Modal Orbits at Forward End - S=3.0 No Damping, Angular Modes Only 88

3.25 Modal Orbits at Forward End - S=0.2 89

3.26 Modal Orbits at Forward End - S=0.4 90

3.27 Modal Orbits at Forward End - S=0.6 91

3.28 Modal Orbits at Forward End - S=0.629 92

3.29 Modal Orbits at Forward End - S=0.8 93

3.30 Modal Orbits at Forward End - S=1.0 94

3.31 Modal Orbits at Forward End - S=1.2 95

3.32 Modal Orbits at Forward End - S=1.6 96

3.33 Modal Orbits at Forward End - S=2.0 97

3.34 Modal Orbits at Forward End - S=2.4 98

3.35 Modal Orbits at Forward End - S=2.8 99

4.1 Inertial and Body-Fixed Axes of Infinitesimal Disk Section of Rotor / Shaft Element of Length $\delta\zeta$. $Oxyz$ is parallel to the inertial frame of reference, $O\xi\eta\zeta$ is a body fixed coordinate system coincident with the principal axes. ϕ_x, ϕ_y and ωt are Euler angles relating the two systems and ξ', η' are parallel to $O\xi$ and $O\eta$. 117

4.2 Rotor / Shaft Section Precessing at Angular Frequency ω_n Relative to Frame of Reference Rotating at ω. 118

4.3 Relation Between Shear Slope, Bending Slope and Neutral Axis Slope in the $O\xi\zeta$ and $O\eta\zeta$ Planes. ϕ_η and ϕ_ξ are the bending slopes, ψ_η and ψ_ξ, the shear slopes and ξ' and η' the neutral axis slopes in the $O\xi\zeta$ and $O\eta\zeta$ planes respectively. 119

4.4 Natural Frequencies of First Two Bending Modes for a Uniform Rotor at Zero RPM vs. Distributed Bearing Stiffness - No Shear. Length 2500mm, Diam. 200mm, Bearing Length 200mm (L/D = 1.0). 120

4.5 Outline of Rotor Model Analyzed. The Bearings are Assumed Identical of Length 200mm and Diam. 200mm. 121

4.6 Modal Frequencies in Rotating Frame vs. Speed for Central Rotor with Asymmetric Mass and Diametral Stiffness Moments of Area, Uniform Axisymmetric Shaft, No Shear Deflection. 122

4.7 Modal Frequencies in Inertial Frame vs. Speed for Central Rotor with Asymmetric Mass and Stiffness Diametral Moments of Area, Uniform Axisymmetric Shaft, No Shear Deflection. 123

4.8 Modal Frequencies in Rotating Frame vs. Speed for Central Rotor with Asymmetric Mass and Stiffness Diametral Moments of Area, Uniform Axisymmetric Shaft, with Shear Deflection. 124

4.9 Modal Frequencies in Inertial Frame vs. Speed for Central Rotor with Asymmetric Mass and Stiffness Diametral Moments of Area, Uniform Axisymmetric Shaft, with Shear Deflection. 125

4.10 Modal Frequencies in Rotating Frame vs. Speed for Central Rotor with Asymmetric Diametral Mass Moments of Area, but Axisymmetric Stiffness, Uniform Axisymmetric Shaft, with Shear Deflection. 126

4.11 Modal Frequencies in Inertial Frame vs. Speed for Central Rotor with Asymmetric Diametral Mass Moments of Area, but Axisymmetric Stiffness, Uniform Axisymmetric Shaft, with Shear Deflection. 127

4.12 Instability Regions for a Flexible Rotor / Shaft System Having Non-Axisymmetric Stiffness, Supported by Distributed Axisymmetric Bearings. $q = 2(J_{\xi\xi} - J_{\eta\eta})/(J_{\xi\xi} + J_{\eta\eta})$. The instability around the fundamental resonance is not included. 128

4.13 Modal Frequencies vs. Speed for q = 0.45 and Zero Damping. 129

4.14 Uniform Non-Axisymmetric Rotor on Point Bearing Supports. 130

5.1 Notation Used in Analysis of Journal in Circular Cylindrical Bearing. The local film thickness $h = c(1 + \varepsilon \cos\theta)$ where c is radial clearance, ε is the ratio of the eccentricity e to the radial clearance and θ the angular position measured relative to the line of centres. 144

5.2 Rectangular Element, Notation Within Element. 145

5.3 Non-Dim Pressure Profile at Mid-Bearing Span with Reynolds' Boundary Condition. L/D=1.0, ε=0.4. Pressure = Non-Dim. Pressure times $\mu\,(R/c)^2\,\omega_j$, where μ is absolute viscosity, R/c is ratio of journal radius to radial clearance and ω_j is the angular velocity of the journal. 146

5.4 Attitude Angle of Journal Within a Bearing 147

5.5 Sommerfeld Number S, Versus Eccentricity Ratio, ε for Four Values of Length to Diameter Ratio L/D. 148

5.6 Attitude Angle ψ, Versus Eccentricity Ratio ε, for Four Values of Length to Diameter Ratio L/D Ratio. 149

5.7 Non-Dimensionalized Pressure Profile with Reynolds Boundary Condition for L/D=1.0 and ε=0.4. Pressure = Non-Dim. Pressure times $\mu\,(R/c)^2\,\omega_j$, where μ is absolute viscosity, R/c is ratio of journal radius to radial clearance and ω_j is the angular velocity of the journal. 150

6.1 Nomenclature for a Tilting-Pad, N = point on the pad surface, θ = angular location of N from line of centres (L.O.C.), θ_p = pivot location, O_p = pad centre of curvature, O_b = centre of pivot circle, O_j = journal centre, ω_j = journal angular velocity, h = film thickness at N. 161

6.2 Definitions of Pad Clearance c_p and Bearing Clearance c. R_p = pad radius of curvature, R_b = radius of pivot circle. 162

6.3 Notation for Film Thickness Calculation; h = total film thickness at point N, h_{nt} film thickness at N without any pad tilt, h_t = film thickness contribution due to pad tilt alone. 163

6.4 Pad Arrangement for Case Analyzed. The pads are located symmetrically around the bearing with each pad extending for 80° circumferentially. 164

6.5 Typical Pad Arrangements of Five - Pad Bearings. The upper sketch is a load-on-pad arrangement and the lower one is a load-between-pads arrangement. 165

6.6 Illustration of Pad Orientation During Normal Operation. 166

6.7 Eccentricity Ratio ε vs. Inverse Sommerfeld Number S^{-1} for Four Pad Tilting - Pad Bearing. 167

6.8 Non - Dimensionalized Stiffness Coefficient vs. Inverse Sommerfeld Number S^{-1} (based on pad clearance c_p). 168

6.9 Non - Dimensionalized Damping Coefficient vs. Inverse Sommerfeld Number S^{-1} (based on pad clearance c_p). 169

6.10 Pressure Profiles on Each Pad of Four Pad Tilt - Pad Bearing. 170

7.1 Instability Regions for a Flexible Rotor with Speed - Dependent Bearing Stiffness and Damping as Calculated for a Tilting - Pad Bearing. 179

7.2 Modal Frequencies vs. Speed for q = 0.45 with Speed - Dependent Bearing Stiffness and Damping as Calculated for a Tilting - Pad Bearing. 180

7.3 Instability Regions for a Flexible Rotor with Speed - Dependent Bearing Stiffness and Damping, Damping 25% Less Than Calculated. 181

7.4 Speed at Which 1st. Forward Mode Becomes Unstable and Modal Frequency vs. Rotor Internal Damping for a Symmetric Rotor (Modal Frequency re Inertial Frame of Reference). 182

A.1 Determination of Direction of Precession. $\underline{r}$ and $\underline{v}$ are the position and precessional velocity of a point on the shaft centre - line $O' - \zeta'$, i.e. the deflected axis of the rotor. 197

A.2 Equivalence of Complex and Amplitude / Phase Representations. . . 200

C.1 Small Deflections of Journal Centre Parallel and Perpendicular to the Line of Centres (journal - bearing), Showing Contributions to the Incremental Forces due to Rotation of the Fluid Force Components. . 227

Nomenclature

Chapters 3 and 4.

x, y , z	inertial coordinates.
H_x, H_y	momentum components re inertial frame.
ϕ_x ϕ_y	angular displacements about inertial axes.
ξ, η, ζ	coordinates in rotating reference frame.
H_ξ, H_η	momentum components re rotating frame.
ϕ_ξ ϕ_η	angular displacements about axes of rotating reference frame.
ω	angular frequency of rotation of rotor / shaft system rad/s.
ρ	density kg/m^3
A	cross-sectional area m^2.
l	element length m.
$J_{\xi\xi}$, $J_{\eta\eta}$, $J_{\zeta\zeta}$	principal values of inertia tensor matrix **J** in rotating coordinate frame.
t	time s.
τ	non-dimensional time equals ωt.
$\{\phi^a\}$	angular displacement vector at a point within an element.
$\{H\}$	angular momentum vector at a point within an element.
$\mathbf{\Phi^a}$	angular displacement vector.

$\mathbf{H}$	angular momentum vector.
$\mathcal{T}_i^e$	element kinetic energy due to angular motion.
$\mathcal{T}_m^e$	element kinetic energy due to linear motion.
$\mathcal{T}^e$	total element kinetic energy.
δ	first variation. Also $(J_{\xi\xi} - J_{\eta\eta})/(J_{\xi\xi} + J_{\eta\eta})$ for rigid rotor analysis (Stammers' notation).
λ	complex eigenvalue. Also $2(J_{\zeta\zeta})/(J_{\xi\xi} + J_{\eta\eta})$ for rigid rotor analysis (Stammers' notation).
$[m]$	mass matrix per unit length per unit density for an element cross section - Equation 4.7.
$[g]$	'Coriolis / gyroscopic' matrix for an element cross-section - Equation 4.7.
$[y]$	'centrifugal' matrix for an element cross-section - Equation 4.7.
$\{\phi\}$	linear and angular displacement vector.
$[N]^T$	Shape function or 'Cardinal basis' for finite element approximation.
$\{\Phi^e\}$	element nodal displacement vector.
$[B]$	matrix of cubic polynomial interpolation functions.
$[T]$	matrix relating the cardinal basis to the polynomial interpolation functions matrix.
E	Young's modulus of elasticity.
G	shear modulus.
$\mathcal{K}$	section shape factor.
$\beta_\xi,\ \beta_{\eta\eta}$	$E.J_{\xi\xi}/(\mathcal{K}.G.A)$ and $E.J_{\eta\eta}/(\mathcal{K}.G.A)$ respectively.
$[M^e]$	consistent element mass matrix.
$[G^e]$	consistent element Coriolis / gyroscopic matrix.

$[Y^e]$	consistent element 'centrifugal' matrix.
$[K^e]$	consistent element stiffness matrix.
U^e	element strain energy.
ψ_ξ, ψ_η	shear slopes.
$[K_b]$	consistent bearing stiffness matrix.
$[M_g]$	global mass matrix.
$[G_g]$	global 'Coriolis / gyroscopic' matrix.
$[K_g]$	global stiffness matrix.
$[K_g^b]$	global bearing stiffness matrix.
$[Y_g]$	global 'centrifugal' matrix.
$\{\Phi_g\}$	global linear/angular displacement vector.

Chapters 5,6 and 7

θ	angular position within an element relative to cicumferential mid point.
$\overline{\theta}$	global angular position within a bearing element.
θ_g	global angular position of mid point of a bearing element.
$\Delta\theta$	angle subtended by bearing element at journal centre.
l	axial length of element.
R, R_j	journal radius.
R_b	bearing radius.
R_p	pad radius of curvature.
c	radial clearance of bearing.
c_p	pad radial clearance.

ε	e/c eccentricity ratio.
m	pad preload.
h	local film thickness.
θ_p	global angular position of pad pivot.
θ_1	global angular position of pad leading edge.
$h1t$	film thickness at pad leading edge due to pad tilt alone.
p	fluid film local pressure (above atmospheric).
μ	absolute viscosity.
ω_j	journal angular velocity.
ω_b	bearing angular velocity.
ω_c	angular velocity of line of centres.
$\{p^e\}$	vector of element nodal pressures.
$\{p_g\}$	vector of global nodal pressures.
$\{p_g^*\}$	vector of non - dimensionalized global nodal pressures.
$I^e(p)$	element functional for Reynolds' equation.
$\{G\}$	shape function for pressures within an element.
pel_i	mean pressure over i'th element.
D	bearing diameter.
L	bearing length.
W	bearing load.
N	journal speed (R.P.M.).
S	Sommerfeld number = $W.(c/R)^2/(L.D.N.\mu)$
F_r	resultant radial fluid force on journal.
F_t	resultant tangential fluid force on journal.

$\overline{F}_r$	non - dimensional resultant radial fluid force on journal.
$\overline{F}_t$	non - dimensional resultant tangential fluid force on journal.
ψ	bearing attitude angle.
$[C_s^e], [C_b^e]$	element coefficient matrices of the displacement and velocity vectors respectively, due to external damping.
$[C_{int}^e]$	element coefficient matrix due to internal damping.
W_{nc}	work due to non - conservative forces.

Chapter 1

Introduction

In Jeffcott's much cited 1919 paper [1], the response of a simple rotor with a weightless shaft and pinned - pinned bearings was analyzed. The behaviour of such a system, as set out by Jeffcott, is essentially as taught today in industry seminars on balancing, including the expressions 'critical speed' and 'heavy spot', which he probably coined.

Jeffcott made no assumption about the frequency of precession that would be caused by simple unbalance, but proved that for this axi - symmetric system, it would indeed be synchronous with rotation. He derived the frequency of maximum unbalance response and the amplitude at that speed for a given level of viscous damping.

The addition to the model of oil - film bearings and seals, working fluids, a support structure which is usually of non - symmetric stiffness and a rotor which may have non - axisymmetric properties and internal hysteretic damping, introduces major complexities to the mathematics and various mechanisms of unstable vibration. Some simplifying assumptions can be made. For instance for machine trains where a process steam turbine or motor drives a compressor through a gear coupling or other flexible coupling, it is generally assumed that coupling of lateral vibration between machines is negligible.

This has been shown in most cases to be a reasonable assumption, but the problem remains very difficult. However where machines are coupled with solid couplings or are strongly coupled (from a vibrational point of view) through the structure, e.g. as in vertical pump - sets, this assumption cannot be made.

The inability to accurately predict rotordynamic phenomena, particularly instability problems, has resulted in many very expensive retro - fits [2] and in the writer's own consulting experience, the total replacement of a process steam turbine [3]. Modelling the solid, elastic parts of the rotor and support structure is amenable to standard methods such as the lumped mass / transfer matrix approach for beam structures such as shafts. The Rayleigh-Ritz method has been used for

many years for coupling several admissible functions (i.e. shapes which satisfy the boundary conditions such as mode shapes) [4] in order to analyze the elastic vibrations of structures, and more recently, finite element methods have become common for determining the natural frequencies and mode shapes of the structures.

The motion-dependent forces generated in the fluids were first modelled for rotating equipment in the late 40's. In contrast, the motion dependent aerodynamic forces, responsible for wing divergence and flutter, have been incorporated into aeroelastic analyses since well before World War II. Theodorsen's detailed paper[5] in 1935 derived the oscillatory aerodynamic forces using potential flow theory. The expressions for these forces were, in turn, incorporated into the mathematical model of the airplane structure, from which flutter and divergence 'critical speeds' could be derived.

In rotating equipment, the counterparts of flutter; oil whirl and oil/aerodynamic whip, have been well characterized and can be readily identified with appropriate instrumentation. The term 'whirl' is used widely but with various interpretations. The most common usage, which will be used in this thesis, refers to the precessional motion of a rotor or of a journal within a bearing, at some circular frequency, which may be the same as the rotor rotational frequency (synchronous whirl), subsynchronous i.e. at a frequency below that of rotation speed, or supersynchronous. To further characterize the precessional frequency, it may be subharmonic i.e. at a frequency equal to an exact fraction of rotation speed or harmonic, equal to an exact multiple of rotation speed and which is therefore phase-locked to any whirl component at rotational speed frequency. There is not universal agreement on the terminology, particularly of 'synchronous' and 'harmonic'. However, the above meanings seem to be the most widely used.

The term 'swirl' has been coined and is generally applied to the motion of the fluid rather than that of a rotor. Also 'subrotative' is sometimes used for subharmonic. 'Oil-whirl' or 'journal-whirl' as Newkirk and Taylor described it [6] is a self-excited instability which can occur at any speed below the first lateral rotor / bearing / structure 'critical speed' which is characterized by a precessional frequency equal to typically 43%- 48% of rotation speed and which therefore tracks rotation speed [7, 8]. The writer has on one occasion, seen evidence of some oil whirl above the first critical. Charles Jackson, an experienced field engineer, author of [9] confirms this (private communication) and Muszynska, [10] develops an analytical mechanism for it, but it is rare and seems, at least at present, to be of little consequence.

'Whip' prefaced by 'oil', 'aerodynamic', 'steam', or 'gas' depending on the swirling fluid driving the motion is characterized by a precessional frequency essentially equal to that of the first critical speed (natural frequency) and which can occur when

rotation speed exceeds approximately twice the first critical frequency. That is to say, this frequency is essentially constant for increasing rotor speed and the instability can occur at a speed such that this natural frequency is a lower eigenvalue of the system than the oil whirl frequency. There are other causes of 'resonant whip', which will be discussed below under 'Internal Friction'. Oil-whirl is an instability localized to a bearing and can cause severe damage to the bearing although in many instances does not because the motion reaches a limit cycle. The rotor motion generally involves no excitation of the elastic modes of the rotor, the entire rotor moving as a rigid body with the journals. Whip involves a natural mode of the rotor/bearing system and can cause severe damage to bearings, seals or the rotor. However, there are many machines operating with a small amount of whip. That is, vibration signals show a persistent component of vibration at the first rotor/bearing natural frequency (critical) with no deleterious effects. This suggests that there are 'degrees' of instability. That is to say that although the presence of some subsynchronous vibration at a natural frequency implies self excitation, the amplitude is self limiting because the non-linear behaviour of the bearing stiffness and damping becomes significant for large journal motion.

Although Newkirk made the distinction between oil-whirl and whip in 1925 on the basis of experiments and Robertson confirmed this analytically in 1933 [11], the low frequency tracking phenomenon seems to have been absent from later studies by Newkirk [12], Lund [13] (his results show it but it is not discussed) and the very detailed work by Gunter [14]. In these later studies, attention was confined to the conditions necessary for whirl or whip at speeds exceeding the first critical speed only.

From the point of view of the industrial 'end-user' of turbo- machinery, a precise understanding of the dynamics of his machine is rather academic, except in so far as knowing what is to be the 'fix' and in assigning liability for the problem, e.g. the pump or the motor manufacturer. In order to protect the end user, many standards have been developed which can be used for specifying acceptance levels of vibration, e.g. American Petroleum Institute Standard 612 [15] and International Association for Standardization - (I.S.O.) 3945 [16].

These standards specify vibration limits, either seismic i.e. on the machine casing (usually bearing housing) vibration relative to ground, or shaft displacement relative to the bearing housing. In the case of the A.P.I. Standards, which are widely used on this continent, detailed acceptance procedures are set out for proving a machine on the test stand. This has in the past included a limit on the crest factor or 'Q' value of the resonance peak in vibration measured when passing through the 'critical speeds' during a run-down of the machine. This is usually defined today as the ratio of the resonant frequency to the bandwidth at the 3 dB down point, i.e. at an amplitude equal to 0.707 times the peak value.

This gave a measure of protection in effectively demanding a minimum level of damping in the lateral bending modes, thereby limiting the response due to residual unbalance and, hopefully, the sensitivity of those modes to instability. Recently this provision has been removed, to the regret of some specialists in the field, but presumably because of the possible use of 'anti- swirl' devices which can eliminate 'whip' even in a machine with a high 'Q'. The writer has experience of such an installation [17] in which an anti - swirl seal system [18] was used most successfully.

Unfortunately, such test procedures do not guarantee a trouble- free machine because the loading conditions can rarely be simulated adequately on the test stand and the properties of the machine foundation are unlikely to be the same as the field installation. There has been considerable progress in the modelling and understanding of fluid induced forces in turbomachinery in the last few years, particularly with respect to instability. However, the models developed do not represent all machinery configurations or operating conditions and many aspects of the behaviour of rotating machines are not fully understood and are treated empirically at best.

This thesis develops as its main theme, methods for analyzing a rotor - shaft system in a rotating frame using finite element methods. This permits the investigation of the effects on rotor stability of a lack of axi-symmetry in both mass and stiffness of the rotor.

In Chapter 2 selected references are described, taken from the large number of studies carried out since the turn of the century. The development of the mathematics for motion of a rigid non-axisymmetric rotor in a rotating frame of reference is described in Chapter 3 and the effect of bearing fluid swirl on a rigid rotor assembly is also investigated. A finite-element model for a non-axisymmetric flexible rotor system is constructed in Chapter 4 and the stability of such a system without damping and with bearings having constant distributed stiffness is investigated.

Chapters 5 and 6 are devoted to the development of finite element models for plain and tilting - pad bearings respectively to obtain their stiffness and damping characteristics. An improved model for investigating the stability of a flexible non - axisymmetric rotor system is then analyzed in Chapter 7, incorporating the stiffness and damping characteristics obtained for a four pad tilting - pad bearing. The effects of the inclusion of internal damping is also investigated in Chapter 7 for an axisymmetric rotor system.

Chapter 2

Literature Review

2.1 Scope of Review

The number of publications directly or indirectly applicable to the behaviour of rotating machinery is extremely large. The field is sufficiently broad that it embraces highly mathematical studies in learned journals and industry - oriented journals concerned with routine maintenance of machinery. The machinery studied extends from the NASA space shuttle to a single stage pump in a water treatment plant. Therefore this review is of necessity selective. It is intended to demonstrate the extent of our knowledge to-date and to indicate that even with all these studies, the subject is sufficiently complex that there is considerable scope for further research.

2.2 Instabilities and Bearing Coefficients

Hagg, [19] in his abstract, groups oil whirl and whip together, but notes that the 'upper limit of whirling frequency has been found to be one half rotational frequency in the general case'; this limit being reached for the case of an unloaded bearing. This therefore does not include the 'tracking' oil whirl phenomenon but only the essentially constant frequency 'whip' instability. Hagg sets up the equations of motion for a single bearing (rigid rotor) as:

$$m\frac{d^2x}{dt^2} + c\frac{dx}{dt} + K_1x - D_1y = 0, \tag{2.1}$$

$$m\frac{d^2y}{dt^2} + c\frac{dy}{dt} + K_2y + D_2x = 0, \tag{2.2}$$

or

$$\begin{bmatrix} m & 0 \\ 0 & m \end{bmatrix}\begin{Bmatrix} \ddot{x} \\ \ddot{y} \end{Bmatrix} + \begin{bmatrix} c & 0 \\ 0 & c \end{bmatrix}\begin{Bmatrix} \dot{x} \\ \dot{y} \end{Bmatrix} + \begin{bmatrix} K_1 & -D_1 \\ +D_2 & K_2 \end{bmatrix}\begin{Bmatrix} x \\ y \end{Bmatrix} = \begin{Bmatrix} 0 \\ 0 \end{Bmatrix}, \tag{2.3}$$

where: x and y are lateral displacements, m is the mass of the rotor, c is the viscous damping coefficient (axisymmetric), K_1 and K_2 are the direct stiffness coefficients in the x and y directions and D_1 and D_2 are the cross - coupling stiffness coefficients, see Figure 2.1. Note that the x and y are measured from the equilibrium position, so the weight mg does not enter the equations.

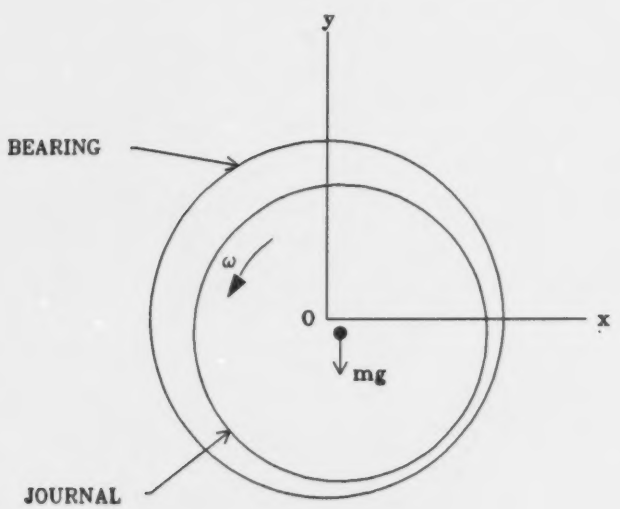

Figure 2.1: Equations of Motion of Centre of Mass of Simple Rotor - Equation of Motion in y Dir. $-K_2y - c\dot{y} - D_2x = m\ddot{y}$, Equation of Motion in x Dir. $-K_1x - c\dot{x} + D_1y = m\ddot{x}$.

The above equations come from considering a small perturbation in position of the journal so that the pressure field remains unchanged. The cross - coupling stiffness terms arise from geometry changes only. Assuming a solution of the form $x = A_1e^{\lambda t}$, $y = A_2e^{\lambda t}$ and applying Routh's stability criterion to the characteristic equation in λ^4, a necessary and sufficient condition for stability is obtained:

$$(K_1 - K_2)^2 + 2c^2\left(\frac{K_1}{m} + \frac{K_2}{m}\right) > 4D_1D_2, \tag{2.4}$$

or

$$(K_{xx} - K_{yy})^2 + 2c^2\left(\frac{K_{xx}}{m} + \frac{K_{yy}}{m}\right) > -4K_{xy}K_{yx}, \tag{2.5}$$

which demonstrates the destabilizing nature of large cross- coupling terms. This analysis does not yield any cross-coupling terms which arise due to Coriolis effect of the rotor translation and simultaneous precession. The latter effect is considered by Hagg in an analysis of a centred (unloaded) bearing for which the equations of motion in terms of polar coordinates; ϵ, shaft radial displacement from the journal equilibrium position (bearing centre in this case) and θ, precession angle:

$$m\frac{d^2\epsilon}{dt^2} - m\epsilon\left(\frac{d\theta}{dt}\right)^2 + B\Omega\epsilon\cos\gamma + c\frac{d\epsilon}{dt} = 0, \tag{2.6}$$

$$m\epsilon\frac{d^2\theta}{dt^2} + 2m\frac{d\epsilon}{dt}\frac{d\theta}{dt} + D\epsilon\frac{d\theta}{dt} - B\Omega\epsilon\sin\gamma = 0, \tag{2.7}$$

where:

$B\Omega\epsilon$ = the bearing resultant force at angle γ to the horizontal.
Ω = rotational speed ($B = K/\Omega$), C, D =damping coefficients.

These are non-linear equations unless $d\theta/dt$, the precessional velocity, is assumed constant. Then applying Routh's criterion to the resulting characteristic equation, Hagg derives the stability criterion:

$$\frac{D^2\cos\gamma}{mB\sin^2\gamma} > \Omega$$

at the threshold of instability, but $D = \Omega B\sin\gamma/(d\theta/dt)$ which therefore yields:

$$\Omega B\cos\gamma > m\left(\frac{d\theta}{dt}\right)^2.$$

Considering the continuity equation for an incompressible fluid gives an upper limit of $d\theta/dt = \Omega/2$. This then yields:

$$\frac{4B\cos\gamma}{m} > \Omega.$$

However $B\Omega\cos\gamma = K$ is the spring constant of the film which means that

$4K/m > \Omega$ or $\omega_n = \Omega/2$ or the speed should not exceed twice the first lateral critical speed for stability. This is the now well known criterion for the *possible* onset of oil whip. As a means of avoiding oil whip, Hagg investigated, analytically and experimentally, the behaviour of tilt-pad bearings which were just becoming popular at the time. Hagg's procedure was to use an approximate form of Reynolds' equation for laminar incompressible flow between plates (approximate because the tangential velocity is dependent on precessional angular motion which is therefore neglected in the plate formulation). The pressure is integrated over the pad with boundary condition of zero pressure at each end of the pad. The work done per cycle of precession by the rotor on the oil film is derived. This work is set equal to that done by viscous drag for circular precession at eccentricity ϵ with precession frequency ω. i.e. $= 2\pi\epsilon^2\omega$ resulting in a viscous damping coefficient:

$$c = \frac{n\mu}{2\eta^3}\left(\frac{l^3w^3}{l^2+w^2}\right)$$

where: l = length of pad, w = width of pad, η = radial clearance, μ = absolute viscosity, n = number of pads. This would give a direct damping coefficient only C_{xx} or C_{yy}. Because Coriolis is not considered, no cross-coupled damping coefficients are derived. However, for tilt-pad bearings these are usually very small. Hagg reasons that for instability to occur, the work done per cycle of displacement, by the oil film pressures due to journal rotation, must be greater than the damping energy, or work done on the oil film by the vibrating rotor. For the tilt-pad bearing, the work done by the principal bearing force during one complete cycle is shown to be approximately zero. This ignores the small frictional force so that the journal force on a pad can be considered to always act through the pivot point of the pad. This is not the case for a cylindrical sleeve bearing so that this integral is not zero in the latter case. Hence the tilt-pad bearing should be resistant to instability, which of course it is and was so demonstrated by Hagg's experiments. Reference [20] extended the previous study to include shaft flexibility. The stability criterion was experimentally modified to:

$$(K_1 - K_2)^2 + \frac{2}{m}\left(\frac{B_1^2K_1}{1+K_1/K_s} + \frac{B_2^2K_2}{1+K_2/K_s}\right) > 4D_1D_2, \qquad (2.8)$$

where the damping coefficient of the previous formula has been separated into B_1 and B_2 for x and y directions and K_s is the shaft flexibility.

Using the above stability criterion and the expression for film pressure we obtain:

$$p = \left(\frac{R}{c}\right)^2 \mu N \alpha \epsilon^\beta \left(\frac{\epsilon}{c}\right),$$

where: R = radius, c = clearance, ϵ = eccentricity, μ = absolute viscosity, α and β are dimensionless constants, and e = base of natural logarithms. This expression was deduced by Hagg from data produced by Needs [21] using an electrical analogue simulation of a one dimensional Reynold's equation for a 120°, partial arc bearing. From this the stiffness and damping coefficients were derived and a flexible rotor stability criterion was obtained:

$$\frac{\lambda A^2}{\phi}\left[\left(\frac{R}{c}\right)^2 \frac{\mu N}{p}\right]^2 > \frac{cN^2}{g}, \tag{2.9}$$

where:

$$\lambda = \left(\frac{K_1}{1 + K_1/K_s} + \frac{4K_2}{1 + K_2/K_s}\right) / (K_1 + K_2),$$

$$A = \left[\frac{(L/D)^2}{1 + (L/D)^2}\right][1 - \epsilon/2c]^{-3},$$

and ϕ is a dimensionless constant. λ has a fixed value for each specific value of the rigid support natural frequency and therefore of N_c (i.e. $30\omega_n/\pi$) and A has a definite value for the bearing parameter $\left[\left(\frac{R}{c}\right)^2 \mu N/p\right]$. Therefore, the dimensionless parameter $\lambda A^2/\phi$ has a definite value for each pair of:

$$\left\{\left[(R/c)^2 \mu n/p\right], \left[c(N_c)^2/g\right]\right\}.$$

This permits the expression of the stability criterion as a family of curves representing the stability boundaries by holding cN_c^2/g constant and varying:

$$\left\{\left[(R/c)^2 \mu n/p\right], cN/g\right\}$$

to determine each crossing of the boundary.

This resulted in a very practical family of curves for a simple rotor with fluid film bearings where the first lateral mode only is considered (the most common case in practise).

The above criterion was verified with an electrical analogue to within 10% accuracy and an experimental rig consisting of a small steam turbine was used to check the theory for several partial arc bearings as well as full cylindrical sleeve bearings, as well as a full cylindrical sleeve bearing with a circular central groove. The results agreed fairly well quantitatively with theory and qualitatively well with field experience, in

terms of the trends in stability for changes in bearing clearance and oil viscosity for different speed ranges of operation and the effect of shaft flexibility.

The effect of oil film properties on the unbalance response of rotors was investigated by Hagg and Sankey [22]. However, in this case the effective stiffness and damping coefficients were experimentally determined at rotation speed. In these experiments, only direct stiffness and damping coefficients were determined. It is presumed that this was because only direct (diagonal) terms could be accommodated in the analysis, at that time.

2.3 Derivation of Bearing Coefficients - Laminar Flow

In order to derive stiffness and damping coefficients for hydrodynamically lubricated bearings, some form of Reynolds' equation is generally used. This implicitly assumes that inertia forces are negligible, i.e. the Reynolds number is sufficiently low that viscous forces are dominant and that laminar, Couette flow prevails (there are no Taylor vortices) [23] - the Taylor number:

$$T_a = U_i d/\nu\sqrt{d/R_i} < 41.3,$$

where: U_i = peripheral velocity of inner cylinder, d = gap width, R_i = radius of inner cylinder, ν = kinematic viscosity.

Reynolds' equation for a slipper bearing, Figure 2.2 can be expressed as: [24, 25]:

$$\frac{\partial}{\partial x}\left(h^3\rho\frac{\partial p}{\partial x}\right)+\frac{\partial}{\partial y}\left(h^3\rho\frac{\partial p}{\partial y}\right)=6\mu\left[\frac{\partial}{\partial x}(h\rho U)+\frac{\partial}{\partial y}(h\rho W)\right]+12\mu\rho(w_h-w_o), \tag{2.10}$$

where: μ = dynamic viscosity, p = pressure, ρ = density, U, W are velocities of the boundary in the x and z directions.
For incompressible flow this becomes:

$$\frac{\partial}{\partial x}\left(h^3\frac{\partial p}{\partial x}\right)+\frac{\partial}{\partial y}\left(h^3\frac{\partial p}{\partial y}\right)=6\mu\left[\frac{\partial}{\partial x}(hU)+\frac{\partial}{\partial y}(hW)\right]+12\mu(w_h-w_o). \tag{2.11}$$

Sternlicht [26] used this form of Reynolds' equation with $(w_h - w_o) = V'$ the squeeze film velocity around the bearing, using an iterative finite difference method. This yields the eight coefficients of the equation of motion:

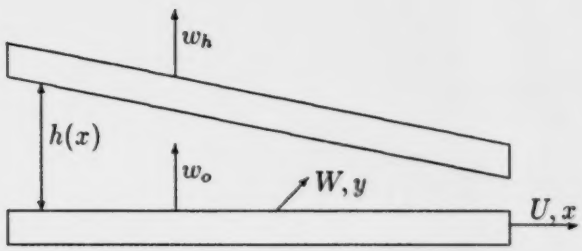

Figure 2.2: Slipper Bearing

$$\begin{bmatrix} m & 0 \\ 0 & m \end{bmatrix} \begin{Bmatrix} \ddot{x} \\ \ddot{y} \end{Bmatrix} + \begin{bmatrix} B_{xx} & B_{xy} \\ B_{yx} & B_{yy} \end{bmatrix} \begin{Bmatrix} \dot{x} \\ \dot{y} \end{Bmatrix} + \begin{bmatrix} K_{xx} & K_{xy} \\ K_{yx} & K_{yy} \end{bmatrix} \begin{Bmatrix} x \\ y \end{Bmatrix} = \begin{Bmatrix} G\cos(\omega t + \phi) \\ G\sin(\omega t + \phi) \end{Bmatrix}. \tag{2.12}$$

The damping cross - coupling terms B_{xy} and B_{yx} are stated to be negligible. The above form of Reynolds' equation can be modified to a more convenient expression for a rotor.

The local velocity at A, Figure 2.3, tangent to the surface at A is U where

$$U = \omega R - \dot{x}_j \cos\theta - \dot{z}_j \sin\theta \quad h = c(1 + \varepsilon\cos\theta), \quad \varepsilon = e/c$$

If W = 0 and $w_o = 0$ then ignoring second order terms:

$$\frac{\partial}{\partial x}\left(h^3\frac{\partial p}{\partial x}\right) + \frac{\partial p}{\partial y}\left(h^3\frac{\partial}{\partial y}\right) = 6\mu\left[R\omega\left\{1 - 2\frac{\dot{\alpha}}{\omega}\right\}\frac{\partial h}{\partial x} + 2\dot{e}\cos\theta\right]. \tag{2.13}$$

This is Lund and Sternlicht's starting point [27].

Their procedure was then to derive expressions for radial and tangential forces in terms of the eccentricity ratio ε, attitude angle α, the squeeze film velocity $\dot{e}$ the non - dimensionalized precessional velocity $\dot{\alpha}/\omega$, ω, the bearing geometry and oil viscosity. They then expand these expressions (which involve integration around the oil film, carried out numerically) in a Taylor series for a perturbation from the equilibrium position. Retaining first order terms only and returning to a non - rotating frame of reference the coefficients of dx, $d\dot{x}$, dy, $d\dot{y}$ become the stiffness and damping coefficients in the inertial frame i.e.

$$dF_x = -K_{xx}dx - C_{xx}d\dot{x} + K_{xy}dy + C_{xy}d\dot{y}, \tag{2.14}$$

$$dF_y = K_{yx}dx - C_{yx}d\dot{x} + K_{yy}dy + C_{yy}d\dot{y}. \tag{2.15}$$

The stiffness and damping coefficients so derived are functions of the geometry of the bearing, the eccentricity, the attitude angle and the time derivatives of the latter two. Lund and Sternlicht eliminate the term $\partial f/\partial\left(\frac{\dot{\alpha}}{\omega}\right)$ stating that as the Taylor expansion is about an equilibrium position where $\dot{\alpha}$ and $\dot{\varepsilon}$ both equal zero, that $\partial f/\partial\left(\frac{\dot{\alpha}}{\omega}\right) =$ zero.

However, this does not follow. In fact, if it did, then by the same reasoning the similar term; $\partial f/\partial\left(\frac{\dot{\varepsilon}}{\omega}\right)$ would also be zero. If however, it is reasoned that $\dot{\alpha}$ is merely constant i.e. a constant precession rate (or zero as is the case for the equilibrium position) then the result in the paper follows, without any condition (other than the 'small' assumption implicit in the linearization) on $\dot{\varepsilon}$. Therefore the stiffness and damping coefficients so derived are valid at the given eccentricity ratio i.e. for small deflections from that position.

In order to use standard analytical procedures for unbalance response and stability calculations, it was necessary to reduce the coefficient matrices to 'equivalent' diagonal matrices i.e. eliminating the cross - coupling terms. As these terms are not always equal and are usually opposite in sign (in Lund and Sternlicht's analysis they are of equal magnitude but opposite sign), this transformation cannot be achieved by a rotation of coordinate axes to find a set of principal axes. Using the response of a simple rotor with bearings having direct stiffness and damping coefficients only, Lund and Sternlicht obtained equivalent diagonal matrices. This equivalence was therefore dependent on the rotor configuration and, further was only valid for one lateral bending mode. It was essentially equivalent to a modal method of analysis with one mode only. For many rotors, operating well below the second lateral mode (critical speed), this model would suffice.

Lund extended this analysis [28] to the more complicated geometry of the tilting - pad bearing. The same basic theory as above was used and applied to each pad. Overall coefficients were then derived by summing over the pads. The cross - coupling terms were found to be ignorable (except at pad resonance). This is as Hagg had found and is the major reason for adoption of this design, as it indicates a greatly reduced tendency to instability.

The pad resonance derives from the rotational motion of the individual pads resulting in a 'critical mass', (an unfortunate use of the phrase), i.e. the mass of the pad for which this oscillatory motion becomes resonant for a given rotational speed, oil viscosity and pad geometry.

Lund used the bearing coefficients for oil film bearings in [13] in which he modelled a complete rotor, including bearing, aerodynamic effects and hysteretic friction in the rotor.

In the introduction to [13] it is stated that the calculated 'criticals' on the basis of rigid bearings, is often borne out on the test stand in-spite-of flexible fluid film bearings because of the stiffening effect of the damping in the bearings. This may have been experience restricted to a certain class of machines or due to the characteristics of the particular test stand. It has been the writers experience that many compressor sets in the petro-chemical industry and turbine- generator sets, that the name plate critical speed(s) are often removed from that determined by measurement of vibration signals during start-ups and run-downs, by several hundred R.P.M..

Lund also states that 'the true critical' is the damped natural frequency rather than the undamped natural frequency, often calculated at that time. In industry and in rotor dynamics trouble - shooting particularly, the speed of maximum unbalance response is generally regarded as the 'critical'. This is, after all, what is measured in the field and what matters to the user.

The term 'critical' is perhaps an unfortunate one in that many 'criticals' are so heavily damped as to be most uncritical but some operators still accelerate madly through that speed range incurring other system problems. Donald E. Bently coined the term 'balance resonance' which is more appropriate but not widely used. In practical terms the speed of maximum unbalance response and the damped natural frequency are very close. Lund's analysis of a simple rotor in plain bearings shows a pair of roots, (eigenvalues) which appear to 'track' rotation speed at a fraction of approximately 0.5 over most of the speed range. This pair of forward or backward modes are regarded by Lund as the 'first' modes, distinct from the rotor 'critical'. At instability it is the first mode which goes unstable and at a frequency $\approx 0.5\times$ rotor speed. Lund makes the point that this is not the first critical which has become unstable. However this result looks very like that of Muszynska [7], i.e. that the 'tracking' eigenvalue is the 'oil whirl' mode and when the rotor speed rises above twice the first 'critical speed', this critical now becomes the lower of the two eigenvalues and becomes unstable (or may do so in the absence of sufficient external damping).

One may also reason that the 'tracking mode' has begun to couple with the rotor critical as their frequencies approach, resulting in two new coupled modes. In such a case, as with aircraft flutter, one of the two modes generally goes less stable (the one with inherently less damping such as a bending mode) while the other goes more stable.

Lund's model for the rotor was derived from the lumped mass transfer matrix method, analogous to that of Myklestad's or Prohl, [29, 30] incorporating frequency - dependent hysteretic damping and oil - film coefficients as described above. In his analysis Lund retains all the backward precession modes (sometimes ignored by other writers) and in fact notes that it is the first backward mode which, for that rotor, had the greatest unbalance response and was therefore, in practical terms the first critical of the rotor.

In an analysis of the same rotor, using tilting - pad bearings, to prevent oil whip instability, Lund also included the effect of floating ring seals, behaving essentially as unloaded bearings and thereby creating a destabilizing mechanism. In fact they were shown to cause an instability within the speed range of the compressor which did not occur without the inclusion of the seal in the model. Unfortunately this lesson had to be re-learned in the design of the space shuttle fuel pumps - below. Details of the seal model were not given in the paper, but it is presumed that the same laminar, incompressible flow was assumed, permitting the use of Reynolds's equation.

In Prohl's paper, referred to above [30], the rotor was discretized into an equivalent system of disks and massless shaft sections. Vibration is assumed to be planar (no damping is included) and the bearings are considered isotropic. Stiffnesses, both angular and linear are assumed independent of speed. The equations of motion for an arbitrary section of shaft yields the shear force and moment at the station 'n' in terms of those at station 'n-1', the elastic properties of the beam element and the unbalance force on the element. The bending moment, shear force, rotation (in the plane of the shaft) and lateral displacement at a point on the rotor is then a linear function of these quantities, along the rotor up to that point, for a given speed.

Using a two step tabular process, firstly a unit shear force is assumed at one end, moment = 0, and the deflections and rotations are derived along the rotor. Then similarly for a unit moment and zero shear at one end the deflections and rotations are derived along the rotor.

This is essentially a means of deriving a dynamic 2x2 flexibility matrix for the rotor from one end to the other. For a critical speed the moment at the end must be zero. Therefore, the procedure is repeated for increments of speed to determine these speeds. Lund and Orcutt, some 20 years later [31] improved upon Prohl's method by including non - isotropic bearings with unequal cross - coupling terms stiffness and damping coefficients. This therefore resulted in elliptical shaft orbits and the inability to determine principal axes. Because of the low viscosity lubricant used in

the particular machine analyzed, the flow regime was turbulent and the coefficients had to be derived accordingly (see below). To accommodate damping, displacements along the rotor are represented in complex form as are the bearing stiffness and damping coefficients i.e. they were represented as complex impedances:

$$Z_{xx} = K_{xx} + i\omega B_{xx} \qquad Z_{xy} = K_{xy} + i\omega B_{xy} \quad etc.$$

The beam element relationships are derived in a manner similar to Prohl. Lund and Orcutt developed the theory for using distributed mass and moment of inertia, but did not use it in the paper as it was considered an unnecessary complication.

In carrying out the calculation of shear and bending moment for each speed increment (with appropriate changes in bearing coefficients), Lund and Orcutt extended the analysis by setting the bending moment to zero at the rotor end and thereby derived the displacements and rotations along the rotor for each speed i.e. a complete unbalance response. This analysis therefore also provided the orbit shapes along the rotor at all speeds and whether the modes being excited were forward or backward precession.

Lund [34] also developed a modal method for rotor - bearing systems including damping. The normal procedure for decoupling equations of motion using the normal modes of a system, requires that the mass and stiffness matrices be symmetric. To permit such a method to be used for the case involving the non - symmetric cross - coupling terms generated by fluid - film bearings (and seals), it was necessary to develop an othogonality criterion for non - symmetric matrices.

Lund sets up a complex eigenvalue problem for free vibration of the rotor / bearing system, which can be solved for its eigenvalues which occur as complex conjugate pairs, and an associated set of eigenvectors. Then replacing the coefficient matrices by their transposes and reversing the direction of rotation (mathematically in the gyroscopic term of the element equation of motion), a second complex eigenvalue problem is set up. This has the same complex eigenvalues as the first analysis but for non - symmetric matrices, yields a different set of eigenvectors (complementary or left eigenvectors). These two sets of eigenvectors permit the decoupling of the equations of motion of the rotor.

2.4 Tilting - Pad Bearings

Tilting pad (or pivoted pad) bearings started to be used about forty years ago and are today the rule rather than the exception for high speed turbomachinery, where the freedom from 'oil-whirl' or 'oil-whip' instability is their major advantage over plain cylindrical, elliptical or fixed lobe type bearings.

For most tilting - pad arrangements the stiffness and damping coefficient matrices, referred to a coordinate system along and perpendicular to the line of centres, (bearing - journal), have zero or small cross terms K_{xy}, C_{xy} etc. i.e. principal coordinates can be found. This is not the case with the fixed geometry bearings. With no circulatory terms, there is no tendency to drive the journal in a forward precessing mode.

Unfortunately, this freedom from these two types of instability sometimes causes them to be used as a cure for all types of instability problems in rotating machinery, occasionally making matters worse. Steam or gas swirl in the seals of a steam turbine or gas compressor can produce a 'whip' i.e. an instability in which the first lateral vibration mode of the rotor - shaft system becomes unstable in very much the same way as is caused by oil swirl in a bearing.

If the existing fixed geometry bearings are then replaced by tilting pad bearings, the situation may well worsen because generally the latter provide less external damping to the rotor system.

Boyd and Raimondi [35] in 1953, were possibly the first to publish an analysis of the performance of tilting pad bearings. They compared their performance with that of plain bearings and concluded that apart from the stability question, there was no advantage over the plain bearing. Indeed the plain bearing had some advantages, particularly in heat rejection capability. However, this analysis was for pads which had zero preload, i.e. the pads had the same centre of curvature as the bearing. The bearing in this context is regarded as the circle through the points on the pad surfaces immediately above the pivots.

In their subsequent paper, [36] in 1962, Boyd and Raimondi investigated the variation of load bearing capability with pad curvature (preload), the self aligning capability of pads with preload, and means of preventing 'spragging' which is when the leading edge of a pad contacts the journal.

As mentioned above, Lund [28] derived stiffness and damping coefficients for individual pads, using Reynolds' equation to derive the pressure profile and taking the gradients of the resulting forces on the journal. Lund also investigated the stability of pad rotational vibration and determined the maximum moment inertia of the pad for stability.

It is evident from the literature of that time (the 60's), that other advantages of tilting pad bearings were being realised. Not only did tilting - pad bearings have the advantage of inherent stability but the ability to change the loading capability (a high load capability is not always good) and thereby oil temperature rise, by changing the curvature of the pads in a given bearing assembly, was a very useful means of changing bearing characteristics without a major design change.

The fact that tilting - pad bearings provide less external damping to the rotor - shaft system than fixed geometry bearings, can be a problem even when there is no non-synchronous instability problem such as the gas or steam-induced whip referred to above. The lower damping can result in a high response to mass imbalance, particularly when traversing rotor 'critical speeds'. Further, it was discovered that the predicted damping coefficients were higher than actually found in practice. The primary reason for this appears to be the effect of a change in pad curvature under load and of pivot deflection.

Ettles [37] 1980 devised a very comprehensive procedure for analysis of tilting pad bearings which included the effects of pad distortion, oil temperature variation and which analyzed the whole bearing simultaneously rather than each pad at a time. This involved 6 nested iterative loops in the computer code. To make the computer time acceptable, Ettles used a one dimensional analysis for the oil film pressure distribution, assuming the axial pressure profile could be expressed in terms of the circumferential pressure at mid - span $p = P(1 - y)^2$, where p is the pressure at non - dimensional distance y from the bearing centre and P is the pressure at the centre, for a particular circumferential position. This procedure compared well with measurements for static load and stiffness and was about 30 - 40% high for damping coefficients.

From the point of view of a rotor - shaft system, the bearings are spring - mass - damper systems between the shaft journal and support pedestal or ground if one regards the pedestal as rigid. They therefore can be regarded as complex impedances. Even if one ignores pad mass / inertia, the damping force applied to the rotor by the bearing will depend on the frequency of vibration, and therefore on the eigenvalue solution. The procedure used by several authors is to select this frequency, usually referred to as the 'reduced frequency' as equal to the undamped natural frequency of the particular mode of interest or equal to the rotation speed if one is interested in the frequency response of the rotor system for varying speed.

Rouch, [38], 1983 accounted for pad pivot flexibility and pad mass /inertia by introducing extra linear and angular degrees of freedom for the pad. Rouch then coupled his bearing model with a flexible rotor and showed, as expected that the closer the assumed reduced frequency was to the frequency of the least stable mode, the lower was the log - decrement of that mode, i.e. the less stable.

Lund and Pederson, [39], 1987 developed an approximate method for including pad flexibility by including an equivalent change in clearance. They showed a damping coefficient reduction with decreasing film thickness (increasing load) of up to 20 percent for a film thickness at the pivot equal to 20 percent of nominal clearance and about 5 percent reduction for a pivot film thickness equal to 50 percent of nominal clearance. The effective pad - film stiffness was affected far less.

Earles et al. [40, 41] ,1990, used a finite element model of the pad to account for pad flexibility rather than the curved beam model used by previous authors. The pad elements were two dimensional. This analysis showed similar reductions in damping due to pad flexibility as had Lund and Pederson.

Their subsequent stability analysis showed a lower stability threshold for assumed reduced frequency equal to the eigenvalue rather than equal to rotation speed as would be expected. They also showed lower threshold speeds for inclusion of pad flexibility and pivot flexibility. It is most significant that they found pivot flexibility considerably more significant than pad flexibility. Pad flexibility reduced the onset of instability from 9500 RPM for the rigid pivot to 9250 RPM. Pivot flexibility reduced it to 8000 RPM.

The effect of heat transfer between the fluid film and its surroundings was investigated by Knight and Barrett [42], 1988. This showed little change in damping coefficient for a $30°C$ temperature difference in inlet oil temperature but the stiffness coefficient was lower by from 10% to 30% for the lower inlet temperature. It should be said that the greater difference was at low speeds where it is of least significance. At the speeds where instability is possible, the difference was smaller.

Kim and Rodkiewicz [43], 1991 investigated the effect of inlet pressure build - up including heat transfer effects and variable viscosity. The viscosity was assumed to vary according to $\eta = \eta_{in} exp[\beta(T_{in} - T)]$ where T, T_{in} are local and inlet temperatures, η and η_{in} are local and inlet absolute viscosities and β is a constant.

They found, among other effects, that the maximum pressure in the film could increase by about 20% due to inlet pressure build - up. However they assumed an infinite length bearing and a 'linear' slider for their analysis. The recommendation that inlet pressure build-up has such a significant effect that it should be considered in the design of tilting pad bearings would seem a little premature. More realistic configurations including a whole bearing assembly should be analyzed with due regard for satisfying the Reynolds' pressure boundary condition at all of the pads' trailing edges, before such a strong conclusion can be supported.

2.5 Finite Element Analysis for Bearings

Most of the work on the derivation of bearing coefficients used the method of finite differences until the 1970's when the finite element method was first applied to fluid mechanics problems. The variational calculus approach is most commonly used in fluid mechanics. The finite element representation of a bearing lubrication problem using Reynolds' equation is described in [44] and [45]. Both direct and variational approaches are described in the paper.

The variational statement for the incompressible Reynolds' differential lubrication equation is that the pressure field minimizes the functional $I(p)$ and satisfies the pressure and flow boundary conditions (unless the pressure boundary conditions are specified on the whole boundary):

$$I(p) = \int\int_A \left[\left(\frac{\rho h^3}{24\mu} \nabla p - \rho h \overline{U} - \frac{\rho h^3 B}{12\mu} \right) \cdot \nabla p + \left(\frac{\partial(\rho h)}{\partial t} + \rho v_d \right) p \right] dA + \int_{S_q} \rho Q p \, ds, \tag{2.16}$$

where ρ = density (constant), h = film thickness, $\overline{U}$ is the average velocity of the two bearing surfaces, B is the body force, μ = the absolute viscosity, v_d is the leakage velocity through a porous bearing, A = area, Q = is the leakage flow at the boundary and S_q is the segment of boundary over which there leakage flow is specified.

This functional representation can be shown to be equivalent to the differential equation form of Reynolds' equation :

$$\nabla \cdot \left(\frac{\rho h^3}{12\mu} \nabla p \right) = \nabla \cdot \left(\rho h \overline{U} + \frac{\rho h^3}{12\mu} B \right) + \frac{\partial(\rho h)}{\partial t} + \rho v_d, \tag{2.17}$$

subject to the flow boundary condition :

$$Q = \rho \boldsymbol{q} \cdot \boldsymbol{n} \equiv h\left(\rho\overline{\boldsymbol{U}} + \frac{\rho h^2}{12\mu}\boldsymbol{B} - \frac{\rho h^2}{12\mu}\nabla p^*\right) \cdot \boldsymbol{n}, \tag{2.18}$$

where p^* is some distribution of p which satisfies the Reynolds' equation. This boundary condition is that the average flow normal to the boundary corresponds with that specified.

Body forces can usually be ignored for a bearing. Therefore for a non - porous bearing Equation 2.16 can be re-stated as:

$$I(p) = \int\int_A \left\{\frac{\rho h^3}{24\mu}\left[\left(\frac{\partial p}{\partial x}\right)^2 + \left(\frac{\partial p}{\partial y}\right)^2\right] - \rho h\left[U_x\frac{\partial p}{\partial x} + U_y\frac{\partial p}{\partial y}\right] + \frac{\partial(\rho h)}{\partial t}p\right\} dA$$

$$+ \int_{S_q} [q_x n_x + q_y n_y]\, p\, ds \tag{2.19}$$

or

$$I(p) = \int\int_A \left\{\frac{\rho h^3}{24\mu}\left(\frac{\partial p}{\partial x_j}\right)\left(\frac{\partial p}{\partial x_j}\right) - \rho h U_j\frac{\partial p}{\partial x_j} + \frac{\partial(\rho h)}{\partial t}p\right\} dA + \int_{S_q} q_j n_j p\, ds \tag{2.20}$$

(sum on j).

This is the form of the equation used by Allaire et al. [46]. The field variables within an element can be expressed as a function of the nodal values of the element, using an interpolation function which is some function of the geometrical coordinates. This results in an expression of the form:

$$p_k(\chi_i) = \{N(\chi_i)\}^T\{p\}_{k(nodes)} = N_i\, p_{i(nodes)} \qquad \text{(sum on } i\text{)} \tag{2.21}$$

The $\{N(\chi_i)\}$ are referred to as a normal or cardinal basis and k is the element number ($i = 1$ to r where $r =$ number of nodes per element). χ_i are functions of the spatial coordinates local to the element x_j where for a 2 - dimensional element, $j = 1,2$ i.e. (x,y) coordinates. Similarly expressions can be set up for the other field variables, which in this case are U_x, U_y and $\partial h/\partial t$. The interpolation functions need not be the same for all field variables.

The natural basis is determined as follows for (for example) a 2 - dimensional quadrilateral element with a bi-linear interpolation function:

$$p_k(\chi_i) = a_1 + a_2x_1 + a_3x_2 + a_4x_1x_2$$

where $\chi_i = a_1,\ a_2x_1,\ a_3x_2,\ a_4x_1x_2$ for $i = 1$ to 4

and the a_i are constants. Therefore for node 1 letting $x_j = x_{j1}$:

$$p_1 = a_1 + a_2 x_{11} + a_3 x_{21} + a_4 x_{11} x_{21} \tag{2.22}$$

and similarly for the other nodes, 2, 3, 4. Hence:

$$\begin{Bmatrix} p_1 \\ p_2 \\ p_3 \\ p_4 \end{Bmatrix}_k = \begin{bmatrix} 1 & x_{11} & x_{21} & x_{11}x_{21} \\ 1 & x_{12} & x_{22} & x_{12}x_{22} \\ 1 & x_{13} & x_{23} & x_{13}x_{23} \\ 1 & x_{14} & x_{24} & x_{14}x_{24} \end{bmatrix}_k \begin{Bmatrix} a_1 \\ a_2 \\ a_3 \\ a_4 \end{Bmatrix}_k \tag{2.23}$$

or

$$\{p\}_k = [T]_k \{a\}_k.$$

Therefore :

$$\{a\}_k = [T]_k^{-1} \{p\}_k.$$

Then :

$$p_k(\chi_i) = \{1 \;\; x_1 \;\; x_2 \;\; x_1 x_2\}_k \, [T]_k^{-1} \, \{p\}_k.$$

Therefore the normal basis is given by :

$$\{N_k(\chi_i)\}^T = \{1 \;\; x_1 \;\; x_2 \;\; x_1 x_2\}_k [T]_k^{-1} \text{ for element } k \text{ i.e. no sum on } k$$

For the general case, (any interpolation function) and dropping the k and χ for simplicity we can write for a given element:

$$\begin{aligned} p &= \{N\}^T \{p\} = N_i p_i \\ U_x &= \{N\}^T \{U_x\} = N_i U_{x_i} \\ U_y &= \{N\}^T \{U_y\} = N_i U_{y_i} \\ \dot{h} &= \{N\}^T \{\dot{h}\} = N_i \dot{h}_i \, . \end{aligned} \tag{2.24}$$

The above uses the same $\{N\}$ for all the field variables (actions). Now

$$\frac{\partial p}{\partial x} = \left\{ \frac{\partial N}{\partial x} \right\}^T \{p\} = \{p\}^T \left\{ \frac{\partial N}{\partial x} \right\}, \tag{2.25}$$

$$\frac{\partial p}{\partial y} = \left\{ \frac{\partial N}{\partial y} \right\}^T \{p\} = \{p\}^T \left\{ \frac{\partial N}{\partial y} \right\}. \tag{2.26}$$

If we now substitute these approximate expressions for p, U_x, U_y, $\dot{h}$, $\partial p/\partial x$, $\partial p/\partial y$ in Equation 2.20 and then minimise this equation by setting its derivative $\partial I/\partial \{p\}^T = 0$ we obtain:

$$[K_p]\{p\} = \{q\} - [K_{U_x}]\{U_x\} - [K_{U_y}]\{U_y\} - [K_h]\{\dot{h}\} \tag{2.27}$$

where :

$$K_{p_{ij}} = -\int\int_A \frac{\rho h^3}{12\mu}\left[\frac{\partial N_i}{\partial x}\frac{\partial N_j}{\partial x} + \frac{\partial N_i}{\partial y}\frac{\partial N_j}{\partial y}\right] dA$$

$$K_{U_x\,ij} = \int\int_A \rho h \frac{\partial N_i}{\partial x} N_j \, dA$$

$$K_{U_y\,ij} = \int\int_A \rho h \frac{\partial N_i}{\partial y} N_j \, dA$$

$$K_{\dot{h}\,ij} = -\int\int_A \rho N_i N_j \, dA$$

$$q_i = \int_{S_q} Q N_i \, dS.$$

The [K]'s are known as 'fluidity' matrices. They are influence coefficient matrices for the various 'actions'. The element matrices can now be assembled into system or 'global' matrices by matching the pressures at the element nodes and the corresponding flows on the right hand side of Equation 2.27. This set of equations has the same form as the element equations 2.27 except that it now consists of square matrices $n \times n$ and vectors $1 \times n$, where n is the total number of system nodes.

The pressure boundary conditions permit the modification of $[K_p]$ and flow boundary conditions are automatically taken care of on the right hand side of Equation 2.27. Then we have a set of algebraic equations to solve for the nodal pressures p instead of the differential equations we started out with. Hence for given surface velocities, film thickness, density and squeeze rate, we can determine the pressure distribution.

Allaire et al. [46] used the fluidity approach to calculate pressure distribution using triangular elements and linear interpolation functions for pressure within the elements. They assumed ρ, h, U_x, U_y and $\dot{h}$ all constant within each element. It was determined that aligning the element diagonals approximately in line with the direction of the pressure gradient optimized the accuracy and reduced computing time. Also, varying the grid spacing in the circumferential direction directly as the film thickness helped reduce computing time. Allaire et al. considered the use of quadrilateral elements but concluded that the improved accuracy over triangular elements could simply be offset by increasing the number of triangular elements. Huebner and Thornton [45] consider the quadrilateral element preferable. Calculating the pressure field as above presumes we know the values of the film thickness h. This depends on the load, i.e. we have to determine the equilibrium position. For given bearing surface velocities, the bearing develops a film thickness profile corresponding to a pressure profile which can support the load. Therefore, an iterative calculation is required to determine h around the bearing at equilibrium.

Allaire et al. carried out numerical differentiation with respect to the inertial displacements and velocities x, y, $\dot{x}$ and $\dot{y}$ to produce curves of bearing coefficients versus Sommerfeld number. These could then be used in bearing stability calculations as described above in the earlier studies and for unbalance response and critical speed calculations. In fact, the University of Virginia set up a joint University - industry program to make a suite of computer codes available to designers and users of rotating machinery.

2.6 Turbulent Flow Bearing Coefficients

Although, for most bearings with normal lubricants, the assumption of laminar flow is justifiable, this is not always the case. In pump sets, where the pumpage, often water, may be used as the lubricant, the flow in the bearing annulus can be turbulent. In addition the flow through the inter-stage seals may also be turbulent.

Ng and Pan [47] developed a lubrication equation for turbulent flow of the same form as Reynolds' equation for laminar flow. Their starting point was the expression for the time averaged Navier - Stokes (momentum) equation which in indicial form[1] can be expressed as:

$$\frac{\partial}{\partial t}\left[\overline{\rho}\,\overline{u_i} + \overline{\rho' u_i'}\right] + \left[\overline{\rho}\,\overline{u_j}\,\overline{u_i}\right]_{,j} + \left[\overline{\rho u_i' u_j'}\right]_{,j} =$$

$$-\overline{p}_{,i} + \left[\overline{\tau_{ij}} - \overline{u_j}\overline{\rho' u_i'} - \overline{\rho' u_j'}\,\overline{u_i'} - \overline{\rho' u_j' u_i'}\right]_{,j}$$

where ρ is density, u_i, u_j are the ith and jth components of velocity (i and j take values 1,2,3), the overbar denotes the time averaged quantity and the primes denote a perturbation in the quantity from the mean, the $_{,i}$ and $_{,j}$ denote partial differentiation with respect to the ith and jth components of displacement x_i, x_j, p is pressure and τ is the viscous shear stress. For incompressible steady flow, ignoring the mean flow inertia terms, this reduces to :

$$\overline{\tau_{ij}}_{,j} - (\rho\overline{u_i' u_j'})_{,j} = \overline{p}_{,i}$$

where $-\rho\overline{u_i' u_j'}$ is the Reynolds' stress $= \tau_{ij}'$

[1] Ng and Pan did not use indicial notation. The writer has done so for compactness to set up the starting point in Ng and Pan's paper.

or in cartesian tensor form [25]:

$$\begin{pmatrix} \sigma'_x & \tau'_{xy} & \tau'_{xz} \\ \tau'_{yx} & \sigma'_y & \tau'_{yz} \\ \tau'_{zx} & \tau'_{zy} & \sigma'_z \end{pmatrix} = -\rho \begin{pmatrix} \overline{u'^2} & \overline{u'v'} & \overline{u'w'} \\ \overline{v'u'} & \overline{v'^2} & \overline{v'w'} \\ \overline{w'v'} & \overline{w'v'} & \overline{w'^2} \end{pmatrix}.$$

Therefore:

$$(\overline{\tau_{ij}} + \tau'_{ij}),_j = -\overline{p},_i$$

but

$$\tau'_{ij} = \varepsilon\rho\overline{u_i},_j$$

where ε is the 'eddy diffusivity'. Therefore:

$$\tau'_{ij} = \mu\left(\frac{\varepsilon}{\nu}\right)\overline{u_i},_j$$

$$\tau_{ij} = \mu\overline{u_i},_j + \mu\left(\frac{\varepsilon}{\nu}\right)\overline{u_i},_j$$

or

$$\tau_{ij} = \mu\left(1 + \frac{\epsilon}{\nu}\right)\overline{u_i},_j = \overline{p},_i \quad . \tag{2.28}$$

Ng and Pan make use of Reichardt's formula for ϵ/ν, with constants determined by their own experiments, and the relationship:

$$\tau_{ij},_j = p,_i$$

to integrate equation 2.28 to obtain the velocity profile across the annular channel.

After some considerable manipulation, an equation having the same form as the Reynolds' lubrication equation is obtained. The integration procedure assumes that the flow field can be represented as a small perturbation of 'turbulent Couette' flow. This permitted Ng and Pan's colleague, F.K. Orcutt at Mechanical Technology Inc., to develop bearing coefficients for turbulent flow for tilting - pad bearings[48].

A rigorous treatment of turbulent flow in an annulus was carried out by Yamada [49]. This work concerns only situations when the Reynolds number is sufficiently high that Taylor vortices (a pattern of vortices about stationary circumferential axes) are no longer formed, i.e. the flow is completely turbulent. Yamada examines theoretically and experimentally, flow in the annulus between concentric cylinders, including axial and circumferential components of velocity and assuming turbulent 'law of the wall' velocity profiles. Thus the velocity distribution in the axial direction obeys a law of the form:

$$v = v_0 \left(\frac{2y}{s}\right)^{\frac{1}{n}}$$

where s = radial clearance, y = distance from the wall, v_0 = max velocity (at the mid point), n = constant to be determined by experiment.

Also, the frictional resistance coefficient is of the form

$$\lambda = cR_e^{-\alpha}$$

where R_e = axial Reynolds' number, $= v_{mean}s/\nu$, ν is the kinematic viscosity and c, α are constants.

For the circumferential direction with turbulent flow, the same power law results. The circumferential velocity u at radial position y is:

$$u = \frac{u_1}{2}\left(\frac{2y}{s}\right)^{\frac{1}{n}}$$

for

$$0 \leq \frac{s}{2}$$

and

$$u_1 - u = \frac{u_1}{2}\left[2\frac{(s-y)}{s}\right]^{\frac{1}{n}}$$

for

$$\frac{s}{2} \leq y \leq s$$

where u_1 is the circumferential velocity of the inner cylinder $= r\omega$, the outer cylinder remaining stationary.

Using $n = 7$ (7th. power law) and c, α deduced from experiment in the above expressions result in a friction factor for combined axial and circumferential flow:

$$\lambda = 0.26R_e^{-0.24}\left[1 + \left(\frac{7}{8}\right)^2\left(\frac{R_\omega}{2R_e}\right)^2\right]^{0.38} \tag{2.29}$$

for which the general expression is:

$$\lambda = cR_e^{-\alpha}\left[1 + \left(\frac{n}{n+1}\right)^2\left(\frac{R_\omega}{2R_e}\right)^2\right]^{\frac{1-\alpha}{2}}$$

where R_ω is the Reynolds' number for circumferential flow. Yamada indicates that for pipe flow using a 7th. power law $u/U = (y/R)^{\frac{1}{n}}$ with $n = 7$, Blazius' equation is obtained, viz $\lambda = 0.27R_e^{-0.25}$. However, Blazius formula was actually deduced to be $\lambda = 0.3164R_e^{-0.25}$ for smooth pipes [25, 50]. But Blazius defined R_e as $(v_{mean}d/n$ for the pipe. Thus for the limiting case of the annulus becoming a pipe, the clearance $s \rightarrow r_2$ in which case Yamada's $R_e(axial)$ becomes $v_{mean}r_2/\nu = v_{mean}\frac{d}{2}/\nu$; i.e. $R_e(Blazius) = 2R_e(Yamada)$. This indeed leads to the two expressions being equivalent.

Therefore using Blazius' rule, the case of concentric cylinders with a 7th. power law would result in a friction factor for combined axial and circumferential flow:

$$\lambda = 0.27\,R_e^{-\frac{1}{4}}\left[1 + \left(\frac{7}{8}\right)^2\left(\frac{R_\omega}{2\,R_e}\right)^2\right]^{\frac{3}{8}} \tag{2.30}$$

which is very close to that derived by Yamada. In Black et al's papers, discussed below, this latter expression was used to derive stiffness, damping and inertia coefficients for turbulent flow through seals. Black [51] makes the same assumption as Ng and Pan, that turbulent flow in the annulus can be considered a perturbation superimposed on a 'mean Couette flow'. Then for axial flow through the annulus the pressure gradient is:

$$\frac{dp}{dz} = -2\frac{\lambda_a}{c}\frac{1}{2}\rho w^2$$

where w is the mean axial velocity, c is the radial clearance and λ_a is the axial friction coefficient.

Black takes his expression for λ_a from Yamada's paper (the Blazius' law version) expressing it as:

$$\lambda_a = 0.079R_e^{-0.25}\left[1 + \left(\frac{7}{8}\right)^2\left(\frac{R_r}{R_e}\right)^2\right]^{0.375}.$$

The difference between this and Yamada's form, above, is because $\lambda(Yamada) \equiv 4\lambda(Black)$. Also $R_e(Black) = 2R_e(Yamada)$ i.e. Black's usage was consistent with that of Blazius. Using the stress law $\tau = 1/8\lambda\rho U^2$ where ρ = density, U = shaft peripheral velocity, Black derives a linearized expression for circumferential pressure distribution in terms of the local clearance for the eccentric journal, shaft peripheral speed, mean velocity increment due to the pressure gradient and the local (around the journal) rotational Reynold's number.

Having expressions for axial and circumferential pressure gradient, in terms of mean axial velocity and circumferential, pressure induced, mean perturbation velocity, these velocities are eliminated from the continuity equation for an incompressible fluid at the angular position corresponding to the local clearance. A pressure field equation is thus derived which has the same form as Reynolds' equation for the laminar régime.

The rest of their paper was concerned with the load bearing capabilities of a bearing which had a substantial axial flow component, as a function of Sommerfeld number and bearing clearance. However, Black concludes that stiffness and damping coefficients would depend solely on journal position.

In his almost simultaneous and widely referenced paper, [52] effective fluid stiffness damping and inertia coefficients are derived for a centred shaft, executing small vibrations within an annular seal.

Starting with the integral form of the continuity equation for an incompressible fluid subject to the squeeze action of the shaft within the seal, and the linear momentum equation along the annular passage, Black postulates small deviations about the average axial fluid velocity due to the perturbations in lateral shaft position and derives a lateral force:

$$F_y = -\epsilon k(D) y$$

where $k(D)$ can be approximated by:

$$k(D) = \mu_0 + \mu_1 T D + \mu_2 T^2 D^2$$

where:

$$T = \frac{L}{V}, \quad \epsilon = \frac{\pi}{6\lambda}\left(\frac{\sigma}{1.5 + 2\sigma}\right) RP, \quad \sigma = \frac{\lambda L}{y_0}$$

where: λ = friction coefficient, y_0 = radial clearance, P = pressure differential across the seal, R = seal radius.

Therefore, the coefficients $\epsilon\mu_0$, $\epsilon\mu_1 T$ $\epsilon\mu_2 T^2$ can be considered stiffness, damping and inertia coefficients for the fluid, which were added to the corresponding terms for the rotor to derive an expression for the unbalance response in the normal fashion. Black extended the analysis to include speed dependent pressure drop across the seal, resulting in an increase of damping coefficient with speed and a 'negative fluid mass' effect.

In order to investigate fluid whip instability, Black considers fully developed 'turbulent Couette flow' within the annular space, in the circumferential direction i.e. mean fluid rotation velocity equal to half the shaft speed $\omega/2$. Then considering a frame of reference rotating at $\omega/2$, expressions are developed for the radial component of the fluid forces in the rotating frame. These are transformed to the inertial frame

and the equation of motion for free vibration is so derived. The stability boundary is then determined by inspecting the complex eigenvalues and finding the condition for a quasi - stable solution.

The frequency of precession given by this analysis is:

$$\Omega = \frac{\omega}{2}$$

where

$$\omega = 2\sqrt{\frac{s + \epsilon\mu_0}{m}}$$

where s and m are respectively the shaft stiffness and mass, i.e. the precession is at a frequency equal to a half shaft rotation speed, when the rotation speed is a little higher than twice the rotor critical speed.

Black further considers the case for speed dependent pressure drop across the seal and includes external viscous damping to develop a stability boundary for a centrifugal pump. Black and Jensen [53] extended the study above to include circumferential pressure - induced flow which is the dominant effect in a bearing. However, in the seal application this is assumed small compared with the axial flow. This resulted in a modification to the μ_0, μ_1, μ_2 coefficients as a function of the length/radius ratio of the seal.

In [53] the concept of 'rotary receptance' r/F is introduced for an unbalanced journal (or subject to some rotating force F) producing a precession radius r. The integral forms of the continuity and momentum equations are used, allowing for circumferential and axial flow for an incompressible fluid. The friction head loss per unit length along the seal is assumed, as in the previous study, proportional to velocity squared and Yamada's [49] coefficient of friction is used. The friction coefficient is assumed constant within the annulus and average velocities are used in the momentum equation (the radial velocity profile across the fluid gap is not accounted for).

The differential equation for pressure perturbation distribution with respect to non - dimensionalized axial position and time is derived as a function of radial journal perturbation and the constants of the seal. Then assuming a harmonic variation in pressure and radial position perturbation, and integrating around the seal, the radial force is found in terms of a complex dynamic stiffness and the radial displacement amplitude. The components of the dynamic stiffness can then be resolved into hydraulic 'inertia', 'damping' and 'stiffness' components in terms of the μ_0, μ_1 and μ_2 parameters, derived in the previous study, [52].

Evaluation of the differential equation for a practical range of seal parameters permitted a modification to the μ's due to fluid circulation, so that the modified values may be used in the matrix formulation of the equations of motion for fluid in the seal annulus:

$$\begin{Bmatrix} F_y \\ F_z \end{Bmatrix} = \frac{-\pi RP}{\lambda} \begin{bmatrix} \left(\mu_0 - \frac{1}{4}\mu_2\omega_s^2 T^2\right) & \frac{1}{2}\mu_1\omega_s T \\ -\frac{1}{2}\mu_1\omega_s T & \left(\mu_0 - \frac{1}{4}\mu_2\omega_s^2 T^2\right) \end{bmatrix} \begin{Bmatrix} y \\ x \end{Bmatrix}$$

$$+ \begin{bmatrix} \mu_1 T & \mu_2\omega_s T^2 \\ -\mu_2\omega_s T_2 & \mu_1 T \end{bmatrix} \begin{Bmatrix} \dot{y} \\ \dot{x} \end{Bmatrix} + \begin{bmatrix} \mu_2 T^2 & 0 \\ 0 & \mu_2 T^2 \end{bmatrix} \begin{Bmatrix} \ddot{y} \\ \ddot{x} \end{Bmatrix}. \qquad (2.31)$$

Finally Black and Jenssen investigated the case of high eccentricity of the journal within the seal. The perturbation about the steady - state position was still assumed small but the axial and circumferential Reynolds' numbers and friction factors were allowed to vary around the annulus. The stiffness characteristics were then evaluated by a numerical solution and only showed significant differences from the centred journal for high eccentricity ratios. This assumes that, under the conditions of high eccentricity, the 'turbulent Couette flow' assumption for the velocity profile is still valid.

The results of [53] show that the velocity and acceleration terms arising from the fluid in the seals, strongly control the displacement response, to the extent of totally suppressing the first lateral mode 'critical' of the pump rotor and the onset of 'whip' instability. This is in agreement with several field investigations the writer has carried out on water and petro - chemical pump - sets, in which the first 'critical' was undetectable on run - ups or shut - downs.

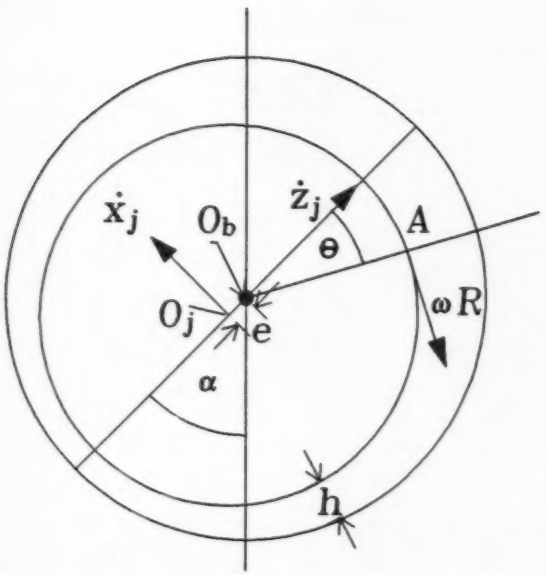

Figure 2.3: **Journal Precessing in Bearing Annulus: The journal has components of precessional velocity $\dot{x}_j$, $\dot{z}_j$ and constant angular velocity ω. O_j and O_b are the journal and bearing centres.**

2.7 Internal Friction

The phenomenon of instability induced by internal damping, has been the subject of considerable analysis, [54, 55, 56, 14, 57], perhaps because of its counter - intuitive aspect. To the field engineer, it is a phenomenon which typically occurs in machines such as compressors which have 'stacked' rotors, which, if not very precisely assembled, can generate internal friction damping i.e. within the rotor rather than externally applied through, for instance, the viscous damping of a fluid film bearing. It is not a common occurrence but can be very severe and sudden when it does occur.

In 1924 Kimball [54, 55] demonstrated that the presence of internal friction (viscous or coulomb), leads to a tangential disturbing force which is at approximately the first resonant frequency (critical speed) of the rotor. The direction of this disturbing force is such as to promote whirling i.e. in the direction of rotation, when the rotation speed is above the first resonance, and so as to suppress whirling when rotation speed is below the first resonance.

Ehrich [56] showed that the unstable mode need not necessarily be the fundamental mode but is generally the mode closest to one half rotation speed. This does not agree with [54, 57, 14]. However, the re-excitation of the first mode 'whip' due to fluid - induced forces occurs at speeds above twice the first (or other) critical speed frequency. It is therefore possible that where internal damping is insufficient to cause instability below twice the first critical, the combined destabilizing effects of fluid whip and internal damping cause instability at a speed in the vicinity of twice the first critical.

Both Gunter and Tondl examine several different configurations to evaluate the behaviour of internal damping. The case of a simple 'Jeffcott' rotor with internal viscous damping can be very easily analyzed to demonstrate the principle. Referring to Figure 2.4,

$$z = x + iy \qquad and \qquad \zeta = \xi + i\eta$$

are the complex displacements of the centre of the rotor referred to an inertial reference frame, and referred to a frame of reference rotating at the rotor speed respectively. Therefore the transformation between the two systems is:

$$z = \zeta e^{i\omega t}$$

For a simple horizontal unbalanced rotor with its centre of gravity ε from the geometric centre, we have an equation of motion referred to the inertial frame [57]:

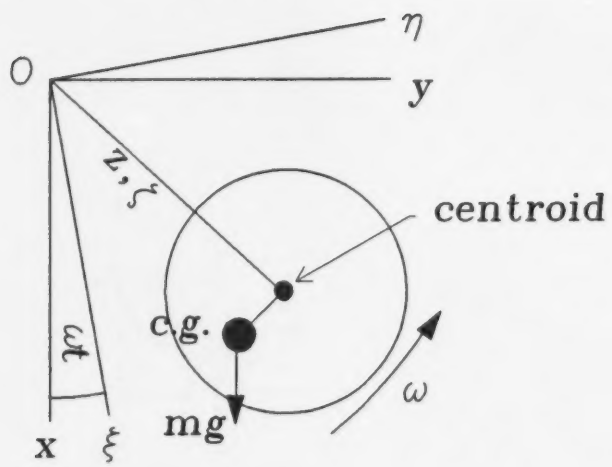

Figure 2.4: Simple Rotor with Internal Friction

$$m\ddot{z} + c\dot{z} + kz = mg + m\varepsilon\omega^2 e^{i\omega t}.$$

Transforming this to the rotating frame, and adding a term for internal damping P_v:

$$m(\ddot{\zeta} + 2i\omega\dot{\zeta} - \omega^2\zeta) + c(\dot{\zeta} + i\omega\zeta) + k\zeta - P_v = mge^{-i\omega t} + m\varepsilon\omega^2. \quad (2.32)$$

For simple viscous damping $P_v = -h\dot{\zeta}$ and we can return to the inertial frame to get:

$$\ddot{z} + D\dot{z} + \delta(\dot{z} - i\omega z) + \Omega^2 z = g + \varepsilon\omega^2 e^{i\omega t}$$

where:

$$D = c/m, \qquad \delta = h/m, \qquad \Omega^2 = k/m.$$

[2] This is a linear homogeneous ordinary differential equation, which has a solution:

$$z = Z_1 e^{i\lambda_1 t} + Z_2 e^{i\lambda_2 t} + Z_\epsilon e^{i\omega t} + Z_g.$$

The first two terms are solutions of the complementary function and the second two are a particular solution which describe the rotor response due to unbalance and the rotor weight.

$$Z_\epsilon = R_\epsilon e^{-i\phi} \qquad \text{and} \qquad Z_g = R_g e^{\psi}$$

where

$$R_\epsilon = \frac{\epsilon\omega^2}{\sqrt{[(\Omega^2 - \omega^2)^2 + D^2\omega^2]}}$$

and

$$\tan\phi = \frac{D\omega}{\Omega^2 - \omega^2}$$

also:

$$R_g = \frac{g}{\sqrt{\Omega^4 + \delta^2\omega^2}}$$

and

$$\tan\psi = \frac{\delta\omega}{\Omega^2}.$$

Therefore the particular solution demonstrates that the internal friction has the effect of deflecting the deflection due to gravity, an angle ψ and reduces the magnitude of the deflection due to gravity. The unbalance produces the response of a circular orbit of radius R_ϵ at a circular frequency ω. The $\lambda_{1,2}$ are the roots of the characteristic equation:

$$\lambda^2 - i\lambda(D + \delta) - \Omega^2 + i\delta\omega = 0 \tag{2.33}$$

i.e.

$$\lambda_{1,2} = \frac{1}{2}i(D + \delta) \pm \sqrt{[\Omega^2 - \frac{1}{4}(D + \delta)^2 - i\delta\omega]}.$$

One of these eigenvalues (the positive square root) corresponds to the forward precessing mode and the other to the backward precessing mode. The backward mode solution will disappear with time.

[2]Tondl used k for damping coefficient, c for stiffness coefficient and κ for (damping coefficient)/m. The writer has used k for stiffness coefficient, c for damping coefficient, which is the usual convention, and D for c/m

Using the Routh - Hurwitz criterion on Equation 2.33 yields the necessary and sufficient condition for stability:

$$\omega < \Omega\left(1 + \frac{D}{\delta}\right). \tag{2.34}$$

Note that Ω is the undamped natural frequency. This very simple condition illustrates well the effect of the ratio of external to internal damping on stability.

The analysis for the case of internal hysteretic damping is rather more complex. Starting with Equation 2.32, Tondl [57] uses:

$$P_v = -h\,(max|\zeta|)\,\frac{\dot{\zeta}}{|\dot{\zeta}|}\,.$$

Changing to polar coordinates ρ and ϕ in the rotating frame of reference:

$$\zeta = \rho e^{i\phi}$$

and equating real and imaginary parts, two coupled equations in ρ and ϕ are obtained:

$$\ddot{\rho} - \rho\dot{\phi}^2 - 2\rho\omega\dot{\phi} + (\Omega^2 - \omega^2)\rho + D\dot{\rho} + \frac{\delta(max|\rho|)\dot{\rho}}{\left|\sqrt{\dot{\rho}^2 + \rho^2\dot{\phi}^2}\right|} = g\cos(\omega t + \phi) \tag{2.35}$$

$$\rho\ddot{\phi} + 2\dot{\rho}\dot{\phi} + 2\omega\dot{\rho} + D(\omega + \dot{\phi}) + \frac{\delta(max|\rho|)\rho\dot{\phi}}{\left|\sqrt{\dot{\rho}^2 + \rho^2\dot{\phi}^2}\right|} = -gsin(\omega t + \phi). \tag{2.36}$$

A particular solution of Equation 2.35 and Equation 2.36 is an orbit of radius $\rho = R$ and a precessional velocity $\dot{\phi} = -\omega$. This is satisfied by $\phi = -\omega t + \phi_0$, where R and ϕ_0 are constants defined by:

$$R\Omega^2 = gcos\phi_0, \qquad \delta(R) = g\sin\phi_0.$$

This represents the static condition under the gravity and hysteretic friction loading - see Figure 2.5.

A perturbation is postulated: $\rho \rightarrow (\rho_0 + r)$ and $\phi \rightarrow \phi_0 + \psi$ where r and ψ are small. Then after some considerable manipulation and retaining only first order terms, two differential equations are derived in terms of these perturbations.

$$\ddot{r} + \left(D + \frac{\delta(R)}{R\omega}\right)\dot{r} + \Omega^2 r + \delta(R)\psi = 0, \tag{2.37}$$

and

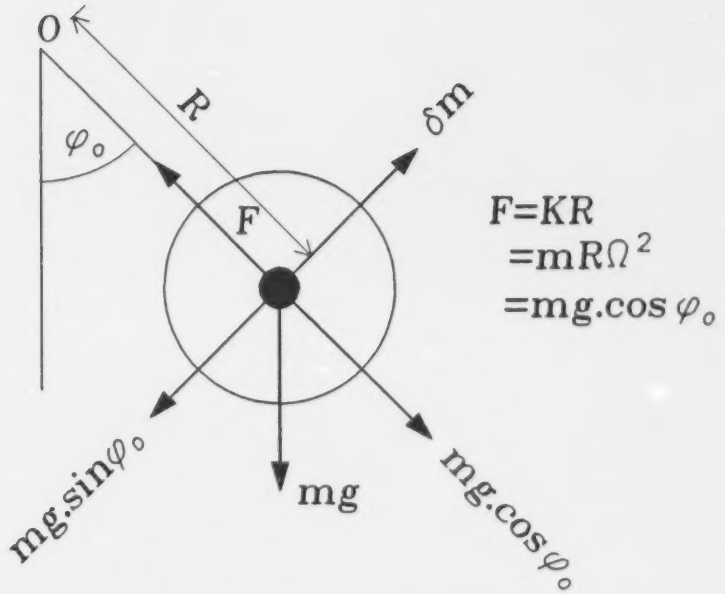

Figure 2.5: Static Deflection Under Gravity and Friction Loading

$$R\ddot{\psi} + DR\dot{\psi} + R\Omega^2\psi - \delta'(R)r = 0 \tag{2.38}$$

where δ' is $\partial\delta/\partial R$. Assuming a solution of the form $r = r_0 e^{\lambda t}$ and $\psi = \psi_0 e^{\lambda t}$ results in a characteristic equation:

$$\lambda^4 + \lambda^3\left(2D + \frac{\delta}{R\omega}\right) + \lambda^2\left[2\Omega^2 + D\left(D + \frac{\delta}{R\omega}\right)\right]$$

$$+ \lambda\left(2D + \frac{\delta}{R\omega}\right)\Omega^2 + \Omega^4 + \frac{\delta\delta'}{R} = 0. \tag{2.39}$$

Applying the Routh - Hurwitz criterion, as above results in the necessary and sufficient condition for stability at all speeds:

$$\delta\delta' < D^2 R\Omega^2 \tag{2.40}$$

which is again in the form of the ratio of internal damping to external damping.

2.8 Space Shuttle Turbo - Pumps

D.W. Childs has published numerous papers from 1969 until quite recently on the rotordynamic analyses of the liquid hydrogen and liquid oxygen fuel turbopumps of the U.S. space shuttle main engine. The history of the development of these pumps illustrates most strongly, the influence of the fluid forces on the dynamics of rotating machines and the difficulty in adequately modelling these forces.

In [58] Childs developed an elegant procedure for analyzing a rotating elastic body using body - fixed axes. The initial application for this had been spin - stabilized spacecraft. The formulation requires an inertial coordinate system $\{x, y, z\}$; a body - fixed coordinate system $\{x_0, y_0, z_0\}$ moving with the rotating undeformed body, with the origin coincident with the centre of mass of the undeformed rotating body; a set of n coordinate systems $\{x_i, y_i, z_i\}$ with origins at the centres of mass of each of the n elastically connected bodies; and finally a fourth set of n coordinate systems $\{\tilde{x}_i, \tilde{y}_i, \tilde{z}_i\}$ with origins at the elastically displaced centres of mass of the n elastically connected rigid bodies.

Thus, the position of a particle in the i'th rigid body with respect to the $\{x_i, y_i, z_i\}$ system, is determined by the elastic deformation of the $\{\tilde{x}_i, \tilde{y}_i, \tilde{z}_i\}$ system and its position within that system. The transformation from the $\{x_i, y_i, z_i\}$ system to the $\{x_0, y_0, z_0\}$ system is a simple translation for each i.

Childs sets up the equations of motion for the individual rigid bodies with respect to the inertial frame and defines the angular motion of the $\{x_0, y_0, z_0\}$ system via Newton's 2nd law applied to the whole rotor. The equations of motion of the i'th rigid body are then restated using the kinematic relationships in a form that includes the elastic deformations and their rates of change relative to an observer in the body (vehicle) - fixed coordinate system $\{x_0, y_0, z_0\}$.

The assumptions of linear theory are made that the deformations can be stated in terms of a reference undeformed configuration and that deflections are linear functions of the applied loads. This implies that the orthogonal transformation of vectors from the $\{x_0, y_0, z_0\}$ to the $\{\tilde{x}_i, \tilde{y}_i, \tilde{z}_i\}$ system, becomes the identity matrix for small values of the Euler angles, i.e. that changes in loads due to changes in geometry are negligible.

The applied loads can be expressed as the product of a stiffness matrix (banded) premultiplying a deflection vector consisting of the linear and angular deformations of the n discrete rigid bodies. This permits the elimination of internal forces in the equations of motion by substitution of the stiffness matrix coefficients and deflections in the $\{x_0, y_0, z_0\}$ system. The result is then a set of differential equations of motion in the body - fixed coordinate system:

$$[M]\left\{\hat{\ddot{x}}\right\}_0 + [C]\left\{\hat{\dot{x}}\right\}_0 + [K]\{x\}_0 = \{F\}_0 - \{P\}_0 - \{S\}_0,$$

where $\{x\}_0$ is a vector of linear and angular elastic deformations. The $\hat{}$ denotes as seen by an observer moving with the $\{x_0, y_0, z_0\}$ coordinate system. Also $\{\hat{x}\}_0 = \{x\}_0$ for small angular deflections. $\{F\}_0$ is a vector of applied forces and moments at the i'th mass, $\{P\}_0$ is a vector containing terms involving the linear acceleration of the centre of mass of the whole vehicle in the inertial frame and $\{S\}_0$ contains terms in $\Omega \times \Omega$ and Ω, where Ω is the angular velocity of the whole body, i.e. these are angular inertia terms of the body in the inertial frame. Having set up the equations of motion, modal coordinates are used and modal damping introduced via a modal damping matrix.

In [59, 60] the above method of analysis is applied to the space shuttle fuel pumps. Bearing constraints are introduced by means of spring stiffnesses at the bearing locations. Two bending modes were used in the response analysis, derived from an independent eigenvalue analysis. External damping was accounted for by direct (no cross - coupling) damping coefficients at the bearings i.e. due to damping in the roller bearings only.

In [60] it was predicted that the first 'rigid body' mode of the rotor would be unstable for a damping coefficient $\zeta = 0.02$ at speeds above 51000 RPM. This was not considered a problem as the normal maximum operating speed was 30000 RPM (this was given as 37500 RPM in later references). No fluid forces were included in this analysis. The type of stability analysis used involved examining the response of the coupled bending modes and the frequency of the whirl mode as a function of time, during a simulated run - up for a given level of hysteretic modal damping.

In [61] the model was improved considerably by including seal forces as stiffness, damping and inertia matrices, derived using the formulation of Black (above). The structural response and stability analyses carried out in [61, 62] bare a close resemblance to those used for aircraft structural vibration response due to propeller unbalance and flutter respectively. For both the response and stability analyses, a set of normal modes of the system are required. these are derived from a set of admissible functions by use of the Rayleigh - Ritz method. These admissible functions consisted of free - free elastic bending modes of the rotor, calculated separately plus 'rigid - body' modes of the rotor on its elastic bearing / support structure.

Generally in turbomachinery, the mode which becomes unstable is a forward precessing mode [63, 64], although there is some evidence that backward modes can be unstable for rotors [2]. This appears to be most likely in the case of overhung rotors. This was the case for the structural failure 'whirl flutter' cases studied for the De Havilland Dash - 7 aircraft (outside the flight envelope). In [60] backward whirl modes appear to have been ignored, which was probably alright for the hydrogen pump, but the oxygen pump has overhung impellers and it would have been safer to include these modes. Childs predicted [61] 'a serious rotordynamic instability problem' for the fuel (hydrogen) pump involving a re - excitation of the first bending forward precession mode. He also found via parametric studies that the stability was increased if support stiffness asymmetry was increased. This was also the case for the Dash - 7 analysis and it is understood from contacts with Kraftswerkunion (Federal Republic of Germany) engineers, that they have used this as a means of controlling instabilities in steam turbines. In the Dash - 7 instance it was reasoned that asymmetry decoupled lateral and vertical modes thus making the excitation of a whirl mode less likely.

The prediction of an instability problem was correct [62] resulting in hardware damage on the test stand and a research program to improve seal design [65] to control this instability. Hirs' method of deriving seal coefficients [66] was used for this work [65, 67].

A similar analysis was carried out on the oxygen pumps [61, 68]. In this case the transient response calculation predicted a potentially excessive lateral rotor displacement and consequent rub. However it showed that instability was possible but unlikely. It was reasoned that although the results predicted instability for $\zeta = 0.02$ that because the rotor is essentially solid, the ξ would be lower than this. Also the analysis predicted instability at a speed only a little higher than the frequency of the unstable mode, which was considered unlikely because classical 'whip' usually occurs when the rotation speed is above approximately twice the frequency of the unstable mode. This is of course not the case for internal friction (above).

However, the first mode did prove unstable [69]. In addition vibration became excessive at high speed, associated with excitation of the second lateral bending mode (critical speed) of the rotor system. This second mode at 32500 CPM is very close to the 30380 RPM full power level speed required for circumpolar orbital missions of the space shuttle. This was a very undesirable situation, the more so because this mode is lightly damped. The above results led to considerable research into seal optimization to control instability, including [70, 71, 72] on helically grooved seals, seals with various surface roughnesses and sawtooth seals respectively for turbulent flow.

These pumps are very high speed, of an unusual structural design and have highly unusual working fluids. However the problems they posed were essentially similar to those in their more prosaic industrial counterparts. The analyses carried out to make these machines fully operational can be extremely useful for other applications.

2.9 Discussion

The subject of rotor - dynamics is not at all new. There have been many excellent research papers on the subject from around the turn of the century and, perhaps more significantly there is a great deal of unpublished knowledge and expertise in industry. In spite of this history, there are still many operational machine problems which are never completely understood, even if they are eventually solved by trial.

The trends in turbomachinery design in recent years are to lighter, higher speed, higher load rotors. This is particularly noticeable in Canada because much of the machinery in the petrochemical industry is of recent design and manufacture. Thus, the elastic / hydrodynamic behaviour of rotors has therefore become of major importance at the design stage. There is therefore scope for considerably more study and this thesis is one contribution, intended to add a little more understanding of some aspects of instability phenomena.

Chapter 3

Rigid Rotor Analysis

The majority of rotating machinery trains in the oil and petrochemical industries, as well as the power generation industry, with the very notable exception of turbine - generator sets, consist of a motor or steam turbine driver, a gear - box and a one or two case compressor. The rotors are generally coupled by flexible couplings, of either a gear type or a diaphragm type. In a few cases, solid couplings are used.

Each of the rotors of such trains generally runs at an operating speed either below or above the first lateral natural frequency (critical speed) of that specific rotor/support structure. In a minority of cases they run above the second critical speed.

Although some lateral vibration is transmitted through flexible couplings, the dynamic behaviour of each rotor is dominated by the properties of that rotor - shaft, the fluid forces in the bearings and seals of that case and the support stiffness and damping of that machine case.

Also, in most cases, the first two lateral modes involve only a little strain energy of bending of the rotor, the motion, particularly the stability of the motion of the rotor assembly, being largely determined by the characteristics of the bearings and seals.

In this chapter, the equations of motion for a rigid rotor are set up in as general a manner as possible, in rotating coordinates and in inertial coordinates. The approach used for the rotating coordinate derivation takes considerable inspiration from Brosens [73]. The mathematical procedure used is however, rather different and permits a more complex model, which can be analyzed with modern computing methods unavailable to Brosens.

The exercise of setting up equations of motion in a rotating frame of reference is only used in this chapter to demonstrate the effects of asymmetric diametral moments of inertia and axial centre of gravity location for a system with two lateral displacement degrees of freedom and two angular displacement degrees of freedom of a rigid rotor. In Chapter 4, rotating coordinates will be employed for the more useful case of asymmetric lateral stiffness, such as would be found in a cracked rotor or a rotor of laminated construction.

In the second half of this chapter, the effect on stability of oil 'swirl' (the mean circumferential flow within the bearing or seal annulus) is examined and the results correspond to those observed in the field. The stiffness and damping matrices are set up in such a way that the off - diagonal terms are split into symmetric and skew parts. In this way, the case of circulatory coefficients due to fluid swirl can be accommodated as well as the case of the conservative symmetric matrices.

The expressions for the stiffness and damping coefficients generated by a cylindrical, fluid film bearing are then derived in such a way that they can be inserted into the general formulation.

All of the equations are set up in non - dimensional form.

3.1 Rotating Coordinate Frame

3.1.1 Rate of Change of Momentum

For a rigid body, the angular momentum is:

$$\underline{H} = \underline{J}\,\underline{\omega} \qquad \text{in tensor form}$$

Where $\underline{H}$, $\underline{J}$ and $\underline{\omega}$ are the angular momentum vector, moment of inertia tensor and angular velocity vector respectively. Expressing this equation in terms of matrix components referred to an inertial frame of reference, (Figure 3.1) we have:

$$\begin{Bmatrix} H_x \\ H_y \\ H_z \end{Bmatrix} = \begin{pmatrix} J_{xx} & -J_{xy} & -J_{xz} \\ -J_{yx} & J_{yy} & -J_{yz} \\ -J_{zx} & -J_{zy} & J_{zz} \end{pmatrix} \begin{Bmatrix} \omega_x \\ \omega_y \\ \omega_z \end{Bmatrix} \tag{3.1}$$

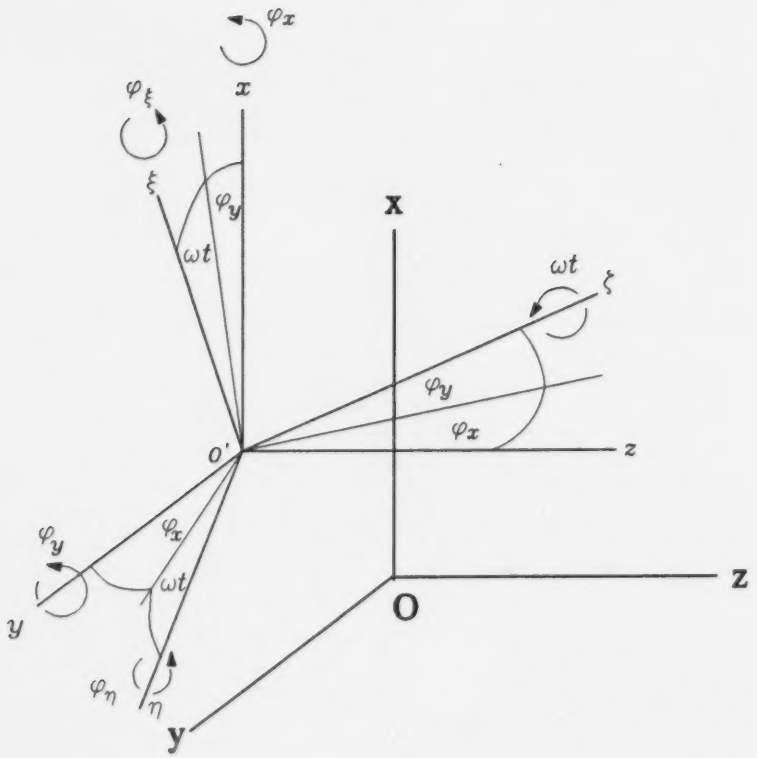

Figure 3.1: Inertial and Body - Fixed Coordinate Systems. The $Oxyz$ axes are inertial and the axes $O'\xi\eta\zeta$ are fixed in the rotating body. The angles ϕ_x, ϕ_y and ωt are the standard 'Euler' angles. $O\zeta$ is the the axis of rotation of the rotor and the C.G. is at O'.

The components of the moment of inertia matrix, which we can abbreviate to $(J)_{xyz}$, vary with angular position ωt where ω is the rotation speed of the rotor and t is time, but the components of the inertia tensor referred to a basis fixed in the rotating body, are constant. We will refer to this matrix of constant coefficients as $(J)_{\xi\eta\zeta}$ where $O_{\xi\eta\zeta}$ is the coordinate frame fixed in the spinning and deflecting body. The two matrices are related by three basis rotations:

$$(J)_{xyz} = (Q_3)^T (Q_2)^T (Q_1)^T (J)_{\xi\eta\zeta} (Q_1) (Q_2) (Q_3), \tag{3.2}$$

where:

$$(Q_1) = \begin{pmatrix} \cos\tau & \sin\tau & 0 \\ -\sin\tau & \cos\tau & 0 \\ 0 & 0 & 1 \end{pmatrix}, \tag{3.3}$$

$$(Q_2) = \begin{pmatrix} \cos\phi_y & 0 & -\sin\phi_y \\ 0 & 1 & 0 \\ \sin\phi_y & 0 & \cos\phi y \end{pmatrix},$$

$$(Q_3) = \begin{pmatrix} 1 & 0 & 0 \\ 0 & \cos\phi_x & \sin\phi_x \\ 0 & -\sin\phi_x & \cos\phi x \end{pmatrix},$$

where ϕ_x, ϕ_y and $\tau(=\omega t)$ are the three components of angular rotation with respect to the inertial frame. These are, in fact Euler angles. The components of the angular velocity vector $\underline{\omega}$ in terms of the angles ϕ_x, ϕ_y and their derivatives with respect to time, the spin velocity ω and time t can be expressed as:

$$\begin{Bmatrix} \omega_x \\ \omega_y \\ \omega_z \end{Bmatrix} = \begin{Bmatrix} \phi_{x,t} + \omega \sin\phi_y \\ \phi_{y,t} \cos\phi_x - \omega \sin\phi_x \cos\phi_y \\ \omega \cos\phi_y \cos\phi_x + \phi_{y,t} \sin\phi_x \end{Bmatrix}. \tag{3.4}$$

It is convenient to express derivatives with respect to the angle τ as 'non-dimensional time'. Therefore the 'dot' operator is defined as $\partial/\partial\tau$, then:

$$\frac{\partial}{\partial\tau} = \frac{1}{\omega}\frac{\partial}{\partial t}.$$

Then for small angular deflections ϕ_x, ϕ_y:

$$\begin{Bmatrix} \omega_x \\ \omega_y \\ \omega_z \end{Bmatrix} = \omega \begin{Bmatrix} \dot{\phi}_x + \phi_y \\ \dot{\phi}_y - \phi_x \\ 1 \end{Bmatrix}.$$

where:

$$\dot{\phi}_x = \frac{\partial \phi_x}{\partial \tau} \qquad \dot{\phi}_y = \frac{\partial \phi_y}{\partial \tau}.$$

In the following analysis, we are only interested in the lateral vibration, angular and linear, not rolling or torsional vibration. Therefore we can drop the equation for H_z. Carrying out the three basis rotations, the angular momentum vector becomes:

$$\begin{Bmatrix} H_x \\ H_y \end{Bmatrix} = \omega \begin{bmatrix} J_{11} & J_{12} & J_{13} \\ J_{21} & J_{22} & J_{23} \end{bmatrix} \begin{Bmatrix} (\dot{\phi}_x + \phi_y) \\ (\dot{\phi}_y - \phi_x) \\ 1 \end{Bmatrix} \tag{3.5}$$

where:

$$J_{11} = \tfrac{1}{2}(J_{\xi\xi} + J_{\eta\eta}) + \tfrac{1}{2}(J_{\xi\xi} - J_{\eta\eta}) \cos 2\tau + J_{\xi\eta} \sin 2\tau - 2J_{\xi\zeta}\, \phi_y \cos \tau + 2J_{\eta\zeta}\, \phi_y \sin \tau$$

$$J_{12} = \tfrac{1}{2}(J_{\xi\xi} - J_{\eta\eta}) \sin 2\tau - J_{\xi\eta} \cos 2\tau + \phi_x(J_{\xi\zeta} \cos \tau - J_{\eta\zeta} \sin \tau) - \phi_y(J_{\zeta\xi} \sin \tau + J_{\zeta\eta} \cos \tau)$$

$$J_{13} = [-\tfrac{1}{2}(J_{\xi\xi} + J_{\eta\eta}) - \tfrac{1}{2}(J_{\xi\xi} - J_{\eta\eta}) \cos 2\tau]\phi_y + \tfrac{1}{2}(J_{\xi\xi} - J_{\eta\eta})\phi_x \sin 2\tau + J_{\zeta\zeta}\phi_y - J_{\xi\eta}\phi_x \cos 2\tau - J_{\xi\eta}\phi_y \sin 2\tau - (J_{\xi\zeta} \cos \tau - J_{\eta\zeta} \sin \tau)$$

$$J_{21} = \tfrac{1}{2}(J_{\xi\xi} - J_{\eta\eta}) \sin 2\tau - \phi_y(J_{\eta\zeta} \cos \tau + J_{\xi\zeta} \sin \tau) + \phi_x(J_{\zeta\xi} \cos \tau - J_{\zeta\eta} \sin \tau) - J_{\xi\eta} \cos 2\tau$$

$$J_{22} = \tfrac{1}{2}(J_{\xi\xi} + J_{\eta\eta}) - \tfrac{1}{2}(J_{\xi\xi} - J_{\eta\eta}) \cos 2\tau + \phi_x(J_{\xi\zeta} \sin \tau + J_{\eta\zeta} \cos \tau) + \phi_x(J_{\zeta\xi} \sin \tau + J_{\zeta\eta} \cos \tau) - J_{\xi\eta} \sin 2\tau$$

$$J_{23} = -\tfrac{1}{2}(J_{\xi\xi} - J_{\eta\eta})\phi_y \sin 2\tau + \tfrac{1}{2}(J_{\xi\xi} + J_{\eta\eta})\phi_x - \tfrac{1}{2}(J_{\xi\xi} - J_{\eta\eta})\phi_x \cos 2\tau - J_{\zeta\zeta}\phi_x + J_{\xi\eta}\phi_y \cos 2\tau - J_{\xi\eta}\phi_x \sin 2\tau - (J_{\xi\zeta} \sin \tau + J_{\eta\zeta} \cos \tau).$$

Carrying out the matrix multiplication and ignoring terms which are of second order, the terms which are first order in ϕ_x and ϕ_y cancel out, except for those which multiply $J_{\zeta\zeta}$. Therefore the right hand side of Equation 3.5 can be rearranged as follows:

$$\begin{Bmatrix} H_x \\ H_y \end{Bmatrix} =$$

$$= \omega \begin{bmatrix} \left[\frac{(J_{\xi\xi}+J_{\eta\eta})}{2} + \frac{(J_{\xi\xi}-J_{\eta\eta})}{2}\cos 2\tau + J_{\xi\eta}\sin 2\tau\right] & \left[\frac{(J_{\xi\xi}-J_{\eta\eta})}{2}\sin 2\tau - J_{\xi\eta}\cos 2\tau\right] & \left[-J_{\xi\zeta}\cos\tau + J_{\eta\zeta}\sin\tau\right] \\ \left[\frac{(J_{\xi\xi}-J_{\eta\eta})}{2}\sin 2\tau - J_{\xi\eta}\cos 2\tau\right] & \left[\frac{(J_{\xi\xi}+J_{\eta\eta})}{2} - \frac{(J_{\xi\xi}-J_{\eta\eta})}{2}\cos 2\tau - J_{\xi\eta}\sin 2\tau\right] & \left[-J_{\xi\zeta}\sin\tau - J_{\eta\zeta}\cos\tau\right] \end{bmatrix} \begin{Bmatrix} \dot{\phi}_x \\ \dot{\phi}_y \\ 1 \end{Bmatrix}$$

$$+ \omega \begin{bmatrix} 0 & J_{\zeta\zeta} \\ -J_{\zeta\zeta} & 0 \end{bmatrix} \begin{Bmatrix} \phi_x \\ \phi_y \end{Bmatrix} \tag{3.6}$$

.

The first expression on the right hand side of Equation 3.6 represents the angular momentum vector in a non rotating frame and the second is a gyroscopic term brought about by the motion in a rotating frame referred to the inertial coordinate reference frame.

Differentiating with respect to τ and noting that:

$$\frac{\partial}{\partial t} = \omega \frac{\partial}{\partial \tau}$$

the rate of change of angular momentum with respect to time (indicated by $_{,t}$) is

then:

$$\left\{ \begin{array}{c} H_{x,t} \\ H_{y,t} \end{array} \right\} =$$

$$\omega^2 \left[\begin{array}{ccc} \left[\frac{(J_{\xi\xi}+J_{\eta\eta})}{2} + \frac{(J_{\xi\xi}-J_{\eta\eta})}{2}\cos 2\tau \right. & \left[\frac{(J_{\xi\xi}-J_{\eta\eta})}{2}\sin 2\tau \right. & \left[-J_{\xi\zeta}\cos\tau \right. \\ \left. +J_{\xi\eta}\sin 2\tau\right] & \left. -J_{\xi\eta}\cos 2\tau\right] & \left. +J_{\eta\zeta}\sin\tau\right] \\ \left[\frac{(J_{\xi\xi}-J_{\eta\eta})}{2}\sin 2\tau \right. & \left[\frac{(J_{\xi\xi}+J_{\eta\eta})}{2} - \frac{(J_{\xi\xi}-J_{\eta\eta})}{2}\cos 2\tau \right. & \left[-J_{\xi\zeta}\sin\tau \right. \\ \left. -J_{\xi\eta}\cos 2\tau\right] & \left. -J_{\xi\eta}\sin 2\tau\right] & \left. -J_{\eta\zeta}\cos\tau\right] \end{array} \right] \left\{ \begin{array}{c} \ddot{\phi}_x \\ \ddot{\phi}_y \\ 0 \end{array} \right\}$$

$$+ \omega^2 \left[\begin{array}{ccc} \left[-(J_{\xi\xi}-J_{\eta\eta})\sin 2\tau \right. & \left[(J_{\xi\xi}-J_{\eta\eta})\cos 2\tau \right. & \left[J_{\xi\zeta}\sin\tau \right. \\ \left. +2J_{\xi\eta}\cos 2\tau\right] & \left. +2J_{\xi\eta}\sin 2\tau\right] & \left. +J_{\eta\zeta}\cos\tau\right] \\ \left[(J_{\xi\xi}-J_{\eta\eta})\cos 2\tau \right. & \left[(J_{\xi\xi}-J_{\eta\eta})\sin 2\tau \right. & \left[-J_{\xi\zeta}\cos\tau \right. \\ \left. +2J_{\xi\eta}\sin 2\tau\right] & \left. -2J_{\xi\eta}\sin 2\tau\right] & \left. +J_{\eta\zeta}\sin\tau\right] \end{array} \right] \left\{ \begin{array}{c} \dot{\phi}_x \\ \dot{\phi}_y \\ 1 \end{array} \right\}$$

$$+ \omega^2 \left[\begin{array}{cc} 0 & J_{\zeta\zeta} \\ -J_{\zeta\zeta} & 0 \end{array} \right] \left\{ \begin{array}{c} \dot{\phi}_x \\ \dot{\phi}_y \end{array} \right\}. \qquad (3.7)$$

The first 2 by 3 matrix on the right hand side of Equation 3.7 is a function of the matrix components of $(J)_{\xi\eta\zeta}$ and the angle (non - dimensional time) τ. Therefore it is abbreviated in the following to $[J_{\xi\eta\zeta\tau}]$. The skew 2 by 2 matrix is abbreviated to $[J_{\zeta\zeta}]$. Similarly, the column vectors of Equation 3.7 are abbreviated to $\{H_{xyz}\}_{,t}$, $\{\ddot{\phi}_{xyz}\}$ and $\{\dot{\phi}_{xyz}\}$ then:

$$\{H_{xyz}\}_{,t} = \omega^2 [J_{\xi\eta\zeta\tau}]\{\ddot{\phi}_{xyz}\} + \omega^2 \left[\dot{J}_{\xi\eta\zeta\tau}\right]\left\{\dot{\phi}_{xyz}\right\} + \omega^2 [J_{\zeta\zeta}]\left\{\dot{\phi}_{xyz}\right\}. \qquad (3.8)$$

We now have the rate of change of angular momentum in terms of components referred to an inertial frame; angular displacement, velocity and acceleration vectors also referred to an inertial frame and coefficient matrices whose components are cyclic in τ. To change the R.H.S. vectors to a rotating reference frame we have:

$$\left\{ \begin{array}{c} \phi_x \\ \phi_y \end{array} \right\} = \left[\begin{array}{ccc} \cos\tau & -\sin\tau & 0 \\ \sin\tau & \cos\tau & 0 \end{array} \right] \left\{ \begin{array}{c} \phi_\xi \\ \phi_\eta \end{array} \right\}. \qquad (3.9)$$

Denoting the rotation matrix as $[Q]$ and differentiating with respect to τ we have:

$$\{\dot{\phi}_{xyz}\} = [\dot{Q}]\{\phi_{\xi\eta\zeta}\} + [Q]\{\dot{\phi}_{\xi\eta\zeta}\} \tag{3.10}$$

$$\{\ddot{\phi}_{xyz}\} = [\ddot{Q}]\{\phi_{\xi\eta\zeta}\} + 2[\dot{Q}]\{\dot{\phi}_{\xi\eta\zeta}\} + [Q]\{\ddot{\phi}_{\xi\eta\zeta}\} \tag{3.11}$$

. Substituting for the angular inertial acceleration, velocity and displacement vectors in Equation 3.8 we have:

$$\{H_{xyz}\}_{,t} = \omega^2 [J_{\xi\eta\zeta\tau}] \left\{ \left[\ddot{Q}\right] \{\phi_{\xi\eta\zeta}\} + 2\left[\dot{Q}\right] \left\{\dot{\phi}_{\xi\eta\zeta}\right\} + [Q] \left\{\ddot{\phi}_{\xi\eta\zeta}\right\} \right\}$$

$$+ \omega^2 \left[\dot{J}_{\xi\eta\zeta\tau}\right] \left[\left[\dot{Q}\right] \{\phi_{\xi\eta\zeta}\} + [Q] \left\{\dot{\phi}_{\xi\eta\zeta}\right\} \right]$$

$$+ \omega^2 [J_{\zeta\zeta}] \left[\left[\dot{Q}\right] \{\phi_{\xi\eta\zeta}\} + [Q] \left\{\dot{\phi}_{\xi\eta\zeta}\right\} \right] .$$

The coefficient matrices can be conveniently non-dimensionalized using the same procedure as Stammers [74] and Brosens (Stammers notation has been retained). For the inertia asymmetry term,

$$\delta = \frac{J_{\xi\xi} - J_{\eta\eta}}{J_{\xi\xi} + J_{\eta\eta}},$$

and for the gyroscopic term,

$$\lambda = \frac{2J_{\zeta\zeta}}{J_{\xi\xi} + J_{\eta\eta}}.$$

The cross - product of inertia terms are respectively:

$$\gamma = \frac{2J_{\xi\eta}}{J_{\xi\xi} + J_{\eta\eta}} \qquad \sigma_1 = \frac{2J_{\xi\zeta}}{J_{\xi\xi} + J_{\eta\eta}} \qquad \sigma_2 = \frac{2J_{\eta\zeta}}{J_{\xi\xi} + J_{\eta\eta}}.$$

Then the Equation 3.7 can be written:

$$\left\{ \begin{array}{c} H_{x,t} \\ H_{y,t} \end{array} \right\} =$$

$$\frac{\omega^2 (J_{\xi\xi} + J_{\eta\eta})}{2} \left[\left[\begin{array}{cc} [(1+\delta)\cos\tau + \gamma\sin\tau] & [-(1-\delta)\sin\tau - \gamma\cos\tau] \\ [(1+\delta)\sin\tau - \gamma\cos\tau] & [(1-\delta)\cos\tau - \gamma\sin\tau] \end{array} \right] \left\{ \begin{array}{c} \ddot{\phi}_\xi \\ \ddot{\phi}_\eta \end{array} \right\} +$$

$$\left[\begin{array}{ccc} -2\sin\tau & -2\cos\tau & (\sigma_1\sin\tau + \sigma_2\cos\tau) \\ 2\cos\tau & -2\sin\tau & (-\sigma_1\cos\tau + \sigma_2\sin\tau) \end{array} \right] \left\{ \begin{array}{c} \dot{\phi}_\xi \\ \dot{\phi}_\eta \\ 1 \end{array} \right\} +$$

$$\left[\begin{array}{cc} \lambda\sin\tau & \lambda\cos\tau \\ -\lambda\cos\tau & \lambda\sin\tau \end{array} \right] \left\{ \begin{array}{c} \dot{\phi}_\xi \\ \dot{\phi}_\eta \end{array} \right\} +$$

$$\left[\begin{array}{cc} [(\delta-1)\cos\tau + \gamma\sin\tau] & (1+\delta)\sin\tau - \gamma\cos\tau] \\ [(\delta-1)\sin\tau - \gamma\cos\tau] & [-(1+\delta)\cos\tau - \gamma\sin\tau] \end{array} \right] \left\{ \begin{array}{c} \phi_\xi \\ \phi_\eta \end{array} \right\} +$$

$$\left[\begin{array}{cc} \lambda\cos\tau & -\lambda\sin\tau \\ \lambda\sin\tau & \lambda\cos\tau \end{array} \right] \left\{ \begin{array}{c} \phi_\xi \\ \phi_\eta \end{array} \right\} \Bigg]. \qquad (3.12)$$

To refer the L.H.S. to the rotating coordinate system we have:

$$\left\{ \begin{array}{c} H_\xi \\ H_\eta \end{array} \right\}_{,t} = \left[\begin{array}{cc} \cos\tau & \sin\tau \\ -\sin\tau & \cos\tau \end{array} \right] \left\{ \begin{array}{c} H_x \\ H_y \end{array} \right\}_{,t} = [Q]^T \{H_{xyz}\}_{,t} \,. \qquad (3.13)$$

Therefore, pre - multiplying Equation 3.12 by $[Q]^T$, the rate of change of angular momentum with respect to time, in rotating coordinates becomes:

$$\left\{ \begin{array}{c} H_{\xi,t} \\ H_{\eta,t} \end{array} \right\} = \omega^2 \frac{(J_{\xi\xi} + J_{\eta\eta})}{2} \left[\left[\begin{array}{cc} (1+\delta) & -\gamma \\ -\gamma & (1-\delta) \end{array} \right] \left\{ \begin{array}{c} \ddot{\phi}_\xi \\ \ddot{\phi}_\eta \end{array} \right\} \right.$$

$$+ \left[\begin{array}{cc} 0 & (-2+\lambda) \\ (2-\lambda) & 0 \end{array} \right] \left\{ \begin{array}{c} \dot{\phi}_\xi \\ \dot{\phi}_\eta \end{array} \right\}$$

$$\left. + \left[\begin{array}{cc} (\delta - 1 + \lambda) & -\gamma \\ -\gamma & (-\delta - 1 + \lambda) \end{array} \right] \left\{ \begin{array}{c} \phi_\xi \\ \phi_\eta \end{array} \right\} + \left\{ \begin{array}{c} \sigma_2 \\ -\sigma_1 \end{array} \right\} \right]. \qquad (3.14)$$

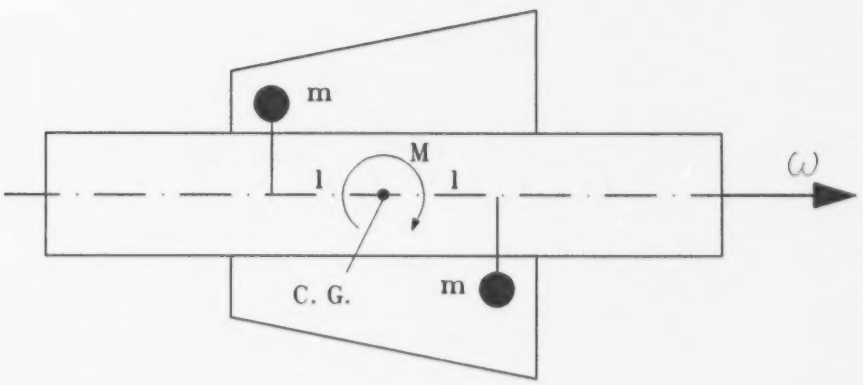

Figure 3.2: Dynamic Imbalance. The two equal concentrated masses equidistant, both axially and radially from the C.G. will produce a rotating moment in the plane of the rotor when rotating but be balanced when stationary, i.e. about a diameter.

The γ cross-product is generally small compared with σ_1 or σ_2 for most practical rotors. The latter represent the 'dynamic' imbalance of the rotor. It is referred to as dynamic imbalance because it is possible to have a non zero $J_{\xi\zeta}$ and/or $J_{\eta\zeta}$ but have the centre of gravity at the geometric centroid. Then the rotor would be balanced when stationary but would experience a couple when rotating. Such imbalance would tend to excite the second or 'conical' mode of a rotor but not the first or 'cylindrical' mode. Figure 3.2 shows a simple case.

Similarly, for linear momentum with no inertial coupling between angular and linear motion (the coordinates chosen to be at the centre of gravity of the body:

$$\left\{ \begin{array}{c} L_{\xi,t} \\ L_{\eta,t} \end{array} \right\} = \omega^2 m \left[\left[\begin{array}{cc} 1 & 0 \\ 0 & 1 \end{array} \right] \left\{ \begin{array}{c} \ddot{\xi} \\ \ddot{\eta} \end{array} \right\} + \left[\begin{array}{cc} 0 & -2 \\ 2 & 0 \end{array} \right] \left\{ \begin{array}{c} \dot{\xi} \\ \dot{\eta} \end{array} \right\} + \left[\begin{array}{cc} -1 & 0 \\ 0 & -1 \end{array} \right] \left\{ \begin{array}{c} \xi \\ \eta \end{array} \right\} - \left\{ \begin{array}{c} \bar{\xi} \\ \bar{\eta} \end{array} \right\} \right] \tag{3.15}$$

The last vector represents the 'static' imbalance of the rotor, i.e. the coordinates of the centre of gravity in the ξ, η plane through the C.G.

3.1.2 Stiffness and Damping Forces / Moments

The rate of change of linear and angular momentum vector, in a rotating frame, for a rigid non - symmetrical rotor can be set equal to the restoring moment due to damping and stiffness forces for bearings with cross - coupling terms (cross - coupling terms within the bearing coefficient matrices, coupling between angular and linear motion because the centre of gravity is not, in general mid way between the bearings). The forces and moments applied to/about the rotor c.g. due to the effective stiffness of the bearing and support structure can be expressed in an inertial frame of reference as:

$$\left\{ \begin{array}{c} F_x \\ F_y \\ M_x \\ M_y \end{array} \right\} = - \left[\begin{array}{cccc} k_{xx} & k_{xy} & k_{x\phi_x} & k_{x\phi_y} \\ k_{yx} & k_{yy} & k_{y\phi_x} & k_{y\phi_y} \\ k_{\phi_x x} & k_{\phi_x y} & k_{\phi_x \phi_x} & k_{\phi_x \phi_y} \\ k_{\phi_y x} & k_{\phi_y y} & k_{\phi_y \phi_x} & k_{\phi_y \phi_y} \end{array} \right] \left\{ \begin{array}{c} x \\ y \\ \phi_x \\ \phi_y \end{array} \right\}$$

To determine the influence coefficients in terms of the individual bearing stiffness coefficients (the two bearings assumed identical), and the axial position of the rotor c.g., we consider a pure unit displacement of each coordinate in turn. This normal procedure is complicated by the inclusion of cross - coupling terms at each bearing, which may not be symmetric ($k^b_{xy} \neq k^b_{yx}$).Consider a unit deflection in the x direction as shown in Figure 3.3.

The applied forces and moments at/about the c.g. to maintain this configuration are the stiffness coefficients:

$$\begin{aligned} k_{xx} &= 2k^b_{xx} \\ k_{yx} &= 2k^b_{yx} \\ k_{\phi_x x} &= k^b_{yx}(l_1 - l_2) \\ k_{\phi_y x} &= -k^b_{xx}(l_1 - l_2) \end{aligned}$$

Similarly for a unit y deflection as shown in Figure 3.4 we have the stiffness coefficients:

$$\begin{aligned} k_{yy} &= 2k^b_{yy} \\ k_{xy} &= 2k^b_{xy} \\ k_{\phi_x y} &= k^b_{yy}(l_1 - l_2) \\ k_{\phi_y y} &= -k^b_{xy}(l_1 - l_2) \end{aligned}$$

For a unit ϕ_x angular deflection (Figure 3.5):

$$\begin{aligned} k_{\phi_x \phi_x} &= k^b_{yy}(l_1^2 + l_2^2) \\ k_{x\phi_x} &= k^b_{xy}(l_1 - l_2) \\ k_{y\phi_x} &= k^b_{yy}(l_1 - l_2) \\ k_{\phi_y \phi_x} &= -k^b_{xy}(l_1^2 + l_2^2) \end{aligned}$$

And for a unit ϕ_y angular deflection (Figure 3.6):

$$\begin{aligned} k_{\phi_y \phi_y} &= k^b_{xx}(l_1^2 + l_2^2) \\ k_{x\phi_y} &= -k^b_{xx}(l_1 - l_2) \\ k_{y\phi_y} &= -k^b_{yx}(l_1 - l_2) \\ k_{\phi_x \phi_y} &= -k^b_{yx}(l_1^2 + l_2^2) \end{aligned}$$

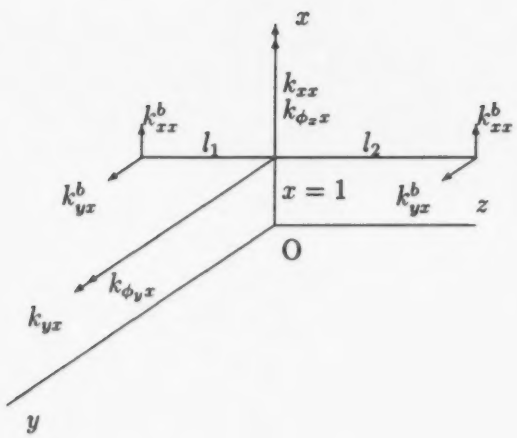

Figure 3.3: Stiffness Coefficients due to Unit x Deflection

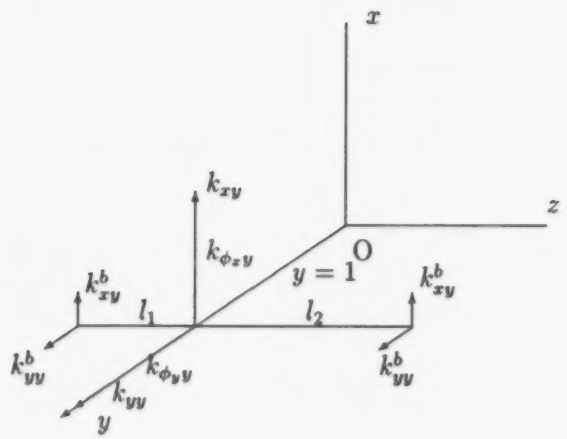

Figure 3.4: Stiffness Coefficients due to Unit y Deflection

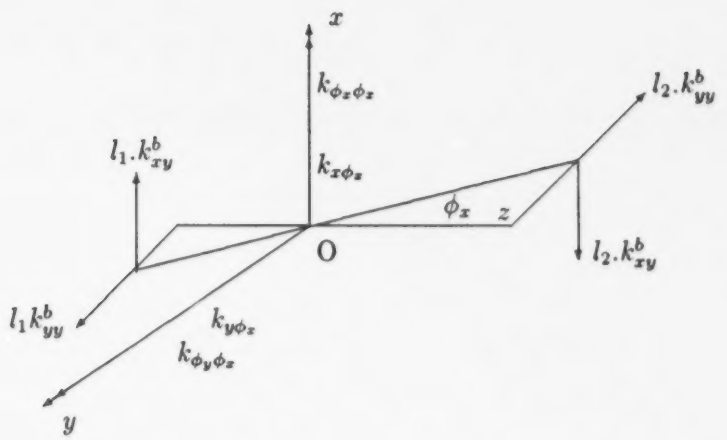

Figure 3.5: Stiffness Coefficients due to Unit ϕ_x Deflection

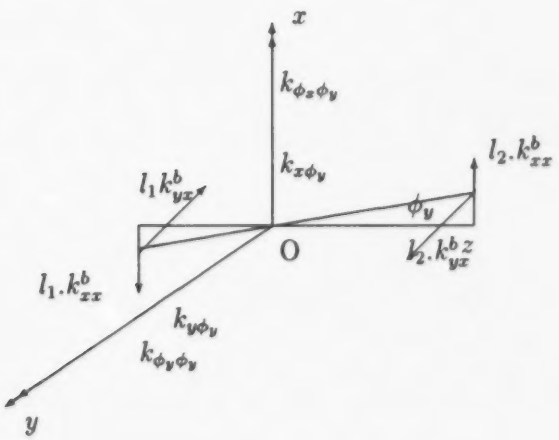

Figure 3.6: Stiffness Coefficients due to Unit ϕ_y Deflection

Letting $(l_1 + l_2) = 2l$, $l_1 = (l - s)$ and $l_2 = (l + s)$ the stiffness matrix can then be written:

$$2\begin{bmatrix} k^b_{xx} & k^b_{xy} & -k^b_{xy}.s & k^b_{xx}.s \\ k^b_{yx} & k^b_{yy} & -k^b_{yy}.s & k^b_{yx}.s \\ -k^b_{yx}.s & -k^b_{yy}.s & k^b_{yy}(l^2+s^2) & -k^b_{yx}(l^2+s^2) \\ k^b_{xx}.s & k^b_{xy}.s & -k^b_{xy}(l^2+s^2) & k^b xx(l^2+s^2) \end{bmatrix}.$$

The 'stiffness' force can then be expressed in terms of a stiffness matrix containing non - dimensional stiffnesses and the lengths s and l:

$$\begin{Bmatrix} F_x \\ F_y \\ M_x \\ M_y \end{Bmatrix}^k = -\begin{bmatrix} m\omega_c^2 & 0 & 0 & 0 \\ 0 & m\omega_c^2 & 0 & 0 \\ 0 & 0 & \frac{(J_{\xi\xi}+J_{\eta\eta})}{2}\omega_0^2\left(1+\left(\frac{s}{l}\right)^2\right) & 0 \\ 0 & 0 & 0 & \frac{(J_{\xi\xi}+J_{\eta\eta})}{2}\omega_0^2\left(1+\left(\frac{s}{l}\right)^2\right) \end{bmatrix}$$

$$\times \begin{bmatrix} (1-\epsilon) & (-\alpha+\beta) & (\alpha-\beta)s & (1-\epsilon)s \\ (-\alpha-\beta) & (1+\epsilon) & (-1-\epsilon)s & (-\alpha-\beta)s \\ \frac{(\alpha+\beta)s}{(l^2+s^2)} & \frac{(-1-\epsilon)s}{(l^2+s^2)} & (1+\epsilon) & (\alpha+\beta) \\ \frac{(1-\epsilon)s}{(l^2+s^2)} & \frac{(-\alpha+\beta)s}{(l^2+s^2)} & (\alpha-\beta) & (1-\epsilon) \end{bmatrix} \begin{Bmatrix} x \\ y \\ \phi_x \\ \phi_y \end{Bmatrix}, \qquad (3.16)$$

where non - dimensionalized stiffness coefficients are defined as:

$$\epsilon = \frac{k_{\phi_x\phi_x} - k_{\phi_y\phi_y}}{k_{\phi_x\phi_x} + k_{\phi_y\phi_y}} \qquad \alpha = \frac{k_{\phi_x\phi_y} + k_{\phi_y\phi_x}}{k_{\phi_x\phi_x} + k_{\phi_y\phi_y}} \qquad \beta = \frac{k_{\phi_x\phi_y} - k_{\phi_y\phi_x}}{k_{\phi_x\phi_x} + k_{\phi_y\phi_y}}.$$

Characteristic linear and angular frequencies are defined as:

$$\omega_c^2 = \frac{k_{xx} + k_{yy}}{2m} = \frac{k^b_{xx} + k^b_{yy}}{m} \qquad \omega_0^2 = \frac{k_{\phi_x\phi_x} + k_{\phi_y\phi_y}}{J_{\xi\xi} + J_{\eta\eta}}(\text{sym}) = \frac{2(k^b_{xx} + k^b_{yy})l^2}{J_{\xi\xi} + J_{\eta\eta}},$$

i.e. the characteristic frequencies, used for non - dimensionalizing the equations, are those linear and angular natural frequencies which a rigid body would have, if its C.G. were mid - way between the bearings, and the bearings had only direct stiffness coefficients both equal to the mean of the actual direct stiffness coefficients.

The damping forces / moments on the rotor can be expressed in a similar manner, ignoring the damping cross-coupling terms:

$$\begin{Bmatrix} F_x \\ F_y \\ M_x \\ M_y \end{Bmatrix}^c =$$

$$-\begin{bmatrix} 2m\zeta_c\omega_c & 0 & 0 & 0 \\ 0 & 2m\zeta_c\omega_c & 0 & 0 \\ 0 & 0 & (J_{\xi\xi}+J_{\eta\eta})\zeta_0\omega_0\left(1+\left(\frac{s}{l}\right)^2\right) & 0 \\ 0 & 0 & 0 & (J_{\xi\xi}+J_{\eta\eta})\zeta_0\omega_0\left(1+\left(\frac{s}{l}\right)^2\right) \end{bmatrix}$$

$$\times \begin{bmatrix} (1-\nu) & 0 & 0 & (1-\nu)s \\ 0 & (1+\nu) & (-1-\nu)s & 0 \\ 0 & \frac{(-1-\nu)s}{(l^2+s^2)} & (1+\nu) & 0 \\ \frac{(1-\nu)s}{(l^2+s^2)} & 0 & 0 & (1-\nu) \end{bmatrix} \begin{Bmatrix} \dot{x} \\ \dot{y} \\ \dot{\phi}_x \\ \dot{\phi}_y \end{Bmatrix}, \tag{3.17}$$

where the damping asymmetry term (ignoring c_{xy}, c_{yx} terms) is defined as:

$$\nu = \frac{c_{\phi_x\phi_x} - c_{\phi_y\phi_y}}{c_{\phi_x\phi_x} + c_{\phi_y\phi_y}}$$

and characteristic damping factors are defined by the relationships:

$$2\zeta_c\omega_c = \frac{c_{xx}+c_{yy}}{2m} = \frac{c^b_{xx}+c^b_{yy}}{m} \qquad 2\zeta_0\omega_o = \frac{c_{\phi_x\phi_x}+c_{\phi_y\phi_y}}{J_{\xi\xi}+J_{\eta\eta}} = 2\frac{(c^b_{xx}+c^b_{yy})l^2}{J_{\xi\xi}+J_{\eta\eta}}.$$

Now to change to a rotating frame of reference we have for small deflections:

$$\begin{Bmatrix} x \\ y \\ \phi_x \\ \phi_y \end{Bmatrix} = \begin{bmatrix} \cos\tau & -\sin\tau & 0 & 0 \\ \sin\tau & \cos\tau & 0 & 0 \\ 0 & 0 & \cos\tau & -\sin\tau \\ 0 & 0 & \sin\tau & \cos\tau \end{bmatrix} \begin{Bmatrix} \xi \\ \eta \\ \phi_\xi \\ \phi_\eta \end{Bmatrix} \tag{3.18}$$

and:

$$\begin{Bmatrix} F_\xi \\ F_\eta \\ M_{\phi_\xi} \\ M_{\phi_\eta} \end{Bmatrix} = \begin{bmatrix} \cos\tau & \sin\tau & 0 & 0 \\ -\sin\tau & \cos\tau & 0 & 0 \\ 0 & 0 & \cos\tau & \sin\tau \\ 0 & 0 & -\sin\tau & \cos\tau \end{bmatrix} \begin{Bmatrix} F_x \\ F_y \\ M_{\phi_x} \\ M_{\phi_y} \end{Bmatrix}. \tag{3.19}$$

Therefore, changing the stiffness and damping forces to a rotating frame of reference, in a manner similar to the momentum vector, we can express the four equations of motion as:

$$\begin{Bmatrix} L_{\xi,t} \\ L_{\eta,t} \\ H_{\xi,t} \\ H_{\eta,t} \end{Bmatrix} = \omega^2 \begin{bmatrix} m & 0 & 0 & 0 \\ 0 & m & 0 & 0 \\ 0 & 0 & \left(\frac{J_{\xi\xi}+J_{\eta\eta}}{2}\right) & 0 \\ 0 & 0 & 0 & \left(\frac{J_{\xi\xi}+J_{\eta\eta}}{2}\right) \end{bmatrix} \left[\begin{bmatrix} 1 & 0 & 0 & 0 \\ 0 & 1 & 0 & 0 \\ 0 & 0 & (1+\delta) & -\gamma \\ 0 & 0 & -\gamma & (1-\delta) \end{bmatrix} \begin{Bmatrix} \ddot{\xi} \\ \ddot{\eta} \\ \ddot{\phi}_\xi \\ \ddot{\phi}_\eta \end{Bmatrix} \right.$$

$$+ \begin{bmatrix} 0 & -2 & 0 & 0 \\ 2 & 0 & 0 & 0 \\ 0 & 0 & 0 & (-2+\lambda) \\ 0 & 0 & (2-\lambda) & 0 \end{bmatrix} \begin{Bmatrix} \dot{\xi} \\ \dot{\eta} \\ \dot{\phi}_\xi \\ \dot{\phi}_\eta \end{Bmatrix}$$

$$\left. + \begin{bmatrix} -1 & 0 & 0 & 0 \\ 0 & -1 & 0 & 0 \\ 0 & 0 & (\delta-1+\lambda) & -\gamma \\ 0 & 0 & -\gamma & (-\delta-1+\lambda) \end{bmatrix} \begin{Bmatrix} \xi \\ \eta \\ \phi_\xi \\ \phi_\eta \end{Bmatrix} - \begin{Bmatrix} \bar{\xi} \\ \bar{\eta} \\ -\sigma_2 \\ \sigma_1 \end{Bmatrix} \right] =$$

$$= -\omega \begin{bmatrix} m & 0 & 0 & 0 \\ 0 & m & 0 & 0 \\ 0 & 0 & \left(\frac{J_{\xi\xi}+J_{\eta\eta}}{2}\right) & 0 \\ 0 & 0 & 0 & \left(\frac{J_{\xi\xi}+J_{\eta\eta}}{2}\right) \end{bmatrix} \begin{bmatrix} 2\zeta_c\omega_c & & & \\ & 2\zeta_c\omega_c & & \\ & & 2\zeta_0\omega_0 & \\ & & & 2\zeta_0\omega_0 \end{bmatrix}$$

$$\times \left[\begin{bmatrix} & \nu_1 & \\ & (\tau) & \end{bmatrix} \begin{Bmatrix} \xi \\ \eta \\ \phi_\xi \\ \phi_\eta \end{Bmatrix} + \begin{bmatrix} & \nu_2 & \\ & (\tau) & \end{bmatrix} \begin{Bmatrix} \dot{\xi} \\ \dot{\eta} \\ \dot{\phi}_\xi \\ \dot{\phi}_\eta \end{Bmatrix} \right]$$

$$- \begin{bmatrix} m & 0 & 0 & 0 \\ 0 & m & 0 & 0 \\ 0 & 0 & \left(\frac{J_{\xi\xi}+J_{\eta\eta}}{2}\right) & 0 \\ 0 & 0 & 0 & \left(\frac{J_{\xi\xi}+J_{\eta\eta}}{2}\right) \end{bmatrix} \begin{bmatrix} \omega_c^2 & 0 & 0 & 0 \\ 0 & \omega_c^2 & 0 & 0 \\ 0 & 0 & \omega_0^2 & 0 \\ 0 & 0 & 0 & \omega_0^2 \end{bmatrix} \begin{bmatrix} & \epsilon & \\ & (k_{ij},\tau) & \end{bmatrix} \begin{Bmatrix} \xi \\ \eta \\ \phi_\xi \\ \phi_\eta \end{Bmatrix}. \tag{3.20}$$

Then, pre - multiplying by the inverse of the mass /inertia matrix, dividing through by ω^2, and non - dimensionalizing the linear deflections, the equations of motion can be written:

$$\begin{bmatrix} 1 & 0 & 0 & 0 \\ 0 & 1 & 0 & 0 \\ 0 & 0 & (1+\delta) & -\gamma \\ 0 & 0 & -\gamma & (1-\delta) \end{bmatrix} \begin{Bmatrix} \ddot{\xi}/l \\ \ddot{\eta}/l \\ \ddot{\phi}_\xi \\ \ddot{\phi}_\eta \end{Bmatrix} + \begin{bmatrix} 0 & -2 & 0 & 0 \\ 2 & 0 & 0 & 0 \\ 0 & 0 & 0 & (-2+\lambda) \\ 0 & 0 & (2-\lambda) & 0 \end{bmatrix} \begin{Bmatrix} \dot{\xi}/l \\ \dot{\eta}/l \\ \dot{\phi}_\xi \\ \dot{\phi}_\eta \end{Bmatrix}$$

$$+ \begin{bmatrix} -1 & 0 & 0 & 0 \\ 0 & -1 & 0 & 0 \\ 0 & 0 & (\delta-1+\lambda) & -\gamma \\ 0 & 0 & -\gamma & (-\delta-1+\lambda) \end{bmatrix} \begin{Bmatrix} \xi/l \\ \eta/l \\ \phi_\xi \\ \phi_\eta \end{Bmatrix} + \begin{bmatrix} 2\zeta_c\frac{\omega_c}{\omega} & & & \\ & 2\zeta_c\frac{\omega_c}{\omega} & & \\ & & 2\zeta_0\frac{\omega_0}{\omega} & \\ & & & 2\zeta_0\frac{\omega_0}{\omega} \end{bmatrix}$$

$$\times \left[\begin{bmatrix} & \nu_1 & \\ & (\nu, s/l, \tau) & \end{bmatrix} \begin{Bmatrix} \xi/l \\ \eta/l \\ \phi_\xi \\ \phi_\eta \end{Bmatrix} + \begin{bmatrix} & \nu_2 & \\ & (\nu, s/l, \tau) & \end{bmatrix} \begin{Bmatrix} \dot{\xi}/l \\ \dot{\eta}/l \\ \dot{\phi}_\xi \\ \dot{\phi}_\eta \end{Bmatrix} \right]$$

$$+ \begin{bmatrix} \omega_c^2/\omega^2 & 0 & 0 & 0 \\ 0 & \omega_c^2/\omega^2 & 0 & 0 \\ 0 & 0 & \omega_0^2/\omega^2 & \\ 0 & 0 & 0 & \omega_0^2/\omega^2 \end{bmatrix} \begin{bmatrix} & \epsilon \quad (k_{ij}, s/l, \tau) & \end{bmatrix} \begin{Bmatrix} \xi/l \\ \eta/l \\ \phi_\xi \\ \phi_\eta \end{Bmatrix}$$

$$= \begin{Bmatrix} \bar{\xi}/l \\ \bar{\eta}/l \\ -\sigma_2 \\ \sigma_1 \end{Bmatrix}, \tag{3.21}$$

where the elements of the above matrices are:

$$\begin{aligned}
\epsilon_{1,1} &= (1 - \epsilon\cos 2\tau - \alpha\sin 2\tau) \\
\epsilon_{1,2} &= (\epsilon\sin 2\tau - \alpha\cos 2\tau + \beta) \\
\epsilon_{1,3} &= (-\epsilon\sin 2\tau + \alpha\cos 2\tau - \beta)s/l \\
\epsilon_{1,4} &= (1 - \epsilon\cos 2\tau - \alpha\sin 2\tau)s/l \\
\\
\epsilon_{2,1} &= (\epsilon sin2\tau - \alpha\cos 2\tau - \beta) \\
\epsilon_{2,2} &= (1 + \epsilon\cos 2\tau + \alpha\sin 2\tau) \\
\epsilon_{2,3} &= (-1 - \epsilon\cos 2\tau - \alpha\sin 2\tau)s/l \\
\epsilon_{2,4} &= (\epsilon\sin 2\tau - \alpha\cos 2\tau - \beta)s/l \\
\\
\epsilon_{3,1} &= (-\epsilon\sin 2\tau + \alpha\cos 2\tau + \beta)s/l \\
\epsilon_{3,2} &= (-1 - \epsilon\cos 2\tau - \alpha\sin 2\tau)s/l \\
\epsilon_{3,3} &= (1 + \epsilon\cos 2\tau + \alpha\sin 2\tau)(1 + (s/l)^2) \\
\epsilon_{3,4} &= (-\epsilon\sin 2\tau + \alpha\cos 2\tau + \beta)(1 + (s/l)^2)
\end{aligned}$$

$$
\begin{aligned}
\epsilon_{4,1} &= (1 - \epsilon\cos 2\tau - \alpha \sin 2\tau)s/l \\
\epsilon_{4,2} &= (\epsilon \sin 2\tau - \alpha\cos 2\tau + \beta)s/l \\
\epsilon_{4,3} &= (-\epsilon \sin 2\tau + \alpha\cos 2\tau - \beta)(1 + (s/l)^2) \\
\epsilon_{4,4} &= (1 - \epsilon\cos 2\tau - \alpha \sin 2\tau)(1 + (s/l)^2) \\
\nu 1_{1,1} &= (\nu \sin 2\tau) \\
\nu 1_{1,2} &= (-1 + \nu\cos 2\tau) \\
\nu 1_{1,3} &= (1 - \nu\cos 2\tau)s/l \\
\nu 1_{1,4} &= (\nu\, s/l \sin 2\tau)
\end{aligned}
$$

$$
\begin{aligned}
\nu 1_{2,1} &= (1 + \nu\cos 2\tau) \\
\nu 1_{2,2} &= (-\nu \sin 2\tau) \\
\nu 1_{2,3} &= (\nu\, s/l \sin 2\tau) \\
\nu 1_{2,4} &= (1 + \nu\cos 2\tau)s/l
\end{aligned}
$$

$$
\begin{aligned}
\nu 1_{3,1} &= (-1 - \nu\cos 2\tau)s/l \\
\nu 1_{3,2} &= \nu\, s/l \sin 2\tau \\
\nu 1_{3,3} &= (-\nu \sin 2\tau)(1 + (s/l)^2) \\
\nu 1_{3,4} &= (-1 - \nu\cos 2\tau)(1 + (s/l)^2)
\end{aligned}
$$

$$
\begin{aligned}
\nu 1_{4,1} &= \nu\, s/l \sin 2\tau \\
\nu 1_{4,2} &= (-1 + \nu\cos 2\tau)s/l \\
\nu 1_{4,3} &= (1 - \nu\cos 2\tau)(1 + (s/l)^2) \\
\nu 1_{4,4} &= (\nu \sin 2\tau)(1 + (s/l)^2)
\end{aligned}
$$

$$
\begin{aligned}
\nu 2_{1,1} &= (1 - \nu\cos 2\tau) \\
\nu 2_{1,2} &= (\nu \sin 2\tau) \\
\nu 2_{1,3} &= (-\nu \sin 2\tau)s/l \\
\nu 2_{1,4} &= (1 - \nu\cos 2\tau)s/l
\end{aligned}
$$

$$
\begin{aligned}
\nu 2_{2,1} &= (\nu \sin 2\tau) \\
\nu 2_{2,2} &= (1 + \nu\cos 2\tau) \\
\nu 2_{2,3} &= (-1 - \nu\cos 2\tau)s/l \\
\nu 2_{2,4} &= (\nu\, s/l \sin 2\tau)
\end{aligned}
$$

$$
\begin{aligned}
\nu 2_{3,1} &= (-\nu\, s/l \sin 2\tau) \\
\nu 2_{3,2} &= (-1 - \nu\cos 2\tau)s/l \\
\nu 2_{3,3} &= (1 + \nu\cos 2\tau)(1 + (s/l)^2) \\
\nu 2_{3,4} &= (-\nu \sin 2\tau)(1 + (s/l)^2)
\end{aligned}
$$

$$
\begin{aligned}
\nu 2_{4,1} &= (1 - \nu \cos 2\tau) s/l \\
\nu 2_{4,2} &= (\nu\, s/l \sin 2\tau) \\
\nu 2_{4,3} &= (-\nu \sin 2\tau)(1 + (s/l)^2) \\
\nu 2_{4,4} &= (1 - \nu \cos 2\tau)(1 + (s/l)^2).
\end{aligned}
$$

The above set of equations reduce to those given in References [73] and [74] for the case of, no axial asymmetry (s/l = zero) and no cross-coupling terms in the stiffness matrix.

3.2 The Eigenvalue Problem

Matrix equation 3.21 is a set of second order ordinary differential equations. Some of the coefficients, those associated with the support stiffnesses, are cyclic at frequency 2ω. If we assume the support stiffness is axisymmetric and there are no cross - coupling support stiffness terms then the cyclic terms become zero. These are the assumptions made in the analyses in this chapter. In this case the matrix Equation 3.21 has constant coefficients.

Such a set of equations can be rearranged as described in Appendix A into twice as many first order ordinary differential equations, which can be expressed as:

$$[A]\{\Phi\} = \left\{\dot{\Phi}\right\}. \tag{3.22}$$

If we assume a solution of the form,

$$\{\Phi\} = \{\Phi_o\}\, e^{\lambda_n t},$$

where $\{\Phi_o\}$ is a constant vector, and λ_n can be complex then,

$$[A]\{\Phi_o\} = \lambda_n \{\Phi_o\}, \tag{3.23}$$

which can be expressed in the form,

$$[[A] - \lambda_n [I]] \{\Phi_o\} = \{0\}. \tag{3.24}$$

For a non-trivial solution, i.e. $\{\Phi_o\} \neq \{0\}$ we require that,

$$\det([A] - \lambda_n [I]) = 0. \tag{3.25}$$

This is the fundamental algebraïc eigenvalue problem. The roots of the characteristic equation in λ_n obtained by evaluating the determinant of Equation 3.25 are the 'eigenvalues' or 'principal roots' of the system of equations. However for all the cases studied in this thesis, the matrix solved is not symmetric and the roots occur in complex conjugate pairs.

The 'QR' method [75] was used to obtain the complex eigenvalues for the cases described in the following sections. The criterion for determining that a mode is unstable is that the real part of the complex eigenvalue be greater than zero. For the undamped cases, the eigenvalues are either purely imaginary or purely real.

3.3 Non-Axisymmetric Rotor Without Damping.

The analysis of a rotor with its C.G. at the axial mid point is shown in Figure 3.7 in which the lateral displacement degrees of freedom were included but which are unaffected by the gyroscopic effects and diametral moment of inertia asymmetry. Therefore this result is in fact identical to that of [73] and was therefore a useful test case.

The modal frequencies versus speed are shown on Figure 3.8. The solutions occur in complex conjugates, so the set of plots are mirror images about the zero frequency line.

The plots shown in Figure 3.9 are also for a rotor with its C.G. at the axial mid point but with a greater diametral moment of inertia asymmetry ($\delta = 0.2$) and with a larger polar moment of inertia ($\lambda = 0.5$). Only those modes which have positive frequencies relative to an inertial frame of reference are included. On this plot the 'flat' zone along the zero frequency axis is very evident. Over this range the real part of the second lowest eigenvalue becomes slightly positive. This instability is of the mode which has zero frequency in the rotating frame of reference, i.e. at a frequency equal to rotation speed relative to an inertial frame. It is therefore the counterpart of a simple rotor at resonance. What would be a single frequency for an axi - symmetric rotor (equal to rotation speed for zero polar moment of inertia), becomes an unstable frequency band for a rotor with asymmetric diametral moments of inertia.

Figure 3.10 shows the variation of stability boundary with c.g. position: mid span (s/l=0), half way between mid span and one bearing (s/l=-0.5) and at one bearing (s/l=-1.0 - not an ideal location as it would unload the bearing). The unstable area occurs at higher speeds with increasing asymmetry. The mode which becomes unstable is consistently that with second lowest natural frequency but the natural frequency of this mode, which consists mostly of angular motion, increases with increasing asymmetry.

For the case of a non-axisymmetrical rotor, the above formulation eliminates cyclic terms in the mass matrix but incurs cyclic terms in the stiffness and damping matrices for non symmetrical bearing/support stiffness and damping. Conversely, formulation of the problem in an inertial frame results in cyclic coefficients in the mass/inertia matrix but avoids them in the stiffness and damping matrices. For an axi - symmetric rotor it is therefore more convenient to use inertial coefficients for machines which commonly have non - axisymmetric support stiffness.

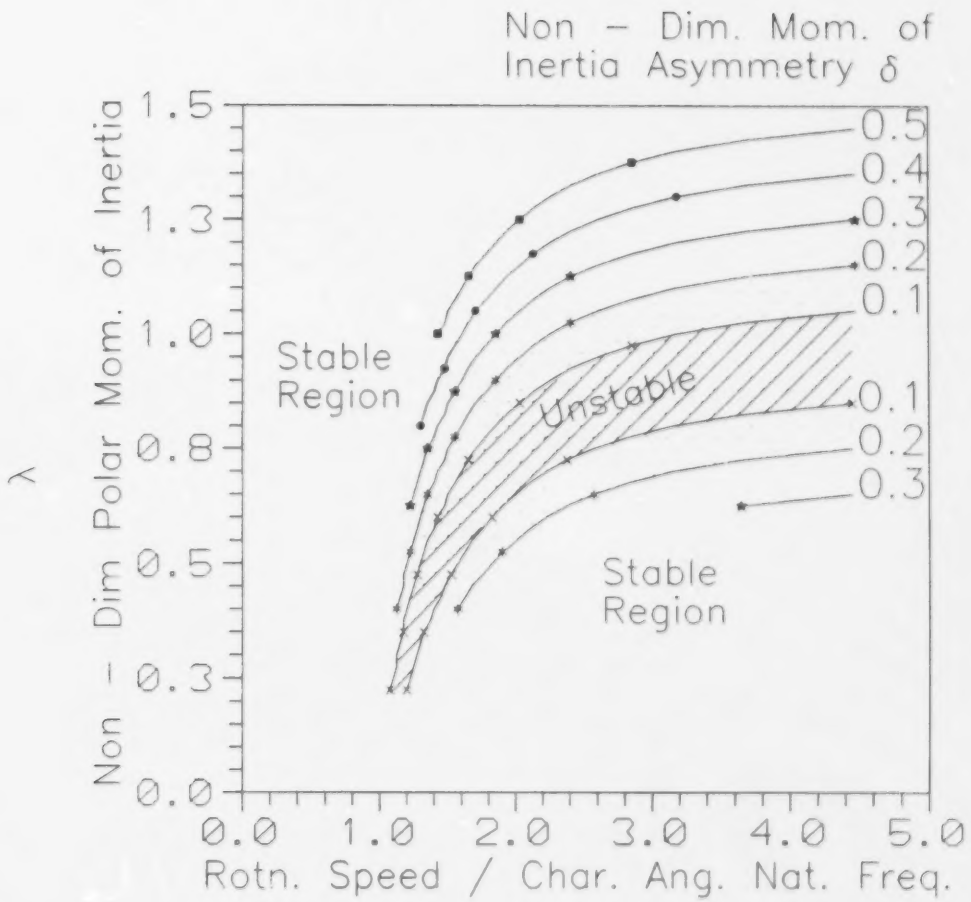

Figure 3.7: Creation of a Region of Instability due to Asymmetry of Diametral Moments of Inertia for a Rigid Rotor with Zero Damping. $\delta = (J_{\xi\xi} - J_{\eta\eta})/(J_{\xi\xi} + J_{\eta\eta})$ **and** $\lambda = 2J_{\zeta\zeta}/(J_{\xi\xi} + J_{\eta\eta})$.

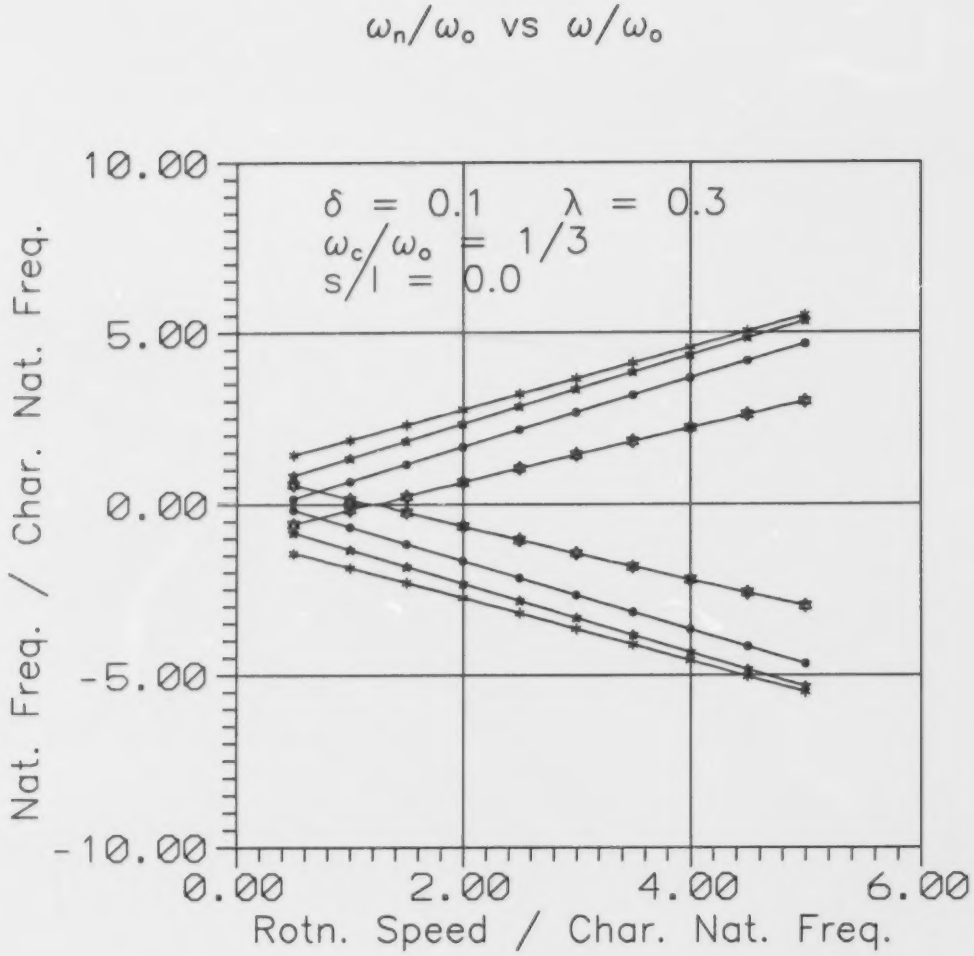

Figure 3.8: Modal Frequencies Relative to Rotating Coordinate Frame of Reference, Corresponding to the Case of $\delta = 0.1$ and $\lambda = 0.3$. The plots with the same symbols correspond to complex conjugate eigenvalues.

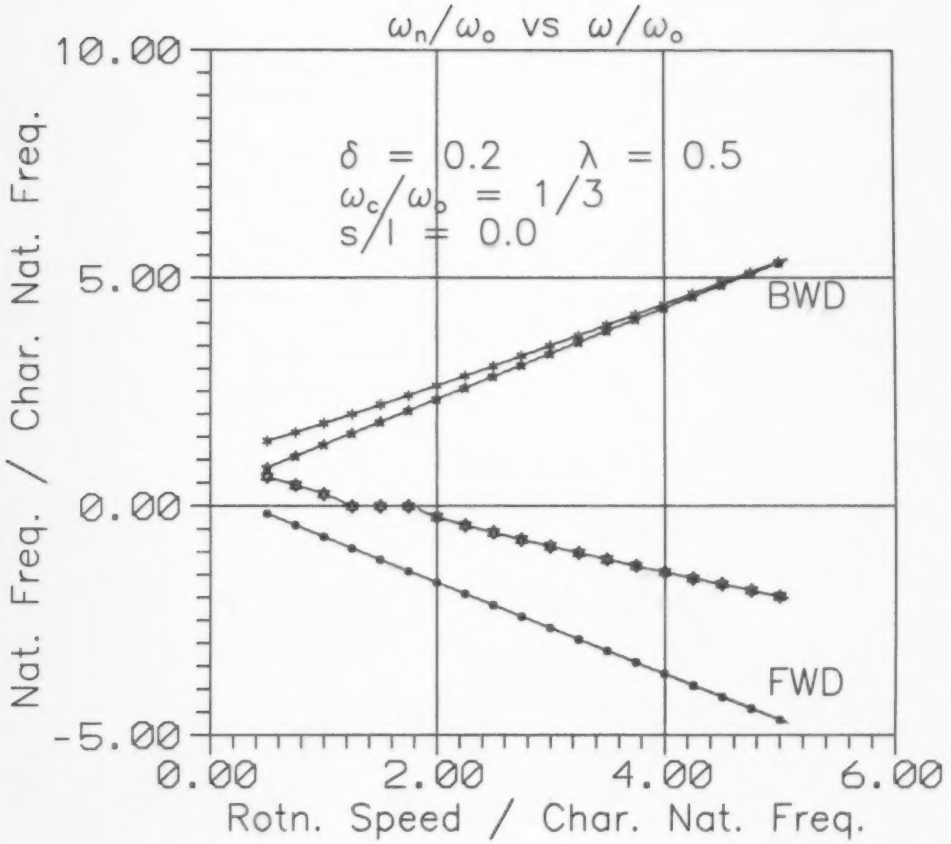

Figure 3.9: Modal Frequencies Relative to Rotating Coordinate Frame of Reference, Corresponding to the Case of $\delta = 0.2$ and $\lambda = 0.5$.

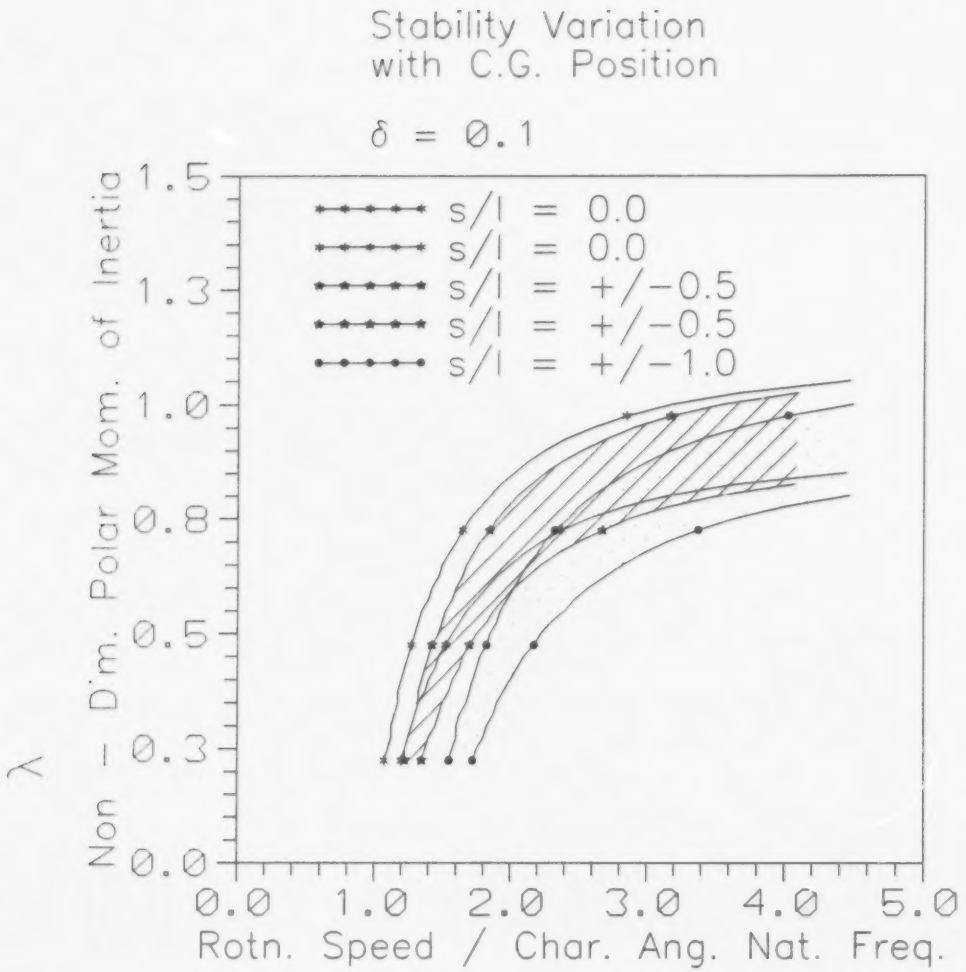

Figure 3.10: Variation of Stability Boundaries with Rotor C.G. Position: at the mid point; half way between mid point and one bearing, and at one bearing. The regions between plots with the same symbol are unstable, e.g. the dotted and cross - hatched regions.

3.4 Inertial Coordinate Formulation

Proceeding in a similar manner to the previous analysis, except omitting the change to a rotating frame of reference, the equation of motion in inertial coordinates for a rigid axi - symmetric rotor can be expressed:

$$\begin{Bmatrix} \ddot{x}/l \\ \ddot{y}/l \\ \ddot{\phi}_x \\ \ddot{\phi}_y \end{Bmatrix} + \begin{bmatrix} 0 & 0 & 0 & 0 \\ 0 & 0 & 0 & 0 \\ 0 & 0 & 0 & (\lambda) \\ 0 & 0 & (-\lambda) & 0 \end{bmatrix} \begin{Bmatrix} \dot{x}/l \\ \dot{y}/l \\ \dot{\phi}_x \\ \dot{\phi}_y \end{Bmatrix} +$$

$$+ \begin{bmatrix} 2\zeta_c \frac{\omega_c}{\omega} & & & \\ & 2\zeta_c \frac{\omega_c}{\omega} & & \\ & & 2\zeta_0 \frac{\omega_0}{\omega}(1+(\frac{s}{l})^2) & \\ & & & 2\zeta_0 \frac{\omega_0}{\omega}(1+(\frac{s}{l})^2) \end{bmatrix} \begin{bmatrix} \nu & \\ (\nu, s/l) & \end{bmatrix} \begin{Bmatrix} \dot{x}/l \\ \dot{y}/l \\ \dot{\phi}_x \\ \dot{\phi}_y \end{Bmatrix}$$

$$+ \begin{bmatrix} (\frac{\omega_c}{\omega})^2 & 0 & 0 & 0 \\ 0 & (\frac{\omega_c}{\omega})^2 & 0 & 0 \\ 0 & 0 & (\frac{\omega_0}{\omega})^2(1+(\frac{s}{l})^2) & \\ 0 & 0 & 0 & (\frac{\omega_0}{\omega})^2(1+(\frac{s}{l})^2) \end{bmatrix} \begin{bmatrix} \epsilon & (k_{ij}, s/l) \end{bmatrix} \begin{Bmatrix} x/l \\ y/l \\ \phi_x \\ \phi_y \end{Bmatrix}$$

$$= \begin{bmatrix} \cos\tau & -\sin\tau & 0 & 0 \\ \sin\tau & \cos\tau & 0 & 0 \\ 0 & 0 & \cos\tau & -\sin\tau \\ 0 & 0 & \sin\tau & \cos\tau \end{bmatrix} \begin{Bmatrix} \bar{\xi}/l \\ \bar{\eta}/l \\ -\sigma_2 \\ \sigma_1 \end{Bmatrix}, \tag{3.26}$$

where:

$$[\epsilon_{ij}] =$$

$$\begin{bmatrix} (1-\epsilon) & (-\alpha+\beta) & (\alpha-\beta)s/l & (1-\epsilon)s/l \\ (-\alpha-\beta) & (1+\epsilon) & (-1-\epsilon)s/l & (-\alpha-\beta)s/l \\ \frac{(\alpha+\beta)s/l}{(1+(s/l)^2)} & \frac{(-1-\epsilon)s/l}{(1+(s/l)^2)} & (1+\epsilon) & (\alpha+\beta) \\ \frac{(1-\epsilon)s/l}{(1+(s/l)^2)} & \frac{(-\alpha+\beta)s/l}{1+(s/l)^2)} & (\alpha-\beta) & (1-\epsilon) \end{bmatrix}$$

$$[\nu_{ij}] = \begin{bmatrix} (1-\nu) & 0 & 0 & (1-\nu)s/l \\ 0 & (1+\nu) & (-1-\nu)s/l & 0 \\ 0 & \frac{(-1-\nu)s/l}{(1+(s/l)^2)} & (1+\nu) & 0 \\ \frac{(1-\nu)s/l}{(1+(s/l)^2)} & 0 & 0 & (1-\nu) \end{bmatrix}.$$

3.4.1 Bearing Coefficients due to Fluid Swirl

If the rotor is supported solely by cylindrical sleeve bearings with a relatively stiff support structure, then we can consider the mechanical impedance of the journal / bearing only, which avoids the extra degrees of freedom due to the pedestal motion. It is then convenient to derive the stiffness and damping coefficients by considering the motion of the bearing fluid with respect to a frame of reference rotating at the mean rotational angular velocity of the fluid within the bearing annulus. This was done in [7] for a simpler system. It is carried out below in matrix form for this system having four degrees of freedom.

Consider a bearing as containing a mass of fluid which is accelerated by the force exerted on it by the shaft and which resists the motion in a manner which can be characterized by a stiffness and damping force.

The forces and moments $\{F\}_s$ applied by the rotor to the fluid masses m_f at each bearing, rotate at ω_s, where $\omega_s = \lambda_s \times \omega$. The λ_s is the 'fluid average circumferential velocity ratio', [7] sometimes called the swirl ratio.

The equation of motion for the two masses of fluid at the ends of the rotor, Figure 3.11, expressed with respect to a coordinate frame rotating at the mean swirl velocity of the fluid in the bearings is then:

$$\{F\}_s = \omega^2 [m_f] \{\ddot{x}\}_s + \omega [c_f] \{\dot{x}\}_s + [k_f] \{x\}_s \tag{3.27}$$

where the dots denote differentiation with respect to τ $(= \omega t)$ as in the previous section,

$$\{F\}_s = \{F_x \;\; F_y \;\; M_x \;\; M_y\}_s^T$$

$$\{x\}_s = \{x \;\; y \;\; \phi_x \;\; \phi_y\}_s^T$$

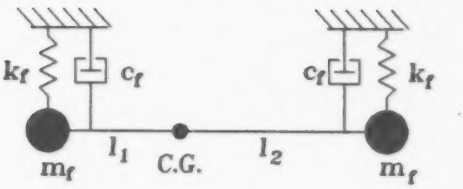

Figure 3.11: Model for Equation of Motion for Swirling Fluid Masses Within Bearings Relative to a Frame of Reference Rotating with the Fluid at Angular Velocity ω_s

$$\{\dot{x}\}_s = \left\{\dot{x}\ \ \dot{y}\ \ \dot{\phi}_x\ \ \dot{\phi}_y\right\}_s^T$$

$$\{\ddot{x}\}_s = \left\{\ddot{x}\ \ \ddot{y}\ \ \ddot{\phi}_x\ \ \ddot{\phi}_y\right\}_s^T$$

$$[m_f] = 2\begin{bmatrix} m_f & 0 & 0 & 0 \\ 0 & m_f & 0 & 0 \\ 0 & 0 & m_f(l^2+s^2) & 0 \\ 0 & 0 & 0 & m_f(l^2+s^2) \end{bmatrix}$$

$$[c_f] = 2\begin{bmatrix} c^b & 0 & 0 & c^b s \\ 0 & c^b & -c^b s & 0 \\ 0 & -c^b s & c^b(l^2+s^2) & 0 \\ c^b s & 0 & 0 & c^b(l^2+s^2) \end{bmatrix}$$

$$[k_f] = 2\begin{bmatrix} k_f^b & 0 & 0 & k_f^b s \\ 0 & k_f^b & -k_f^b s & 0 \\ 0 & -k_f^b s & k_f^b(l^2+s^2) & 0 \\ k_f^b s & 0 & 0 & k_f^b(l^2+s^2) \end{bmatrix}.$$

The vector $\{x\}_s$ represents the linear and angular displacements of the C.G. of the rotor referred to a frame of reference rotating at the fluid swirl speed $\lambda_s\omega$.

Now:

$$\omega_s t = \lambda_s \omega t = \lambda_s \tau. \tag{3.28}$$

Therefore the coordinate transformation to the inertial frame is, in matrix form:

$$\begin{Bmatrix} x \\ y \\ \phi_x \\ \phi_y \end{Bmatrix} = \begin{bmatrix} \cos\lambda_s\tau & \sin\lambda_s\tau & 0 & 0 \\ -\sin\lambda_s\tau & \cos\lambda_s\tau & 0 & 0 \\ 0 & 0 & \cos\lambda_s\tau & \sin\lambda_s\tau \\ 0 & 0 & -\sin\lambda_s\tau & \cos\lambda_s\tau \end{bmatrix}. \tag{3.29}$$

Transforming to an inertial frame of reference in a manner similar to the previous Section, we get the force / moment vector applied by the rotor to the bearing fluid masses:

$$\begin{Bmatrix} F_x/l \\ F_y/l \\ M_x \\ M_y \end{Bmatrix} = 2\omega^2 \begin{bmatrix} m_f & 0 & 0 & 0 \\ 0 & m_f & 0 & 0 \\ 0 & 0 & m_f(l^2+s^2) & 0 \\ 0 & 0 & 0 & m_f(l^2+s^2) \end{bmatrix} \begin{Bmatrix} \ddot{x}/l \\ \ddot{y}/l \\ \ddot{\phi}_x \\ \ddot{\phi}_y \end{Bmatrix} +$$

$$+ 2\omega \begin{bmatrix} c^b & 2\lambda_s\omega m_f & 0 & c^b s/l \\ -2\lambda_s\omega m_f & c^b & -c^b s/l & 0 \\ 0 & -c^b s\, l & c^b(s^2+l^2) & 2\lambda_s\omega m_f l \\ -c^b s\, l & 0 & -2\lambda_s\omega m_f l & c^b(s^2+l^2) \end{bmatrix} \begin{Bmatrix} \dot{x}/l \\ \dot{y}/l \\ \dot{\phi}_x \\ \dot{\phi}_y \end{Bmatrix} +$$

$$+ 2 \begin{bmatrix} [k_f - (\lambda_s\omega)^2 m_f] & \lambda_s\omega c^b & -\lambda_s\omega c^b s/l & k_f s/l \\ -\lambda_s\omega c^b & [k_f - (\lambda_s\omega)^2 m_f] & -k_f s/l & -\lambda_s\omega c^b s/l \\ \lambda_s\omega c^b s\, l & -k_f s l & [(k_f(l^2+s^2) - (\lambda_s\omega)^2 m_f l] & \lambda_s\omega c^b(l^2+s^2) \\ k_f s\, l & \lambda_s\omega c^b s\, l & -\lambda_s\omega c^b(l^2+s^2) & [(k_f(l^2+s^2) - (\lambda_s\omega)^2 m_f l] \end{bmatrix} \begin{Bmatrix} x/l \\ y/l \\ \phi_x \\ \phi_y \end{Bmatrix}. \tag{3.30}$$

Thus, the fluid 'swirl' produces skew terms in the stiffness and damping matrices and terms which reduce the direct stiffness coefficients. The fluid effective mass m_f has been shown to be significant for large bearing eccentricities [7]. It will be assumed, (at least initially) that this is a negligible term. If we have large eccentricity or large orbits, then the problem clearly becomes non - linear, and the present analysis would no longer be adequate. Therefore this is a reasonable assumption, within the bounds of a linear analysis.

If the above matrix expressions for the 'forces' on the rotor (with reversed sign) are inserted into Equation 3.26, we get:

$$\begin{Bmatrix} \ddot{x}/l \\ \ddot{y}/l \\ \ddot{\phi}_x \\ \ddot{\phi}_y \end{Bmatrix} + \begin{bmatrix} 2\zeta_c\frac{\omega_c}{\omega} & & & \\ & 2\zeta_c\frac{\omega_c}{\omega} & & \\ & & 2\zeta_0\frac{\omega_0}{\omega}(1+(\frac{s}{l})^2) & \lambda \\ & & -\lambda & 2\zeta_0\frac{\omega_0}{\omega}(1+(\frac{s}{l})^2) \end{bmatrix}$$

$$\times \begin{bmatrix} 1 & 0 & 0 & s/l \\ 0 & 1 & -s/l & 0 \\ 0 & -\frac{s/l}{(1+(s/l)^2)} & 1 & 0 \\ \frac{s/l}{(1+(s/l)^2)} & 0 & 0 & 1 \end{bmatrix} \begin{Bmatrix} \dot{x}/l \\ \dot{y}/l \\ \dot{\phi}_x \\ \dot{\phi}_y \end{Bmatrix}$$

$$+ \begin{bmatrix} (\frac{\omega_c}{\omega})^2 & 0 & 0 & 0 \\ 0 & (\frac{\omega_c}{\omega})^2 & 0 & 0 \\ 0 & 0 & (\frac{\omega_0}{\omega})^2(1+(\frac{s}{l})^2) & \\ 0 & 0 & 0 & (\frac{\omega_0}{\omega})^2(1+(\frac{s}{l})^2) \end{bmatrix}$$

$$\times \begin{bmatrix} 1 & 2\lambda_s\omega\zeta_c/\omega_c & -2\lambda_s\omega\zeta_c/\omega_c s/l & s/l \\ -2\lambda_s\omega\zeta_c/\omega_c & 1 & -s/l & -2\lambda_s\omega\zeta_c/\omega_c s/l \\ 2\lambda_s\omega\frac{\zeta_0}{\omega_0}\frac{s/l}{(1+(s/l)^2)} & -\frac{s/l}{(1+(s/l)^2)} & 1 & 2\lambda_s\omega\zeta_0/\omega_0 \\ \frac{s/l}{(1+(s/l)^2)} & 2\lambda_s\omega\frac{\zeta_0}{\omega_0}\frac{s/l}{(1+(s/l)^2)} & -2\lambda_s\omega\zeta_0/\omega_0 & 1 \end{bmatrix} \begin{Bmatrix} x/l \\ y/l \\ \phi_x \\ \phi_y \end{Bmatrix}$$

$$= \begin{bmatrix} \cos\tau & -\sin\tau & 0 & 0 \\ \sin\tau & \cos\tau & 0 & 0 \\ 0 & 0 & \cos\tau & -\sin\tau \\ 0 & 0 & \sin\tau & \cos\tau \end{bmatrix} \begin{Bmatrix} \bar{\xi}/l \\ \bar{\eta}/l \\ -\sigma_2 \\ \sigma_1 \end{Bmatrix}. \qquad (3.31)$$

3.4.2 Modal Frequencies and Stability vs. Speed

In the results described in the following, the stability of the rotor motion is investigated, the imbalance forces and moments being set to zero.

Figure 3.12 shows the variation in modal frequencies with speed for a simple rotor with symmetric and asymmetric supports ($\epsilon = 0$ and $\epsilon = 0.2$) for two values of polar moment of inertia ($\lambda = 0.1$ and $\lambda = 0.3$).

As the natural frequencies are non - dimensionalized by the 'characteristic' angular natural frequency ω_0, with a ratio of characteristic linear to angular natural frequencies equal to 0.3, the lower two plots represent the lateral modes and the upper two plots the angular modes which diverge due to the gyroscopic effect.

With the formulation described to this point, one cannot include the swirl terms for the bearing and the asymmetric support as this involves the introduction of more degrees of freedom. This is because the bearing damping is in series with the support, not direct to ground.

Figures 3.13 through 3.17 show the effect of increasing damping with 'swirl'. The plots show the non - dimensionalized real and imaginary parts of the eigenvalues of all the 'physical' modes versus rotor speed. With increasing damping ratio, skew terms of the stiffness matrix become dominant resulting in a complex conjugate pair of eigenvalues of which the 'imaginary' part tends to the 'swirl ratio' λ_s. Therefore, from Figure 3.13 to 3.17 the second mode-pair gradually changes from how one normally expects a second mode to behave, i.e. having natural frequencies which diverge slightly with increasing speed, to a pair of plots slightly diverging from a line having a slope approximately equal to the swirl ratio.

This means that the 'whirl mode' familiar to rotor-dynamicists is in fact the second mode of the rotor system, although at low speeds it is lower in frequency than the first mode-pair.

In all of the plots, the mode with the higher frequency of the first mode-pair becomes unstable ($\alpha_n > 0$) at a low speed which, for high damping ratios, is close to the speed at which the 'whirl mode' intersects the first mode-pair i.e. at frequency coalescence of the two mode-pairs as is the case with flutter mechanisms. However, this mode becomes unstable at low speed even for relatively low damping ratios when the upper pair of modes do not 'track', for example in Figure 3.14. In this case we would have a 'whip' phenomenon without the tracking 'whirl' phenomenon, which is not unusual in practice. Therefore frequency coalescence is not a prerequisite for this kind of instability.

Thus damping within a bearing which is of a design that permits swirl is destabilizing just as internal friction within the rotor as described in Chapter 2. The instability shown in Figures 3.15 through 3.17 is what is observed on actual rotating machines and referred to as 'oil whip' in the case of the driving fluid being the oil in a sleeve bearing. This analysis does not include sources of external damping which would be stabilizing and which in most cases are sufficient to overcome this destabilizing mechanism.

Figure 3.17 for a rotor with c.g. mid way between the rotor centre and one bearing, shows very little change from the symmetric case. The mode with the higher frequency of the second mode-pair, which becomes unstable on all the plots, does so at a slightly higher speed. This is because the second mode has become a little stiffer, and its natural frequency higher.

The instability of the higher of the second mode-pair, is only of academic interest if the first mode has become unstable at a lower speed. However, if the first mode is stabilized by external damping specific to that mode then the second mode is of interest. The second mode becomes unstable for ω_n/ω_0 greater than but approximately equal to 1.0 i.e. it is the forward precessing mode when the frequency of this mode equals the characteristic natural frequency ω_0. This is therefore what would normally be regarded as the second critical speed of the rotor.

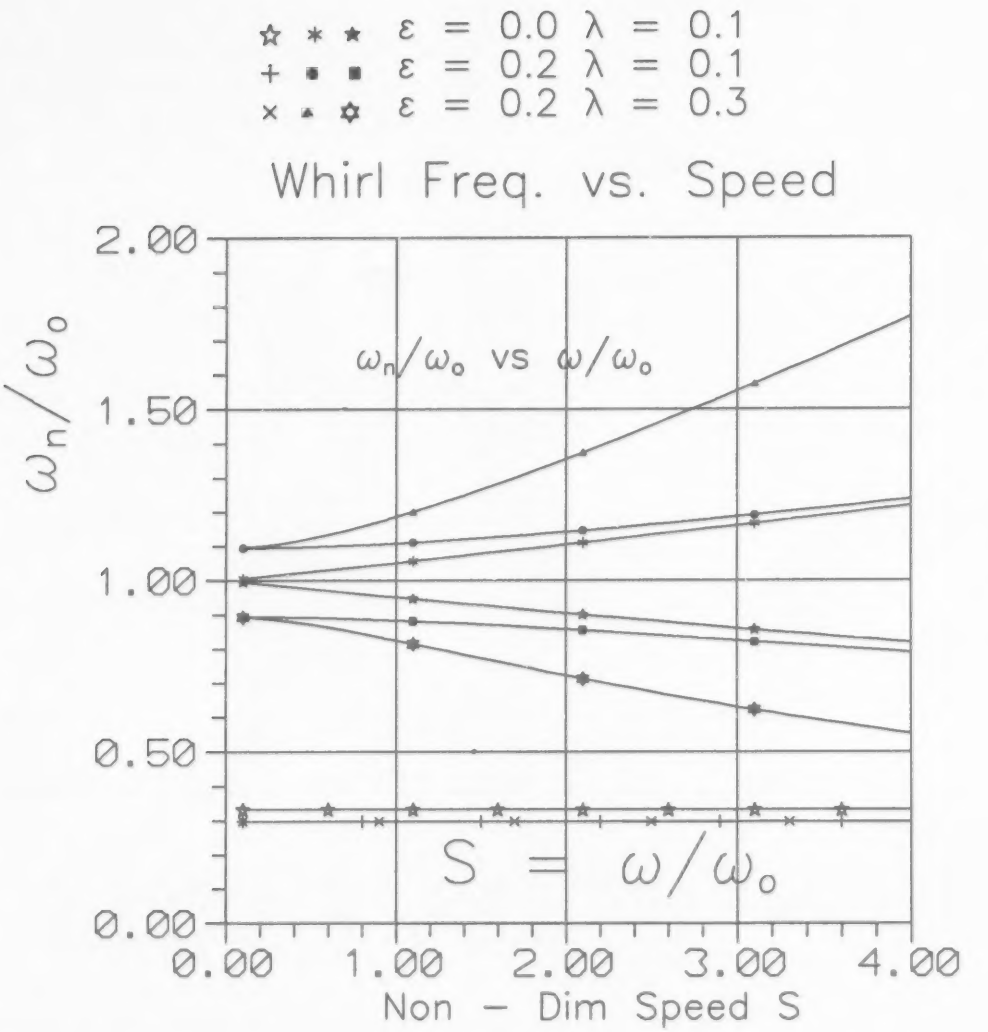

Figure 3.12: Whirl Frequency vs. Speed for No Damping, No Swirl but with Asymmetric Support and Gyroscopic Effects.

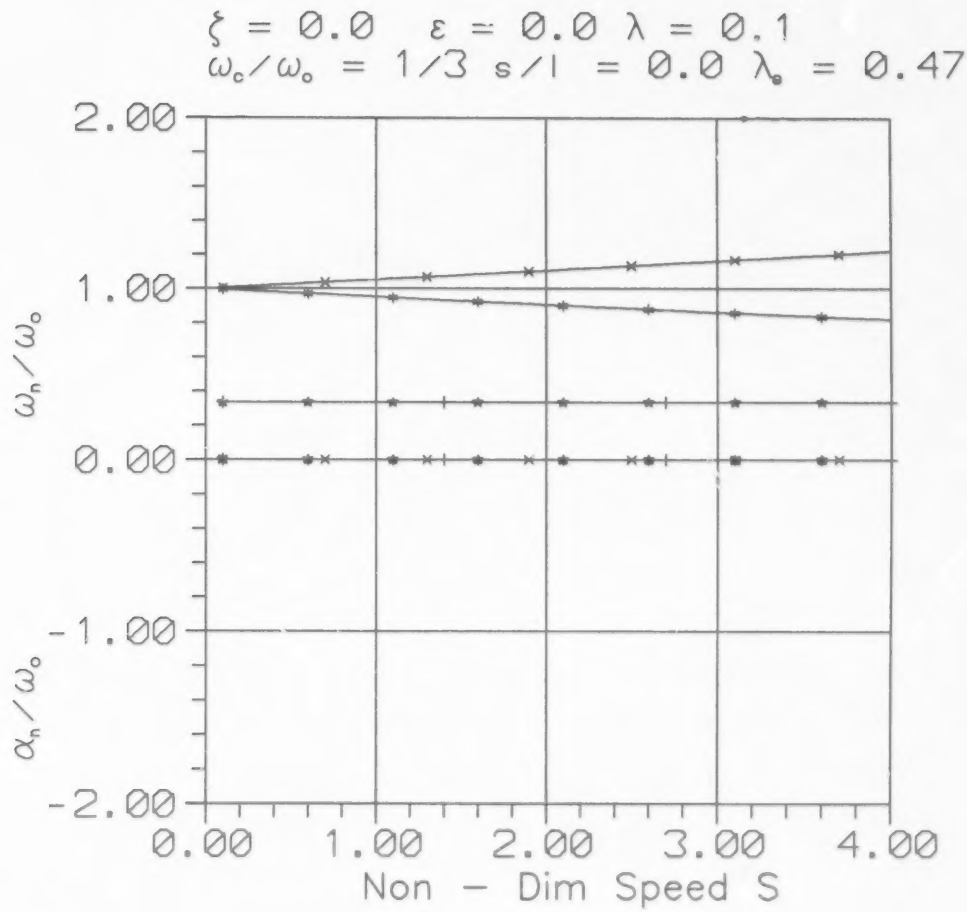

Figure 3.13: Real and Imaginary Parts of Eigenvalue vs. Non - Dimensionalized Speed - No Swirl

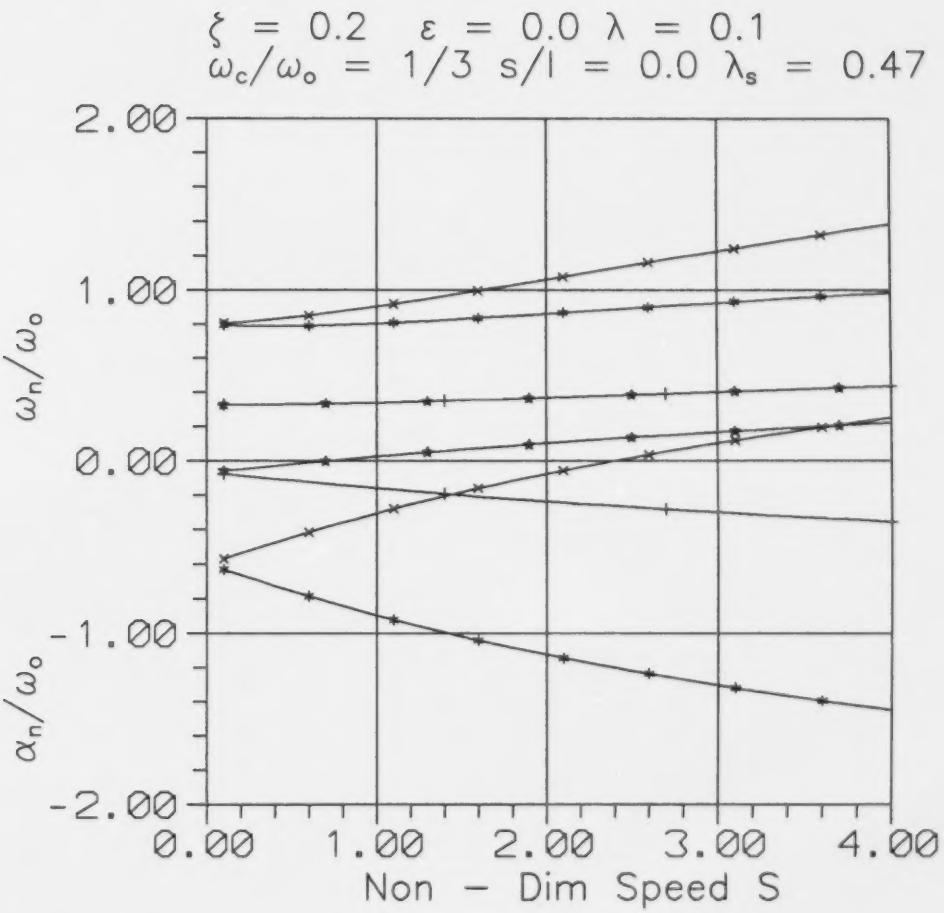

Figure 3.14: Real and Imaginary Parts of Eigenvalue vs. Non - Dimensionalized Speed - Damping Ratio = 0.2

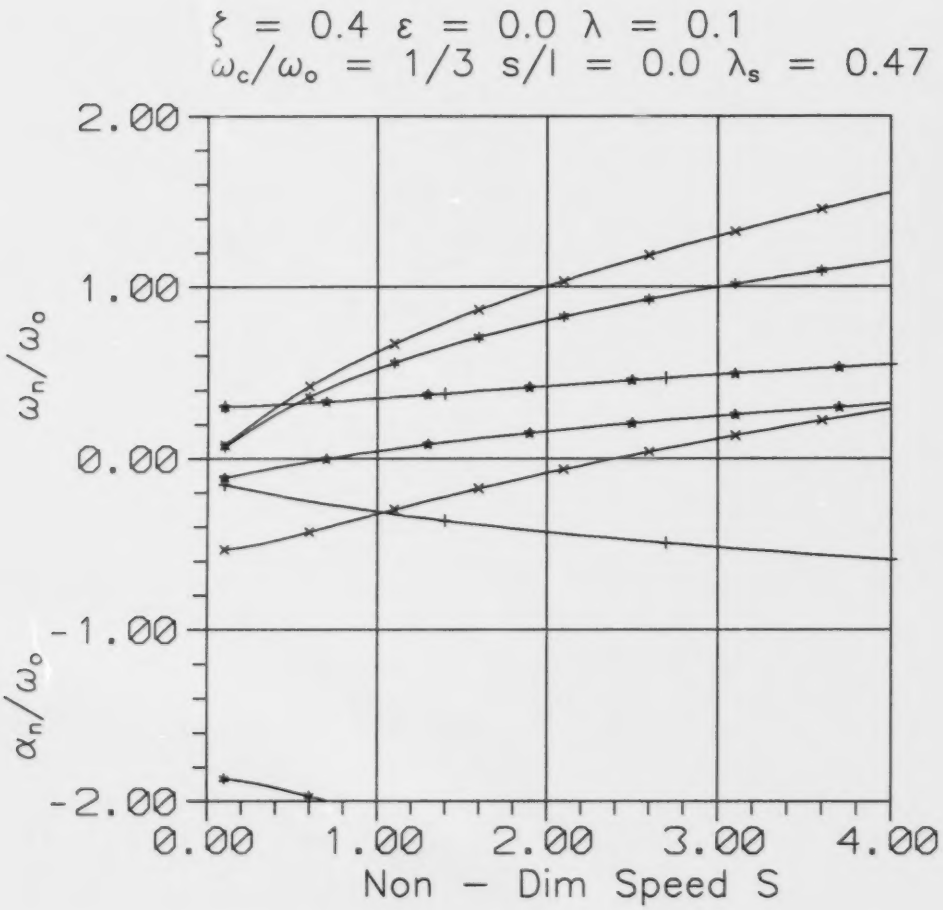

Figure 3.15: Real and Imaginary Parts of Eigenvalue vs. Non - Dimensionalized Speed - Damping Ratio = 0.4

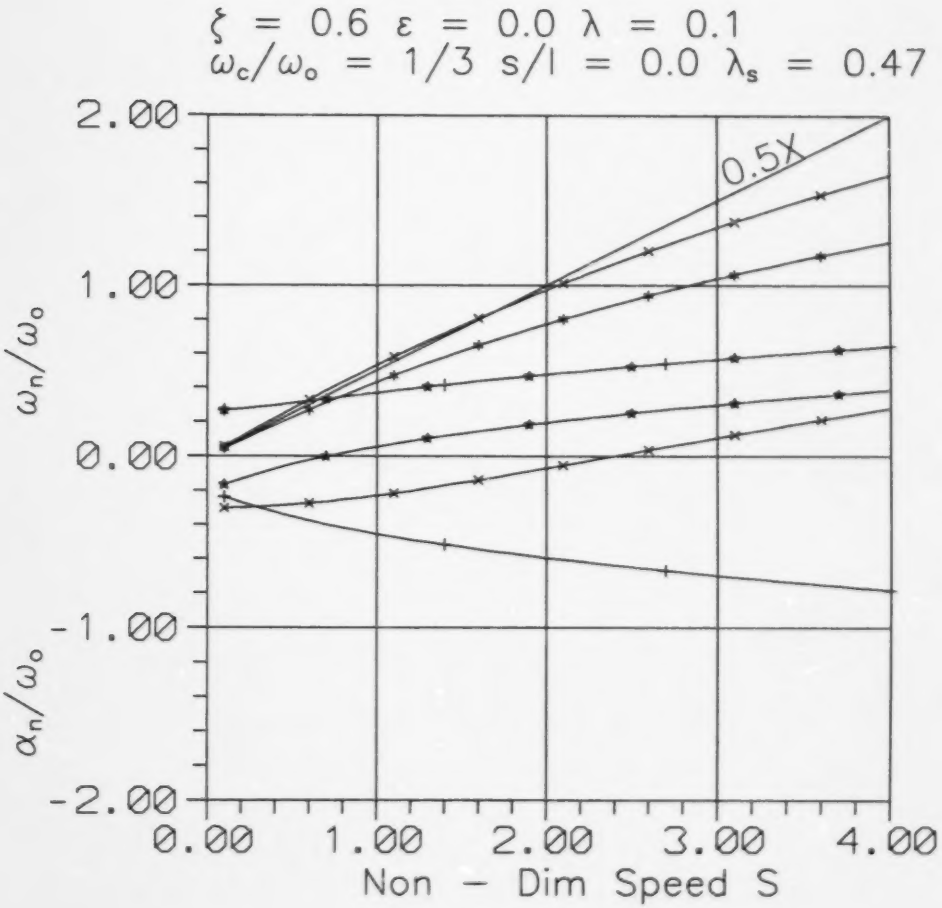

Figure 3.16: Real and Imaginary Parts of Eigenvalue vs. Non - Dimensionalized Speed - Damping Ratio = 0.6

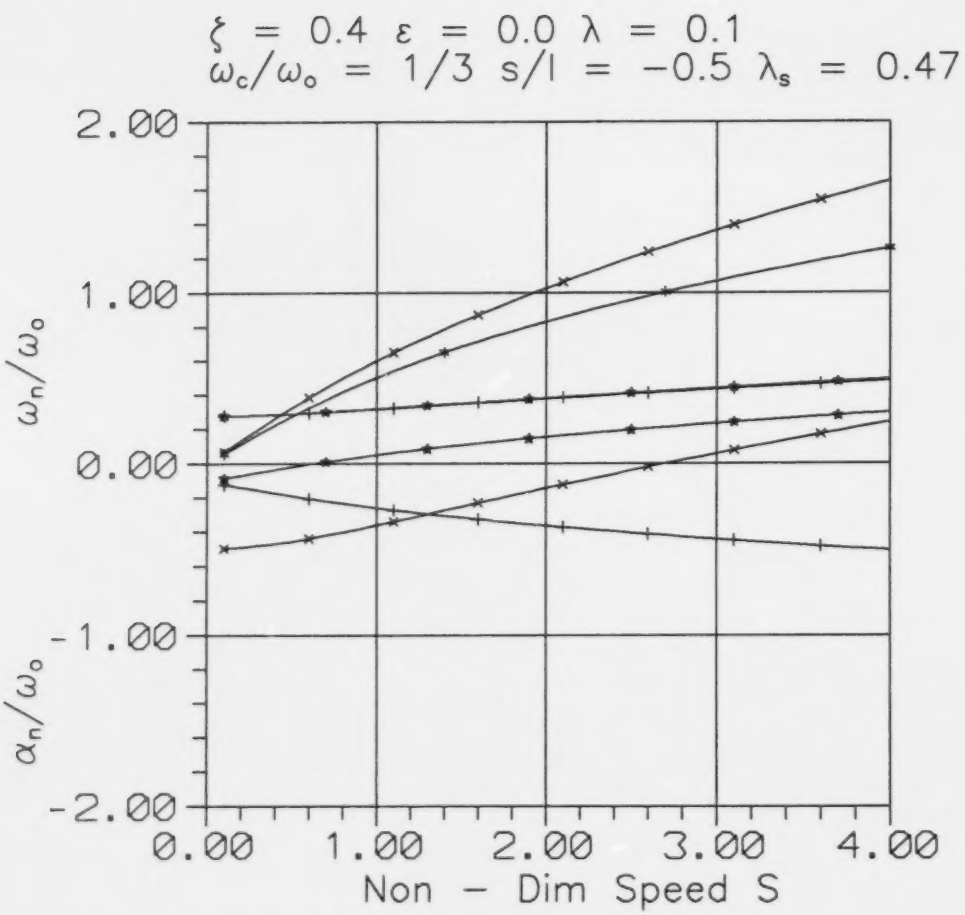

Figure 3.17: Real and Imaginary Parts of Eigenvalue vs. Non - Dimensionalized Speed: C.G. Mid - Way Between Centre and One Bearing - Damping Ratio = 0.4

3.4.3 Modal Orbits

The modal orbits for the upper two modes of Figure 3.12 are shown in Figures 3.18 through 3.24. The lower two modes are simply straight lines (not plotted) because there is no coupling between the linear and angular degrees of freedom of freedom for this case. Figures 3.12 and 3.18 through 3.24 are all of the form shown by Brosens [73] for his two degree of freedom analysis. The upper mode is forward precessing and the lower mode backward precessing. However, when swirl and internal fluid film damping are introduced, the results change significantly.

The modal orbits at the forward end of the rotor (+ve ζ or z) corresponding to Figure 3.17 are shown in Figures 3.25 through Figures 3.35. The modal orbit numbers are in the order of the frequencies of the modes at low speed, i.e. modes 1 and 2 are respectively the lower and upper modes of the pair which 'track' rotation speed at low speeds. Modes 3 and 4 are the predominantly lateral displacement modes which change frequency little with speed. Mode 4 is therefore the first mode to become unstable, followed at high speed by mode 2.

The orbital shapes were calculated as described in the Appendix A.2. The direction of precession can be deduced from the plots by inspecting the symbol location. There is a gap in each plot corresponding to $\omega_n t = 0$ and there is a symbol at the beginning of the plot , but not at the end.

The mode of most interest is number 4, the solid five point star symbols. The direction of precession of this mode is forward as was to be expected and at the point of instability Figure 3.28, its form is circular. This is the behaviour observed on real machines when this form of instability occurs (usually at 11:00 pm on a Friday evening).

Mode 2, the highest frequency mode, is also forward precessing as for the case with no damping. At high speed, when unstable, its orbit is close to circular as for the no damping case. However, mode 1 which was backward precessing in the no damping case is only slightly backward precessing at speeds s = 0.2 through 0.8, Figures 3.25 through 3.30, when the orbit becomes flat. Thereafter this mode also becomes forward precessing. This means that the forward swirl effect has overcome the backward whirl gyroscopic effect.

The results of this analysis are in a reasonable degree of agreement with what is observed on real rotors. The model predicts the instability of the first forward lateral mode (mode 4) at a speed a little above twice the frequency of that mode. The form of the orbit is essentially circular when this instability occurs. The instability of this mode can occur with or without the presence of a mode whose frequency 'tracks' rotation speed. The presence of a mode which 'tracks' appears to depend on the level of damping within a fluid bearing with the presence of fluid 'swirl', i.e. circumferential motion of the fluid in the bearing or seal annulus. The tracking mode is, in fact the second mode (or second pair of modes) which for high damping ratio is of lower frequency than the 'first' mode at low speeds.

A significant question which remains is why the mode which 'tracks' at approximately the swirl ratio times rotation speed, does not become unstable at low speeds, i.e. below the speed at which the mode 4 becomes unstable. In practice, on a machine subject to 'oil whirl' the tracking mode appears able to be unstable up to the speed at which the forward lateral mode, (mode 4 in this study) is lower than the tracking mode. This results in a transition from a large tracking sub-synchronous frequency component to a constant frequency component, the latter being much more severe.

The 'oil whirl' tracking instability is generally of a limit-cycle type, (which is mathematically speaking not an instability) and happens when the bearing is unloaded or completely flooded. The displacement amplitudes within the bearing are relatively large, (close to full clearance) so the problem becomes non - linear and beyond the scope of this analysis. Nevertheless, this analysis does show this to be the second least damped mode and therefore likely to be excited by the swirling fluid, even if not to the extent of becoming unstable. It is possible that what is observed in the field as the tracking phenomenon 'oil whirl', is in fact an excitation of that mode but not an instability in the true sense .

Although this rigid body linear analysis gives some insight into the general behaviour of a reasonably realistic rotor, to be useful it is necessary to include a flexible rotor, and if possible non - linear bearing stiffness and damping properties which is the subject of succeeding chapters.

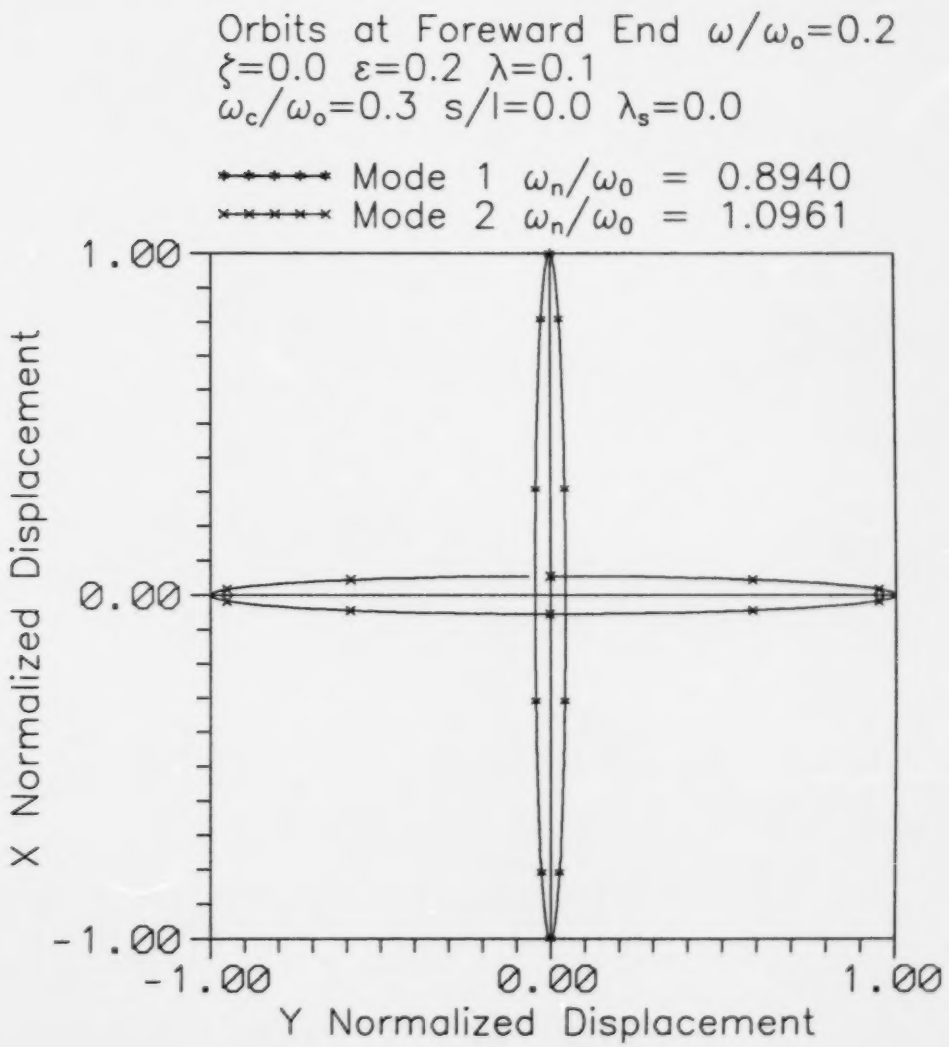

Figure 3.18: Modal Orbits at Forward End - S=0.2 No Damping, Angular Modes Only, Asymmetrical Support Stiffness

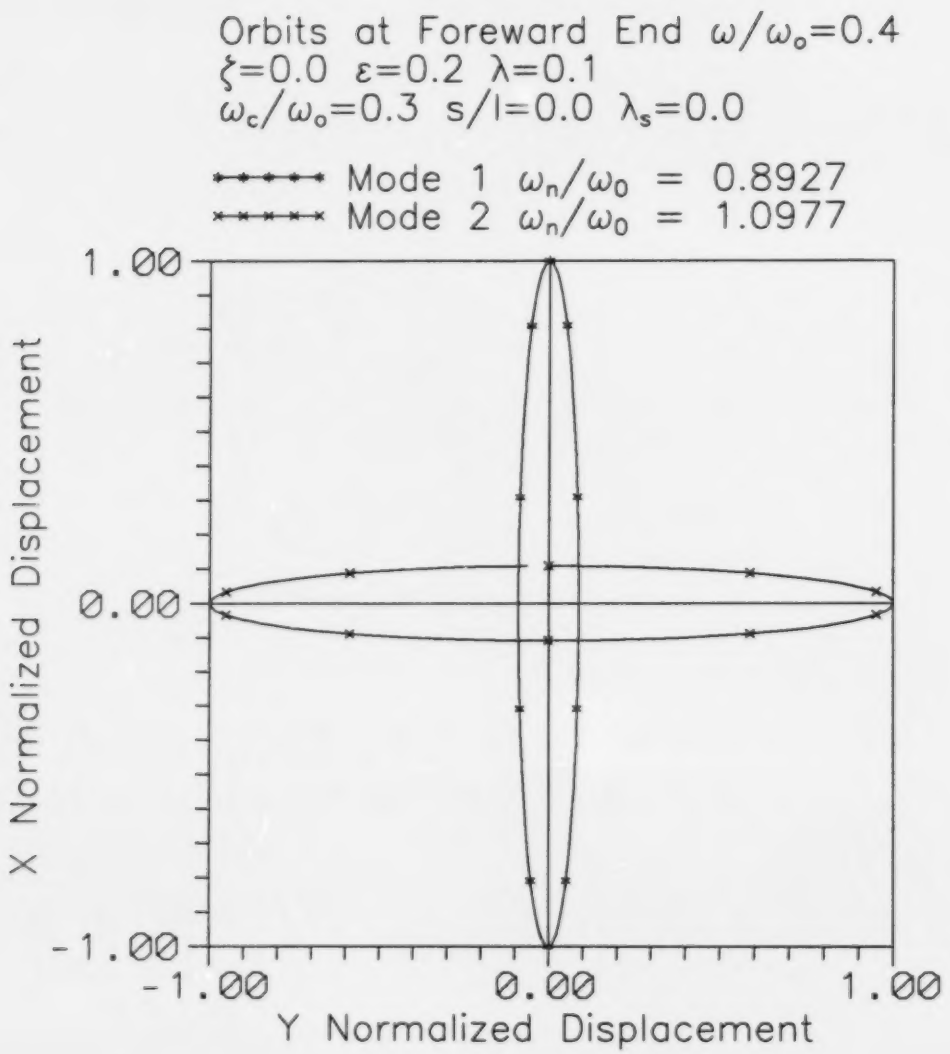

Figure 3.19: Modal Orbits at Forward End - S=0.4 No Damping, Angular Modes Only

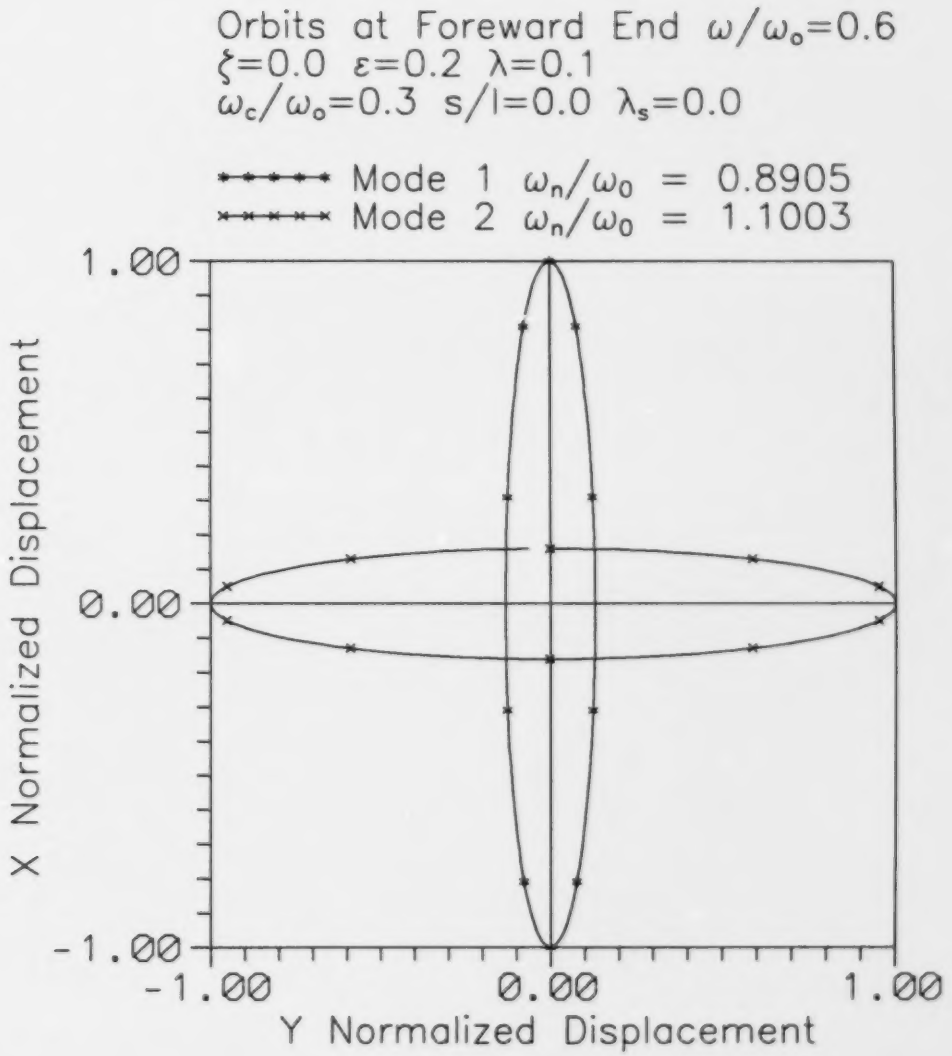

Figure 3.20: Modal Orbits at Forward End - S=0.6 No Damping, Angular Modes Only

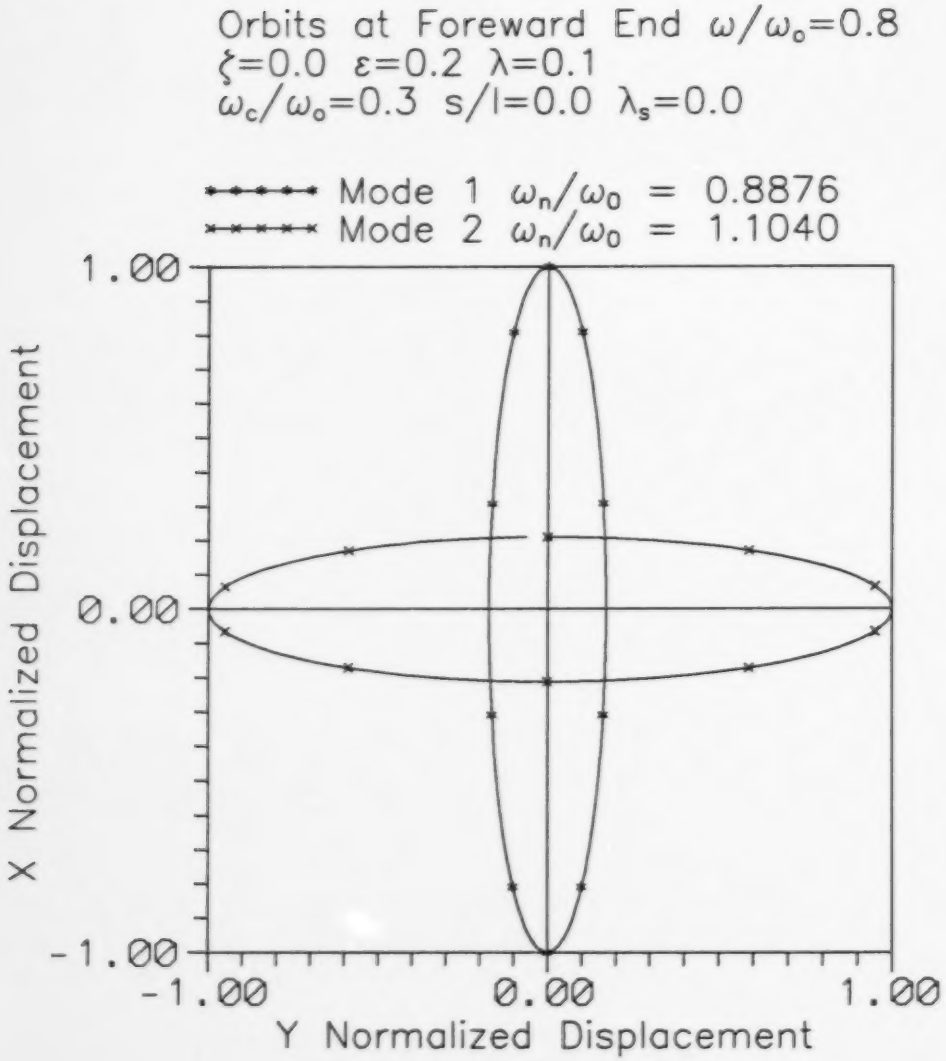

Figure 3.21: Modal Orbits at Forward End - S=0.8 No Damping, Angular Modes Only

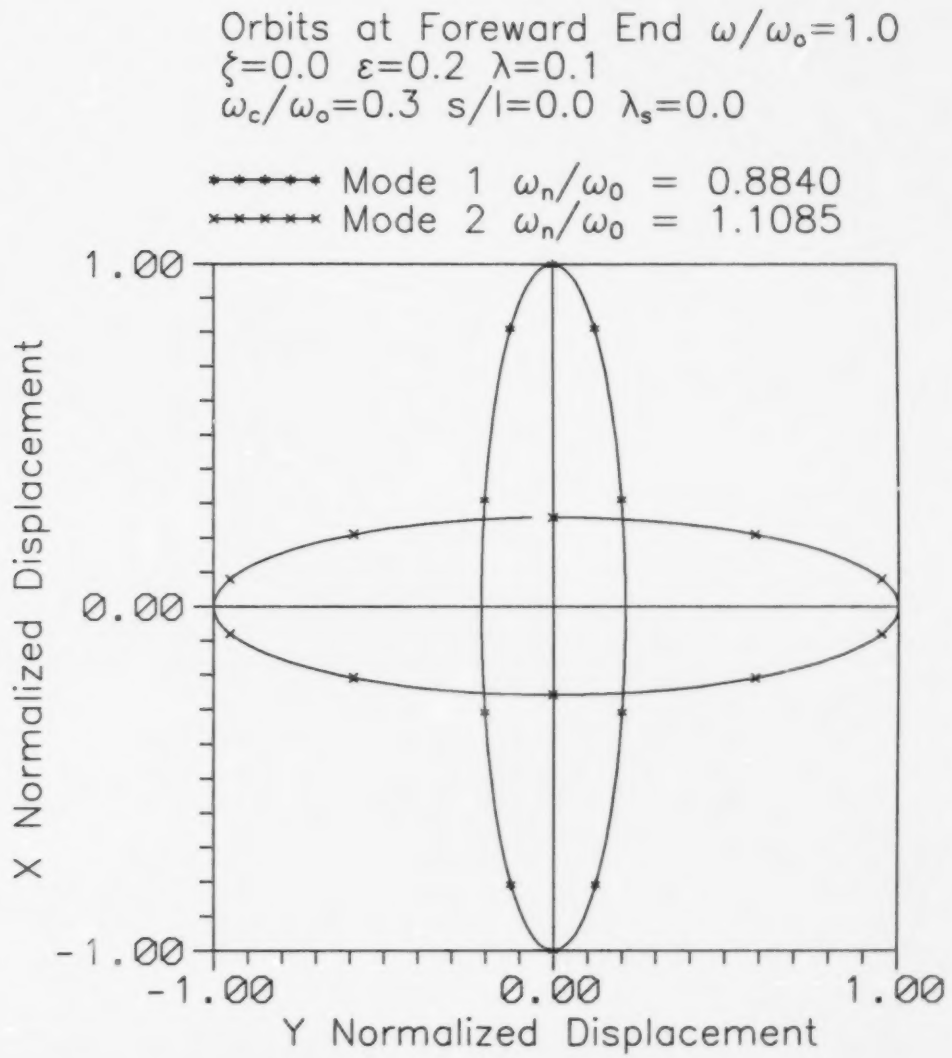

Figure 3.22: Modal Orbits at Forward End - S=1.0 No Damping, Angular Modes Only

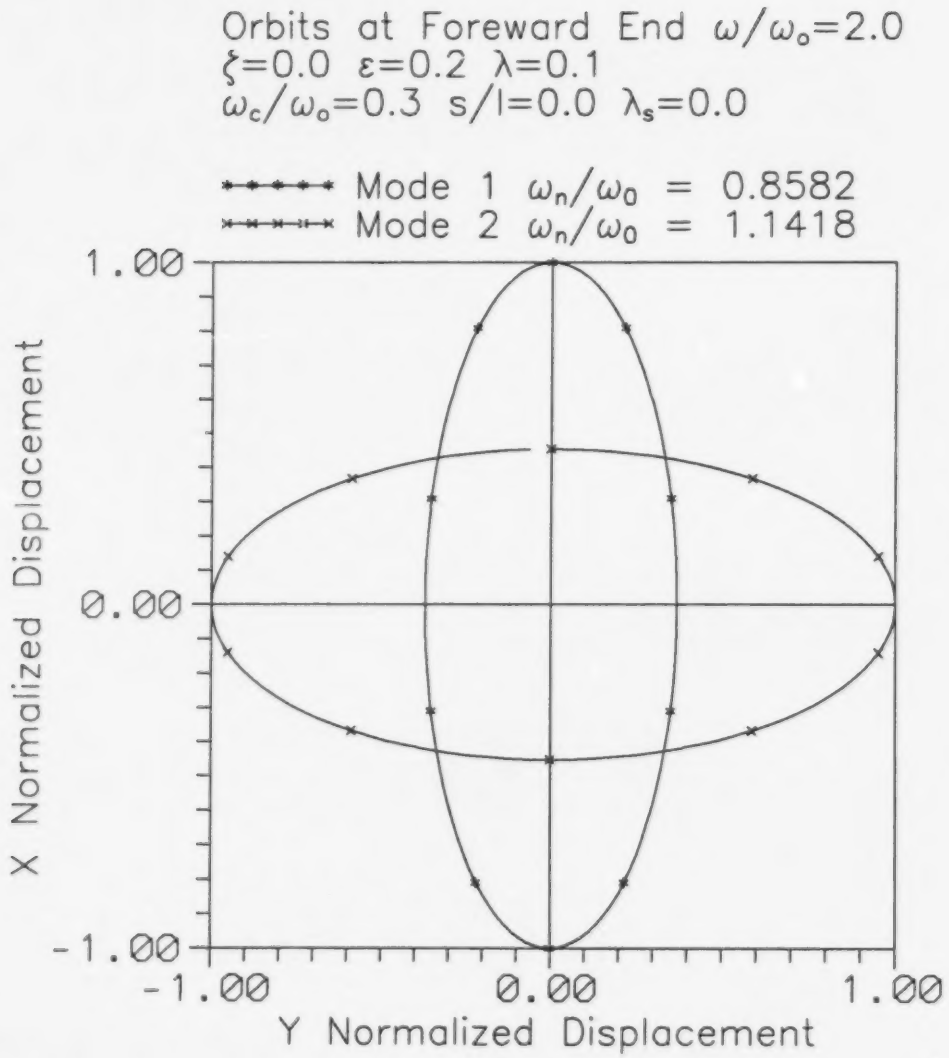

Figure 3.23: Modal Orbits at Forward End - S=2.0 No Damping, Angular Modes Only

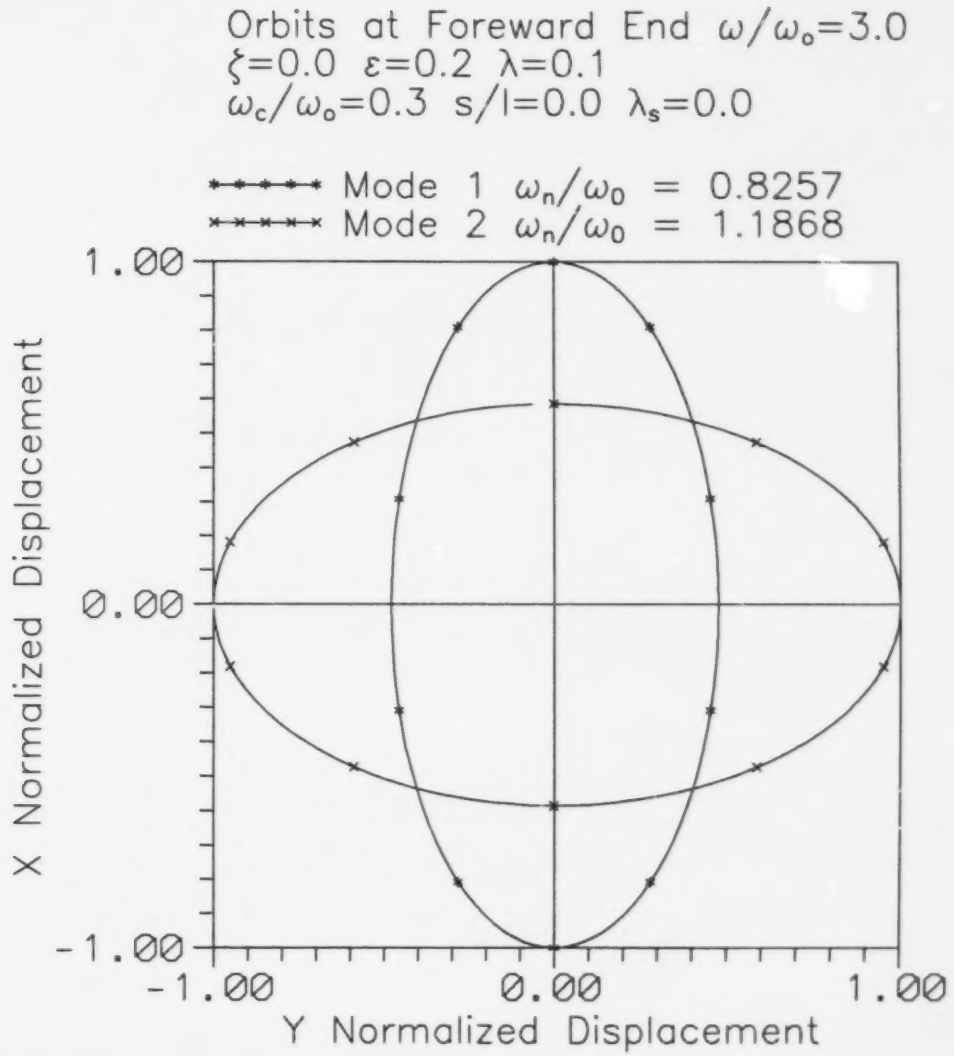

Figure 3.24: Modal Orbits at Forward End - S=3.0 No Damping, Angular Modes Only

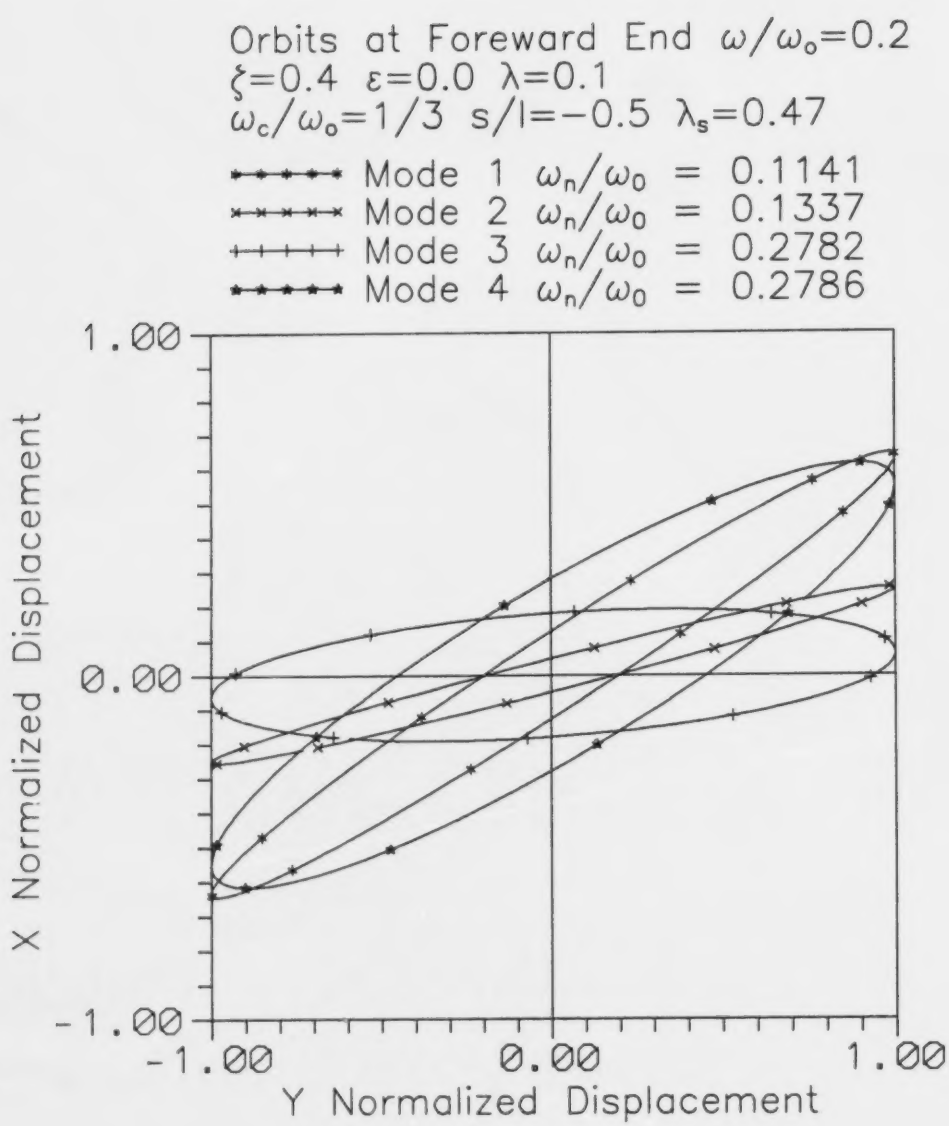

Figure 3.25: Modal Orbits at Forward End - S=0.2

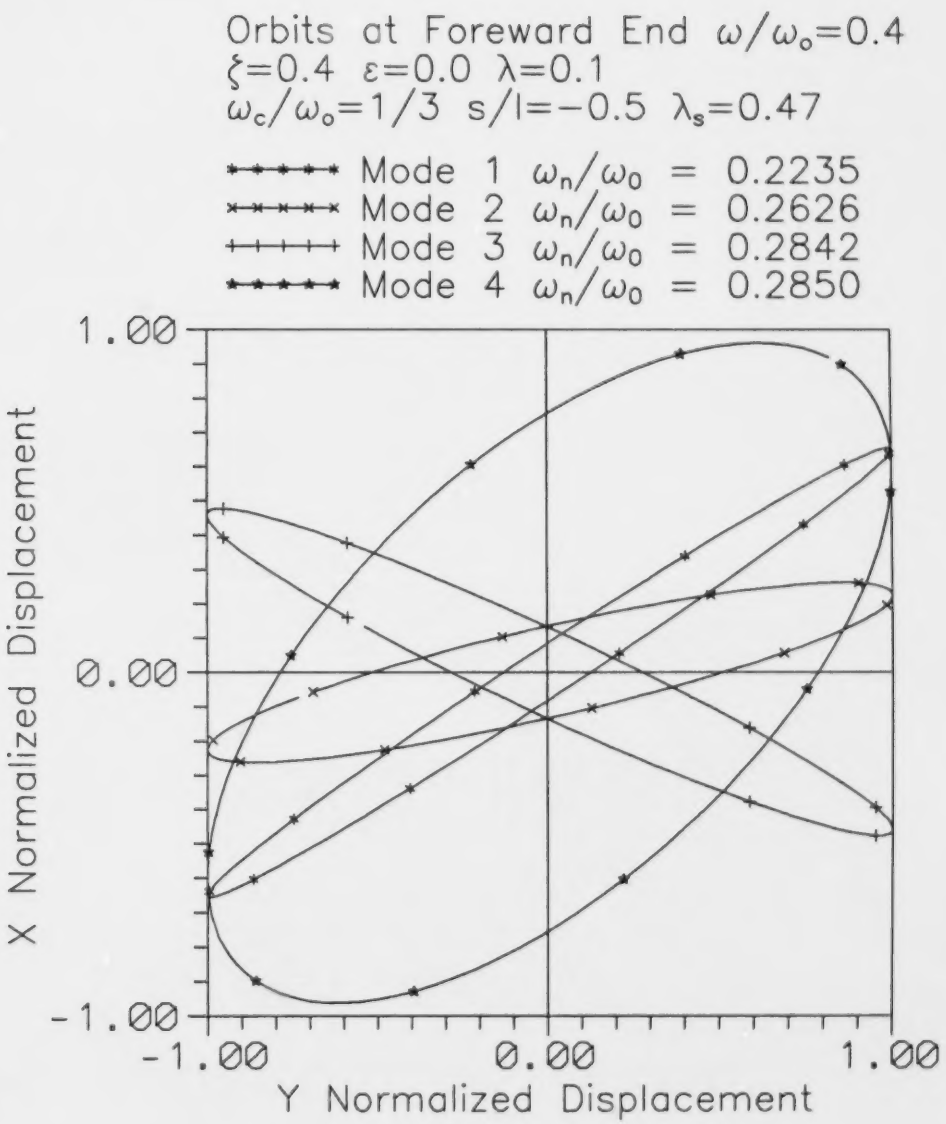

Figure 3.26: Modal Orbits at Forward End - S=0.4

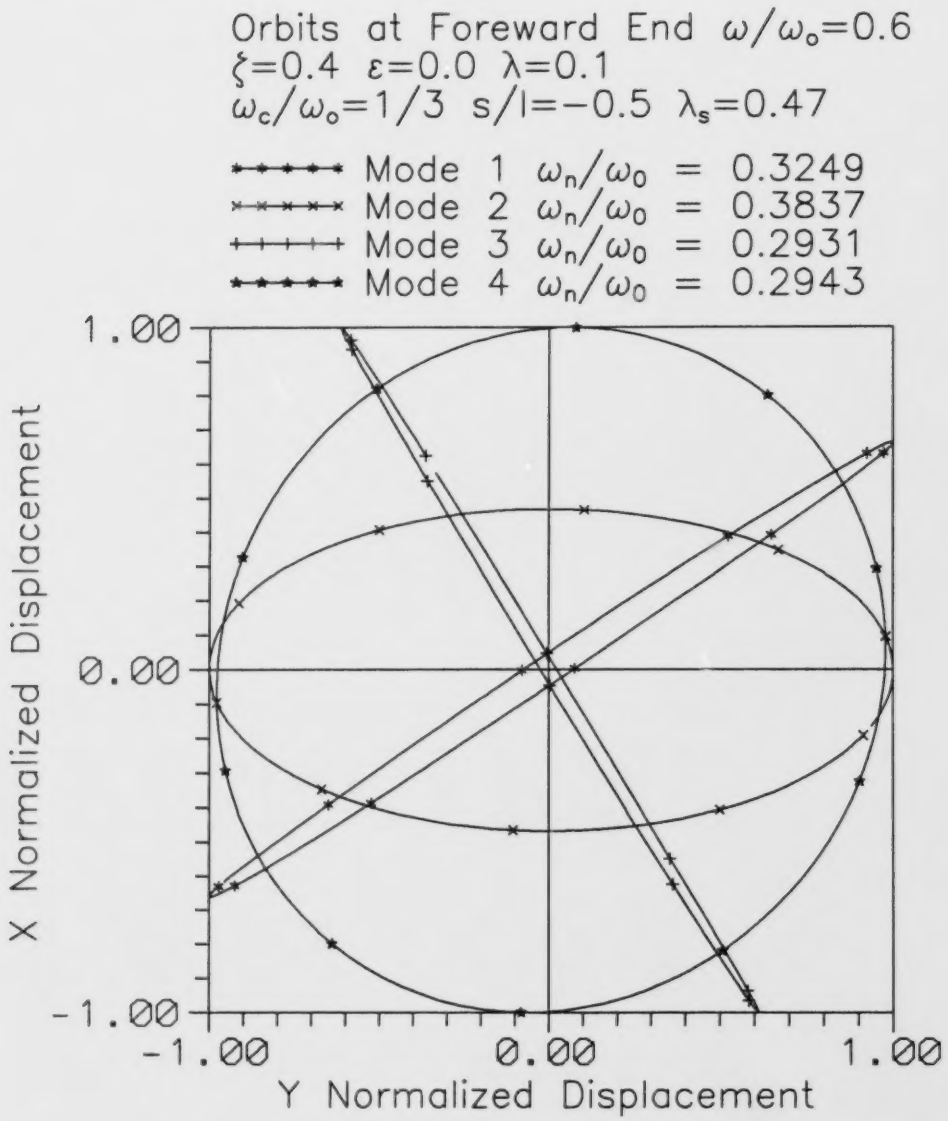

Figure 3.27: Modal Orbits at Forward End - S=0.6

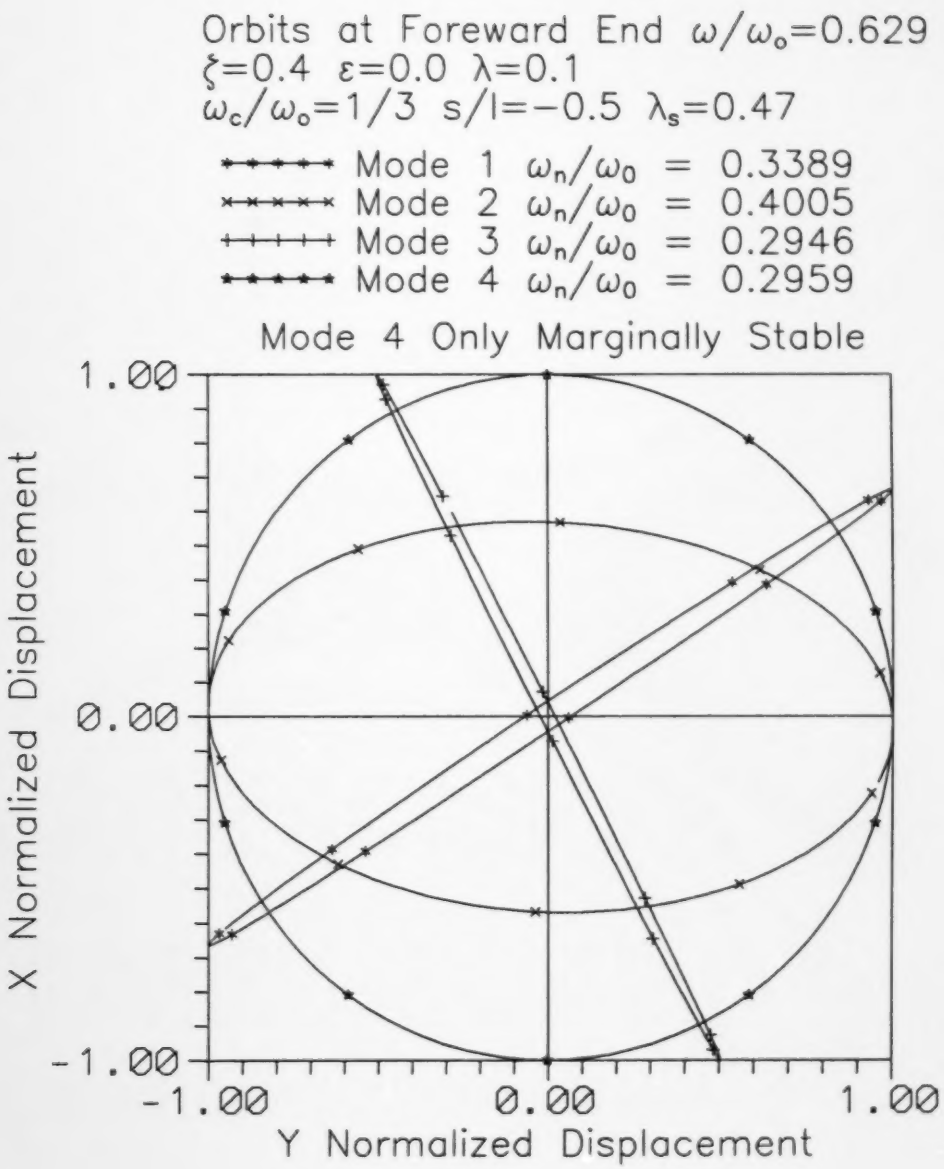

Figure 3.28: Modal Orbits at Forward End - S=0.629

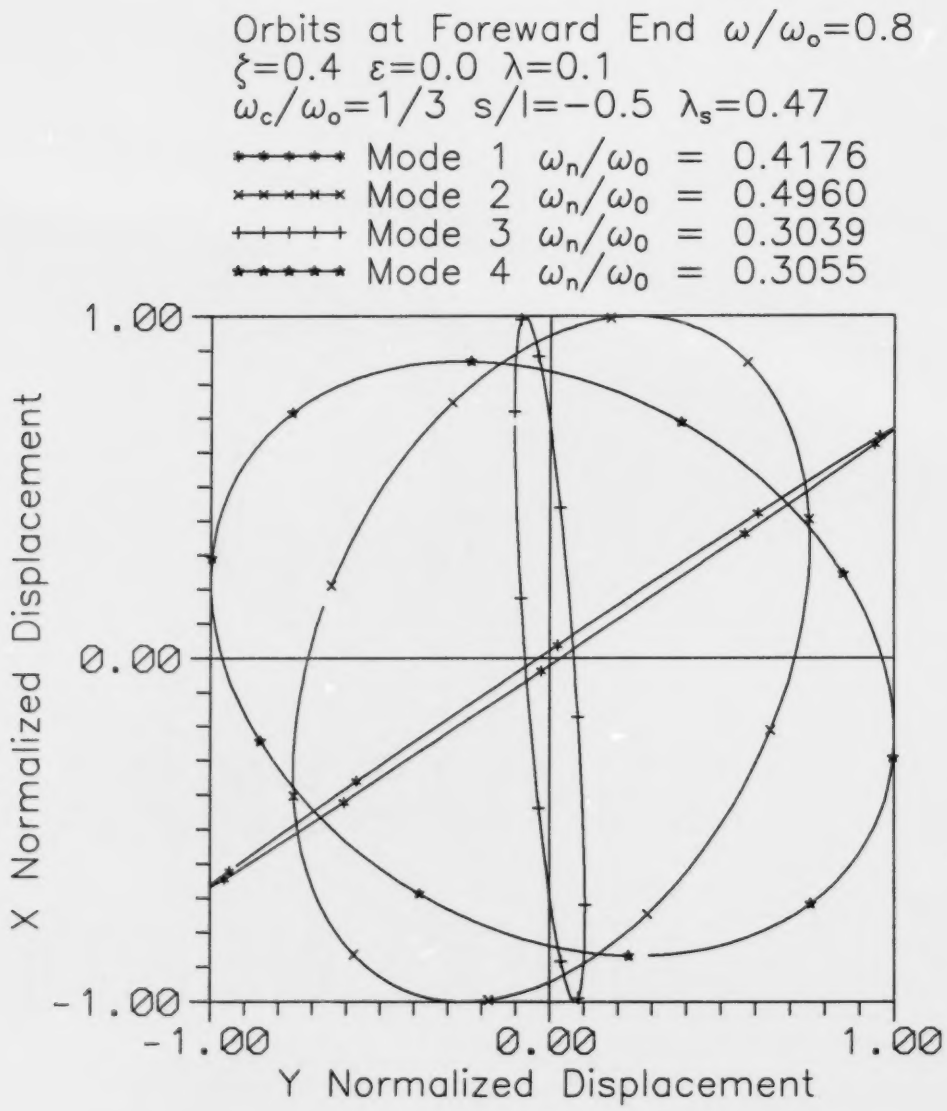

Figure 3.29: Modal Orbits at Forward End - S=0.8

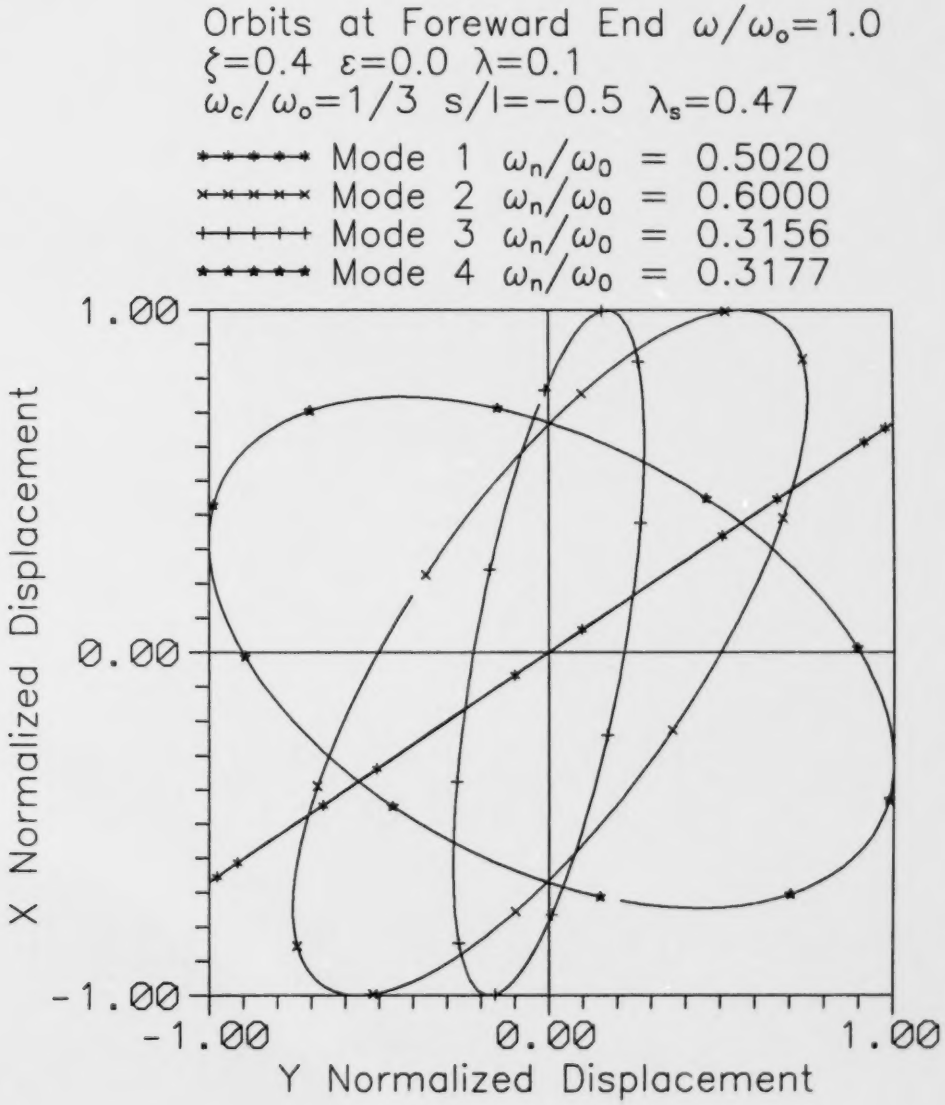

Figure 3.30: Modal Orbits at Forward End - S=1.0

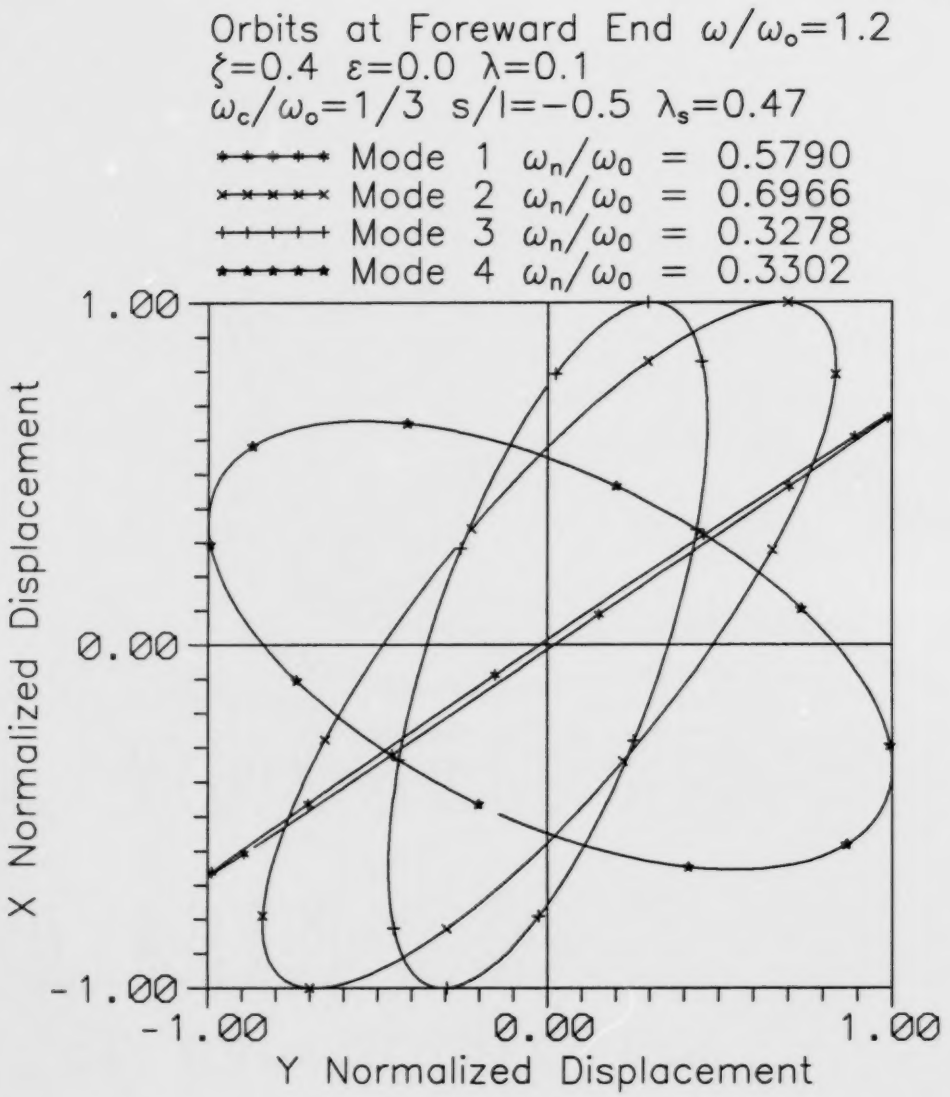

Figure 3.31: Modal Orbits at Forward End - S=1.2

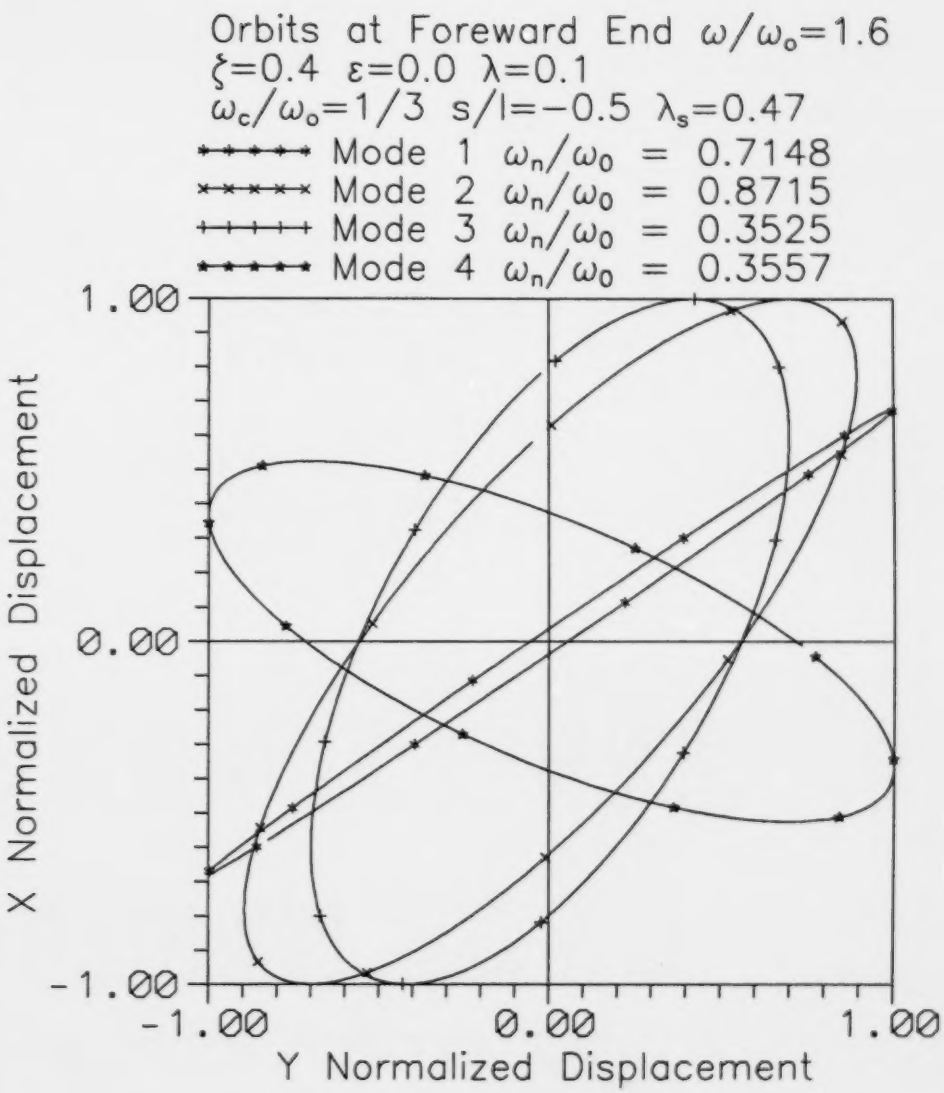

Figure 3.32: Modal Orbits at Forward End - S=1.6

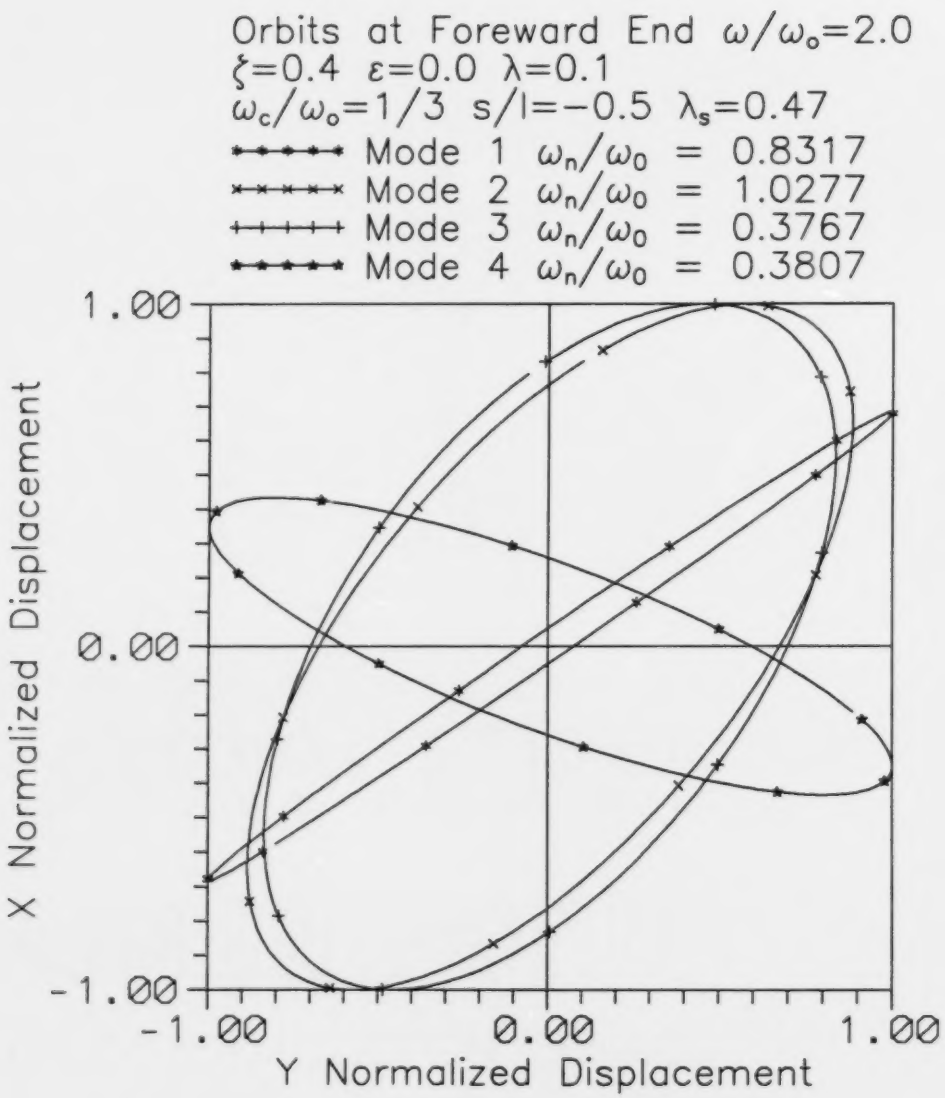

Figure 3.33: Modal Orbits at Forward End - S=2.0

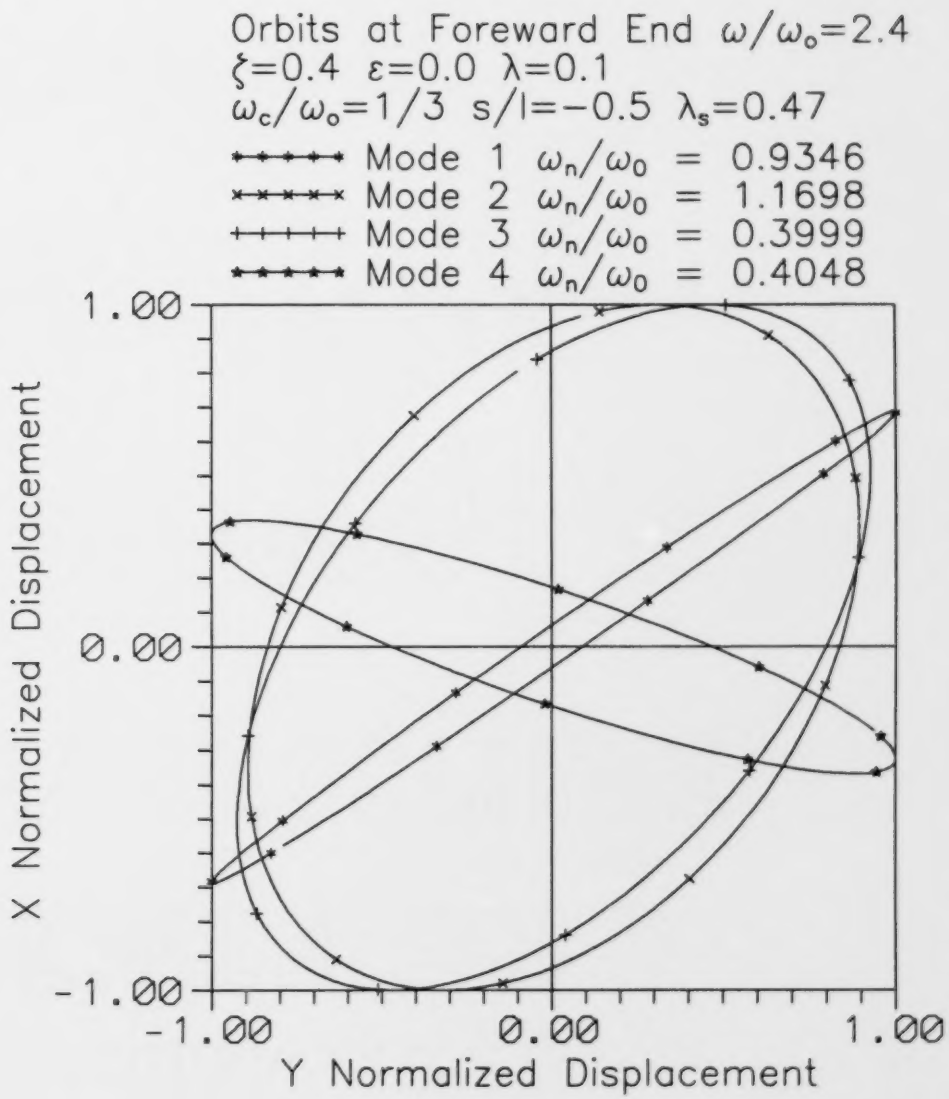

Figure 3.34: Modal Orbits at Forward End - S=2.4

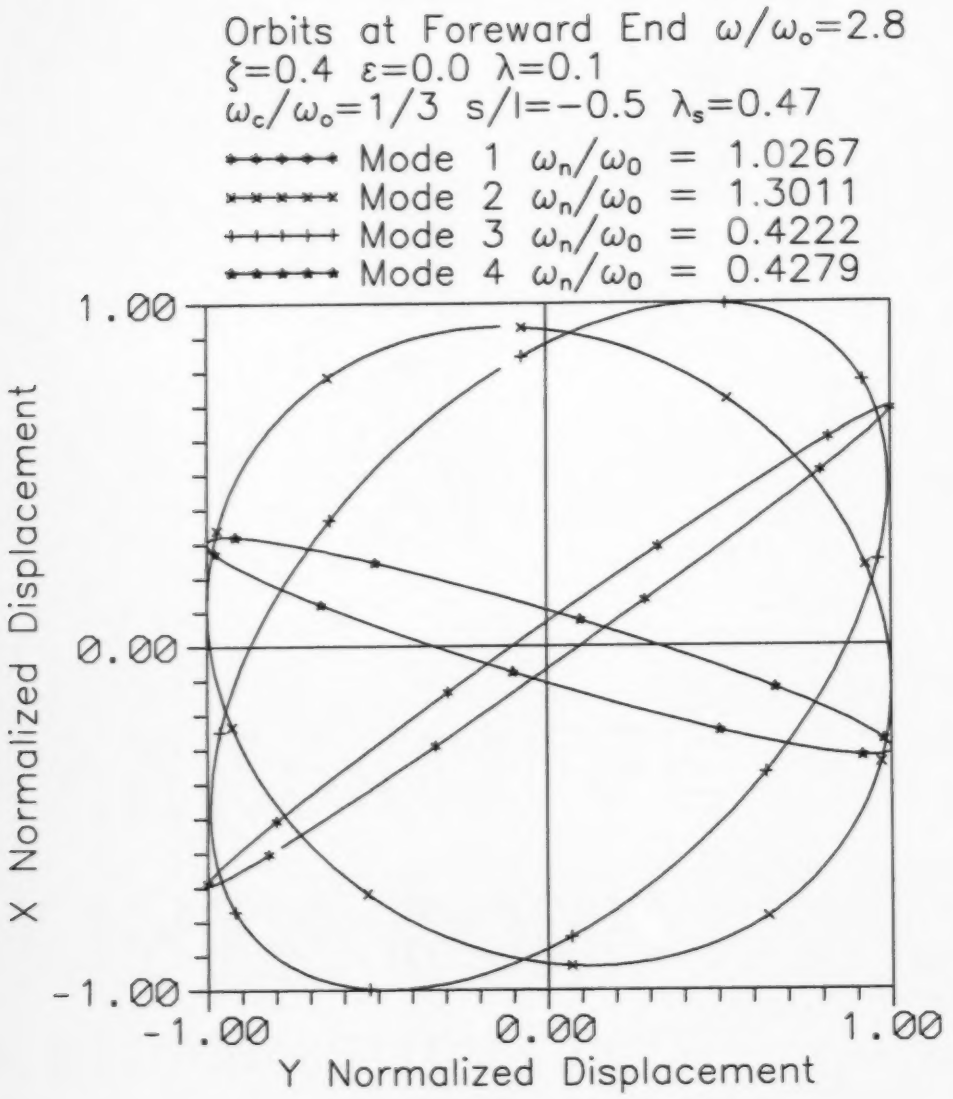

Figure 3.35: Modal Orbits at Forward End - S=2.8

Chapter 4

Flexible Shaft - Rotor

The rotors of most rotating machines are close to axi-symmetric, both in terms of their mass and stiffness properties. However, some industrial machines, for example, power generators, have non-axisymmetric stiffness because of a laminated structure. In addition, if a rotor incurs a crack, then the shaft - rotor stiffness will lose its symmetry. This causes changes in the dynamic behaviour of the machine and the study of this behaviour is of great importance in preventing catastrophic failures. Several commercial surveillance systems and diagnostic procedures are available at the present time dedicated to the detection of cracks through the change in dynamic behaviour.

In the two instances referred to above, the asymmetry in stiffness would not necessarily be accompanied by a mass asymmetry, except for any residual imbalance that is generally easily remedied.

As mentioned in the previous chapter, the behaviour of a non-symmetric rigid rotor was analyzed by P. Brosens in his Ph.D. thesis, [73] and Brosens and Crandall reported their analytical and experimental results in [76]. They showed that the mass asymmetry of a rigid rotor, will produce an unstable speed range around what would normally be the fundamental resonance or first 'critical speed'.

For a flexible shaft, Brosens and Crandall detected, both analytically and by experiment, additional regions of instability due to non-symmetric stiffness.

Bishop and Parkinson [77] also investigated analytically, the behaviour of rotors having some mass and stiffness asymmetry under the steady state load due to the weight of the rotor. Twice per revolution vibration due to asymmetric shaft flexibility is a well known phenomenon to rotating equipment engineers and has recently been used by Muszynska [78] to detect shaft cracks.

Bishop and Parkinson showed that the instability range is bounded approximately by the two critical speeds in each pair of modes. They state that this is due directly to the unequal stiffness. However it can also be due to unequal diametral mass moments of inertia alone, as shown by Brosens and this study. Other zones of instability were not reported by Bishop and Parkinson.

Stammers [74], derived a very similar model to that of Brosens and went on to use Floquet theory to permit the inclusion of cyclic stiffness coefficients due to non-symmetric support stiffnesses. This produced additional speed ranges of instability in the manner of Mathieu's equation.

The purpose of this chapter is to investigate further the stability characteristics of a non-axisymmetric flexible rotor - shaft assembly, using a finite element model, including shear deflection. The equations of motion are developed in a rotating coordinate frame of reference. The bearings are modelled as distributed springs rather than the point stiffness supports commonly used in calculating critical speeds of rotors. The bearings are assumed axisymmetric to avoid cyclic stiffness coefficients. The stability of this model is examined over a speed range typical for an industrial machine and the geometry is chosen to be representative of a typical rotor of an industrial machine.

4.1 Flexible Shaft - Rotor Element Development

4.1.1 Kinetic Energy

The angular momentum vector for a rotor - shaft finite element undergoing small angular displacements can be expressed in terms of the body-fixed moments of inertia, by carrying out three coordinate frame of reference rotations on the matrix of the inertia tensor of an infinitesimal disk section (see Figure 4.1):

$$\left\{ \begin{array}{c} H_x \\ H_y \end{array} \right\}^e = \omega\rho \int_0^l \left(\left[\begin{array}{cc} (J_{\xi\xi}\cos^2\tau + J_{\eta\eta}\sin^2\tau) & (J_{\xi\xi} - J_{\eta\eta})\sin\tau\cos\tau \\ (J_{\xi\xi} - J_{\eta\eta})\sin\tau\cos\tau & (J_{\xi\xi}\sin^2\tau + J_{\eta\eta}\cos^2\tau) \end{array} \right] \left\{ \begin{array}{c} \dot{\phi}_x \\ \dot{\phi}_y \end{array} \right\}^e \right.$$

$$\left. + \left[\begin{array}{cc} 0 & J_{\zeta\zeta} \\ -J_{\zeta\zeta} & 0 \end{array} \right] \left\{ \begin{array}{c} \phi_x \\ \phi_y \end{array} \right\}^e \right) dz, \qquad (4.1)$$

where $J_{\xi\xi}$, $J_{\eta\eta}$, $J_{\zeta\zeta}$ are the principal values of the second moment of area tensor of a section. We choose the coordinate system to coincide with the principal axes so that the cross-products of inertia are zero. The dot operator indicates differentiation with respect to non-dimensionalized time $\tau = \omega t$ where ω is rotation frequency and t is time, just as for the rigid rotor analysis.

The $\{\phi_x \quad \phi_y\}_e^T$ and $\{H_x \quad H_y\}_e^T$ vectors represent the section angular displacement and momentum respectively, referred to the inertial frame of reference. The material density is ρ and motion in the z direction is considered negligible. The 'e' subscript refers to the element.

The kinetic energy of the element, T_i^e, due to angular motion is then given in vector form by:

$$T_i^e = 1/2\ \mathbf{\Phi}^{\mathbf{a}}{}_{,t} \cdot \mathbf{H} = 1/2\omega\ \dot{\mathbf{\Phi}}^{\mathbf{a}} \cdot \mathbf{H} \tag{4.2}$$

where $\mathbf{\Phi}^{\mathbf{a}}{}_{,t}$ and $\mathbf{H}$ are the angular velocity and angular momentum vectors respectively. The 'a' superscript indicates that this vector contains components of angular motion only. In matrix form, this can be expressed as,

$$T_i^e = 1/2\omega \left\{\dot{\phi}^a\right\}^T \{H\}$$

where $\{\phi^a\} = \{\phi_x \quad \phi_y\}^{eT}$ and $\{H\} = \{H_x \quad H_y\}^T$

To express the kinetic energy in terms of coordinates in a rotating reference frame (Figure 4.2),

$$\begin{Bmatrix} \phi_x \\ \phi_y \end{Bmatrix} = \begin{bmatrix} \cos\tau & -\sin\tau \\ \sin\tau & \cos\tau \end{bmatrix} \begin{Bmatrix} \phi_\xi \\ \phi_\eta \end{Bmatrix} \tag{4.3}$$

where ϕ_ξ, ϕ_η are small angular displacements in the rotating coordinates. Making the coordinate transformation results in:

$$T_i^e = 1/2\omega^2\rho \int_0^l \begin{Bmatrix} \dot{\phi}_\xi & \dot{\phi}_\eta \end{Bmatrix} \begin{bmatrix} 0 & -J_{\xi\xi} \\ J_{\eta\eta} & 0 \end{bmatrix} \begin{Bmatrix} \phi_\xi \\ \phi_\eta \end{Bmatrix} +$$

$$\begin{Bmatrix} \phi_\xi & \phi_\eta \end{Bmatrix} \begin{bmatrix} J_{\eta\eta} & 0 \\ 0 & J_{\xi\xi} \end{bmatrix} \begin{Bmatrix} \phi_\xi \\ \phi_\eta \end{Bmatrix} + \begin{Bmatrix} \dot{\phi}_\xi & \dot{\phi}_\eta \end{Bmatrix} \begin{bmatrix} J_{\xi\xi} & 0 \\ 0 & J_{\eta\eta} \end{bmatrix} \begin{Bmatrix} \dot{\phi}_\xi \\ \dot{\phi}_\eta \end{Bmatrix}$$

$$+ \begin{Bmatrix} \phi_\xi & \phi_\eta \end{Bmatrix} \begin{bmatrix} 0 & J_{\eta\eta} \\ -J_{\xi\xi} & 0 \end{bmatrix} \begin{Bmatrix} \dot{\phi}_\xi \\ \dot{\phi}_\eta \end{Bmatrix} + \begin{Bmatrix} \dot{\phi}_\xi & \dot{\phi}_\eta \end{Bmatrix} \begin{bmatrix} 0 & J_{\zeta\zeta} \\ -J_{\zeta\zeta} & 0 \end{bmatrix} \begin{Bmatrix} \phi_\xi \\ \phi_\eta \end{Bmatrix}$$

$$+ \left\{ \phi_\xi \quad \phi_\eta \right\} \begin{bmatrix} -J_{\zeta\zeta} & 0 \\ 0 & -J_{\zeta\zeta} \end{bmatrix} \left\{ \begin{matrix} \phi_\xi \\ \phi_\eta \end{matrix} \right\} d\zeta. \tag{4.4}$$

Taking the first variation and ignoring second order terms:

$$\delta T_i^e = 1/2\omega^2\rho \int_0^l \left(\left\{ \delta\dot{\phi}_\xi \quad \delta\dot{\phi}_\eta \right\} \begin{bmatrix} 0 & -J_{\xi\xi} \\ J_{\eta\eta} & 0 \end{bmatrix} \left\{ \begin{matrix} \phi_\xi \\ \phi_\eta \end{matrix} \right\} +$$

$$\left\{ \dot{\phi}_\xi \quad \dot{\phi}_\eta \right\} \begin{bmatrix} 0 & -J_{\xi\xi} \\ J_{\eta\eta} & 0 \end{bmatrix} \left\{ \begin{matrix} \delta\phi_\xi \\ \delta\phi_\eta \end{matrix} \right\} + 2 \left\{ \delta\dot{\phi}_\xi \quad \delta\dot{\phi}_\eta \right\} \begin{bmatrix} J_{\xi\xi} & 0 \\ 0 & J_{\eta\eta} \end{bmatrix} \left\{ \begin{matrix} \dot{\phi}_\xi \\ \dot{\phi}_\eta \end{matrix} \right\} +$$

$$\left\{ \delta\phi_\xi \quad \delta\phi_\eta \right\} \begin{bmatrix} 0 & J_{\eta\eta} \\ -J_{\xi\xi} & 0 \end{bmatrix} \left\{ \begin{matrix} \dot{\phi}_\xi \\ \dot{\phi}_\eta \end{matrix} \right\} + \left\{ \phi_\xi \quad \phi_\eta \right\} \begin{bmatrix} 0 & J_{\eta\eta} \\ -J_{\xi\xi} & 0 \end{bmatrix} \left\{ \begin{matrix} \delta\dot{\phi}_\xi \\ \delta\dot{\phi}_\eta \end{matrix} \right\} +$$

$$\left\{ \delta\dot{\phi}_\xi \quad \delta\dot{\phi}_\eta \right\} \begin{bmatrix} 0 & J_{\zeta\zeta} \\ -J_{\zeta\zeta} & 0 \end{bmatrix} \left\{ \begin{matrix} \phi_\xi \\ \phi_\eta \end{matrix} \right\} + \left\{ \dot{\phi}_\xi \quad \dot{\phi}_\eta \right\} \begin{bmatrix} 0 & J_{\zeta\zeta} \\ -J_{\zeta\zeta} & 0 \end{bmatrix} \left\{ \begin{matrix} \delta\phi_\xi \\ \delta\phi_\eta \end{matrix} \right\} +$$

$$2 \left\{ \delta\phi_\xi \quad \delta\phi_\eta \right\} \begin{bmatrix} (J_{\eta\eta} - J_{\xi\xi}) & 0 \\ 0 & (J_{\xi\xi} - J_{\eta\eta}) \end{bmatrix} \left\{ \begin{matrix} \phi_\xi \\ \phi_\eta \end{matrix} \right\} \Bigg) d\zeta. \tag{4.5}$$

Similarly for the first variation of the kinetic energy due to linear motion, T_m^e we obtain:

$$\delta T_m^e = 1/2\omega^2\rho A \int_0^l \left(\left\{ \delta\dot{\xi} \quad \delta\dot{\eta} \right\} \left\{ \begin{matrix} \dot{\xi} \\ \dot{\eta} \end{matrix} \right\} + \left\{ \dot{\xi} \quad \dot{\eta} \right\} \left\{ \begin{matrix} \delta\dot{\xi} \\ \delta\dot{\eta} \end{matrix} \right\} +$$

$$\left\{ \delta\dot{\xi} \quad \delta\dot{\eta} \right\} \begin{bmatrix} 0 & -2 \\ 2 & 0 \end{bmatrix} \left\{ \begin{matrix} \xi \\ \eta \end{matrix} \right\} + \left\{ \dot{\xi} \quad \dot{\eta} \right\} \begin{bmatrix} 0 & -2 \\ 2 & 0 \end{bmatrix} \left\{ \begin{matrix} \delta\xi \\ \delta\eta \end{matrix} \right\} +$$

$$\left\{ \delta\xi \quad \delta\eta \right\} \left\{ \begin{matrix} \xi \\ \eta \end{matrix} \right\} + \left\{ \xi \quad \eta \right\} \left\{ \begin{matrix} \delta\xi \\ \delta\eta \end{matrix} \right\} \Bigg) d\zeta, \tag{4.6}$$

where A is the area of the cross section. The first variation of the total kinetic energy can then be expressed as:

$$\delta T^e = \omega^2\rho \int_0^l \left\{\delta\dot{\phi}\right\}^T [m] \left\{\dot{\phi}\right\} + 1/2 \left\{\delta\dot{\phi}\right\}^T [g] \{\phi\} +$$

$$1/2\,\{\delta\phi\}^T\,[g]^T\left\{\dot{\phi}\right\} + \{\delta\phi\}^T\,[y]\,\{\phi\}\,d\zeta \tag{4.7}$$

where:

$$[m] = \text{Diag}\left\{\begin{array}{cccc} A & A & J_{\xi\xi} & J_{\eta\eta}\end{array}\right\}$$

$$\{\phi\}^T = \left\{\begin{array}{cccc} \xi & \eta & \phi_\xi & \phi_\eta\end{array}\right\}$$

$$[g] = \begin{bmatrix} 0 & -2A & 0 & 0 \\ 2A & 0 & 0 & 0 \\ 0 & 0 & 0 & (-2J_{\xi\xi} + J_{\zeta\zeta}) \\ 0 & 0 & (2J_{\eta\eta} - J_{\zeta\zeta}) & 0 \end{bmatrix}$$

$$[y] = \text{Diag}\left\{\begin{array}{cccc} A & A & (J_{\eta\eta} - J_{\zeta\zeta}) & (J_{\xi\xi} - J_{\zeta\zeta})\end{array}\right\}.$$

For the finite element method we assume that the vector $\{\phi\}$ at any location within the element can be expressed in terms of the vectors at the nodes of the element $\{\Phi^e\}$:

$$\{\phi\} = [N]^T\,\{\Phi^e\}$$

where $[N]^T$ is the shape function or 'Cardinal basis' as Baker [79] refers to it, and

$$\{\Phi^e\}^T = \left\{\begin{array}{cccccccc} \xi_1 & \eta_1 & \phi_{\xi_1} & \phi_{\eta_1} & \xi_2 & \eta_2 & \phi_{\xi_2} & \phi_{\eta_2}\end{array}\right\}.$$

Using cubic polynomial interpolation functions and the method of Davis, Henshell and Warburton [80], which assumes a constant shear slope along an element, we can write:

$$[N]^T = [B]^T\,[T] \tag{4.8}$$

where:

$$[B]^T = \begin{bmatrix} \zeta^3/6 & \zeta^2/2 & \zeta & 1 & 0 & 0 & 0 & 0 \\ 0 & 0 & 0 & 0 & \zeta^3/6 & \zeta^2/2 & \zeta & 1 \\ 0 & 0 & 0 & 0 & (\zeta^2/2 + \beta_\xi) & \zeta & 1 & 0 \\ (\zeta^2/2 + \beta_\eta) & \zeta & 1 & 0 & 0 & 0 & 0 & 0 \end{bmatrix} \tag{4.9}$$

and

$$[T] = \text{Diag}\left\{\begin{array}{cccc} l(l^2 + 12\beta_\eta) & l(l^2 + 12\beta_\eta) & l(l^2 + 12\beta_\eta) & l(l^2 + 12\beta_\eta) \\ l(l^2 + 12\beta_\xi) & l(l^2 + 12\beta_\xi) & l(l^2 + 12\beta_\xi) & l(l^2 + 12\beta_\xi)\end{array}\right\}^{-1} \times$$

$$\begin{bmatrix} 12 & 0 & 0 & 6l \\ -6l & 0 & 0 & (-4l^2 - 12\beta_\eta) \\ -12\beta_\eta & 0 & 0 & (l^3 + 6\beta_\eta l) \\ l(l^2 + 12\beta_\eta) & 0 & 0 & 0 \\ 0 & 12 & 6l & 0 \\ 0 & -6l & (-4l^2 - 12\beta_\xi) & 0 \\ 0 & -12\beta_\xi & (l^3 + 6\beta_\xi l) & 0 \\ 0 & l(l^2 + 12\beta_\xi) & 0 & 0 \end{bmatrix}$$

$$\begin{bmatrix} -12 & 0 & 0 & 6l \\ 6l & 0 & 0 & (-2l^2 + 12\beta_\eta) \\ 12\beta_\eta & 0 & 0 & -6\beta_\eta l \\ 0 & 0 & 0 & 0 \\ 0 & -12 & 6l & 0 \\ 0 & 6l & (-2l^2 + 12\beta_\xi) & 0 \\ 0 & 12\beta_\xi & -6\beta_\xi l & 0 \\ 0 & 0 & 0 & 0 \end{bmatrix}, \tag{4.10}$$

where $\beta_\xi = E J_{\xi\xi}/\mathcal{K}GA$, $\beta_\eta = E J_{\eta\eta}/\mathcal{K}GA$ and E is Young's modulus, G is the shear modulus and $\mathcal{K}$ is the section shape factor.

We have,

$$\{\phi\} = [N]^T \{\Phi^e\} = [B]^T [T] \{\Phi^e\}$$

$$\{\delta\phi\} = [B]^T [T] \{\delta\Phi^e\}$$

$$\left\{\dot{\phi}\right\} = [B]^T [T] \left\{\dot{\Phi}^e\right\}$$

$$\left\{\delta\dot{\phi}\right\} = [B]^T [T] \left\{\delta\dot{\Phi}^e\right\}.$$

Thus the first variation of the finite element approximation of the kinetic energy can be written,

$$\delta T^e = \omega^2 \left\{\delta\dot{\Phi}^e\right\}^T [M^e] \left\{\dot{\Phi}^e\right\} + 1/2\omega^2 \left\{\delta\dot{\Phi}^e\right\}^T [G^{e*}] \{\Phi^e\} +$$

$$1/2\omega^2 \{\delta\Phi^e\}^T [G^{e*}]^T \left\{\dot{\Phi}^e\right\} + \omega^2 \{\delta\Phi^e\}^T [Y^e] \{\Phi^e\} \tag{4.11}$$

with the coefficient matrices defined as,

$$[M^e] = \int_0^l \rho[T]^T[B][m][B]^T[T]\, d\zeta$$

$$[G^{e*}] = \int_0^l \rho[T]^T[B][g][B]^T[T]\,d\zeta$$

$$[Y^e] = \int_0^l \rho[T]^T[B][y][B]^T[T]\,d\zeta.$$

$[M^e]$ is the element mass and inertia matrix, i.e. the inertia force contribution to the element kinetic energy. The $[G^{e*}]$ term and its transpose, contain the Coriolis and gyroscopic force and moment contributions respectively, and the $[Y^e]$ represents the 'centrifugal force' contribution, which behaves like a stiffness term in the rotating frame of reference.

4.1.2 Strain Energy

The strain energy of an element undergoing bending and shear deflection can be expressed as:

$$U^e = 1/2\int_0^l \left[EJ_{\eta\eta}\left(d^2\xi_B/d\zeta^2\right)^2 + EJ_{\xi\xi}\left(d^2\eta_B/d\zeta^2\right)^2 + \mathcal{K}G\psi_\eta^2 + \mathcal{K}G\psi_\xi^2\right]d\zeta, \tag{4.12}$$

where ψ_η and ψ_ξ are the shear slopes and ξ and η are chosen to be the section principal axes. This can be written in matrix form as:

$$U^e = 1/2\int_0^l \left[E\left\{\begin{array}{cc}\xi_B'' & \eta_B''\end{array}\right\}\left[\begin{array}{cc}J_{\eta\eta} & 0\\ 0 & J_{\xi\xi}\end{array}\right]\left\{\begin{array}{c}\xi_B''\\ \eta_B''\end{array}\right\} + \mathcal{K}G\left\{\begin{array}{cc}\psi_\xi & \psi_\eta\end{array}\right\}\left\{\begin{array}{c}\psi_\xi\\ \psi_\eta\end{array}\right\}\right]d\zeta, \tag{4.13}$$

where the prime indicates differentiation with respect to ζ and the subscript 'B' refers to the bending component of the angular motion. The shear slopes can be expressed in terms of the total slope and the slope of the neutral axis due to bending, (see Figure 4.3). The upper figure shows the relation between these three slopes for deflection in the ξ, ζ plane, and the lower figure for the η, ζ plane. The shear slopes are ψ_ξ and ψ_η; the slopes of the neutral axis ξ' and η' and the bending slopes ϕ_ξ and ϕ_η. The relations are then,

$$\psi_\xi = \phi_\xi - \eta' \text{ and } \psi_\eta = \phi_\eta - \xi'/;.$$

Substituting these expressions and the cubic polynomial interpolation functions we obtain the finite element approximation of the element strain energy:

$$U^e = 1/2\,\{\Phi^e\}^T \int_0^l E\,[T]^T\,[B'']\,[i]\,[B'']^T\,[T] + \mathcal{K}G\,[T]^T\,[C]\,[C]^T\,d\zeta\,\{\Phi^e\} \qquad (4.14)$$

$$\text{with,} \qquad [i] = \text{Diag}\left\{\, J_{\eta\eta} \;\; J_{\xi\xi} \;\; 0 \;\; 0 \,\right\}$$

$$[C]\,[C]^T = \text{Diag}\left\{\, \beta_\eta^2 \;\; 0 \;\; 0 \;\; 0 \;\; \beta_\xi^2 \;\; 0 \;\; 0 \;\; 0 \,\right\}.$$

The first variation of the strain energy of an element then becomes,

$$\delta U^e = \{\delta\Phi^e\}^T\,[K^e]\,\{\Phi^e\} \qquad (4.15)$$

with the consistent element stiffness matrix $[K_e]$ given by,

$$[K^e] = \int_0^l E\,[T]^T\,[B'']\,[i]\,[B'']^T\,[T] + \mathcal{K}G\,[T]^T\,[C]\,[C]^T\,[T]\,d\zeta. \qquad (4.16)$$

4.1.3 Distributed Bearing Stiffness

For the purposes of this study, bearing stiffness matrix per unit length $[k_b]$ is assumed where:

$$[k_b] = \begin{bmatrix} k_{\xi\xi} & k_{\xi\eta} \\ k_{\eta\xi} & k_{\eta\eta} \end{bmatrix}.$$

The cross terms are not necessarily equal. For a cylindrical sleeve bearing the $k_{\xi\eta}$

and $k_{\eta\xi}$ are often taken to be of equal magnitude and opposite sign due to Coriolis acceleration in the fluid film. For this paper these cross terms are taken to be zero as they would typically be for tilting pad bearings which are now more the rule than the exception for high speed turbomachinery in the oil and petrochemical industries.

Using the principle of virtual work, the work done on the rotor by the bearing is,

$$\delta W_b = -\int_0^l \left\{ \begin{array}{cccc} \delta\xi & \delta\eta & \delta\phi_\xi & \delta\phi_\eta \end{array} \right\} \left[\begin{array}{cccc} k_{\xi\xi} & 0 & 0 & 0 \\ 0 & k_{\eta\eta} & 0 & 0 \\ 0 & 0 & 0 & 0 \\ 0 & 0 & 0 & 0 \end{array} \right] \left\{ \begin{array}{c} \xi \\ \eta \\ \phi_\xi \\ \phi_\eta \end{array} \right\} d\zeta. \qquad (4.17)$$

Then making the finite element approximation we have,

$$\delta W_b = -\{\delta\Phi^e\}^T [K_b^e] \{\Phi^e\}. \qquad (4.18)$$

The distributed bearing stiffness matrix $[K_b^e]$ is given by,

$$[K_b^e] = \int_0^l [T]^T [B] [k_b] [B]^T [T] \, d\zeta.$$

4.1.4 Hamilton's Principle

As bearing circulatory terms and damping are not included in the present study, the forces applied to the rotor by the bearing fluid are conservative. Hamilton's principle may therefore be applied in its original, conservative form.

$$\int_{t_1}^{t_2} \delta(\mathcal{T} - V)\, dt + \int_{t_1}^{t_2} \delta W_b \, dt = 0 \qquad (4.19)$$

where $\mathcal{T}$ and V are kinetic and potential energies respectively and W_b is the work done on the system by the bearing forces.

Therefore for the rotor element we have,

$$\delta \int_{t_1}^{t_2} [\mathcal{T}^e - U^e + W_b^e]\, dt = 0 \qquad (4.20)$$

and in terms of the finite element approximation and non - dimensional time τ,

$$\int_{\tau_1}^{\tau_2} \left[\omega^2 \left\{\delta\dot{\Phi}^e\right\} [M^e] \left\{\dot{\Phi}^e\right\} + 1/2\omega^2 \left\{\delta\dot{\Phi}^e\right\}^T [Ge^*] \{\Phi^e\} + 1/2\omega^2 \{\delta\Phi^e\}^T [G^{e*}]^T \left\{\dot{\Phi}^e\right\}\right.$$

$$\left. + \omega^2 \{\delta\Phi^e\}^T [Y^e] \{\Phi^e\} - \{\delta\Phi^e\}^T [[K^e] + [K_b^e]] \{\Phi^e\}\right] d\tau = 0. \qquad (4.21)$$

Integrating by parts and noting that $\{\delta\Phi^e\} = 0$ at $\tau = \tau_1$ and $\tau = \tau_2$ we get the finite element approximation to the equation of motion for the element:

$$\omega^2 [M^e] \left\{\ddot{\Phi}^e\right\} + \omega^2 [G^e] \left\{\dot{\Phi}^e\right\} + \left[[K^e] + [K_b^e] - \omega^2 [Y^e]\right] \{\Phi^e\} = 0. \qquad (4.22)$$

The 'Coriolis / gyroscopic' matrix $[G^e]$ is defined by,

$$[G^e] = 1/2 \left[[G^{e*}] - [G^{e*}]^T\right].$$

The element equations can now be assembled into a global set of equations for the rotor - shaft bearing system, using the subscript 'g' to indicate coefficient matrices for the global system.

$$\omega^2 [M_g] \left\{\ddot{\Phi}_g\right\} + \omega^2 [G_g] \left\{\dot{\Phi}_g\right\} + \left[[K_g] + \left[K_g^b\right] - \omega^2 [Y_g]\right] \{\Phi_g\} = 0. \qquad (4.23)$$

Letting $\left\{\dot{\Phi}_g\right\} = \{\Psi_g\}$ Equation 4.23 becomes,

$$\begin{Bmatrix} \dot{\Psi}_g \\ \\ \dot{\Phi}_g \end{Bmatrix} = \begin{bmatrix} -[M_g]^{-1}[G_g] & \left([M_g]^{-1}[Y_g] - \omega^{-2}[M_g]^{-1}\left[[K_g] + \left[K_g^b\right]\right]\right) \\ \\ [I] & [0] \end{bmatrix} \begin{Bmatrix} \Psi_g \\ \\ \Phi_g \end{Bmatrix}. \qquad (4.24)$$

Referring to the large matrix of Equation 4.24 as $[A]$ and assuming a solution of the form,

$$\begin{Bmatrix} \Psi_g \\ \Phi_g \end{Bmatrix} = \begin{Bmatrix} \Psi_g \\ \Phi_g \end{Bmatrix}_0 e^{\frac{\lambda}{\omega}\tau} \qquad (4.25)$$

we obtain:

$$\left[[A] - \left(\frac{\lambda}{\omega}\right)[I]\right] \begin{Bmatrix} \Psi_g \\ \Phi_g \end{Bmatrix}_0 = 0. \qquad (4.26)$$

This is an eigenvalue equation of the general (non-symmetric, non skew-symmetric) form.

The lengthy matrix multiplications and integrations over the element length were carried out analytically using the 'Mathematica' computer code by S. Wolfram [81]. Then the 'QR' method of J.H. Wilkinson [75] was used to solve the general eigenvalue problem for the complex roots and the eigenvectors were subsequently derived by an adaptation of the gaussian elimination method to complex eigenvalues and vectors - see Appendix A. The code was written in Fortran and the analyses carried out on both an IBM 6000 computer and on a personal computer with an 80486-25 MHz processor. The details of the coefficient matrices are set out in Appendix B

4.2 Results

4.2.1 Distributed Bearing Stiffness

The plots in Figure 4.4 show the first two shaft - rotor natural frequencies at zero RPM rotor speed for varying bearing stiffness. The bearings were taken to be identical and axi-symmetric, with zero cross-coupling terms, but the stiffnesses were represented as distributed along the length of the bearings. Bending only was considered.

There are two inflections in these curves. The lowest frequency region, below the first inflection, is dominated by the support stiffness which is much lower than the rotor - shaft stiffness. Above the first inflection, where the distributed bearing stiffness is low enough to allow rotation but high enough that there is some shaft - rotor flexing, the modal frequencies are close to those for a simply supported beam, (the dotted lines). Above the second inflection, for high distributed support stiffness, the natural frequencies are asymptotic to those for a clamped - clamped beam, (the solid lines).

These curves were produced for a mathematical model with bearings having a length to diameter ratio (L/D) of 1.0. Even with an L/D of 1.0, it is evidently preferable to use a distributed bearing stiffness rather than point supports. For a uniform rotor - shaft with stiff bearings, it was found that seven elements produced modal frequencies with 0.3% error in the third mode compared with the analytical solution for a clamped - clamped beam and better for the lower modes. This was considered sufficiently accurate.

4.2.2 Stability Analysis

Figure 4.5 shows the geometry of the shaft - rotor bearing system analyzed in this section for three cases. The shaft is considered to be uniform with a central rotor in all three cases. In the first case (Figures 4.6 and 4.7) the central rotor was assumed to have non - axisymmetric diametral mass moments of inertia and asymmetric stiffness but shear deflection was not included. For the second case, (Figures 4.8 and 4.9) shear deflection was included with non-axisymmetric diametral mass and stiffness moments of inertia (i.e. same as Figures 4.6 and 4.7 plus shear). Finally, (Figures 4.10 and 4.11), the shear deflection was included and the non-axisymmetric mass moments of inertia but symmetric stiffness was assumed. The bearing stiffnesses per unit length were the same for all three cases, $0.5.10^9$ N/m/m. For each case the analysis was carried out in the rotating frame of reference and then the same data was converted to the inertial reference frame which is more readily understood. In order to make this conversion the following rule applies.

For a forward precessing mode,

$$f_{in} = f_{rot} + N, \tag{4.27}$$

where f_{in}, f_{rot} are the natural frequencies in the inertial and rotating frames respectively and N is the rotation speed.

For a backward precessing mode,

$$f_{in} = f_{rot} - N. \tag{4.28}$$

The first four pairs of modes only, were plotted as higher modes are rarely of significance in industrial machinery. In all Figures 4.6 to 4.11 the first and third pairs of modes have symmetric mode shapes about the mid point of the rotor - shaft system, and the second and fourth have antisymmetric mode shapes. The antisymmetric modes diverge with speed much more than do the symmetric modes due to the gyroscopic effect.

The eigenvalues, occur as complex conjugates. For the system analyzed here, with no damping but with gyroscopic and Coriolis coefficients, the eigenvalues are, in general either purely imaginary or purely real (with a significant exception described later). Therefore we always have a positive and negative value of the frequency part of the eigenvalue. To determine which roots have physical meaning, we convert these frequencies to the inertial frame according to the above rule and retain only those having positive values. The negative frequencies have no physical meaning in the inertial frame.

For all of the three cases, the same type of unstable speed region around the fundamental resonance occurs as for the rigid rotor case. The analysis was carried out for speed increments of 10 RPM around the region boundaries. Examination of the computer output shows that for Figures 4.6 and 4.7 this is between 8340 and 8610 RPM. The imaginary part of the eigenvalue, in the rotating frame stays at zero while the real part (not plotted) becomes non zero (positive and negative values). For the inertial frame plot this means that over this speed range the frequency of the unstable mode coincides with or 'tracks' rotation speed. In practice, with the damping usually present, this means that the first 'critical speed' would be a little broader range of speeds than for an axisymmetric rotor. The finite element model therefore satisfactorily demonstrates this effect for a fairly practical flexible rotor.

The results for Figures 4.6, 4.7 and Figures 4.10, 4.11 are very similar with respect to the synchronous instability just described. However, the behaviour of, what start off at low speeds, as the fourth backward and second forward modes is interesting. These two modal frequencies approach each other at between 7700 - 7800 RPM, as indicated in Figure 4.10 but do not cross. If the eigenvectors are examined for a particular axial point on the rotor around this speed range, it can be seen, that the direction of precession changes at the point of closest approach. This change of precession direction has to be taken into account when deducing the inertial frame plots. Indeed, if this change were not taking place then one would arrive at a negative frequency in the inertial frame for the second forward mode.

Bishop and Johnson [82] showed that when two modal frequencies are close but not coincident, that cross-coupling damping coefficients cause the frequencies to move closer together by an amount proportional to the product of the two cross-coupling coefficients. In their case these coefficients were assumed equal. In the present analysis, the cross terms are Coriolis and gyroscopic and are therefore skew. Hence the product of these two coefficients would be negative and following the reasoning of Bishop and Johnson, close frequencies would tend to move apart due to gyroscopic and Coriolis coupling.

When asymmetry of the diametral moment of inertia for stiffness is permitted in addition to the mass asymmetry and shear deflection, then we get the results of Figures 4.8 and 4.9. In addition to the unstable speed region when the second forward precessing mode coalesces with rotation speed (zero in the rotating frame), we have two additional regions of instability. These involve coalescence between the first backward and third forward modes and between the second forward and fourth backward modes (and higher order combinations outside the bounds of the plot). These instabilities do not occur if gyroscopic and Coriolis effects are ignored, and occur over a much smaller speed range if only gyroscopic effects are ignored, i.e. the coupling mechanism between the modes is the gyroscopic and, to a lesser degree due to the Coriolis forces. Removing the mass asymmetry does not eliminate the instability. The necessary conditions for this behaviour appear to be stiffness asymmetry and shear deflection.

Frequency coalescence of these pairs of forward and backward modes in the rotating frame means that their frequencies in the inertial frame differ by two times rotation speed.

Figure 4.12 is a plot of the regions of instability for the system analyzed here for various values of stiffness asymmetry and speed. The instability around the fundamental resonance is not shown. Figure 4.13 shows the modal frequencies versus speed for the case of $q = 0.45$.

There are five regions of instability on these two plots. The first occurs when the first backward mode coalesces (couples) with the third forward mode; the second when the second backward and fourth forward modes coalesce and the third when the third backward and fifth forward modes coalesce. The fourth and fifth instabilities are rather complex in nature. After the fifth forward and third backward modes couple, one of the two resulting modes couples with the first forward mode and the other with the second forward mode. Thus the broad area of instability centred around 26000 RPM, (fifth area) Figure 4.12 involves the first backward mode becoming unstable for a second time as the speed is increased. It will be shown in a subsequent chapter that the left boundary of this fifth area of instability meets the right boundary of the first area of instability.

The rotor - shaft system for these plots had axisymmetric mass moments of inerta but the stiffness 2nd. moments of area were made different while maintaining a constant mean 2nd. moment of area, i.e. $J_{\xi\xi} + J_{\eta\eta}$ was constant for varying $J_{\xi\xi} - J_{\eta\eta}$ and the dimensionless variable q was defined as the ratio of the difference to the mean 2nd. moment of area.

4.3 Uniform Flexible Non-Axisymmetric Rotor, Exact Solution

To more fully understand the results of the finite element analysis, it is useful to investigate the behaviour of a simpler system for which an exact solution can be derived. If we consider a uniform, non - axisymmetric shaft - rotor, supported by two bearings with axisymmetric stiffness, see Figure 4.14 then using the variational calculus and Hamilton's principle, the differential equations of motion for such a system are:

$$\omega^2\rho\begin{bmatrix} A & 0 & 0 & 0 \\ 0 & A & 0 & 0 \\ 0 & 0 & J_{\xi\xi} & 0 \\ 0 & 0 & 0 & J_{\eta\eta} \end{bmatrix}\begin{Bmatrix} \ddot{\xi} \\ \ddot{\eta} \\ \ddot{\phi}_\xi \\ \ddot{\phi}_\eta \end{Bmatrix} - \omega^2\rho\begin{bmatrix} 0 & 2A & 0 & 0 \\ -2A & 0 & 0 & 0 \\ 0 & 0 & 0 & (J_{\eta\eta}+J_{\xi\xi}-J_{\zeta\zeta}) \\ 0 & 0 & -(J_{\eta\eta}+J_{\xi\xi}-J_{\zeta\zeta}) & 0 \end{bmatrix}\begin{Bmatrix} \dot{\xi} \\ \dot{\eta} \\ \dot{\phi}_\xi \\ \dot{\phi}_\eta \end{Bmatrix}$$

$$+\left[\mathcal{K}GA\begin{bmatrix} 0 & 0 & 0 & 0 \\ 0 & 0 & 0 & 0 \\ 0 & 0 & 1 & 0 \\ 0 & 0 & 0 & 1 \end{bmatrix} - \omega^2\rho\begin{bmatrix} A & 0 & 0 & 0 \\ 0 & A & 0 & 0 \\ 0 & 0 & (J_{\eta\eta}-J_{\zeta\zeta}) & 0 \\ 0 & 0 & 0 & (J_{\xi\xi}-J_{\zeta\zeta}) \end{bmatrix}\right]\begin{Bmatrix} \xi \\ \eta \\ \phi_\xi \\ \phi_\eta \end{Bmatrix}$$

$$= \begin{bmatrix} \mathcal{K}GA & 0 & 0 & 0 \\ 0 & \mathcal{K}GA & 0 & 0 \\ 0 & 0 & EJ_{\xi\xi} & 0 \\ 0 & 0 & 0 & EJ_{\eta\eta} \end{bmatrix}\begin{Bmatrix} \xi'' \\ \eta'' \\ \phi''_\xi \\ \phi''_\eta \end{Bmatrix} - \mathcal{K}GA\begin{bmatrix} 0 & 0 & 0 & 1 \\ 0 & 0 & 1 & 0 \\ 0 & -1 & 0 & 0 \\ -1 & 0 & 0 & 0 \end{bmatrix}\begin{Bmatrix} \xi' \\ \eta' \\ \phi'_\xi \\ \phi'_\eta \end{Bmatrix}, \tag{4.29}$$

where the dot operator means differentiation with respect to non dimensional time $\tau = \omega t$, the prime means differentiation with respect to axial distance ζ and the variables have the same meaning as in the numerical analyses.

The boundary conditions which the variational approach produces are,

$$-E\begin{bmatrix} 0 & 0 & 0 & 0 \\ 0 & 0 & 0 & 0 \\ 0 & 0 & J_{\xi\xi} & 0 \\ 0 & 0 & 0 & J_{\eta\eta} \end{bmatrix}\begin{Bmatrix} \xi' \\ \eta' \\ \phi'_\xi \\ \phi'_\eta \end{Bmatrix}\Bigg|_o^l - \mathcal{K}GA\begin{bmatrix} 1 & 0 & 0 & 0 \\ 0 & 1 & 0 & 0 \\ 0 & 0 & 0 & 0 \\ 0 & 0 & 0 & 0 \end{bmatrix}\begin{Bmatrix} \xi' \\ \eta' \\ \phi'_\xi \\ \phi'_\eta \end{Bmatrix}\Bigg|_o^l$$

$$+\begin{bmatrix} K_1^b & 0 & 0 & 0 \\ 0 & K_1^b & 0 & 0 \\ 0 & 0 & 0 & 0 \\ 0 & 0 & 0 & 0 \end{bmatrix}\begin{Bmatrix} \xi \\ \eta \\ \phi_\xi \\ \phi_\eta \end{Bmatrix}_{\zeta=0} + \begin{bmatrix} K_2^b & 0 & 0 & 0 \\ 0 & K_2^b & 0 & 0 \\ 0 & 0 & 0 & 0 \\ 0 & 0 & 0 & 0 \end{bmatrix}\begin{Bmatrix} \xi \\ \eta \\ \phi_\xi \\ \phi_\eta \end{Bmatrix}_{\zeta=l} = 0. \quad (4.30)$$

The first term in Equation 4.30 represents the bending moments at the ends of the rotor which are zero for the configuration under consideration. The other terms represent the shear forces and the bearing spring forces for bearings with stiffnesses K_1^b and K_2^b at the ends of the rotor, which cancel each other.

To investigate the stability of the Differential Equation 4.29, about a position of equilibrium, we can set the right hand side to zero. This results in two pairs of ordinary differential equations. The first pair has no stiffness terms, representing only a balance of inertia, Coriolis and centrifugal forces. If we non-dimensionalize the second pair of equations in the same way as for the numerical studies, then using the same notation we get,

$$(1+\delta)\ddot{\phi}_\xi - (2-\lambda)\dot{\phi}_\eta + \left[\frac{\mathcal{K}GA}{\omega^2\rho} + \lambda - 1 + \delta\right]\phi_\xi = 0 \quad (4.31)$$

$$(1-\delta)\ddot{\phi}_\eta + (2-\lambda)\dot{\phi}_\xi + \left[\frac{\mathcal{K}GA}{\omega^2\rho} + \lambda - 1 - \delta\right]\phi_\xi = 0. \quad (4.32)$$

This is of identical form to Gladwell and Stammers' [83] equations for a rigid non-axisymmetric rotor supported by axisymmetric bearings.

It was shown in [83] that for a system represented by such equations of motion in a rotating reference frame, (but with coefficients cyclic at 2ω in the inertial frame), there are two types of unstable region. The first is where rotation speed is between the two 'critical speeds' corresponding to the fundamental resonance as described above. In addition there are two points of limiting stability for each set of λ and δ; i.e. two values of $\mathcal{K}GA/(\omega^2\rho)$ when two eigenvalues coincide (in the rotating frame).

This is precisely the result obtained in the finite element analysis. It is also clear from Equations 4.31 and 4.32, that this result will only be obtained, if δ is non zero, i.e. a non-axisymmetric rotor, and if there are both non - zero gyroscopic and shear terms. These are also the conditions which appeared necessary in the numerical study.

4.4 Discussion

The finite element analysis and computer code described in this chapter predict the type of instability regions for a non-axisymmetric flexible shaft - rotor supported by distributed bearings, similar to the results of analytical studies on rigid rotors and simple flexible rotor systems. That is instability occurs in regions of rotation speeds around the fundamental resonances of the rotor system and when the difference in frequency between modes is a multiple of twice rotation speed in the inertial frame of reference. This latter type of instability only occurs, when both gyroscopic terms and shear deflection are included.

On a practical level, the question arises as to whether such instabilities actually occur in practical rotors. Problems of rough running and strange instabilities at frequencies which do not appear to relate to known mechanisms are quite common and are usually treated by ad - hoc measures, such as changing bearing stiffness, oil temperature and the like or are simply tolerated if the machine can be operated normally.

Having shown that such instabilities are possible for a practical rotor - shaft configuration, it would be a simple matter, in the case of an unexplained instability, to check if the relationships of rotor speed to modal frequencies are as shown here. In addition to the stability analysis, the computer code developed permits the prediction of undamped critical speeds for a non-axisymmetric shaft - rotor system supported on distributed bearings, which is of some practical use. However, the assumptions of constant bearing stiffness and zero damping must detract from the model and addressed in the subsequent chapters.

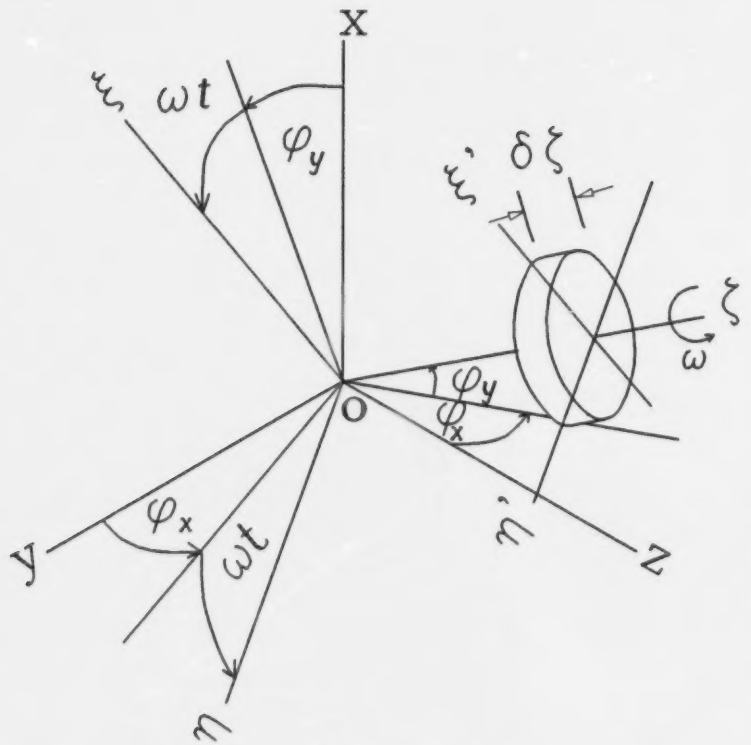

Figure 4.1: Inertial and Body-Fixed Axes of Infinitesimal Disk Section of Rotor / Shaft Element of Length $\delta\zeta$. $Oxyz$ is parallel to the inertial frame of reference, $O\xi\eta\zeta$ is a body fixed coordinate system coincident with the principal axes. ϕ_x, ϕ_y and ωt are Euler angles relating the two systems and ξ', η' are parallel to $O\xi$ and $O\eta$.

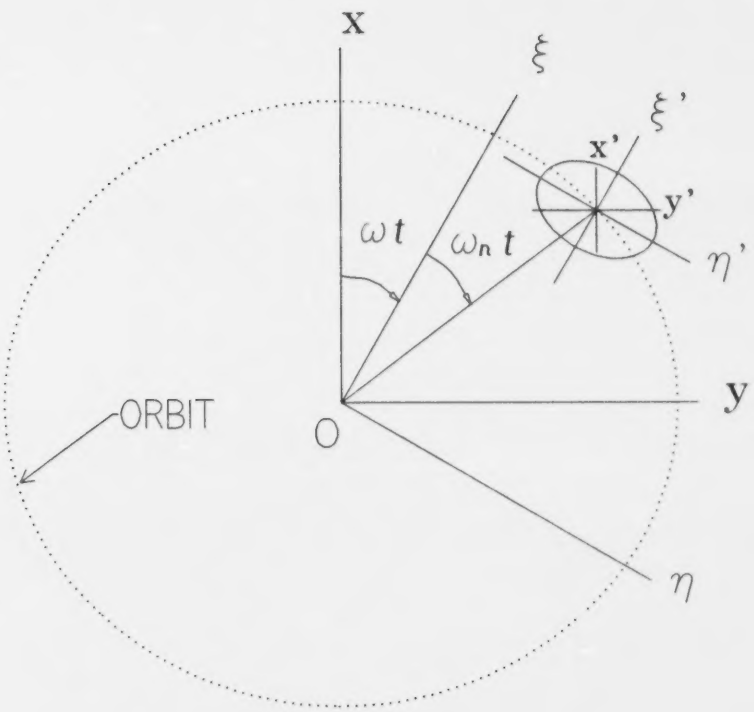

Figure 4.2: Rotor / Shaft Section Precessing at Angular Frequency ω_n Relative to Frame of Reference Rotating at ω.

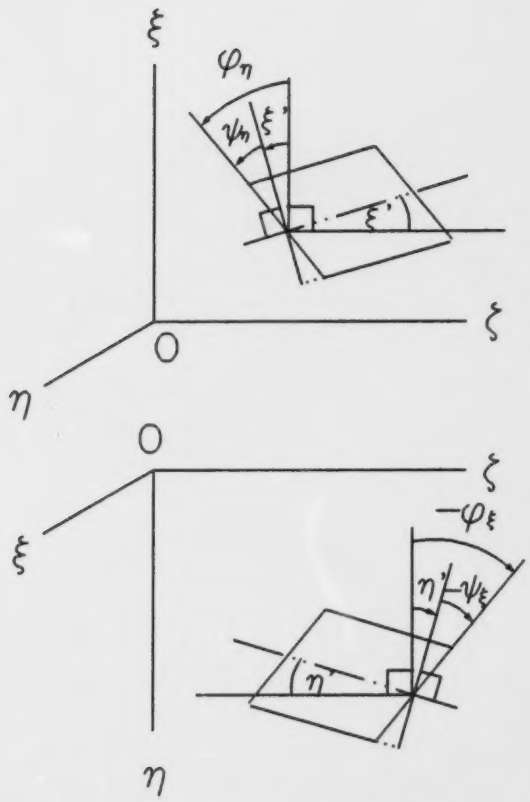

Figure 4.3: Relation Between Shear Slope, Bending Slope and Neutral Axis Slope in the $O\xi\zeta$ and $O\eta\zeta$ Planes. ϕ_η and ϕ_ξ are the bending slopes, ψ_η and ψ_ξ, the shear slopes and ξ' and η' the neutral axis slopes in the $O\xi\zeta$ and $O\eta\zeta$ planes respectively.

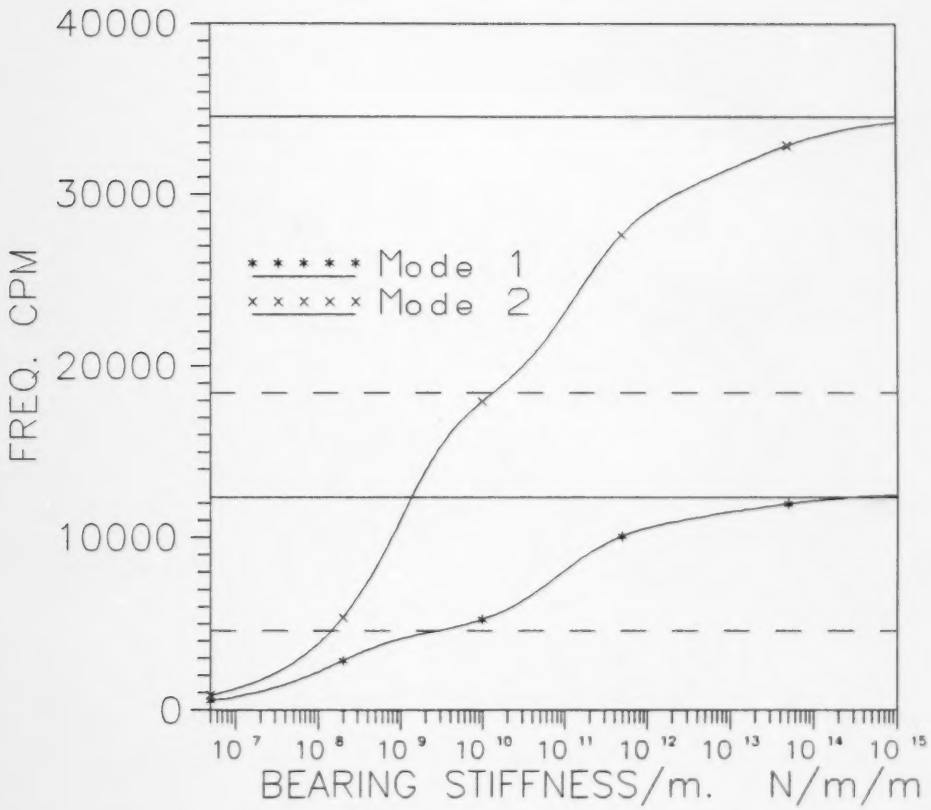

Figure 4.4: Natural Frequencies of First Two Bending Modes for a Uniform Rotor at Zero RPM vs. Distributed Bearing Stiffness - No Shear. Length 2500mm, Diam. 200mm, Bearing Length 200mm (L/D = 1.0).

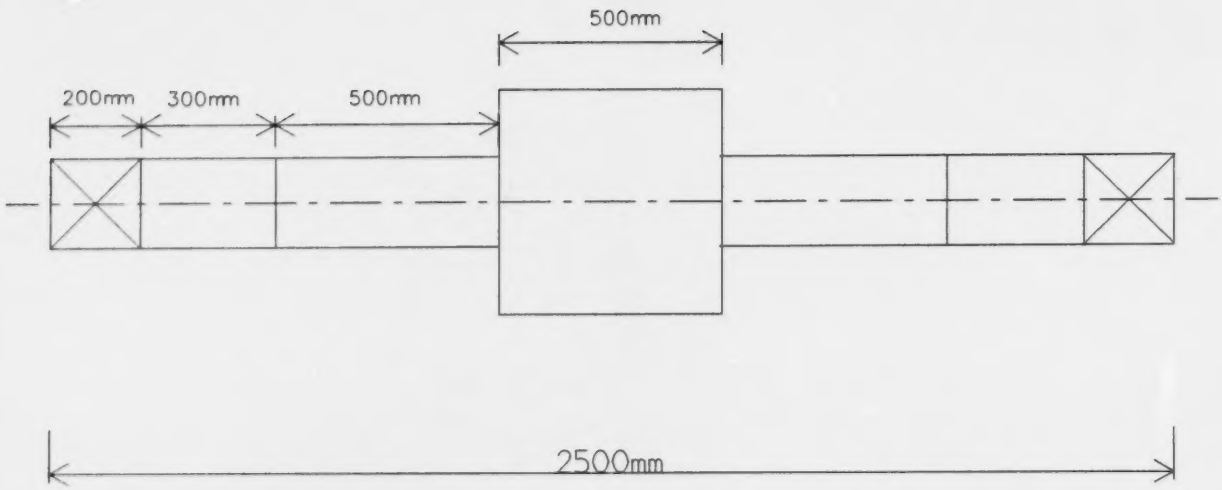

Figure 4.5: Outline of Rotor Model Analyzed. The Bearings are Assumed Identical of Length 200mm and Diam. 200mm.

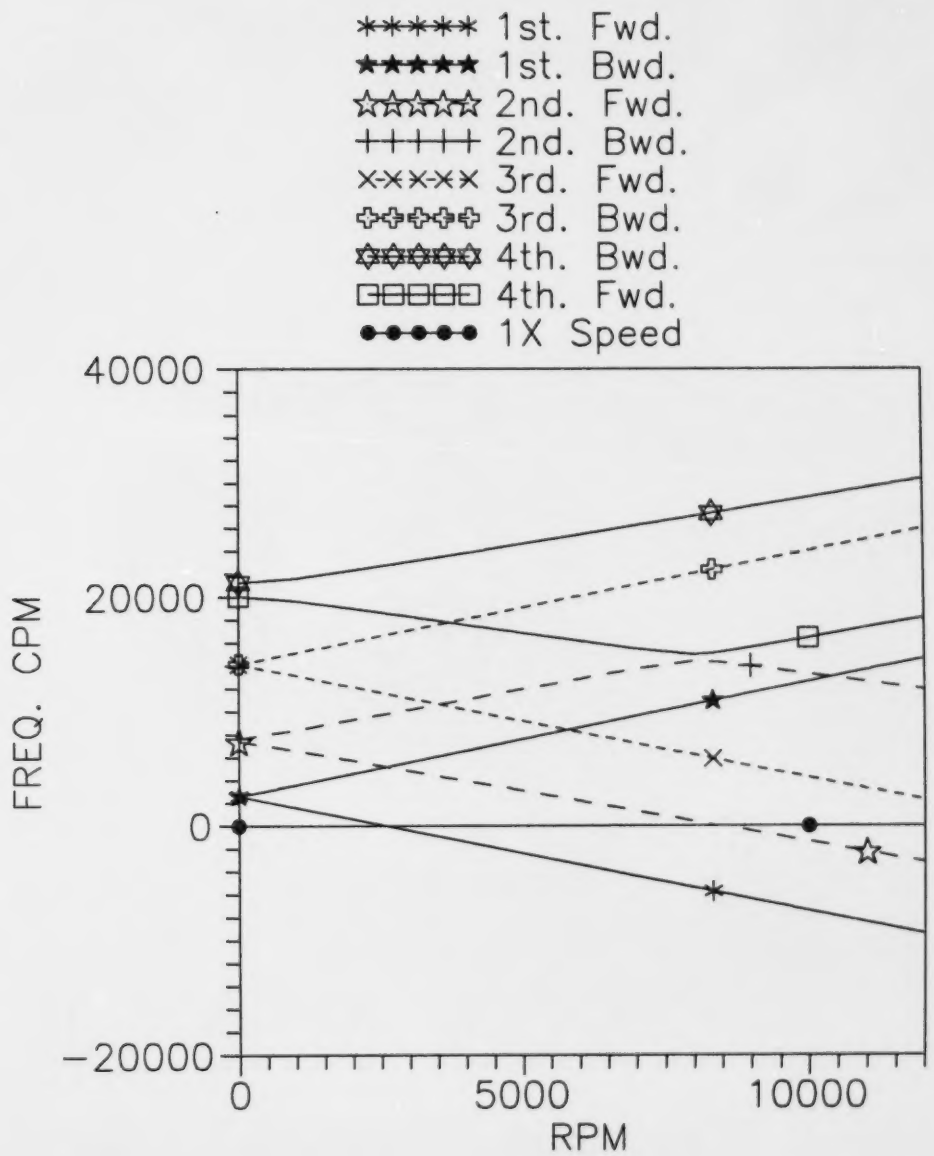

Figure 4.6: Modal Frequencies in Rotating Frame vs. Speed for Central Rotor with Asymmetric Mass and Diametral Stiffness Moments of Area, Uniform Axisymmetric Shaft, No Shear Deflection.

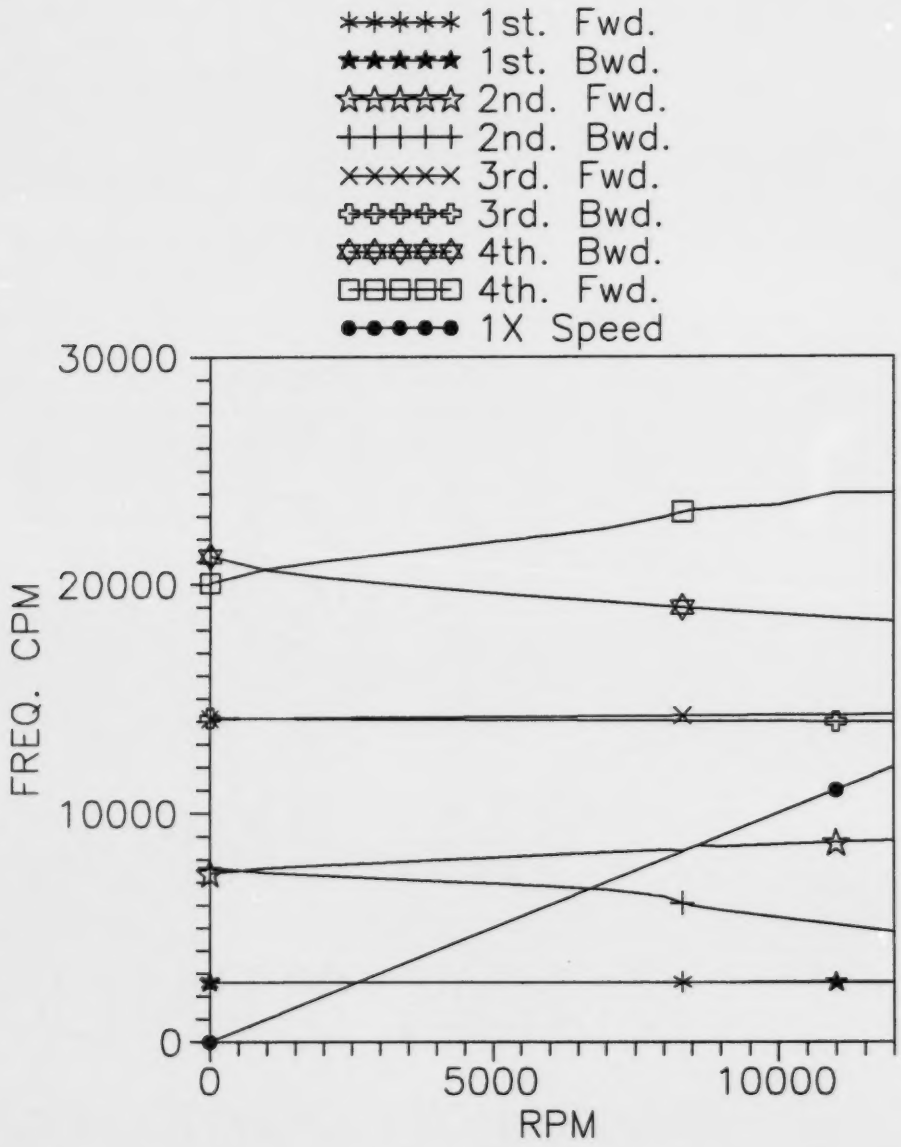

Figure 4.7: Modal Frequencies in Inertial Frame vs. Speed for Central Rotor with Asymmetric Mass and Stiffness Diametral Moments of Area, Uniform Axisymmetric Shaft, No Shear Deflection.

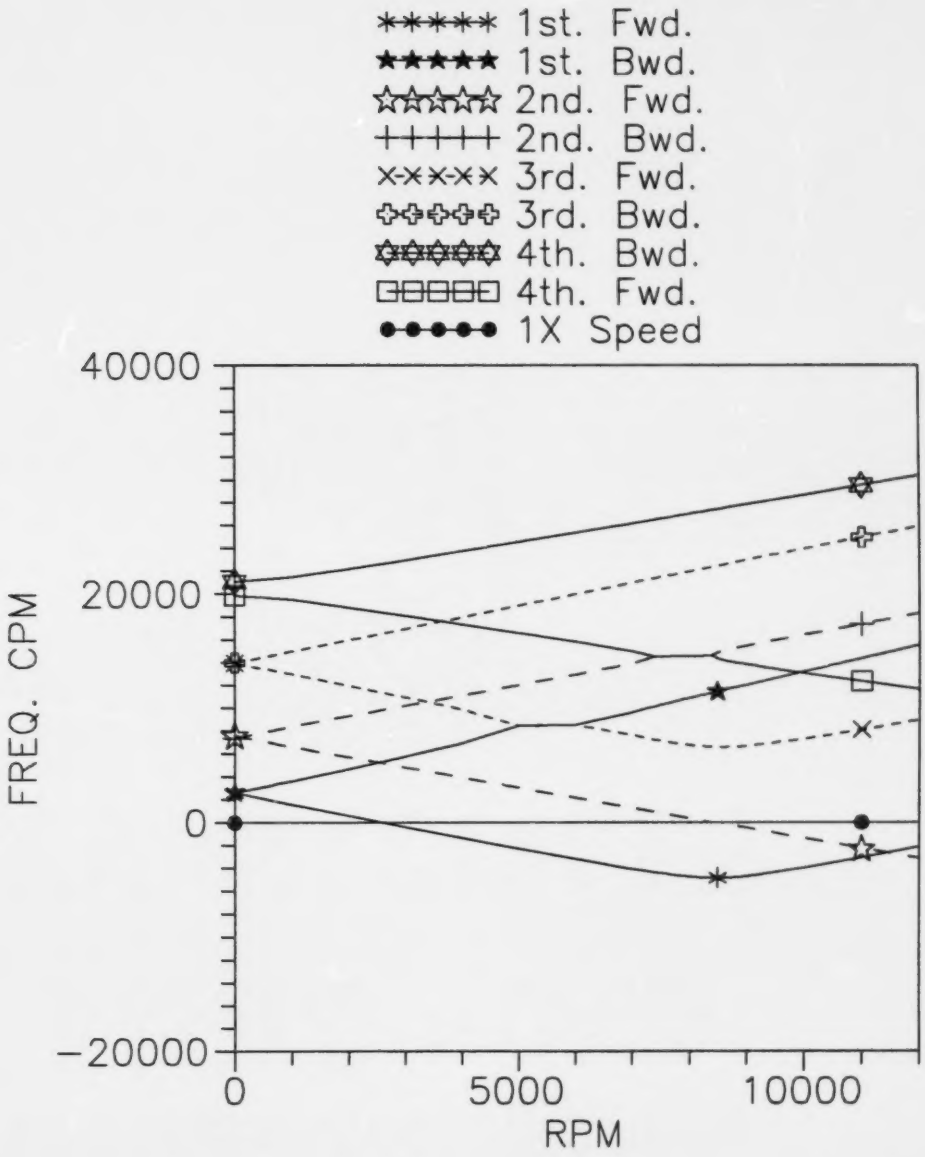

Figure 4.8: Modal Frequencies in Rotating Frame vs. Speed for Central Rotor with Asymmetric Mass and Stiffness Diametral Moments of Area, Uniform Axisymmetric Shaft, with Shear Deflection.

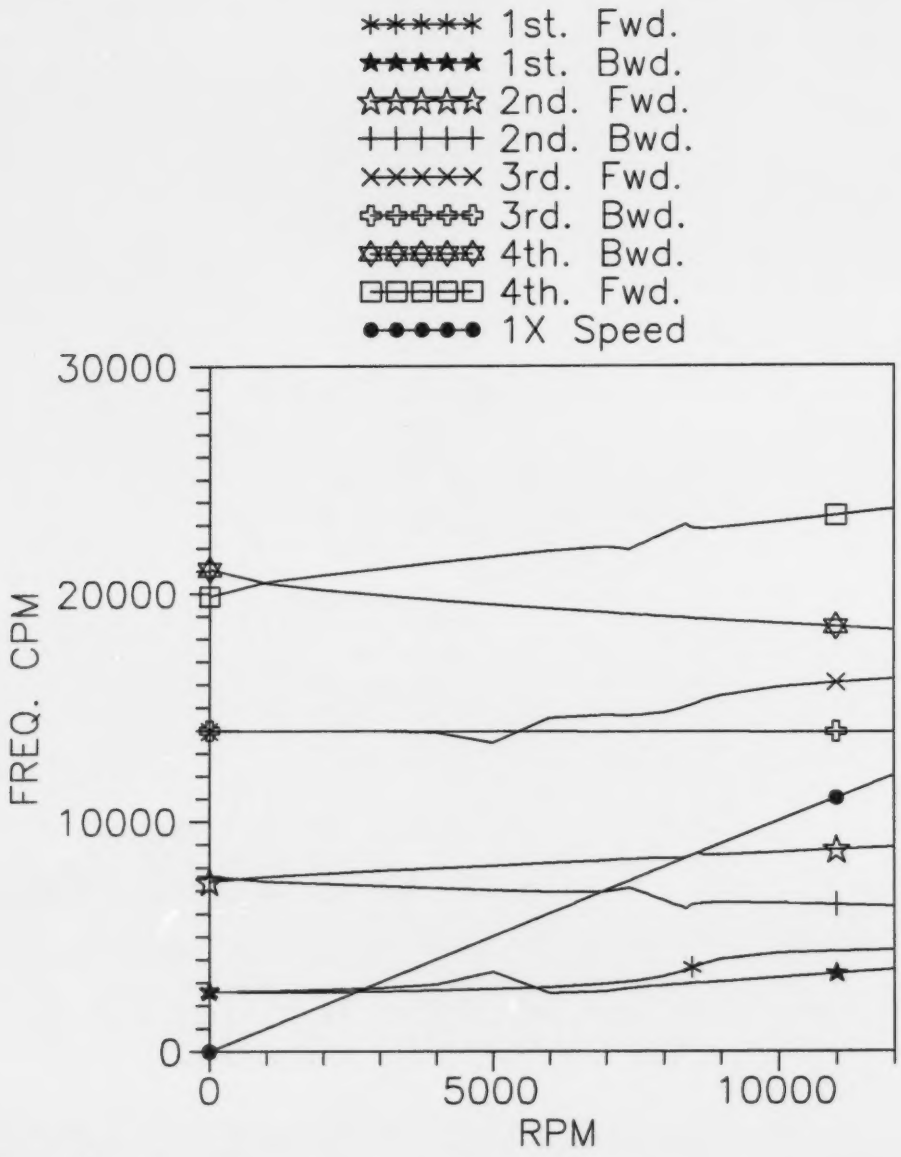

Figure 4.9: Modal Frequencies in Inertial Frame vs. Speed for Central Rotor with Asymmetric Mass and Stiffness Diametral Moments of Area, Uniform Axisymmetric Shaft, with Shear Deflection.

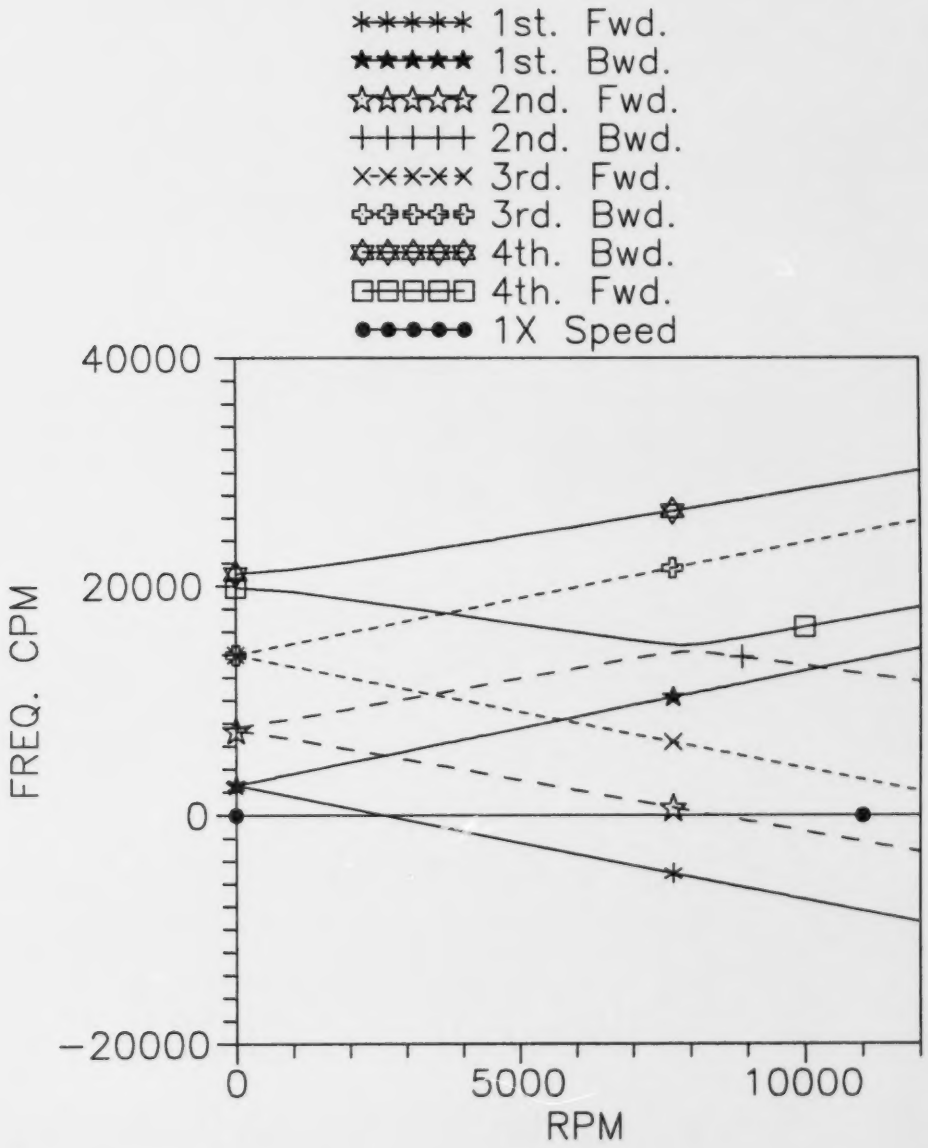

Figure 4.10: Modal Frequencies in Rotating Frame vs. Speed for Central Rotor with Asymmetric Diametral Mass Moments of Area, but Axisymmetric Stiffness, Uniform Axisymmetric Shaft, with Shear Deflection.

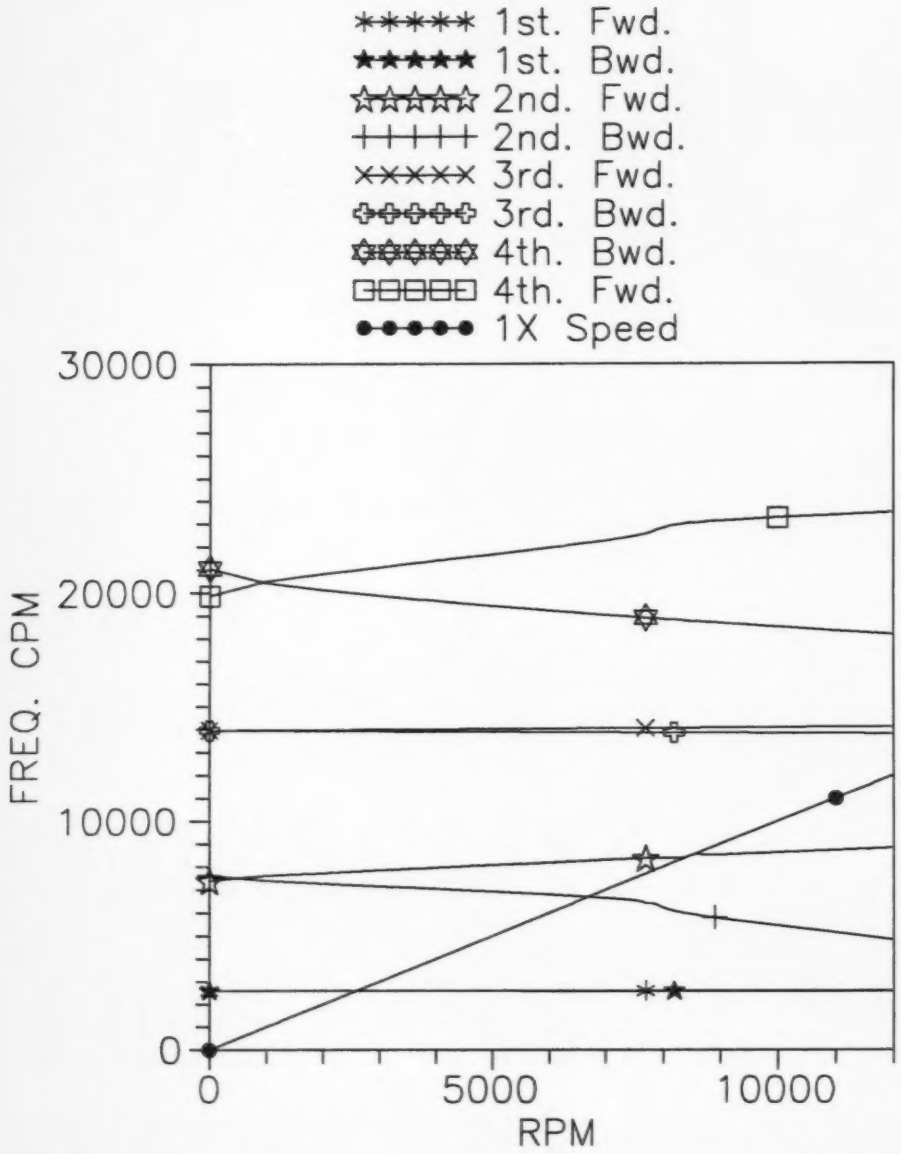

Figure 4.11: Modal Frequencies in Inertial Frame vs. Speed for Central Rotor with Asymmetric Diametral Mass Moments of Area, but Axisymmetric Stiffness, Uniform Axisymmetric Shaft, with Shear Deflection.

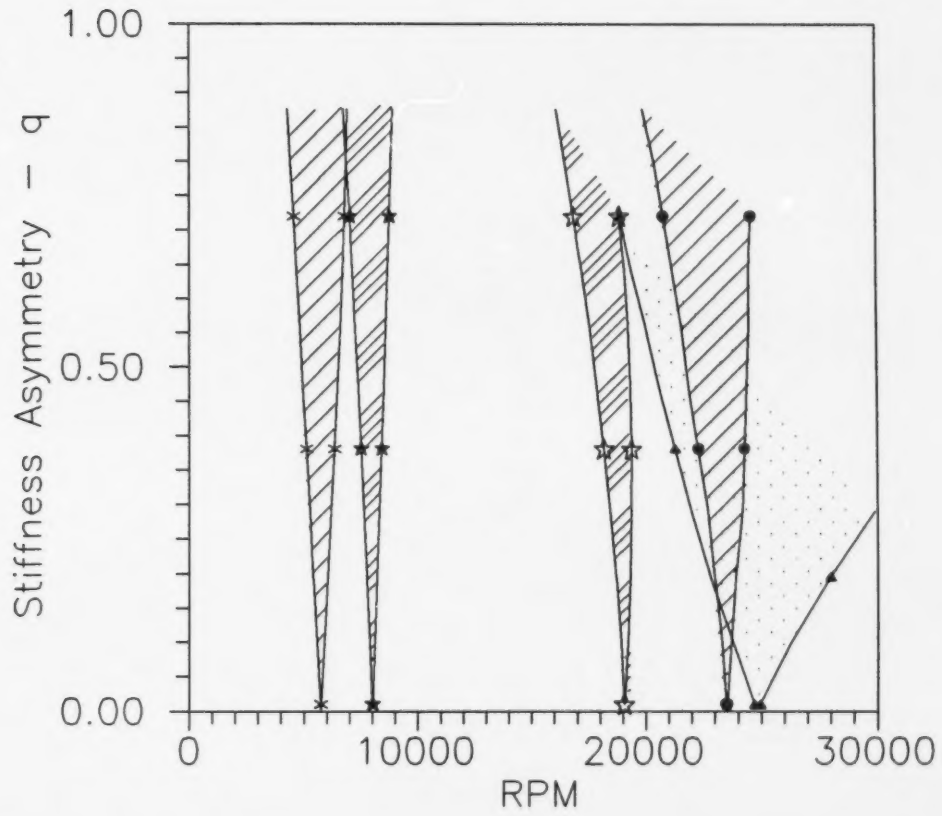

Figure 4.12: Instability Regions for a Flexible Rotor / Shaft System Having Non-Axisymmetric Stiffness, Supported by Distributed Axisymmetric Bearings. $q = 2(J_{\xi\xi} - J_{\eta\eta})/(J_{\xi\xi} + J_{\eta\eta})$. The instability around the fundamental resonance is not included.

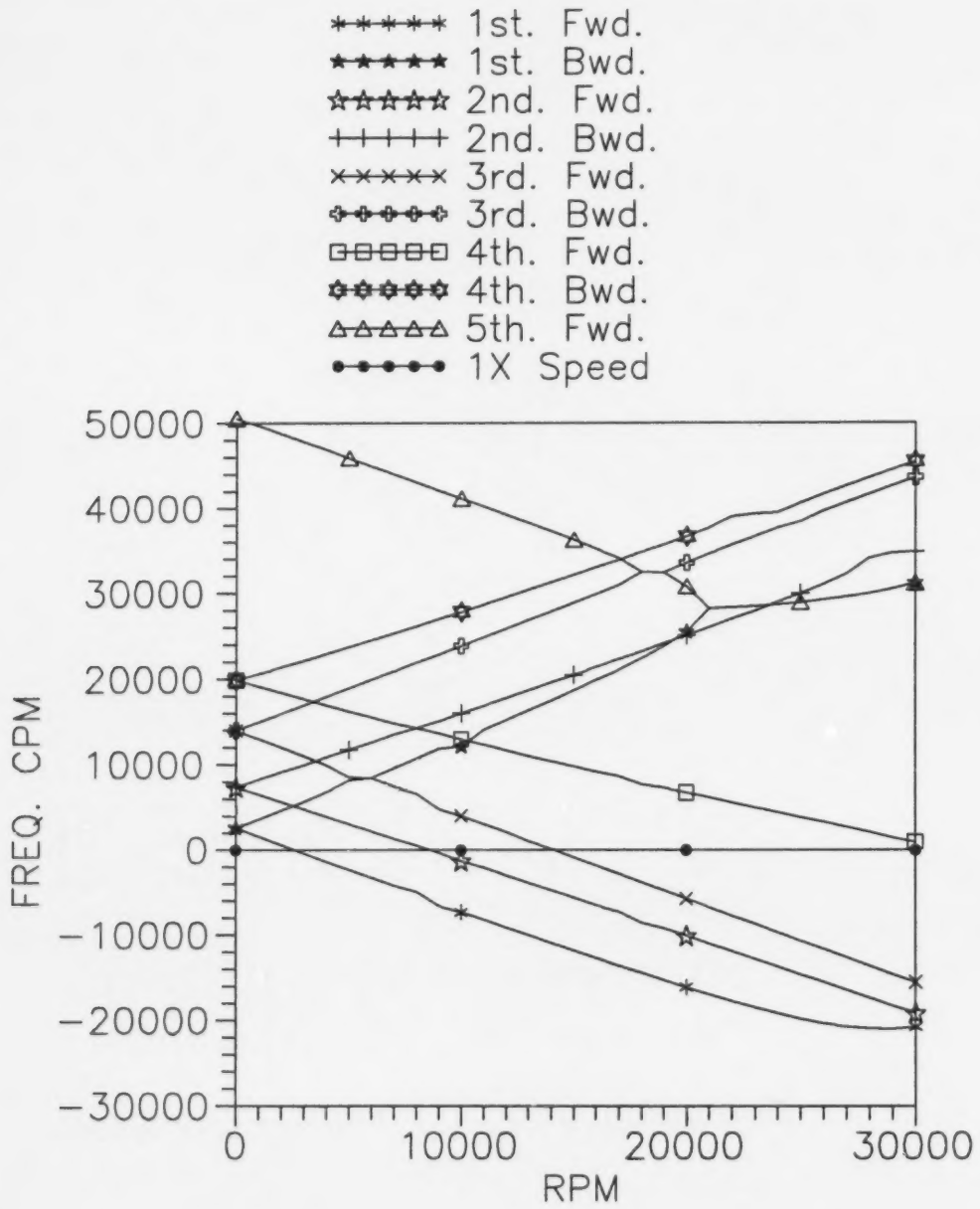

Figure 4.13: Modal Frequencies vs. Speed for q = 0.45 and Zero Damping.

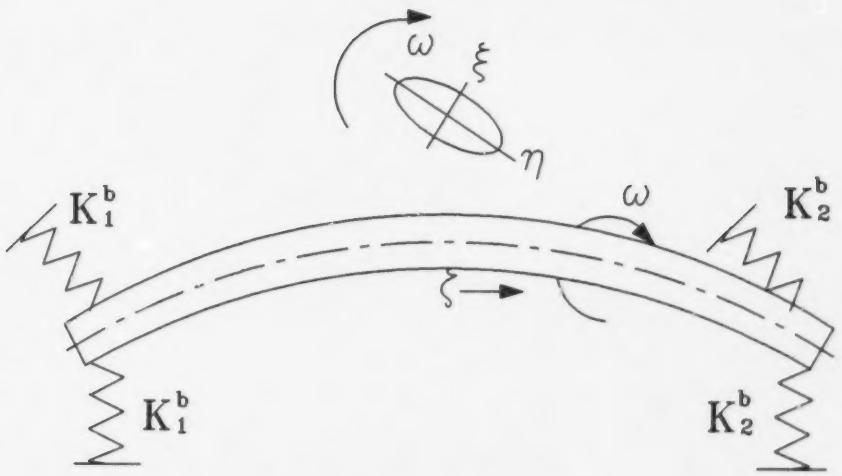

Figure 4.14: Uniform Non-Axisymmetric Rotor on Point Bearing Supports.

Chapter 5

Dynamics of a Plain Journal Bearing

Although there have been many studies on plain and tilting pad bearings, of which some were briefly described in Chapter 2, few of them contain usable data. In addition, the assumptions made, particularly with respect to boundary conditions are generally not described in much detail. The manual prepared by Someya et al. [84] is a notable exception in that their work contains data for many different configurations of bearings. However, in order to have a convenient means with which to derive dynamic coefficients for this and future applications, as well as a means to establish a thorough understanding of the behaviour of a tilting - pad bearing, it was decided to carry out the analyses in this and the subsequent chapter.

This chapter uses the finite element approach to derive, for a plain cylindrical sleeve bearing, the equilibrium position in terms of Sommerfeld number, S, and attitude angle ψ as a function of eccentricity ratio ε. Then, also for given values of the equilibrium value of ε, the rate of change of the fluid forces with respect to ε and $\dot{\varepsilon}$ are derived. The results compare favourably with the work of Cameron Ref. [85] and Pinkus and Sternlich Ref. [86].

5.1 Finite Element Approximation to Reynolds Equation - Steady State

Using the notation of Trumpler [87], Figure 5.1, the pressure field for an incompressible lubricant under laminar flow conditions is described by the following elliptic partial differential equation, known as Reynold's equation, Equation 5.1. This 'unwraps' the bearing film, ignoring the effects of curvature. It therefore considers viscous forces only, no inertia forces.

$$\frac{\partial}{\partial\theta}\left[(1 + \varepsilon\cos\theta)^3 \frac{\partial p}{\partial\theta}\right] + R^2\frac{\partial}{\partial z}\left[(1 + \varepsilon\cos\theta)^3 \frac{\partial p}{\partial z}\right] =$$

$$12\mu\left(\frac{R}{c}\right)^2 [\dot{\varepsilon}\cos\theta - \varepsilon((\omega_j + \omega_b)/2 - \omega_c)\sin\theta] \tag{5.1}$$

where, θ is the angular position relative to the line of centres (journal - bearing), i.e. fixed relative to the rotating journal,
ε is the eccentricity ratio e/c where e is the eccentricity and c is the radial clearance,
R is the journal radius,
z is the axial coordinate,
p is pressure,
μ is the absolute viscosity of the lubricant,
ω_j is the angular velocity of the journal relative to ground,
ω_b is the angular velocity of the bearing relative to ground,
ω_c is the angular velocity of the line of centres relative to ground.
Axial velocity is assumed to be zero.

To use the variational approach, we require a functional which, when extremized will result in Equation 5.1. Euler's theorem states that if the functional,

$$\Xi = \int\int\int_V f\left(x, y, z, \phi, \frac{\partial\phi}{\partial x}, \frac{\partial\phi}{\partial y}, \frac{\partial\phi}{\partial z}\right) dV, \tag{5.2}$$

is to be exremized over V, then the necessary and sufficient condition is that $\phi(x, y, z)$ satisfy the differential equation,

$$\frac{\partial}{\partial x}\left(\frac{\partial f}{\partial(\partial\phi/\partial x)}\right) + \frac{\partial}{\partial y}\left(\frac{\partial f}{\partial(\partial\phi/\partial y)}\right) + \frac{\partial}{\partial z}\left(\frac{\partial f}{\partial(\partial\phi/\partial z)}\right) = \frac{\partial f}{\partial\phi} \tag{5.3}$$

If this condition is applied to the functional $I(p)$,

$$I(p) = \int\int_A \left\{\left(\frac{c}{R}\right)^2 \frac{(1 + \varepsilon\cos\theta)^3}{24\mu}\left[\left(\frac{\partial p}{\partial\theta}\right)^2 + R^2\left(\frac{\partial p}{\partial z}\right)^2\right]\right.$$

$$\left. - \varepsilon\sin\theta\left[\left(\frac{\omega_j + \omega_b}{2}\right) - \omega_c\right]p + \frac{\partial}{\partial t}(1 + \varepsilon\cos\theta)p\right\} dA, \tag{5.4}$$

then Trumpler's form of Reynolds equation results. $I(p)$ is therefore a suitable (not unique) functional.

For steady - state conditions $\dot{\varepsilon} = 0$ and $\omega_c = 0$. The bearing angular velocity ω_b is taken to be zero as it is for most machines.

5.1.1 Bearing Element Development

For the finite element approximation we let the pressure p^e at a point within the element of the bearing film be defined by a function of the pressures at the nodes of the element $\{p^e\}$ and a shape function $\{G\}$:

$$p^e(\theta, z) = \{G\}^T \{p^e\} = \{p^e\}^T \{G\}. \tag{5.5}$$

Then Equation 5.4 becomes for an element,

$$I^e(p) = \int\int_A^e \left[\left(\frac{c}{R}\right)^2 \frac{(1+\varepsilon\cos\overline{\theta})^3}{24\mu} \{p^e\}^T \left[\{G_{,\theta}\}\{G_{,\theta}\}^T + R^2 \{G_{,z}\}\{G_{,z}\}^T \right] \{p^e\} \right.$$

$$\left. - \varepsilon \sin\overline{\theta} \frac{\omega_j}{2} \{p^e\}\{G\} \right] dA, \tag{5.6}$$

for steady state conditions. Note that it is now necessary to distinguish $\overline{\theta}$, the global angular position, from θ the relative angular position within an element. Extremizing Equation 5.6 with respect to $\{p^e\}$ we obtain:

$$\frac{\partial I^e(p)}{\partial \{p^e\}} = \int\int_A^e \left[\left(\frac{c}{R}\right)^2 \frac{(1+\varepsilon\cos\overline{\theta})^3}{12\mu} \left[\{G_{,\theta}\}\{G_{,\theta}\}^T + R^2 \{G_{,z}\}\{G_{,z}\}^T \right] \{p^e\} \right.$$

$$\left. - \varepsilon \sin\overline{\theta} \frac{\omega_j}{2} \{G\} \right] dA. \tag{5.7}$$

If we assume a bilinear dependency of p^e on the local element coordinates θ and z then,

$$p^e = \alpha_1 + \alpha_2\theta + \alpha_3 z + \alpha_4 \theta z, \tag{5.8}$$

where the α's are constants. Thus,

$$p^e = \left\{ 1 \quad \theta \quad z \quad \theta z \right\} \begin{Bmatrix} \alpha_1 \\ \alpha_2 \\ \alpha_3 \\ \alpha_4 \end{Bmatrix}. \tag{5.9}$$

Then referring to Figure 5.2, we can substitute the nodal coordinates to obtain the

pressures at the nodes,

$$\{p^e\}^T = \left\{ \alpha_1 \quad \alpha_2 \quad \alpha_3 \quad \alpha_4 \right\} \begin{bmatrix} 1 & 1 & 1 & 1 \\ \theta_i & \theta_j & \theta_k & \theta_l \\ z_i & z_j & z_k & z_l \\ \theta_i z_i & \theta_j z_j & \theta_k z_k & \theta_l z_l \end{bmatrix}. \tag{5.10}$$

Thus,

$$\{G\}^T = \left\{ 1 \quad \theta \quad z \quad \theta z \right\} \begin{bmatrix} 1 & \theta_i & z_i & \theta_i z_i \\ 1 & \theta_j & z_j & \theta_j z_j \\ 1 & \theta_k & z_k & \theta_k z_k \\ 1 & \theta_l & z_l & \theta_l z_l \end{bmatrix}^{-1}. \tag{5.11}$$

For a rectangular element of length l which subtends an angle $\Delta\theta$ at the centre of the bearing,

$$\{G_{,\theta}\}\{G_{,\theta}\}^T =$$

$$\frac{1}{4l^2\Delta\theta^2} \begin{bmatrix} (l-2z)^2 & -(l-2z)^2 & -(l-2z)(l+2z) & (l-2z)(l+2z) \\ & (l-2z)^2 & (l-2z)(l+2z) & -(l-2z)(l+2z) \\ & Sym & (l+2z)^2 & -(l+2z)^2 \\ & & & (l+2z)2 \end{bmatrix} \tag{5.12}$$

and

$$\{G_{,z}\}\{G_{,z}\}^T = \frac{1}{4l^2\Delta\theta^2} \times$$

$$\begin{bmatrix} (\Delta\theta-2\theta)^2 & (\Delta\theta-2\theta)(\Delta\theta+2\theta) & -(\Delta\theta-2\theta)(\Delta\theta+2\theta) & -(\Delta\theta-2\theta)^2 \\ & (\Delta\theta+2\theta)^2 & -(\Delta\theta+2\theta)^2 & -(\Delta\theta-2\theta)(\Delta\theta+2\theta) \\ & Sym & (\Delta\theta+2\theta)^2 & (\Delta\theta-2\theta)(\Delta\theta+2\theta) \\ & & & (\Delta\theta-2\theta)^2 \end{bmatrix} \tag{5.13}$$

The term $(1+\varepsilon\cos\bar{\theta})^3$ in Equation 5.7, represents the non-dimensionalized film thickness cubed. Allaire [46] assumes this to be constant over the element which involves some small error. This error can be reduced by the following.

If we define θ_g to be the global angular position of the centre of the element, then $\bar{\theta} = \theta_g + \theta$. Then ignoring terms in θ^2 and θ^3,

$$(1 + \varepsilon \cos(\theta_g + \theta))^3 \simeq (1 + \varepsilon \cos \theta_g)^3 - 3\varepsilon\theta \sin \theta_g (1 + \varepsilon \cos \theta_g)^2$$

For the case of 10 circumferential elements over 180° with $\varepsilon = 0.5$, the true values of the non-dimensional film thickness cubed for an element with $\theta_g = \pi$, varies from 0.7830 to 1.2532. Using the above approximation, it varies from 0.7644 to 1.2356 which is a maximum error of 1.4 %. If the thickness is assumed constant then the error in this term would be 25 %. However for small elements (5 degrees circumferential angle), the effect of this correction becomes very small in terms of the Sommerfeld number and dynamic coefficients derived.

Using this approximation therefore, Equation 5.7 becomes,

$$\left\{(1 + \varepsilon \cos \theta_g)^3 \int_{-\frac{\Delta\varrho}{2}}^{\frac{\Delta\varrho}{2}} \int_0^l \left[\{G_{,\theta}\}\{G_{,\theta}\}^T + R^2 \{G_{,z}\}\{G_{,z}\}^T\right] R d\theta\, dz \right.$$

$$\left. -3\varepsilon \sin \theta_g (1 - \varepsilon \cos \theta_g)^2 \int_{-\frac{\Delta\varrho}{2}}^{\frac{\Delta\varrho}{2}} \int_0^l \left[\theta \{G_{,\theta}\}\{G_{,\theta}\}^T + R^2\theta \{G_{,z}\}\{G_{,z}\}^T\right] R d\theta\, dz \right\} \{p^e\}$$

$$= 6\mu \left(\frac{R}{c}\right)^2 \omega_j \int_{-\frac{\Delta\varrho}{2}}^{\frac{\Delta\varrho}{2}} \int_0^l \varepsilon \sin(\theta_g + \theta) \{G\} R d\theta\, dz. \qquad (5.14)$$

Carrying out the integrations of Equation 5.14 we get the element equation:

$$\left\{\frac{(1+\varepsilon\cos\theta_g)^3}{\Delta\theta}\left[\begin{bmatrix} 2 & -2 & -1 & 1 \\ -2 & 2 & 1 & -1 \\ -1 & 1 & 2 & -2 \\ 1 & -1 & -2 & 2 \end{bmatrix} + \frac{R^2\Delta\theta^2}{l^2}\begin{bmatrix} 2 & 1 & -1 & -2 \\ 1 & 2 & -2 & -1 \\ -1 & -2 & 2 & 1 \\ -2 & -1 & 1 & 2 \end{bmatrix}\right]\right.$$

$$\left.-\frac{3}{2}\varepsilon\sin\theta_g(1-\varepsilon\cos\theta_g)^2\left(\frac{R^2\Delta\theta^2}{l^2}\right)\begin{bmatrix} -1 & 0 & 0 & 1 \\ 0 & 1 & -1 & 0 \\ 0 & -1 & 1 & 0 \\ 1 & 0 & 0 & -1 \end{bmatrix}\right\}^e \begin{Bmatrix} p_i \\ p_j \\ p_k \\ p_l \end{Bmatrix}^e$$

$$= 9\mu\left(\frac{R}{c}\right)^2\omega_j\varepsilon\Delta\theta\left[\sin\theta_g\begin{Bmatrix} 1 \\ 1 \\ 1 \\ 1 \end{Bmatrix} + \frac{\Delta\theta\cos\theta_g}{6}\begin{Bmatrix} -1 \\ 1 \\ 1 \\ -1 \end{Bmatrix}\right] \tag{5.15}$$

The element matrix equations 5.15 can now be assembled into a global set of equations of the form:

$$[A(\varepsilon)]\{p_g\} = \mu\left(\frac{R}{c}\right)^2\omega_j\{f_g(\varepsilon)\} \tag{5.16}$$

for a given set of elements, where $[A(\varepsilon)]$ is the assembled matrix of the element coefficient matrices of Equation 5.15, $\{p_g\}$, the global pressure vector, and $\{f_g(\varepsilon)\}$ the assembled, (global) right hand side vectors of Equation 5.15 factored by $\mu\left(\frac{R}{c}\right)^2\omega_j$.

We can define a non - dimensional pressure vector $\left\{p_g^*\right\}$ such that,

$$\{p_g\} = \mu\left(\frac{R}{c}\right)^2\omega_j\left\{p_g^*\right\}$$

and solve the resulting Equation 5.17 for given values of ε.

$$[A(\varepsilon)]\left\{p_g^*\right\} = \{f_g(\varepsilon)\} \tag{5.17}$$

5.1.2 Boundary Conditions

The form of the functional used here is valid for boundary conditions where the pressure is defined over the whole boundary or the flow rate is known to be zero over some of the boundary. Otherwise an additional flow term is necessary in the functional. In this analysis, the lubricant pressure is set to zero (atmospheric pressure in absolute terms) at both axial ends of the bearing.

There are two common assumptions made for the circumferential boundary conditions, the half Sommerfeld condition and the Reynolds condition. The former assumes that the pressure is zero for $180^o < \theta_g < 360^o$. However, this assumption does not satisfy the condition that where p becomes zero, $\partial p/\partial\theta_g$ should also be zero. This more approximates the observed behaviour of bearings, [87].

The Reynolds condition requires both p and $\partial p/\partial\theta_g$ become zero simultaneously at the circumferential location where the film begins to cavitate. This is a little more involved from a computational point of view in that one has to set $\{p_g^*\} = \{0\}$ at some value of θ_g, then adjust this value until $\{\partial p^*/\partial\theta_g\}$ also becomes zero at that point, see Figure 5.3. In practice, this can be done quite quickly by inspection but could clearly be automated.

Having obtained the global non - dimensionalized pressure vector $\left\{p_g^*\right\}$, the mean non - dimensionalized element pressures $\{p_{el}\}$ are calculated by averaging the values for the four nodal pressures of each element. Then the radial and tangential forces applied to the journal by the fluid, F_r and F_t are given by the following,

$$F_r = \mu\left(\frac{R}{c}\right)^2 \omega_j \sum_i p_{el_i} \Delta\theta_i l_i \cos\theta_g^i \tag{5.18}$$

and

$$F_t = \mu\left(\frac{R}{c}\right)^2 \omega_j \sum_i p_{el_i} \Delta\theta_i l_i \sin\theta_g^i \tag{5.19}$$

where $\Delta\theta_i$, l_i and θ_g^i are respectively, the angle subtended at the journal centre, the axial length and the angular position with respect to the line of centres, of the i'th element. The θ_g^i are measured to the centre of the element in the circumferential direction.

For a journal of total length L, diameter $D = 2R$ and speed $N = \omega_j/2\pi$ revs/sec,

$$F_r = \mu\left(\frac{R}{c}\right)^2 N D L \pi \sum_i \left(p_{el_i}\,\Delta\theta_i \frac{l_i}{L}\cos\theta_g^i\right) \tag{5.20}$$

and

$$F_t = \mu\left(\frac{R}{c}\right)^2 N D L \pi \sum_i \left(p_{el_i}\,\Delta\theta_i \frac{l_i}{L}\sin\theta_g^i\right) \tag{5.21}$$

The load W which can be supported is then given by,

$$W^2 = F_r^2 + F_t^2$$

One definition of Sommerfeld number S is,

$$S = \frac{W}{L D N \mu}\left(\frac{c}{R}\right)^2 \tag{5.22}$$

If we define ,

$$\overline{F}_r = \pi \sum_i p_{el_i}\,\Delta\theta_i \frac{l_i}{L}\cos\theta_g^i$$

and

$$\overline{F}_t = \pi \sum_i p_{el_i}\,\Delta\theta_i \frac{l_i}{L}\sin\theta_g^i$$

then,

$$S^2 = \overline{F}_r^2 + \overline{F}_t^2 \tag{5.23}$$

Also the attitude angle ψ which the load W makes with the line of centres is then given by the following, see Figure 5.4.

$$\psi = \arctan\left(-\frac{\overline{F}_t}{\overline{F}_r}\right) \tag{5.24}$$

A computer code was written in Fortran to solve Equation 5.17 for element geometry corresponding to values of length to diameter (L/D) ratio of 0.5, 1.0, 2.0 and 4.0 and for eccentricity ratios $\varepsilon = 0.1$ through 0.85. Higher values than 0.85 gave unreliable results. To obtain better results at higher eccentricity ratios, it would be necessary to use a finer mesh around the location where the film cavitates. The computer code was written to permit unequal rectangular elements. However, this did not seem justified because it is unlikely that Reynolds equation is valid under such conditions. Muszynska [7] showed that recirculation takes place in a cylindrical sleeve bearing at high eccentricity ratios.

The mesh used consisted of 720 equal rectangular elements, 10 axially by a maximum of 72 circumferentially (over 360 degrees), i.e. at 5 degree increments. As the Reynolds condition was employed, the effective mesh used was never greater than 10 by 48, because the Reynolds condition was always satisfied at a circumferential location between 190 and 240 degrees.

In previous studies, some pains were taken to minimise the computer time by varying grid size, element shape and orientation, for example Allaire [46]. This was justified at the time. However with the rather fine mesh used here and using a non-banded solver, the computer runs took only about 2.5 minutes on a desktop computer (80486 25 MHz. C.P.U. with a DOS extender) and about 45 seconds on an IBM 6000.

The results of this analysis, in terms of Sommerfeld number and attitude angle versus eccentricity ratio, are shown in Figures 5.5 and 5.6 respectively. Figure 5.7 is a three dimensional plot of the non - dimensionalized pressure distribution for one of the cases.

The Sommerfeld numbers are very close to those of Cameron [85] for eccentricity ratios below 0.8. Cameron presents the data graphically only and the differences appear to be about one or two percent. The attitude angle calculated here differ by those of Cameron by about 5 degrees at the low to mid values of ε.

Table 5.1 compares the results of the present analysis with those of Pinkus and Sternlicht [86]. The Sommerfeld numbers differ by about 3% or less for $\varepsilon \leq 0.7$ and the attitude angles (given to the nearest degree) are either the same or differ by one degree for $\varepsilon \leq 0.7$.

As instabilities of an 'oil whirl' or 'oil whip' nature generally occur for lightly loaded bearings and therefore for low ε, and given that at high ε the laminar flow assumption is unlikely to be valid, these data would seem to be adequate for determining the equilibrium position at which to investigate stability.

5.2 General (Dynamic) Case

Having determined the steady - state condition in terms of eccentricity ratio ε, Sommerfeld number S and attitude angle ψ, we can include squeeze - film velocity $\dot{\varepsilon}$ in the equations in order to determine damping forces for perturbations about the equilibrium position.

If we apply the finite element approximation to Equation 5.4, retaining the $\dot{\varepsilon}$ term but letting the bearing velocity ω_b and line of centres' velocity ω_c be zero then we obtain a finite element equation for the element as follows:

$$\left\{\frac{(1+\varepsilon\cos\theta_g)^3}{\Delta\theta}\left[\begin{bmatrix} 2 & -2 & -1 & 1 \\ -2 & 2 & 1 & -1 \\ -1 & 1 & 2 & -2 \\ 1 & -1 & -2 & 2 \end{bmatrix} + \frac{R^2\Delta\theta^2}{l^2}\begin{bmatrix} 2 & 1 & -1 & -2 \\ 1 & 2 & -2 & -1 \\ -1 & -2 & 2 & 1 \\ -2 & -1 & 1 & 2 \end{bmatrix}\right]\right.$$

$$\left.-\frac{3}{2}\varepsilon\sin\theta_g(1-\varepsilon\cos\theta_g)^2\left(\frac{R^2\Delta\theta^2}{l^2}\right)\begin{bmatrix} -1 & 0 & 0 & 1 \\ 0 & 1 & -1 & 0 \\ 0 & -1 & 1 & 0 \\ 1 & 0 & 0 & -1 \end{bmatrix}\right\}^e \begin{Bmatrix} p_i \\ p_j \\ p_k \\ p_l \end{Bmatrix}^e$$

$$= 9\mu\left(\frac{R}{c}\right)^2\omega_j\varepsilon\Delta\theta\left[\sin\theta_g\begin{Bmatrix} 1 \\ 1 \\ 1 \\ 1 \end{Bmatrix} + \frac{\Delta\theta\cos\theta_g}{6}\begin{Bmatrix} -1 \\ 1 \\ 1 \\ -1 \end{Bmatrix}\right]$$

$$- 18\mu\left(\frac{R}{c}\right)^2\omega_j\dot{\varepsilon}\Delta\theta\left[\cos\theta_g\begin{Bmatrix} 1 \\ 1 \\ 1 \\ 1 \end{Bmatrix} - \frac{\Delta\theta\sin\theta_g}{6}\begin{Bmatrix} -1 \\ 1 \\ 1 \\ -1 \end{Bmatrix}\right] \qquad (5.25)$$

If we now non - dimensionalize $\dot{\varepsilon}$ by defining,

$$\dot{\varepsilon}' = \frac{\dot{\varepsilon}}{\omega_j}$$

then the right hand side of Equation 5.25 can be expressed as,

$$= \mu \left(\frac{R}{c}\right)^2 \omega_j \Delta\theta \left[9\varepsilon \left(\sin\theta_g \begin{Bmatrix} 1 \\ 1 \\ 1 \\ 1 \end{Bmatrix} + \frac{\Delta\theta \cos\theta_g}{6} \begin{Bmatrix} -1 \\ 1 \\ 1 \\ -1 \end{Bmatrix} \right) \right.$$

$$\left. - 18\dot{\varepsilon}' \left(\cos\theta_g \begin{Bmatrix} 1 \\ 1 \\ 1 \\ 1 \end{Bmatrix} - \frac{\Delta\theta \sin\theta_g}{6} \begin{Bmatrix} -1 \\ 1 \\ 1 \\ -1 \end{Bmatrix} \right) \right]$$

The global equations can then be set up in a similar way to that for the steady - state conditions and solved for combinations of ε and $\dot{\varepsilon}'$. The Reynolds boundary condition occurs at a different circumferential location for non - zero values of $\dot{\varepsilon}'$ than for $\dot{\varepsilon}' = 0$, for a given value of ε. As for the steady - state cases, this typically required two or three computer runs to find this point within the +/-2.5 degrees accuracy of the mesh size used. A comparison of the non - dimensional radial and tangential fluid film forces and attitude angles derived by the F.E. analysis and the finite difference method of Pinkus and Sternlicht [86], is shown in Table 5.2 for $L/D = 1.0, \varepsilon = 0.5$ and for several values of $\dot{\varepsilon}'$.

The values of radial and tangential fluid forces as functions of eccentricity ratio and squeeze film velocity obtained by the present analysis are closely comparable with those cited.

5.3 Stiffness and Damping Coefficients

The stiffness and damping coefficients referred to a coordinate system parallel and perpendicular to the line of centres (journal - bearing) with origin at the journal centre, can be derived from the radial and tangential fluid forces and their derivatives as shown in Appendix C.

For the stiffness matrix we have,

$$\frac{c}{W}\begin{bmatrix} K_{\xi\xi} & K_{\xi\eta} \\ K_{\eta\xi} & K_{\eta\eta} \end{bmatrix} = S^{-1}\begin{bmatrix} -\frac{\overline{F}_x}{\epsilon_o} & -\frac{\partial \overline{F}_t}{\partial \epsilon} \\ \frac{\overline{F}_t}{\epsilon_o} & -\frac{\partial \overline{F}_r}{\partial \epsilon} \end{bmatrix}, \tag{5.26}$$

and for the damping matrix,

$$\frac{c\omega_j}{W}\begin{bmatrix} C_{\xi\xi} & C_{\xi\eta} \\ C_{\eta\xi} & C_{\eta\eta} \end{bmatrix} = S^{-1}\begin{bmatrix} \frac{2\overline{F}_t}{\epsilon_o} & -\frac{\partial \overline{F}_t}{\partial \dot{\epsilon}'} \\ \frac{2\overline{F}_r}{\epsilon_o} & -\frac{\partial \overline{F}_r}{\partial \dot{\epsilon}'} \end{bmatrix}, \tag{5.27}$$

where ξ and η are the tangential and radial coordinates respectively.

The derivatives with respect to ε are conveniently derived by numerical differentiation about the equilibrium value of ε. For the derivatives with respect to $\dot{\varepsilon}'$, it is computationally more efficient to solve directly for the derivative of the global pressure vector with respect to $\dot{\varepsilon}'$ and to then integrate this over the bearing film. However this is only possible for small variations in $\dot{\varepsilon}'$ about zero. This is because, although the Reynolds Equation 5.1 is linear in $\dot{\varepsilon}'$, the requirement that the pressure be always greater than zero is non - linearly dependent on the value of $\dot{\varepsilon}'$. This is why the circumferential position of the Reynolds boundary condition ($p = 0$ and $\partial p/\partial\theta = 0$) has to be determined for each value of ε and $\dot{\varepsilon}'$.

For small perturbations about the equilibrium position, where we can assume the same boundary condition as for $\dot{\varepsilon} = 0$, the element equation is,

$$\left\{\frac{(1+\varepsilon\cos\theta_g)^3}{\Delta\theta}\left[\begin{bmatrix} 2 & -2 & -1 & 1 \\ -2 & 2 & 1 & -1 \\ -1 & 1 & 2 & -2 \\ 1 & -1 & -2 & 2 \end{bmatrix}+\frac{R^2\Delta\theta^2}{l^2}\begin{bmatrix} 2 & 1 & -1 & -2 \\ 1 & 2 & -2 & -1 \\ -1 & -2 & 2 & 1 \\ -2 & -1 & 1 & 2 \end{bmatrix}\right]\right.$$

$$\left.-\frac{3}{2}\varepsilon\sin\theta_g(1-\varepsilon\cos\theta_g)^2\left(\frac{R^2\Delta\theta^2}{l^2}\right)\begin{bmatrix} -1 & 0 & 0 & 1 \\ 0 & 1 & -1 & 0 \\ 0 & -1 & 1 & 0 \\ 1 & 0 & 0 & -1 \end{bmatrix}\right\}^e\begin{Bmatrix} p^i_{,\dot\varepsilon'} \\ p^j_{,\dot\varepsilon'} \\ p^k_{,\dot\varepsilon'} \\ p^l_{,\dot\varepsilon'} \end{Bmatrix}^e$$

$$=-18\mu\left(\frac{R}{c}\right)^2\omega_j\Delta\theta\left[\cos\theta_g\begin{Bmatrix} 1 \\ 1 \\ 1 \\ 1 \end{Bmatrix}-\frac{\Delta\theta\sin\theta_g}{6}\begin{Bmatrix} -1 \\ 1 \\ 1 \\ -1 \end{Bmatrix}\right]. \qquad (5.28)$$

For perturbations in velocity about a non - zero steady - state value of $\dot\varepsilon'$, it would be necessary to carry out a numerical differentiation of the fluid forces with respect to $\dot\varepsilon'$.

For small values of ε_o, i.e. for a journal riding high in the bearing, as for a lightly loaded bearing, the off-diagonal terms become large and approach each other in magnitude. Similarly, the direct terms approach each other. The matrix therefore has strong circulatory coefficients which are destabilizing, as was discussed in Chapters 1 and 2 and demonstrated in Chapter 3.

Consequently this is a major disadvantage of plain bearings for light high - speed rotors but not a problem for such applications as large induction or synchronous motors and generators. This resulted in various more stable fixed geometry, bearing designs such as elliptical (lemon) bore, fixed lobe, offset - halves and pressure - dam, but the tilting - pad bearing is undoubtedly the most successful design and is the subject of the next chapter.

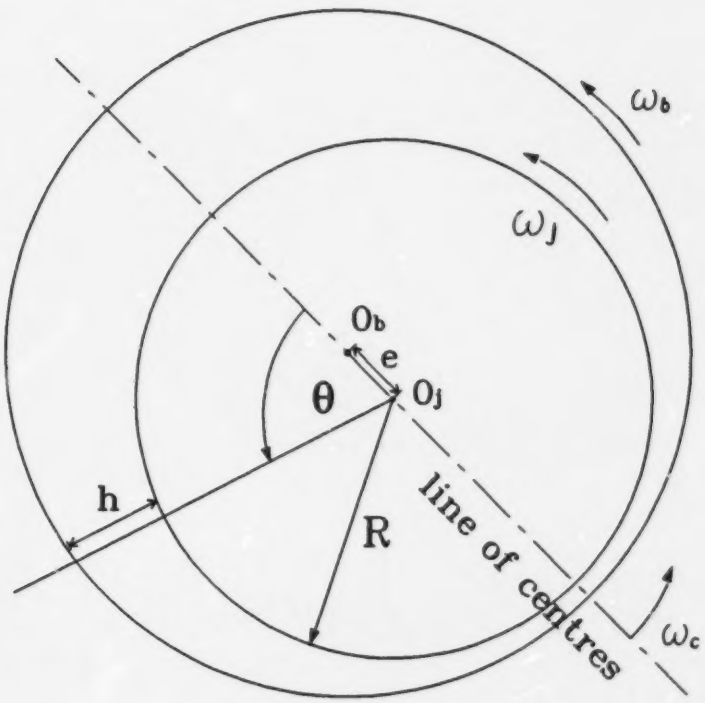

Figure 5.1: Notation Used in Analysis of Journal in Circular Cylindrical Bearing. The local film thickness $h = c(1 + \varepsilon\cos\theta)$ where c is radial clearance, ε is the ratio of the eccentricity e to the radial clearance and θ the angular position measured relative to the line of centres.

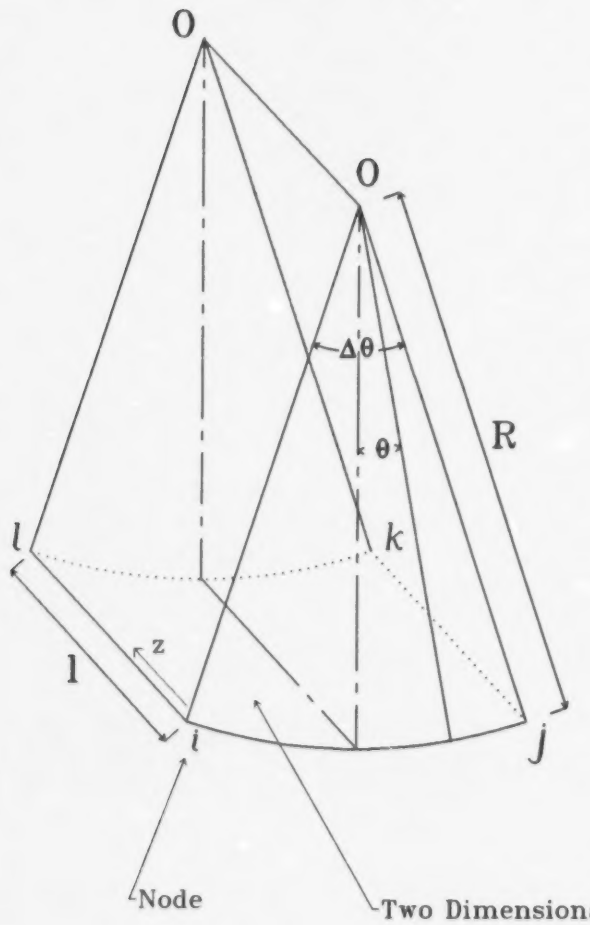

Figure 5.2: Rectangular Element, Notation Within Element.

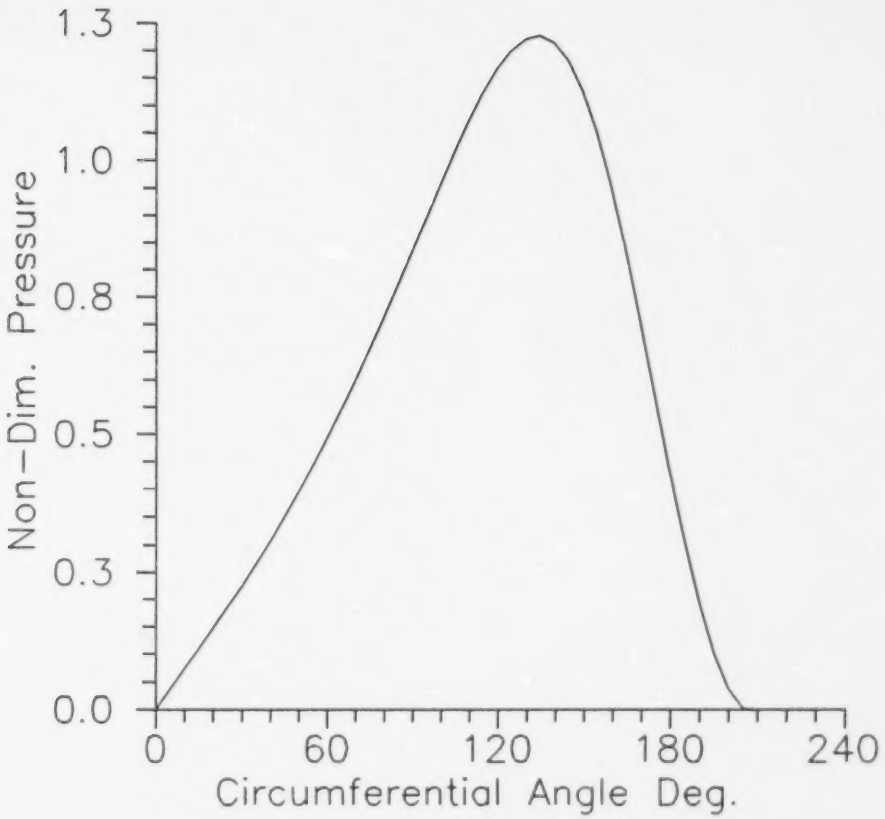

Figure 5.3: Non-Dim Pressure Profile at Mid-Bearing Span with Reynolds' Boundary Condition. L/D=1.0, ε=0.4. Pressure = Non-Dim. Pressure times $\mu\,(R/c)^2\,\omega_j$, where μ is absolute viscosity, R/c is ratio of journal radius to radial clearance and ω_j is the angular velocity of the journal.

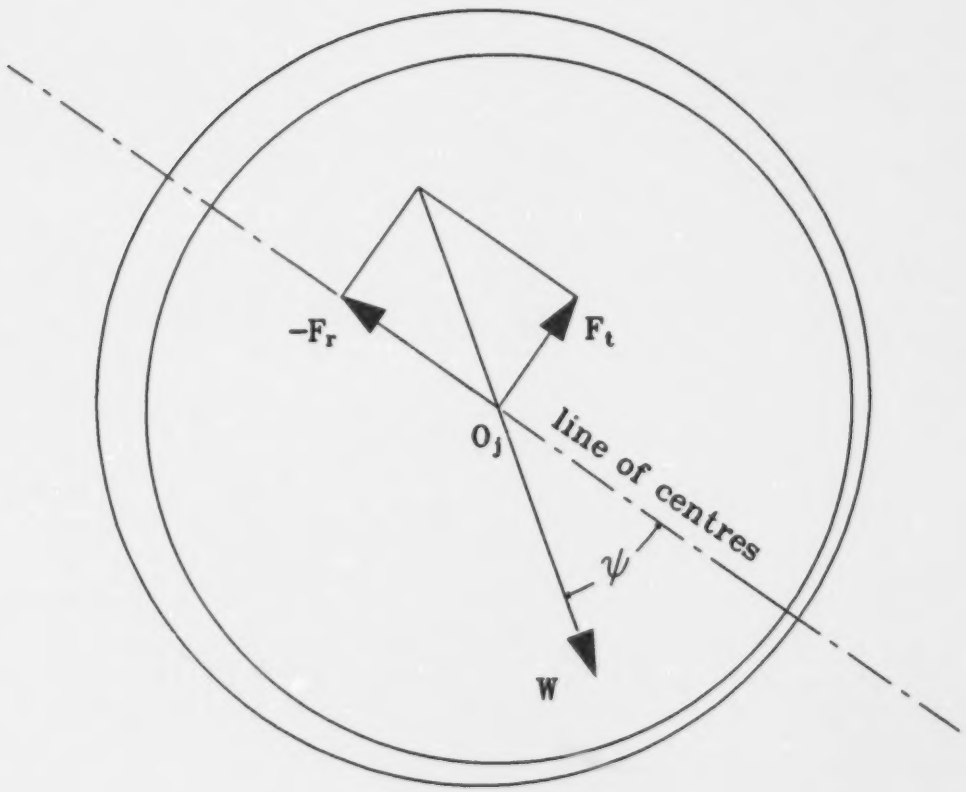

Figure 5.4: Attitude Angle of Journal Within a Bearing

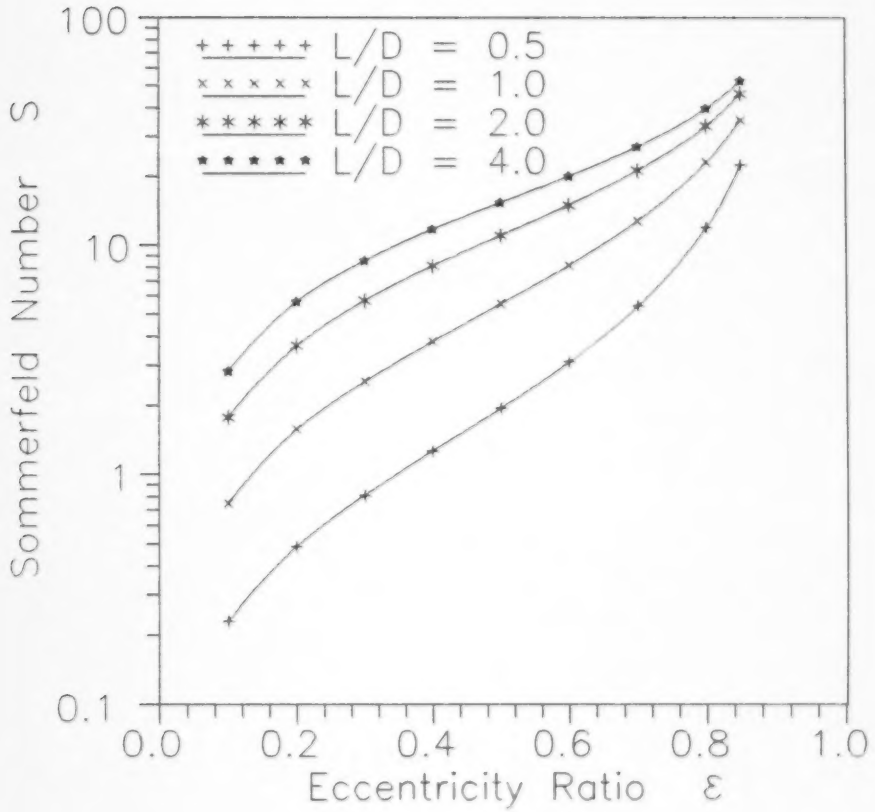

Figure 5.5: Sommerfeld Number S, Versus Eccentricity Ratio, ε for Four Values of Length to Diameter Ratio L/D.

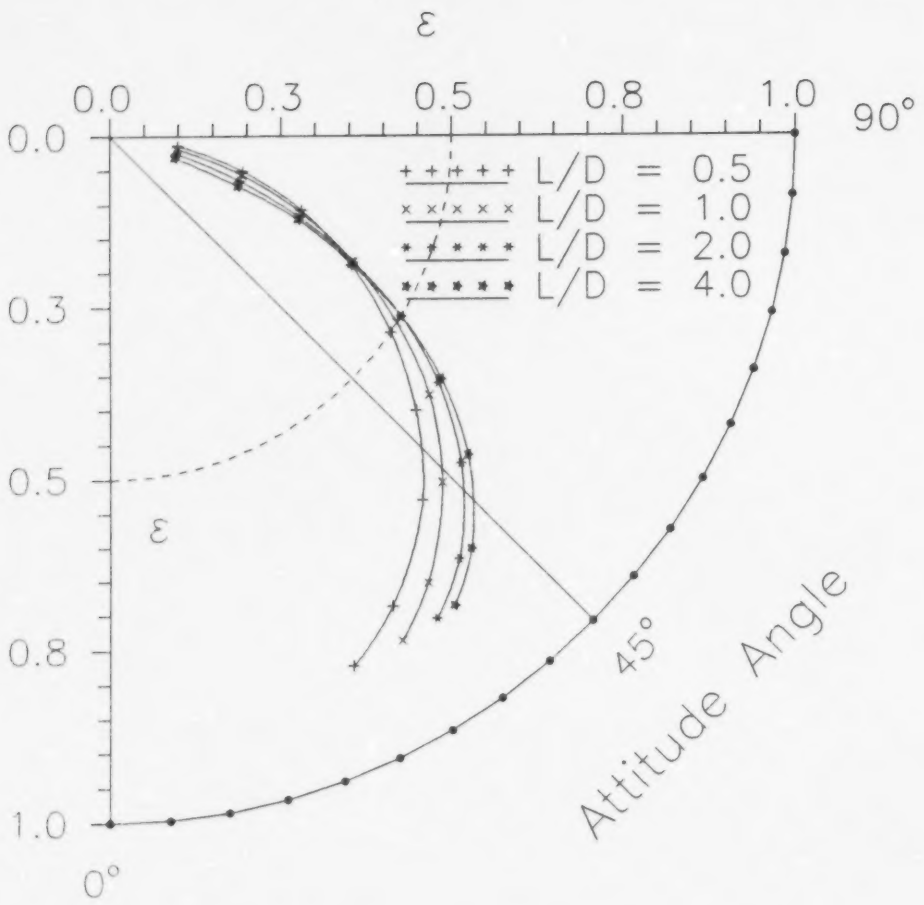

Figure 5.6: Attitude Angle ψ, Versus Eccentricity Ratio ε, for Four Values of Length to Diameter Ratio L/D Ratio.

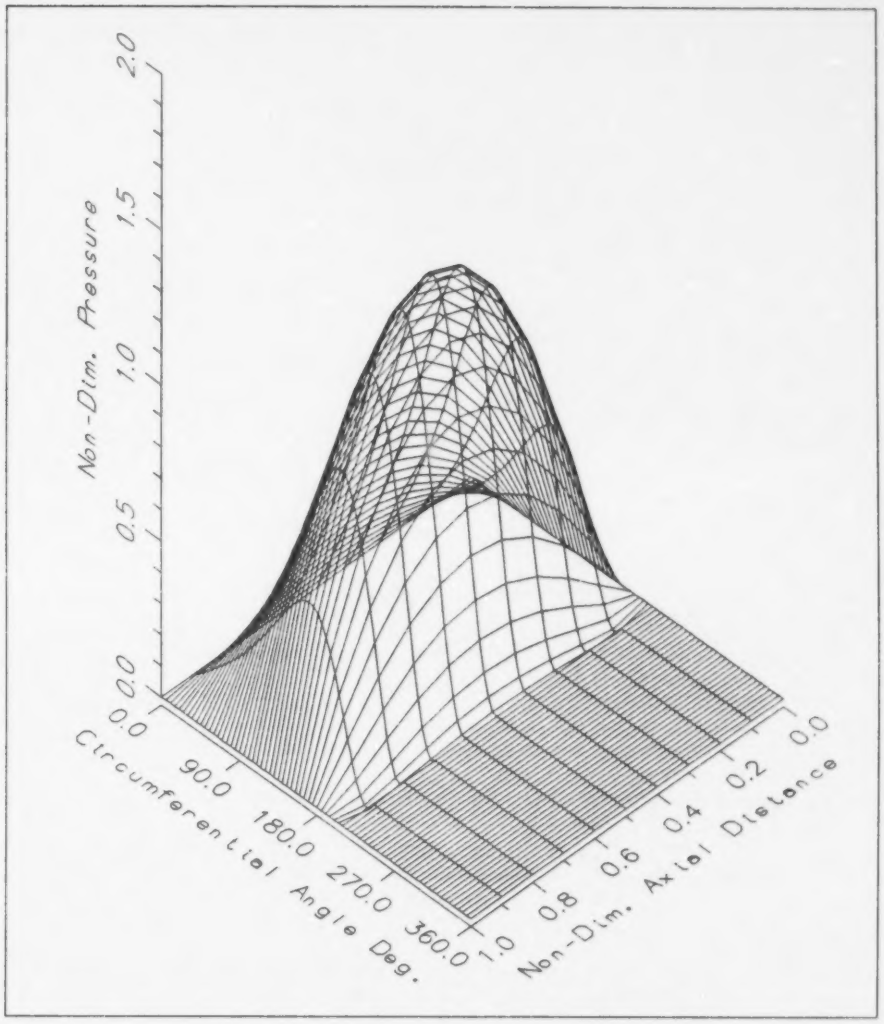

Figure 5.7: Non-Dimensionalized Pressure Profile with Reynolds Boundary Condition for L/D=1.0 and ε=0.4. Pressure = Non-Dim. Pressure times $\mu\,(R/c)^2\,\omega_j$, where μ is absolute viscosity, R/c is ratio of journal radius to radial clearance and ω_j is the angular velocity of the journal.

L/D	ε	Sommerfeld No.		Attitude Angle ψ	
		Ref. [86]	Present Study	Ref. [86]	Present Study
0.5	0.1	0.2326	0.2287	81	82
	0.2	0.4975	0.4865	75	75
	0.3	0.8097	0.8091	68	69
	0.4	1.2739	1.2597	62	62
	0.5	2.0121	1.9426	55	55
	0.6	3.1250	3.1040	48	48
	0.7	5.4054	5.4126	41	41
	0.8	10.8696	11.9683	33	31
	0.85		22.4860		25
	0.9	32.0513		23	
	0.95	84.0336		15	
1.0	0.1	0.7407	0.7453	79	79
	0.2	1.5823	1.5687	74	74
	0.3	2.6178	2.5485	68	68
	0.4	3.8314	3.8026	62	62
	0.5	5.5866	5.5337	56	57
	0.6	8.3333	8.1430	50	51
	0.7	13.0719	12.7784	43	44
	0.8	22.3214	23.0715	36	36
	0.85		35.3382		30
	0.90	52.3560		25	
	0.95	116.9591		16	

Table 5.1: Comparison of Steady - State Data Produced in Present Study and that of Pinkus and Sternlicht

ε	$\dot{\varepsilon}'$	$\pi\dot{\varepsilon}'$	$-\overline{F}_r$		$\overline{F}_t$		Attitude Angle ψ	
			Ref. [86]	Present	Ref. [86]	Present	Ref. [86]	Present
0.5	0.63662	2.0	40.00	38.8493	7.30	6.9332	10.3	10.1
0.5	0.6			36.6296		6.9183		10.7
0.5	0.5			30.5419		6.9157		12.8
0.5	0.47746	1.5	29.50	29.1799	6.80	6.8969	13.0	13.3
0.5	0.4			24.4790		6.8546		15.6
0.5	0.31831	1.0	19.50	19.5241	6.45	6.7808	18.3	19.1
0.5	0.3			18.4435		6.7291		20.0
0.5	0.2			12.5754		6.4048		27.0
0.5	0.15915	0.5	10.50	10.2761	5.70	6.1900	28.5	31.1
0.5	0.1			7.1547		5.7516		38.8
0.5	0.0		2.90	3.0167	4.77	4.6391	59.8	57.0

Table 5.2: Comparison of Dynamic Data Produced in Present Study and that of Pinkus and Sternlicht, (who used $\pi\dot{\varepsilon}'$ as the non - dimensionalized squeeze - film velocity).

Chapter 6

Tilting - Pad Bearings

In this chapter, the finite element approach is used to determine Sommerfeld number, (based on pad clearance) and the stiffness and damping coefficients for a tilting - pad bearing. The pressure profile is determined for each pad and the angular orientation (tilt) of each pad.

The functional for an element of the fluid can be expressed as follows.

$$I^e(p) = \int\int_A \left(\frac{1}{24\mu} \left(\frac{c}{R_j} \right)^2 \left(\frac{h(\theta)}{c} \right)^3 \left[\left(\frac{\partial p}{\partial \theta} \right)^2 + R_j^2 \left(\frac{\partial p}{\partial z} \right)^2 \right] \right.$$
$$\left. + \left(\frac{h'(\theta)}{c} \right) \left[\frac{\omega_j}{2} - \omega_c \right] p + \frac{\partial}{\partial t} \left(\frac{h(\theta)}{c} \right) . p \right) dA. \qquad (6.1)$$

This is the same form as the element functional used for the plane bearing in the previous chapter. The film thickness h (see Figure 6.1), however is no longer simply a function of the eccentricity and the angular location, but also of the tilt of the pad. The prime indicates differentiation with respect to θ.

Referring to Figure 6.2 R_p is the pad radius and the pad clearance c_p is defined as the radial clearance that there would be if the journal and the pad had the same centre of curvature so that,

$$c_p = R_p - R_j.$$

The bearing radius R_b is defined as the radius of the points on the pads immediately above the pivots and the bearing clearance c is therefore defined as,

$$c = R_b - R_j$$

as for the plain bearing. The pad preload m is then

$$m = 1 - \frac{c}{c_p}.$$

The non - dimensional film thickness h_{nt} (Figure 6.3), for a pad with zero tilt can be expressed (after some geometry and algebra) as,

$$\frac{h_{nt}}{c} = -\frac{m}{(1-m)}\cos(\theta-\theta_p) - \frac{R_j}{c} + \varepsilon\cos\theta +$$

$$\left[\frac{R_j}{c} + \frac{1}{(1-m)}\right]\left[1 - \left(\frac{m}{1-m}\right)^2 \frac{(1-\cos^2(\theta-\theta_p))}{(R_j/c+1/(1-m))^2}\right]^{0.5}. \qquad (6.2)$$

As R_j/c is typically of the order of 10^3, the second term under the square root is of the order of 10^{-6} and can be ignored.

Therefore we obtain:

$$\frac{h_{nt}}{c} \simeq \frac{1}{(1-m)}[1 + \varepsilon(1-m)\cos\theta - m\cos(\theta-\theta_p)]. \qquad (6.3)$$

The additional film thickness due to pad tilt h_t is given by the following.

$$h_t = h1t\frac{(\theta_p-\theta)}{(\theta_p-\theta_1)} \qquad (6.4)$$

where θ_p is the angular position of the pad pivot, θ_1 and $h1t$ are respectively the angular position and film thickness due to pad tilt alone, at the pad leading edge.

Therefore we have the complete expression for the film thickness at an angular position θ, and its derivative with respect to *theta*,

$$\frac{h(\theta)}{c} = [1 + \varepsilon(1-m)\cos\theta - m\cos(\theta-\theta_p)]/(1-m) + \frac{h1t}{c}\frac{(\theta_p-\theta)}{(\theta_p-\theta_1)}, \qquad (6.5)$$

and

$$\frac{h'}{c} = \frac{\partial(h/c)}{\partial\theta} = [\varepsilon(m-1)\sin\theta + m\sin(\theta-\theta_p)] - \frac{h1t}{c(\theta_p-\theta_1)}. \qquad (6.6)$$

Putting the element functional into finite element approximation form in the same manner as for the plain bearing, and extremizing with respect to $\{p\}$ we have,

$$\frac{\partial I^e(p)}{\partial \{p\}^T} =$$

$$\int\int_A^e \left[\left(\frac{c}{R_j}\right)^2 \left(\frac{h(\theta)}{c}\right)^3 \frac{1}{12\mu} \left[\{G_{,\theta}\}\{G_{,\theta}\}^T + R_j^2 \{G_{,z}\}\{G_{,z}\}^T\right]\{p\}^e + \right.$$

$$\left. \frac{h'(\theta)}{c}\left[\frac{\omega_j}{2} - \omega_c\right]\{G\} + \frac{\dot{h}(\theta)}{c}\{G\}\right] dA = 0. \tag{6.7}$$

If we choose elements small enough in the circumferential direction, we can take h to be constant over the element and use the angular location of the mid point of the element θ_g for θ. Then we have,

$$\left(\frac{h(\theta_g)}{c}\right)^3 \int\int^e \left[\{G_{,\theta}\}\{G_{,\theta}\}^T + R_j^2 \{G_{,z}\}\{G_{,z}\}^T\right] dA \{p\}^e =$$

$$- \left(\frac{R_j}{c}\right)^2 12\mu \left[\left(\frac{\omega_j}{2} - \omega_c\right)\frac{h'}{c}\int\int^e \{G\}\, dA + \frac{\dot{h}(\theta_g)}{c}\int\int^e \{G\}\, dA\right]. \tag{6.8}$$

For steady - state conditions we take ω_c and $\dot{h}$ to be zero. Then using the same coefficient matrices that were derived in the previous chapter for the plain bearing, we have the finite element approximation to the equation for an element as follows.

$$\left[[1 + \varepsilon(1-m)\cos\theta_g - m\cos(\theta_g - \theta_p)]/(1-m) + \frac{h1t}{c}\frac{(\theta_p - \theta_g)}{(\theta_p - \theta_1)}\right]^3 \times$$

$$\left[\Delta\theta^{-1}\begin{bmatrix} 2 & -2 & -1 & 1 \\ -2 & 2 & 1 & -1 \\ -1 & 1 & 2 & -2 \\ 1 & -1 & -2 & 2 \end{bmatrix} + \frac{R^2\Delta\theta}{l^2}\begin{bmatrix} 2 & 1 & -1 & -2 \\ 1 & 2 & -2 & -1 \\ -1 & -2 & 2 & 1 \\ -2 & -1 & 1 & 2 \end{bmatrix}\right]\{p\}^e =$$

$$- 9\mu\left(\frac{R_j}{c}\right)^2 \omega_j \Delta\theta \left[[\varepsilon(m-1)\sin\theta_g + m\sin(\theta_g - \theta_p)] - \frac{h1t}{c(\theta_p - \theta_1)}\right]\begin{Bmatrix} 1 \\ 1 \\ 1 \\ 1 \end{Bmatrix}. \tag{6.9}$$

The element equations can then be assembled into a global set of equations and the equations solved for the pressure profile for given values of the leading edge non - dimensionalized film thickness due to tilt alone, $h1t/c$ and eccentricity ratio ε. This yields the non - dimensional radial and tangential components of the fluid force on the journal $\overline{F}_r$ and $\overline{F}_t$.

The pads of a tilting - pad bearing self - align such that the resulting moment about the pivot is zero, i.e. that the line of action of the resultant film force passes through the pad pivot. The moment due to surface traction is small compared with that due to the film pressure. Also for a bearing which has a symmetrical pad arrangement with respect to the load line and centrally pivoted pads, the attitude angle is zero [28]. This last point is often verified during field investigations when the shaft position in the bearing is determined by observing the D.C. voltage change on eddy current vibration transducers as a machine runs down to rest. Unless a machine is badly aligned, those with tilting pad bearings usually have shaft positions quite high in the bearing compared with plain bearings, and directly below the bearing centre. Of course the load line need not always be vertical.

Most tilting pad bearings have a symmetrical pad arrangement, which is fortunate as this is much more amenable to analysis than non symmetrical arrangements. The procedure used in this study for a single pad of such a bearing is to find by an iterative procedure, the value of the leading edge film thickness due to tilt alone $h1t/c$ which, for a given value of eccentricity ratio ε, will produce an attitude angle such that the force passes through the pivot. This condition is that $(\pi - \psi = \theta_p)$ where ψ is the calculated attitude angle for the pad force and θ_p is the angular location of the pivot.

Once this position has been derived, the pressure profile has to be checked for negative values. If there are negative values, then the trailing edge boundary condition has to be adjusted in the same way as for the plain bearing to obtain the Reynolds' condition. The same procedure is then used for each pad.

6.1 Load Capability and Dynamic Coefficients

As for the plain bearing, we obtain, for each pad, non-dimensional radial and tangential forces. For a symmetrical bearing, the tangential forces cancel out and the Sommerfeld number is simply the sum of the non-dimensional radial forces. However it is customary for tilting pad bearings to define the Sommerfeld number with respect to the pad clearance c_p rather than the bearing clearance c.

Hence we have for the i'th pad,

$$F_r^i = \mu \left(\frac{R_j}{c}\right)^2 N D L \overline{F}_r^i \tag{6.10}$$

and

$$F_t^i = \mu \left(\frac{R_j}{c}\right)^2 N D L \overline{F}_t^i. \tag{6.11}$$

The Sommerfeld number based on c is,

$$S = \frac{W}{DL}\left(\frac{c}{R_j}\right)^2 \frac{1}{N\mu}.$$

If we define $\overline{S}$ as the Sommerfeld number based on c_p then,

$$\overline{S} = \frac{S}{(1-m)^2}. \tag{6.12}$$

The stiffness coefficient in the radial direction is:

$$K_{xx} = \frac{\partial}{\partial e}\left(\sum_i -F_r\right) = \frac{W}{cS}\frac{\partial}{\partial \varepsilon}\left(\sum_i -\overline{F}_r^i\right).$$

Therefore the non - dimensional stiffness can be written,

$$\frac{c}{W}K_{xx} = S^{-1}\frac{\partial}{\partial \varepsilon}\left(\sum_i -\overline{F}_r^i\right). \tag{6.13}$$

Again it is customary to non dimensionalize with respect to the pad clearance. Thus we get,

$$\frac{c_p}{W}K_{xx} = \overline{S}^{-1}(1-m)^{-3}\frac{\partial}{\partial \varepsilon}\left(\sum_i -\overline{F}_r^i\right) \tag{6.14}$$

or more conveniently,

$$\frac{c_p}{W}K_{xx} = \left[\frac{\partial}{\partial \varepsilon}\left(\sum_i \overline{F}_r^i\right)\right] / \left[(1-m)\left(\sum_i \overline{F}_r^i\right)\right]. \tag{6.15}$$

For a tilting - pad bearing with a pad arrangement symmetric about the load line and the transverse to the load line, see Figure 6.4, the stiffness in the transverse K_{yy} direction is equal to K_{xx}. The K_{xy} and K_{yx} are negligible. This is a common arrangement and the one used in the example below.

The other most common arrangements are symmetrical about the load line only. Figure 6.5 shows two of the most common of these. For such bearings the stiffness along the load - line is higher than in the transverse direction by the radial stiffness of the film on the pad bisected by the load - line. Again the cross terms are negligible.

To derive damping coefficients, the film velocity term $\dot{h}/c$ is added to Equation 6.9. The right hand side of the element equation in finite element form is then,

$$-9\mu\left(\frac{R_j}{c}\right)^2\omega_j\Delta\theta\left[[\varepsilon(m-1)\sin\theta_g + m\sin(\theta_g-\theta_p)] - \frac{h1t}{c(\theta_p-\theta_1)}\right] - 18\dot{\varepsilon}'\cos(\theta_g).$$

Then the non - dimensionalised damping coefficient is given by,

$$\frac{\omega_j c_p}{W}C_{xx} = \left[\frac{\partial}{\partial\dot{\varepsilon}'}\left(\sum_i \overline{F}_r^i\right)\right] / \left[(1-m)\left(\sum_i \overline{F}_r^i\right)\right]. \tag{6.16}$$

These differentiations are carried out numerically using a change in $\varepsilon = 0.001$ and a change in $\dot{\varepsilon}' = 0.01$.

The computer code for the tilting - pad analysis was written in Fortran.

6.2 Analysis of a Four - Pad Tilting - Pad Bearing

The bearing configuration analyzed is a 4 pad load-between-pads arrangement as shown in Figure 6.4. The pads are symmetrically arranged with respect to the load - line and the transverse to the load - line and each pad extends over 80° circumferential angle. The pad preload was taken to be 2/3 and the length to diameter (LOD) ratio was taken to be 1.0.

The mesh used for each pad for the finite element model consisted of 160 rectangular elements, 10 elements axially and 16 circumferentially i.e. elements which subtend 5 degrees at the bearing centre for a pad of total angle equal to 80 degrees.

The steady - state condition for each pad was determined for values of ε from 0.1 to 0.9 in terms of the Sommerfeld number $\overline{S}$ and Figure 6.7 shows the relationship between ε and $\overline{S}^{-1}$ as calculated in the present study and as calculated by Someya et al. [84]. The two sets of results are essentially identical. For a load-between-pads design, ε could be slightly greater than 1.0. However that is not a situation which would normally occur except in the case of severe vertical misalignment on a machine train. The inverse Sommerfeld number is plotted as this is most common in the literature.

Stiffness and damping coefficients are shown in Figures 6.8 and 6.9 respectively. Log - log scales are used as is the norm in the literature. The stiffnesses calculated in this study are higher than those of [84] by 21 - 22% for $\overline{S}^{-1}$ greater than 0.06 but reducing to 7.6% higher at $\overline{S}^{-1} = 0.0144$. The damping coefficients for this study are lower than those of [84] by 10 - 14%.

This comparison is quite close considering the variations of such calculations in the literature although given the identical $\overline{S}^{-1}$ vs, ε values, the differences may be due in part to adjustments made to the values in [84] after the basic calculations.

The non-dimensionalized pressure profiles for the four pads for an eccentricity ratio $\varepsilon = 0.5$ is shown in Figure 6.10. For Pad 1, the trailing edge boundary condition was set at $\theta = 170°$ to approximate the Reynolds condition. The other 3 pads have zero pressure at the trailing edge with no negative pressures.

The lower two pads support the rotor - shaft load plus the small load from the top pads. For steady - state conditions, the top pads serve little purpose. However, during transient conditions, the top pads can restrain the rotor assembly.

Figure 6.6 is a sketch of how the pads orient themselves around the journal (greatly exaggerated). Pads 1 and 2 are almost radially symmetrical with respect to the journal. The journal is a little closer to the trailing edge of Pad 1 than Pad 2. The ratio of leading edge to trailing edge film thickness h_1/h_2 for Pads 1 and 2 is 2.87 and 2.98 respectively. Similarly for the top Pads 3 and 4, h_1/h_2 is 1.94 and 1.92 respectively. Pinkus and Sternlicht [86] showed for a plane slider (zero preload) that maximum load capability was achieved for $h_1/h_2 = 2.2$ but that this increased for increasing pad curvature (increasing preload). Boyd and Raimondi [36] showed similar values to those calculated here but their method of measuring 'crown' of the pad is not readily translatable into preload. Ettles [37] measured film shapes which varied from $h_1/h_2 \simeq 3.5$ for the highest specific loading to $h_1/h_2 \simeq 1.25$ for the lowest specific loading, on a ships bearing at 100 RPM.

6.3 Discussion

The effective stiffness and damping coefficients of the bearing are affected by the mass and flexibility of the pad and of the flexibility and damping of the pivot. This constitutes an additional sub-system which couples with the rotor - shaft system through the bearing film. The studies described in the literature review generally account for this by deriving an equivalent complex impedance matrix for the bearing which is dependent on the complex eigenvalue of the system. Thus one has to choose which eigenvalue to use in order to study the stability of that mode. This choice is easy for a rotating machine as the mode of concern is usually quite clear.

The coefficients derived in this chapter are used in Chapter 7 to evaluate the effect of damping, both internal and external, on the instability mechanism demonstrated in Chapter 4 and [88]. For analysis of a specific real machine, where the quantitative results are of the highest importance, it would be necessary to take account of the pad and support impedances. It is not intended to do that in this study.

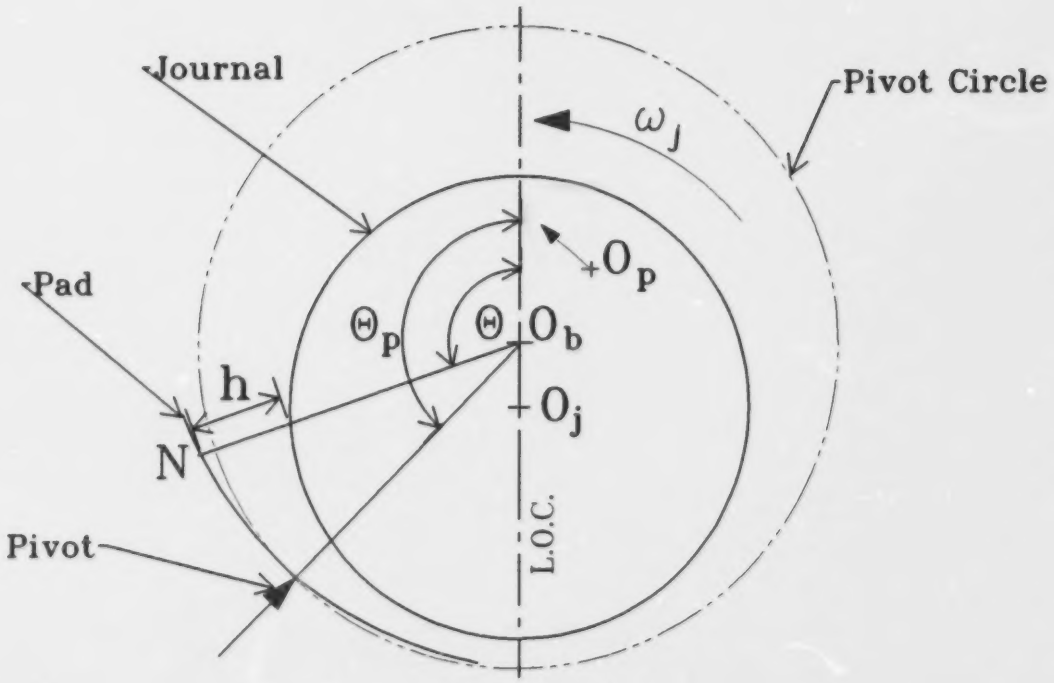

Figure 6.1: Nomenclature for a Tilting-Pad, N = point on the pad surface, θ = angular location of N from line of centres (L.O.C.), θ_p = pivot location, O_p = pad centre of curvature, O_b = centre of pivot circle, O_j = journal centre, ω_j = journal angular velocity, h = film thickness at N.

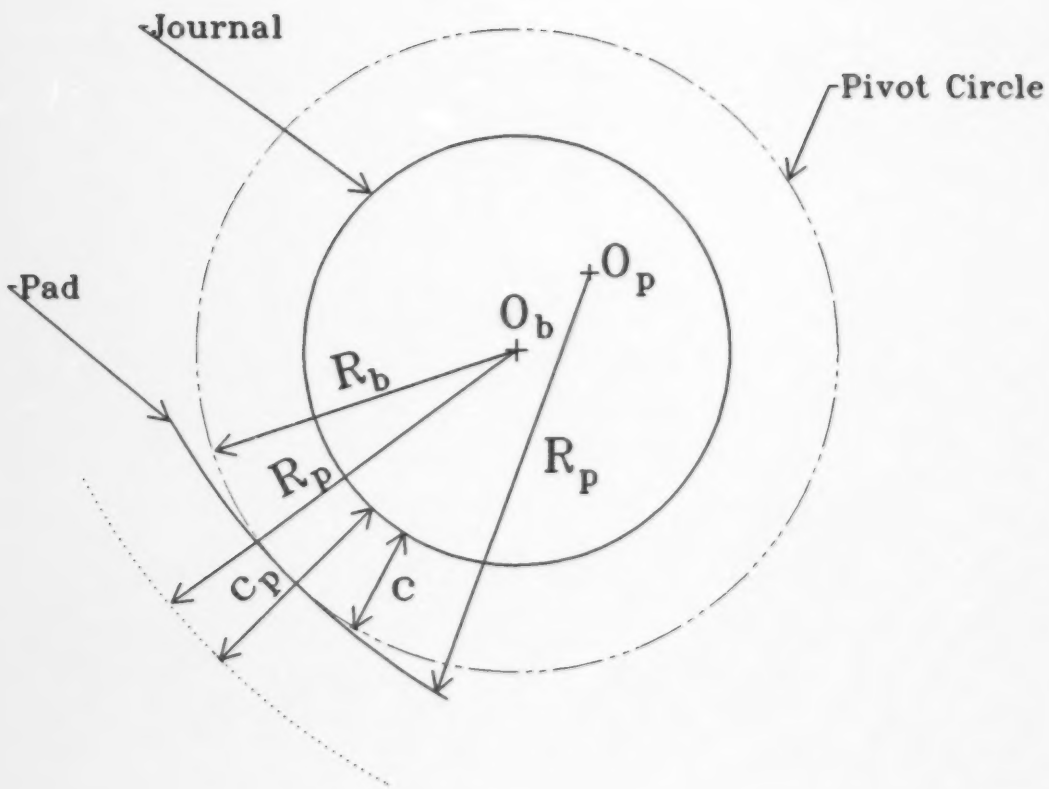

Figure 6.2: Definitions of Pad Clearance c_p and Bearing Clearance c. R_p = pad radius of curvature, R_b = radius of pivot circle.

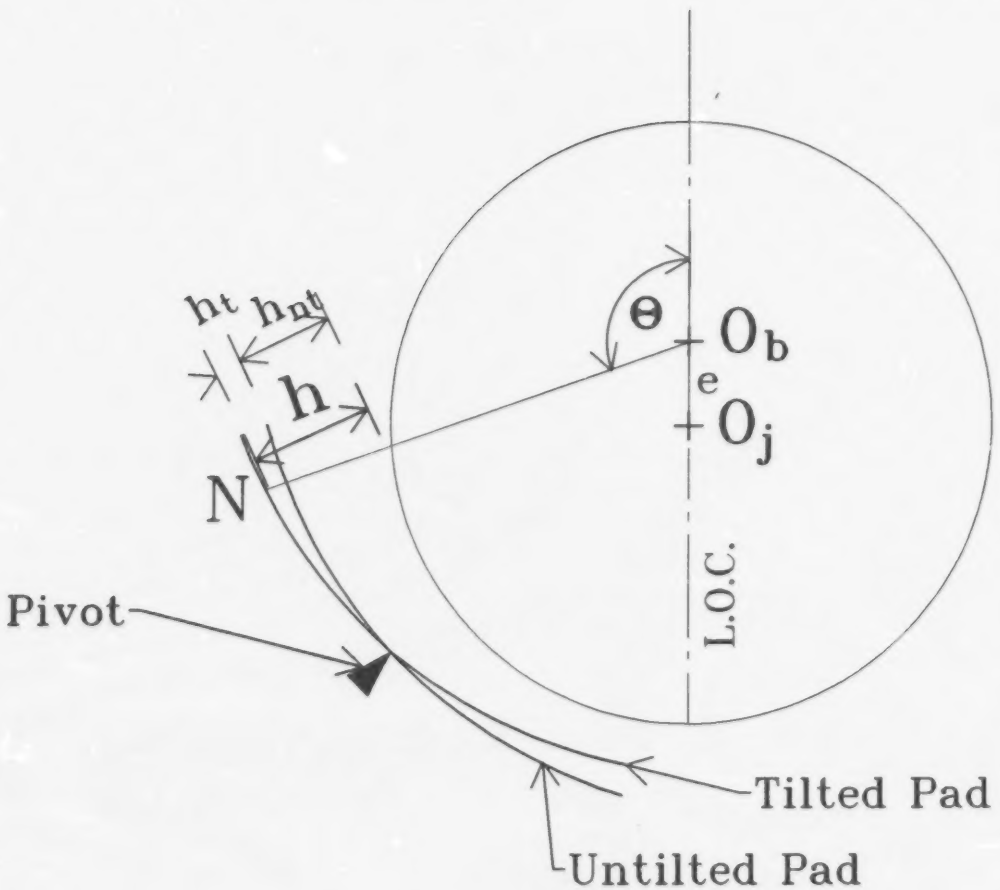

Figure 6.3: **Notation for Film Thickness Calculation; h = total film thickness at point N, h_{nt} film thickness at N without any pad tilt, h_t = film thickness contribution due to pad tilt alone.**

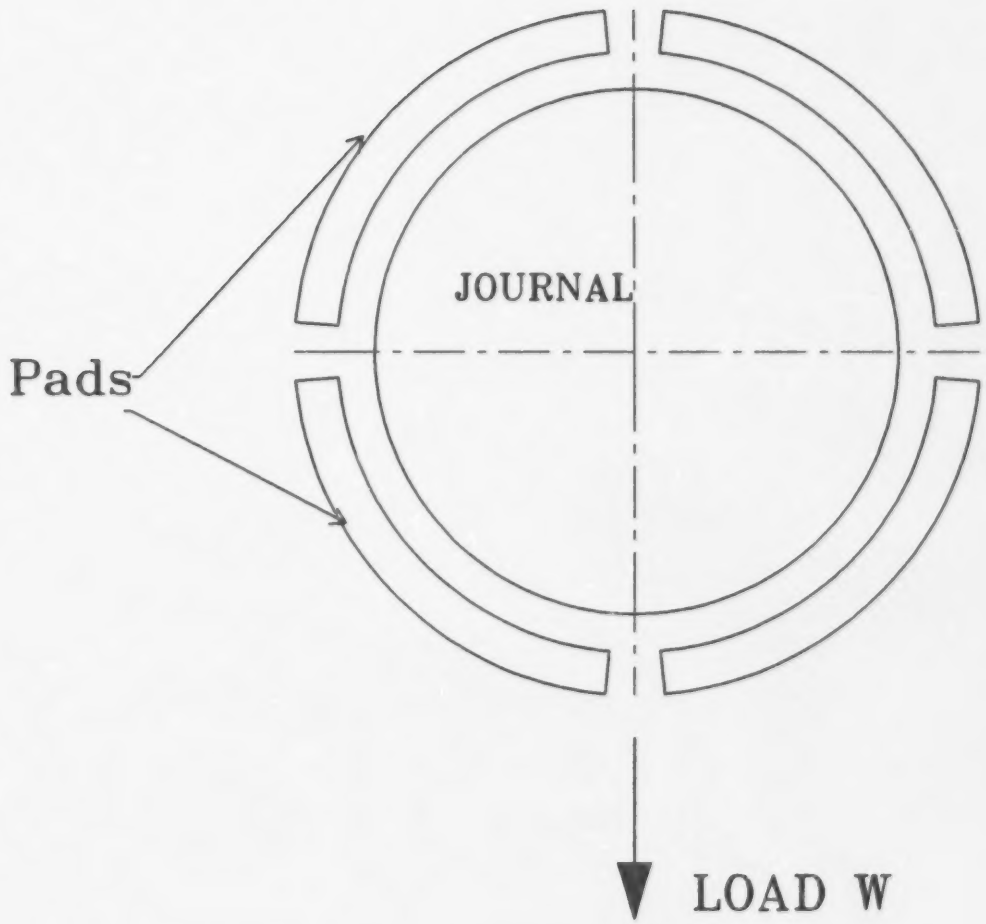

Figure 6.4: Pad Arrangement for Case Analyzed. The pads are located symmetrically around the bearing with each pad extending for 80° circumferentially.

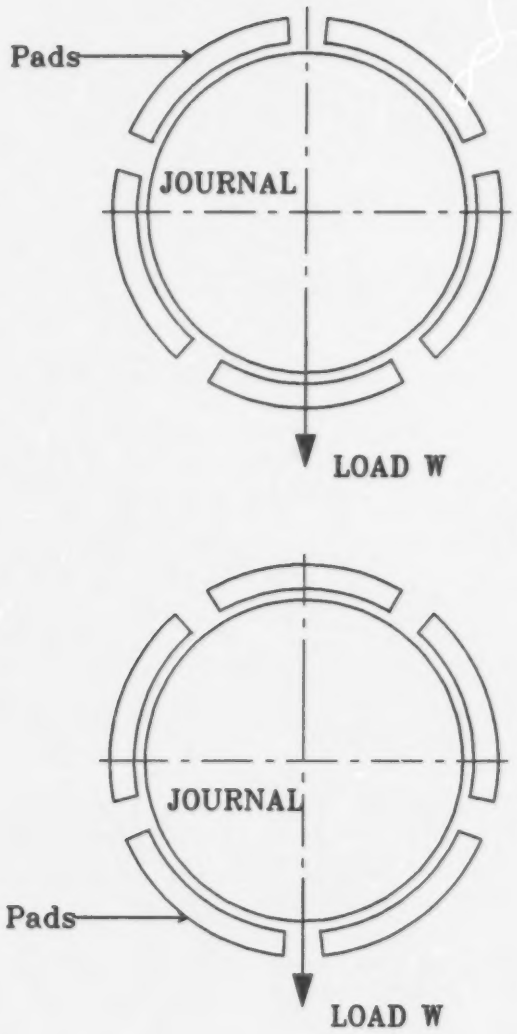

Figure 6.5: **Typical Pad Arrangements of Five - Pad Bearings. The upper sketch is a load-on-pad arrangement and the lower one is a load-between-pads arrangement.**

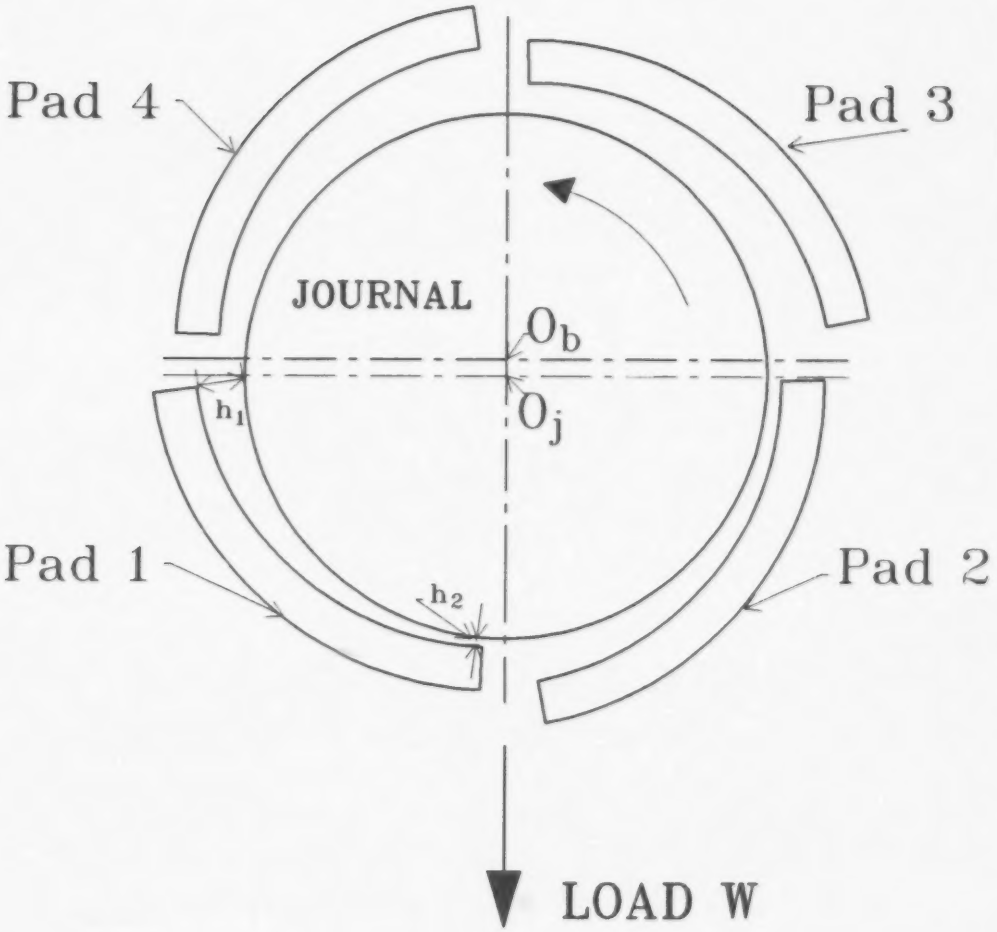

Figure 6.6: Illustration of Pad Orientation During Normal Operation.

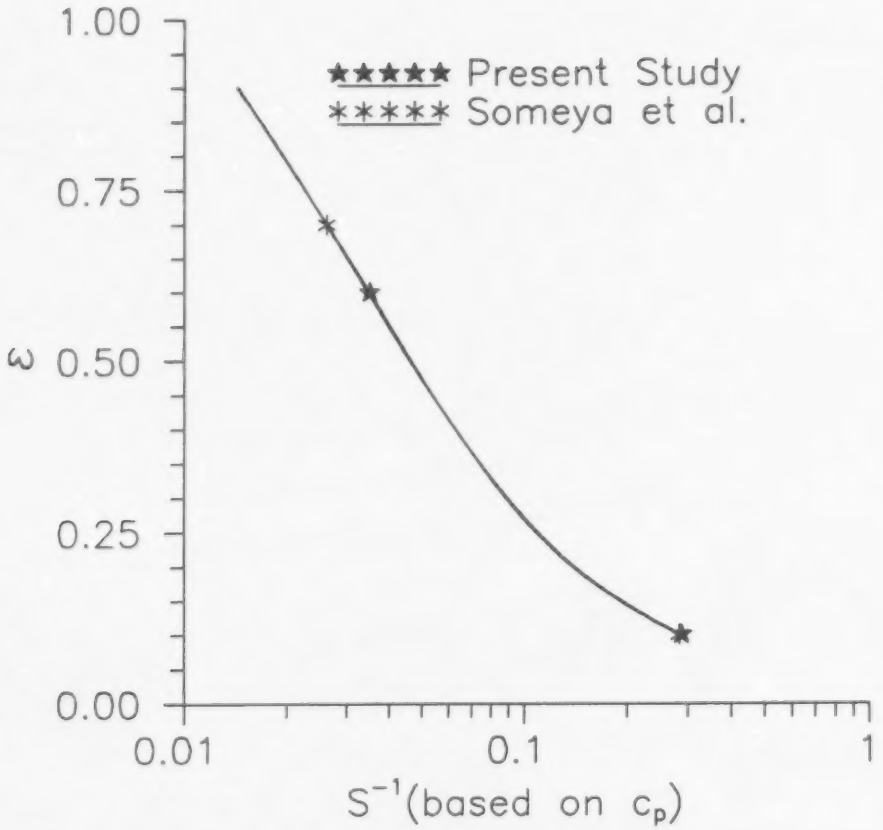

Figure 6.7: Eccentricity Ratio ϵ vs. Inverse Sommerfeld Number S^{-1} for Four Pad Tilting - Pad Bearing.

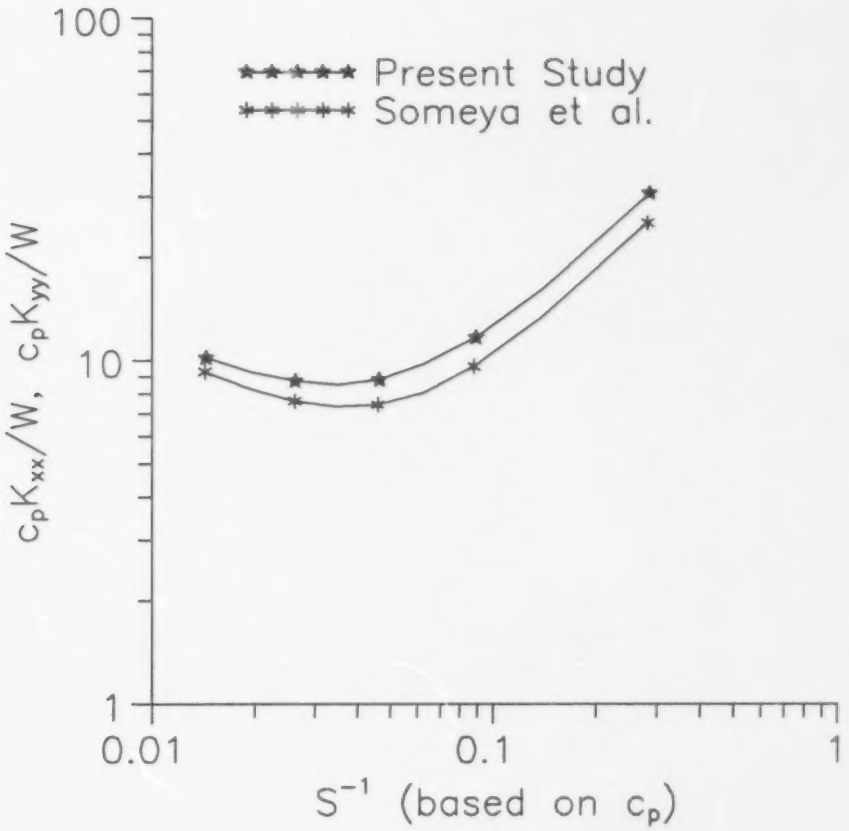

Figure 6.8: Non - Dimensionalized Stiffness Coefficient vs. Inverse Sommerfeld Number S^{-1} (based on pad clearance c_p).

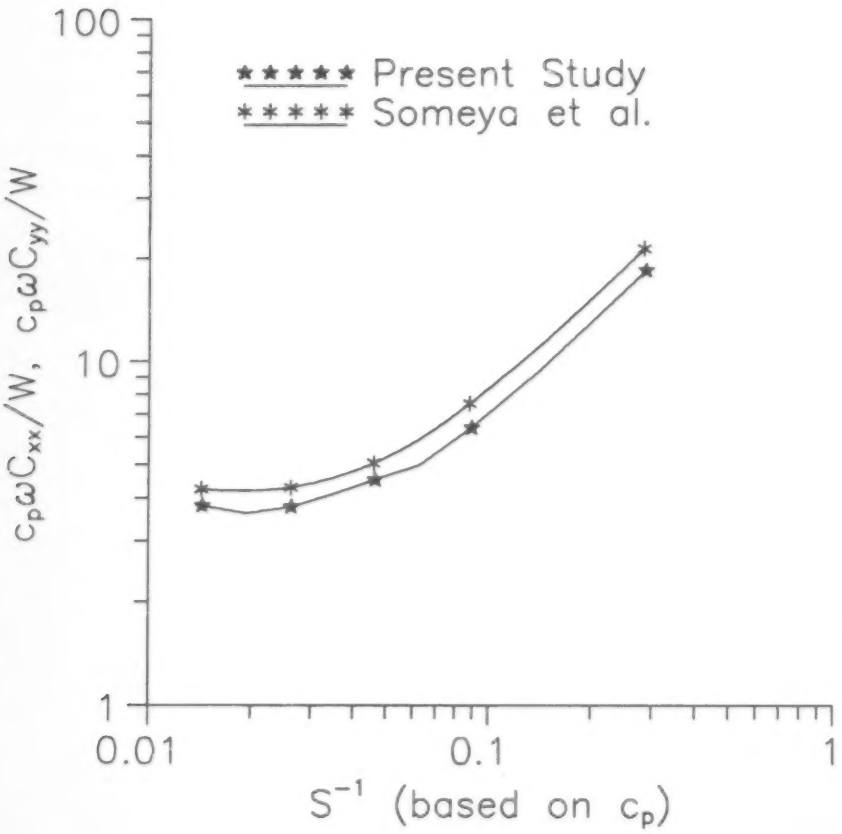

Figure 6.9: Non - Dimensionalized Damping Coefficient vs. Inverse Sommerfeld Number S^{-1} (based on pad clearance c_p).

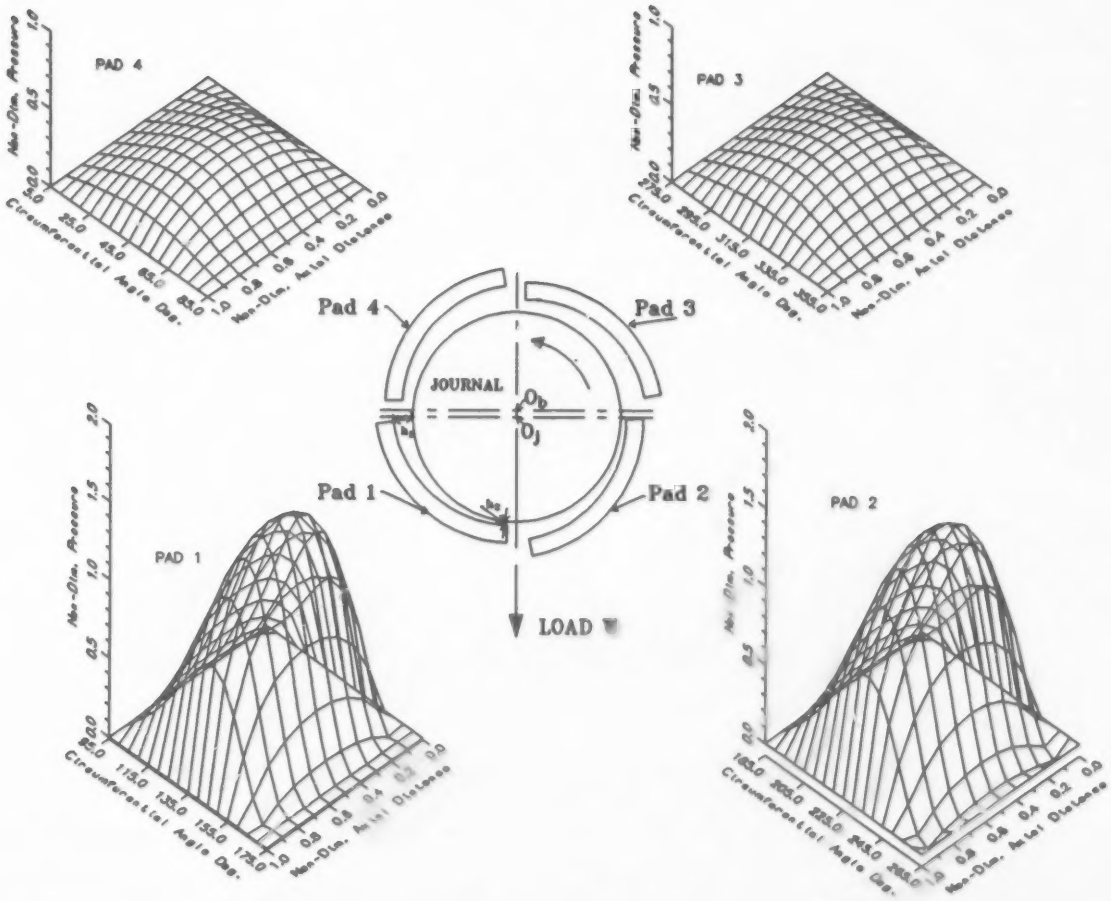

Figure 6.10: Pressure Profiles on Each Pad of Four Pad Tilt - Pad Bearing.

Chapter 7

Flexible Shaft - Rotor with Internal and External Damping.

There are two distinct classes of damping to be considered for a rotating machine; firstly that due to forces generated in the bearing fluid or the working fluid, i.e. external to the rotor - shaft (external damping), and secondly, that due to dissipative forces generated within the rotor - shaft, (internal damping). The former is generally stabilizing and the latter can be destabilizing as described in the literature review, Chapter 2 for a simple rotor.

7.1 Derivation of Damping Terms.

For most machines with journal bearings, the major source of external damping is the bearing fluid. Suppose we have, for a section of shaft supported by a bearing, a damping matrix / unit length,

$$[C] \equiv \begin{bmatrix} C_{xx} & C_{xy} \\ C_{yx} & C_{yy} \end{bmatrix},$$

referred to the inertial frame of reference. The force components per unit length are then given by,

$$\begin{Bmatrix} f_x \\ f_y \end{Bmatrix}_c = -\begin{bmatrix} C_{xx} & C_{xy} \\ C_{yx} & C_{yy} \end{bmatrix} \begin{Bmatrix} x_{,t} \\ y_{,t} \end{Bmatrix}. \tag{7.1}$$

As in Chapters 3 and 4, we define $\tau = \omega t$ and the dot operator as $\partial/\partial\tau$. Thus,

$$\begin{Bmatrix} f_x \\ f_y \end{Bmatrix}_c = -\omega \begin{bmatrix} C_{xx} & C_{xy} \\ C_{yx} & C_{yy} \end{bmatrix} \begin{Bmatrix} \dot{x} \\ \dot{y} \end{Bmatrix}. \tag{7.2}$$

Transforming this equation to the rotating frame of reference,

$$\left\{ \begin{array}{c} f_\xi \\ f_\eta \end{array} \right\}_c = -\omega \left[\begin{array}{cc} \cos\tau & \sin\tau \\ -\sin\tau & \cos\tau \end{array} \right] \left[\begin{array}{cc} C_{xx} & C_{xy} \\ C_{yx} & C_{yy} \end{array} \right] \left[\begin{array}{cc} -\sin\tau & -\cos\tau \\ \cos\tau & -\sin\tau \end{array} \right] \left\{ \begin{array}{c} \xi \\ \eta \end{array} \right\}$$

$$- \omega \left[\begin{array}{cc} \cos\tau & \sin\tau \\ -\sin\tau & \cos\tau \end{array} \right] \left[\begin{array}{cc} C_{xx} & C_{xy} \\ C_{yx} & C_{yy} \end{array} \right] \left[\begin{array}{cc} \cos\tau & -\sin\tau \\ \sin\tau & \cos\tau \end{array} \right] \left\{ \begin{array}{c} \dot{\xi} \\ \dot{\eta} \end{array} \right\}. \qquad (7.3)$$

Carrying out the matrix multiplications we obtain,

$$\left\{ \begin{array}{c} f_\xi \\ \\ f_\eta \end{array} \right\}_c =$$

$$-\omega \left[\begin{array}{cc} \left(-C_{xx}\sin 2\tau/2 + C_{xy}\cos^2\tau \right. & \left(-C_{xx}\cos^2\tau - C_{xy}\sin 2\tau/2 \right. \\ \left. -C_{yx}\sin^2\tau + C_{yy}\sin 2\tau/2\right) & \left. -C_{yx}\sin 2\tau/2 - C_{yy}\sin^2\tau\right) \\ \left(C_{xx}\sin^2\tau - C_{xy}\sin 2\tau/2 \right. & \left(C_{xx}\sin 2\tau/2 + C_{xy}\sin^2\tau \right. \\ \left. -C_{yx}\sin 2\tau/2 + C_{yy}\cos^2\tau\right) & \left. -C_{yx}\cos^2\tau - C_{yy}\sin 2\tau/2\right) \end{array} \right] \left\{ \begin{array}{c} \xi \\ \\ \eta \end{array} \right\}$$

$$- \omega \left[\begin{array}{cc} \left(C_{xx}\cos^2\tau + C_{xy}\sin 2\tau/2 \right. & \left(-C_{xx}\sin 2\tau/2 + C_{xy}\cos^2\tau \right. \\ \left. +C_{yx}\sin 2\tau/2 + C_{yy}\sin^2\tau\right) & \left. -C_{yx}\sin^2\tau + C_{yy}\sin 2\tau/2\right) \\ \left(-C_{xx}\sin 2\tau/2 - C_{xy}\sin^2\tau \right. & \left(C_{xx}\sin^2\tau - C_{xy}\sin 2\tau/2 \right. \\ \left. +C_{yx}\cos^2\tau + C_{yy}\sin 2\tau/2\right) & \left. -Cyx\sin 2\tau/2 + C_{yy}\cos^2\tau\right) \end{array} \right] \left\{ \begin{array}{c} \dot{\xi} \\ \\ \dot{\eta} \end{array} \right\}. \qquad (7.4)$$

These coefficient matrices have elements in which some of the terms are cyclic at frequency 2ω. However for the case of the typical tilting - pad bearing analyzed in Chapter 6, $C_{xx} = C_{yy}$, $C_{xy} = C_{yx} = 0$, $K_{xx} = K_{yy}$ and $K_{xy} = K_{yx} = 0$. Then,

$$\left\{ \begin{array}{c} f_\xi \\ f_\eta \end{array} \right\}_c = -\omega \left[\begin{array}{cc} 0 & -C_{xx} \\ C_{xx} & 0 \end{array} \right] \left\{ \begin{array}{c} \xi \\ \eta \end{array} \right\} - \omega \left[\begin{array}{cc} C_{xx} & 0 \\ 0 & C_{xx} \end{array} \right] \left\{ \begin{array}{c} \dot{\xi} \\ \dot{\eta} \end{array} \right\}. \qquad (7.5)$$

The virtual work δW_b^e done on the rotor - shaft by the stiffness and damping forces from a bearing oil film, can then be expressed as follows:

$$\delta W_b^e = -\int_0^l \left(\omega \left\{ \begin{array}{cc} \delta\xi & \delta\eta \end{array} \right\} \left[\left[\begin{array}{cc} 0 & -C_{xx} \\ C_{xx} & 0 \end{array} \right] \left\{ \begin{array}{c} \xi \\ \eta \end{array} \right\} + \left[\begin{array}{cc} C_{xx} & 0 \\ 0 & C_{xx} \end{array} \right] \right] \left\{ \begin{array}{c} \dot{\xi} \\ \dot{\eta} \end{array} \right\} \right.$$

$$\left. + \left\{ \begin{array}{cc} \delta\xi & \delta\eta \end{array} \right\} \left[\begin{array}{cc} K_{xx} & 0 \\ 0 & K_{xx} \end{array} \right] \left\{ \begin{array}{c} \xi \\ \eta \end{array} \right\} \right) d\zeta, \qquad (7.6)$$

where the integration is taken over the bearing element length.

For internal damping, the equivalent procedure (in terms of a matrix - method analysis) to that of Tondl, - Equation 2.32, whereby the damping coefficient is directly defined in the rotating frame of reference, is to simply add an internal damping coefficient 'C_{int}' to the direct terms of the damping matrix in the equations written with respect to the rotating frame of reference.

In Chapters 5 and 6, the damping coefficients were derived in the non-dimensional form $c\omega C_{ij}/W$ versus Sommerfeld number. For a given bearing geometry, oil viscosity and load, the Sommerfeld number becomes a function of speed alone. Then we can express ωC_{ij} as a function of rotor speed alone. This is described in detail in the example. It is therefore convenient to keep the product ωC_{ij} together in the analysis. For the tilting pad bearing example used we have only $C_{ij} = C_{xx}$ for $i = j$ and zero for $i \neq j$.

Therefore, making the finite element approximation, we can write the virtual work in the following form using the same notation as Chapter 4,

$$\delta W_b^e = -\{\delta\Phi^e\}^T \left(\int_0^l [T]^T [B] [[k_b] + \omega [c_s]] [B]^T [T] \, d\zeta \; \{\Phi^e\} \right.$$

$$\left. \int_0^l [T]^T [B] [\omega [c_b] + \omega [c_{int}]] [B]^T [T] \, d\zeta \left\{ \dot{\Phi}^e \right\} \right), \qquad (7.7)$$

where,

$$[c_s] = \left[\begin{array}{cccc} 0 & -C_{xx} & 0 & 0 \\ C_{xx} & 0 & 0 & 0 \\ 0 & 0 & 0 & 0 \\ 0 & 0 & 0 & 0 \end{array} \right], \qquad [c_b] = \left[\begin{array}{cccc} C_{xx} & 0 & 0 & 0 \\ 0 & C_{xx} & 0 & 0 \\ 0 & 0 & 0 & 0 \\ 0 & 0 & 0 & 0 \end{array} \right]$$

and

$$[c_{int}] = \begin{bmatrix} C_{int} & 0 & 0 & 0 \\ 0 & C_{int} & 0 & 0 \\ 0 & 0 & 0 & 0 \\ 0 & 0 & 0 & 0 \end{bmatrix}.$$

Equation 7.7 can be written as:

$$\delta W_b^e = -\{\delta\Phi^e\}^T [[K_b^e] + \omega [C_s^e]] \{\Phi^e\} - \omega \{\delta\Phi^e\} [[C_b^e] + [C_{int}^e]] \left\{\dot{\Phi}^e\right\}, \quad (7.8)$$

where:

$$[C_s^e] = \int_0^l [T]^T [B] [c_s] [B]^T [T] \, d\zeta,$$

$$[C_b^e] = \int_0^l [T]^T [B] [c_b] [B]^T [T] \, d\zeta,$$

and

$$[C_{int}^e] = \int_0^l [T]^T [B] [c_{int}] [B]^T [T] \, d\zeta.$$

We can then express this virtual work expression as:

$$\delta W_b^e = -\{\delta\Phi^e\}^T [[K_b^e] + \omega [C_s^e]] \{\Phi^e\}$$

$$- \{\delta\Phi^e\}^T [\omega [C_b^e] + \omega [C_{int}^e]] \left\{\dot{\Phi}^e\right\}. \quad (7.9)$$

Thus we have additional terms to include in the coefficients in Equation 4.22, resulting in,

$$\omega^2 [M^e] \left\{\ddot{\Phi}\right\} + \left[\omega^2 [G^e] + \omega [C_b^e] + \omega [C_{int}^e]\right] \left\{\dot{\Phi}^e\right\} +$$

$$\left[-\omega^2 [Y^e] + [K^e] + [K_b^e] + \omega [C_s]\right] \{\Phi^e\} = 0. \quad (7.10)$$

The element equations can then be assembled and rearranged into a global set of first order equations as in Chapter 4:

$$\begin{Bmatrix} \dot{\Psi}_g \\ \\ \dot{\Phi}_g \end{Bmatrix} = \begin{bmatrix} -[M_g]^{-1}[G_g]^* & \left([M_g]^{-1}[Y_g] - \omega^{-2}[M_g]^{-1}\left[[K_g] + \left[K_g^b\right]^*\right]\right) \\ \\ [I] & [0] \end{bmatrix} \begin{Bmatrix} \Psi_g \\ \\ \Phi_g \end{Bmatrix}, \tag{7.11}$$

which is the same form as Equation 4.24 with,

$$[G_g]^* = [G_g] + \frac{1}{\omega^2}[\omega[C_g] + \omega[C_{int}]]$$

and

$$\left[K_g^b\right]^* = \left[K_g^b\right] + \omega[C_s].$$

7.2 Speed Dependent Bearing Coefficients

The values of stiffness and damping coefficients for the bearings were taken from those calculated for the symmetric four pad tilting - pad bearing analyzed in Chapter 6. The computer code was modified to accept the coefficients of two polynomial functions of rotor speed as input, so that the stiffness and damping coefficients could be re-calculated at each speed increment.

For the analysis described in this chapter, the same rotor geometry was assumed as in Chapter 4. For the bearings, it was assumed that these had been designed for an inverse Sommerfeld number $S^{-1} = 0.0465$ at 10000 RPM, which corresponds to an eccentricity ratio ε of 0.5. For this rotor, these values give a ratio of diametral clearance to diameter of 1.82 which is in the normal range.

The two polynomials which closely approximate the stiffness and damping curves, Figures 6.8 and 6.9 are:

$$\frac{c_p K_{xx}}{W} = 10.4896 - 82.1188\,S^{-1} + 1215.63\,S^{-2} - 2383.75\,S^{-3}, \tag{7.12}$$

and

$$\frac{c_p \omega C_{xx}}{W} = 3.69084 - 8.96732\,S^{-1} + 636.683\,S^{-2} - 2583.5\,S^{-3} + 3796.21\,S^{-4}. \tag{7.13}$$

For the Sommerfeld number and design speed selected, Equations 7.12 and 7.13 can be re-written as:

$$\frac{c_p K_{xx}}{W} = 10.4896 - 3.818524.10^{-1}\left(\frac{N}{1000}\right) + 2.628496.10^{-2}\left(\frac{N}{1000}\right)^2 - 2.396732.10^{-4}\left(\frac{N}{1000}\right)^3 \tag{7.14}$$

$$\frac{c_p \omega C_{xx}}{W} = 3.69084 - 4.1698.10^{-2}\left(\frac{N}{1000}\right) + 1.376668.10^{-2}\left(\frac{N}{1000}\right)^2 - 2.597504.10^{-4}\left(\frac{N}{1000}\right)^3 + 1.774987.10^{-6}\left(\frac{N}{1000}\right)^4. \tag{7.15}$$

Thus, the coefficients of Equations 7.14 and 7.15 and the value of the expression $W/c_p.l$ become required input values to the computer program, where l is the length of the bearing. The bearing stiffness coefficient per unit length and ω times the bearing damping per unit length can then be calculated at each speed.

7.3 Results and Discussion - External Damping

Figures 7.1 and 7.3 show the instability regions for the same shaft - rotor analyzed in Chapter 4. The bearing stiffness differs in that it now a function of speed, whereas a constant value was assumed in Chapter 4. Up to 10000 R.P.M., this means that the stiffness assumed in this chapter is about 20 % higher than that in Chapter 4 but then increases considerably with speed.

Two damping cases are considered; the first, Figure 7.1, using the polynomial of Equation 7.15 and the second, Figure 7.3, assuming a 25% reduction in damping for the reasons described in Chapter 6.

Figure 7.2 shows the variation of modal frequencies with speed corresponding to a value of $q = 0.45$ on Figure 7.1. Because of the complicated behaviour around 23000 R.P.M. the data points were determined at 100 R.P.M. increments in order to clearly distinguish the eigenvalues from each other. This involved a great many computer runs and a very tedious procedure of distinguishing the eigenvalues by inspection of the trends of both real and imaginary parts of the eigenvalues with speed.

The speed range used for these plots is 3000 to 30000 R.P.M. At lower speeds the damping becomes very large as the polynomial assumed tends to an approximately constant value for ωC_{xx} for small ω and the results become unrealistic. At very low speeds, of course, we no longer have an oil film and hydrodynamic lubrication. 'Slow - roll' speed for most machines is about 300 to 500 R.P.M.

The same basic instability mechanisms occur as for the undamped cases - compare Figures 7.1 and 7.3 with Figure 4.12 and Figure 7.2 with Figure 4.13. However, some of the instabilities have disappeared. These appear to involve antisymmetric modes which would have relatively greater motion at the bearings than along the shaft - rotor, and would therefore be more affected by bearing damping than would symmetric modes. Such modes are indeed more difficult to excite in practise as is sometimes attempted during acceptance tests.

The first backward mode couples with the third forward mode as for the undamped case but the frequencies simply cross rather than coalesce and an unstable region occurs for $q \geq 0.4$ for the nominal damping case and 0.3 for the 25% reduction in damping. At a higher speed, the first backward mode couples with the fifth forward and the first backward mode again becomes unstable. There is a transition between these two regions at $q = 0.48$ for the nominal case and for $q = 0.47$ for the 25% reduced damping case.

The second unstable region is far less influenced by bearing damping than the first. The mode shape of the first forward mode at the higher speed, has relatively more shaft - rotor flexure compared with motion at the bearings than does the mode shape at the lower speed instability. Thus bearing damping would be less effective at the higher speed.

The other regions of modal instability are of little interest because once one instability has occurred, the problem would no longer be linear, the model no longer valid and in practical terms, one modal instability is quite sufficient.

7.4 Internal Damping

Results for a rotor - shaft system having symmetric stiffness and mass properties only was investigated for this thesis. A few analyses were carried out for cases combining both asymmetry of stiffness and internal damping and the results were interesting enough to warrant further study.

The internal damping was included in the central rotor section of the model only as this is typically where internal damping would occur because of the method of rotor construction and assembly. The internal damping coefficient per unit length was varied from 1000 N/(m/s)/m. The bearing damping assumed was the 25% reduced damping discussed in the previous sections.

The only instability to occur in these calculations involved the first forward precessing mode. Figure 7.4 shows the speed at which the instability onset occurs versus the internal damping coefficient per unit length. Also plotted in Figure 7.4 is the frequency of the first forward mode versus speed. This frequency varies little with speed because the gyroscopic terms are small for symmetric modes.

The behaviour is essentially as described by Tondl [57] and Gunter [14] for simple rotors. It is evident that irrespective of how high the internal damping coefficient is made, (the higher values plotted are quite unrealistic), the instability threshold speed is always above the frequency of the first forward mode (critical speed). This is because the internal damping is stabilizing below the first critical and destabilizing above, as was described in Chapter 2. The model therefore behaves for the finite element model as it should compared with the analytical solutions for the simple 'Jeffcott' rotor and we now have a tool to yield quantitative results for realistic configurations.

For the selected test rotor - shaft system with a design operating speed of 10000 R.P.M. we would want to be assured that it would operate up to at least a 'trip' speed of 12000 R.P.M. Thus we would require that the internal damping coefficient per unit length be not greater than 7000 N/(m/s)/m which represents about 2% of the bearing coefficient /unit length assumed for this case. This is clearly achieved in the majority of machines as this type of instability is quite rare.

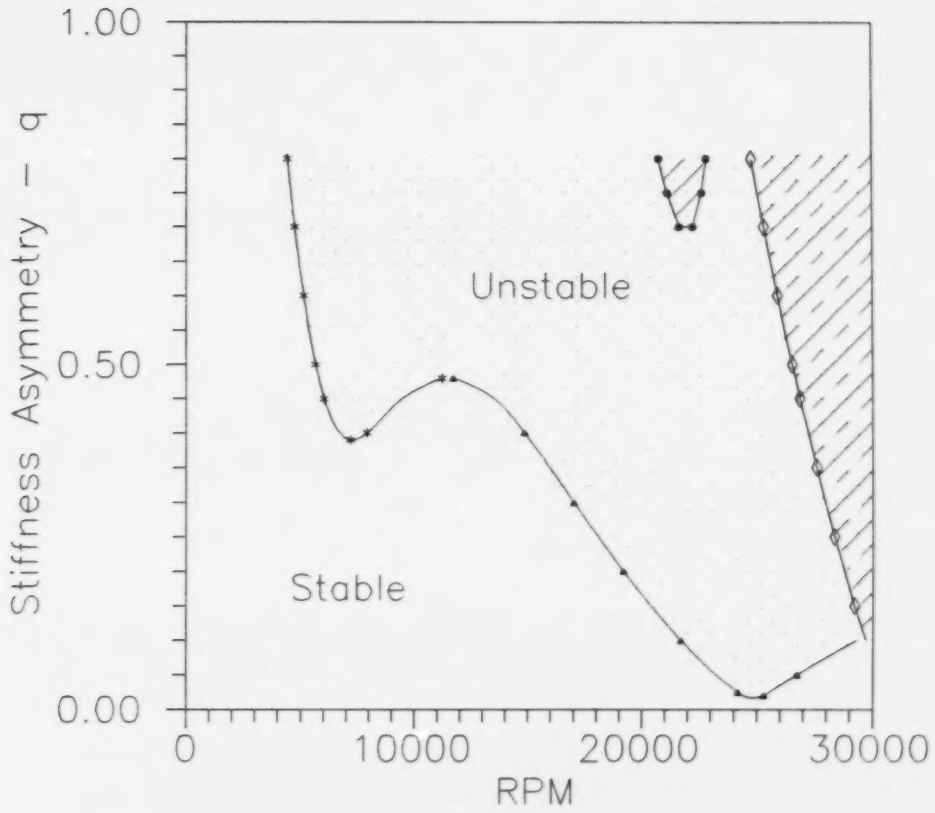

Figure 7.1: Instability Regions for a Flexible Rotor with Speed - Dependent Bearing Stiffness and Damping as Calculated for a Tilting - Pad Bearing.

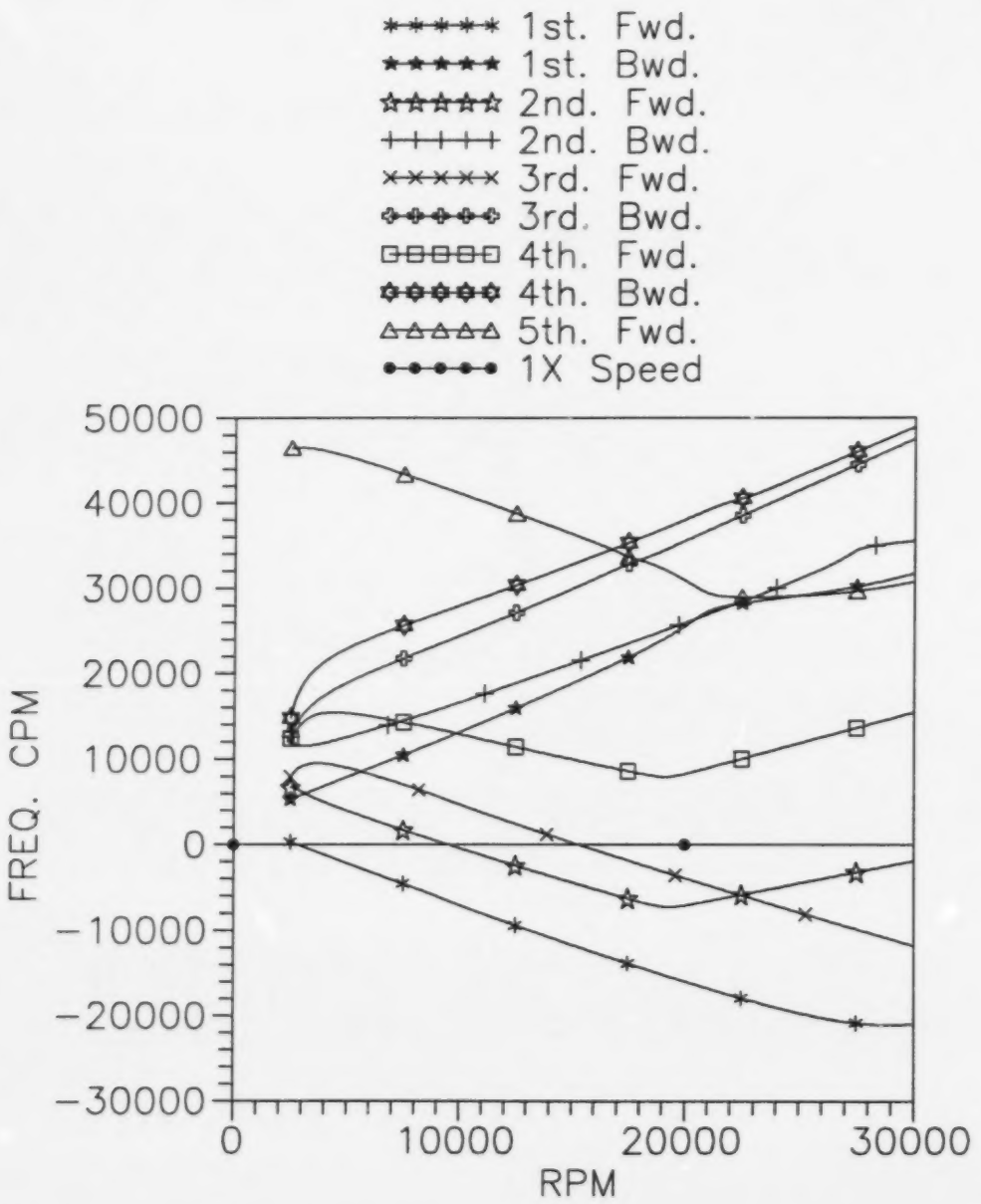

Figure 7.2: Modal Frequencies vs. Speed for q = 0.45 with Speed - Dependent Bearing Stiffness and Damping as Calculated for a Tilting - Pad Bearing.

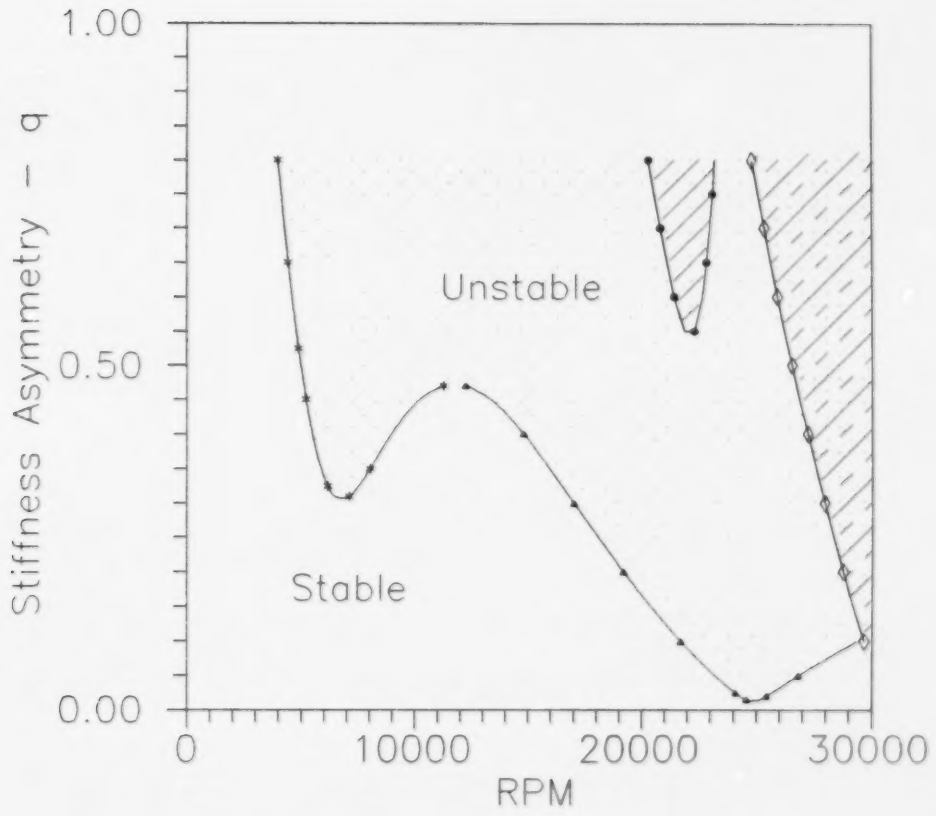

Figure 7.3: Instability Regions for a Flexible Rotor with Speed - Dependent Bearing Stiffness and Damping, Damping 25% Less Than Calculated.

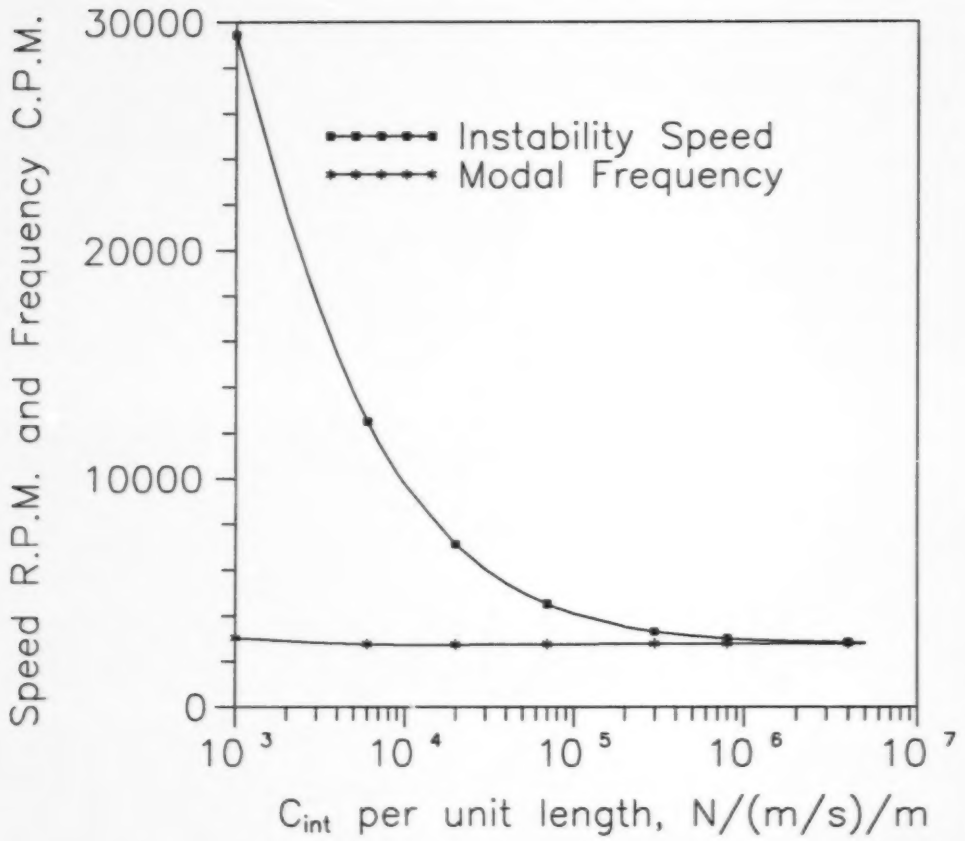

Figure 7.4: Speed at Which 1st. Forward Mode Becomes Unstable and Modal Frequency vs. Rotor Internal Damping for a Symmetric Rotor (Modal Frequency re Inertial Frame of Reference).

Chapter 8

Conclusions and Suggestions for Further Research

The major contribution of this thesis to the study of the dynamic behaviour of rotating machinery is a finite element model for a non - axisymmetric shaft - rotor system, supported by bearings which have speed dependent, distributed stiffness and damping coefficients. The analyses performed with this model have demonstrated the existence of operating speed ranges where instabilities exist in the lateral modes of vibration of the shaft - rotor system.

The most significant of these speed ranges involve instabilities of the first backward - precessing mode. The presence of lateral bending stiffness asymmetry, shear deflection and gyroscopic coupling appear to be prerequisites for this type of instability. These unstable speed ranges are in addition to the region around the fundamental resonance where the first forward mode becomes unstable due to mass asymmetry, as demonstrated by Brosens [73] and Stammers [74] for a rigid rotor. In developing the mathematical model, a rigid rotor was first analyzed and this gave very similar results to those of Brosens and Stammers for a rotor with mass asymmetry.

The phenomena of 'oil whirl' and 'oil whip' were investigated for a rigid rotor with support stiffness and damping coefficients, having circulatory (skew) terms in the stiffness and damping matrices, as would be the case for a plain bearing. This showed the interesting result that the low speed oil whirl mode is in fact the mode which at higher speeds becomes the second 'critical' of the rotor. With hind-sight, this seems an entirely logical result but to the writer's knowledge it has not been reported in the literature.

In the 'oil whirl' - 'oil whip' study the modal orbit shapes were derived for various levels of damping and different speeds. The direction of precession was also derived. The behaviour of these orbits is close to what is observed on field instrumentation during actual machine start - ups.

In order to have realistic bearing dynamic data for the flexible rotor analysis, Chapters 5 and 6 were devoted to the development of a finite element model of the hydrodynamic lubrication problem for plain and tilting - pad bearings respectively. The variational approach was used throughout, and forms of suitable functionals were determined for these analyses. Thermal effects and pad flexibility effects were not considered.

Although there are many papers on similar analyses, much of the actual usable data is proprietary and what data there is in the literature is usually presented without indicating, in detail, the assumptions made.

For the tilting - pad analyses the method used here appears to be a little more rigorous than that in some published papers in that the Reynolds' trailing edge boundary condition was separately determined for each pad including for the small increments of displacement and velocity used for determining the bearing dynamic coefficients.

Having set up the mathematical model in a rotating reference frame, it was convenient to investigate the effect of internal damping on the stability of the lateral rotor - shaft modes of vibration. This was only done for an axisymmetric rotor. The result was the same as for for a simple rotor, in that the first forward mode became unstable at a threshold speed dependent on the level of internal damping for a given level of external damping, but at a speed which is never lower than the frequency of the first natural frequency (first forward mode frequency).

Although there are a significant number of rotating machines which have stiffness asymmetries in two principal planes by virtue of their design, e.g. laminated or slotted rotors, cracked rotors are another major class of machinery which exhibits strongly the effects of asymmetries in lateral bending stiffness. Failures due to cracks are sometimes quite catastrophic involving very high vibration followed by major damage. It is possible that rather than simply failing, such rotors may actually become unstable as part of the failure process. It would be possible, from a knowledge of the modal frequencies of such a machine, to determine whether coincidence of modes in the manner described here was possible within the operating speed range.

There is considerable scope for carrying on this research and building on the tools that have been presented here. The cracked rotor problem could be investigated in greater depth by using the code presented here for a configuration more closely approximating that of a rotor with a crack. Presently the methods of such diagnosis rely partially on the fact that the crack causes the rotor to exhibit a cyclic stiffness in the inertial frame and under gravity loading this produces a twice rotation speed component of vibration and consequently a distinctive orbit shape. However there are other problems that cause similar effects and such a study may help distinguish them from each other.

Another problem involving cracking is the failure of flexible coupling spacers, which the writer has had occasion to diagnose. The code prepared here could be used to model a two - case machine with a flexible coupling, (gear or diaphragm type) to determine if there is a way of distinguishing this problem from simple parallel misalignment.

Backward (or reverse) precession has been observed in machines with large overhung rotors, probably because of large gyroscopic coupling terms. It would be of interest to apply this analysis to such a configuration. It is perhaps noteworthy that in the whirl flutter analysis on the De Havilland - 7 aircraft that the writer was involved with some years ago, the flutter mode was always the first backward precessing mode for structural failure cases which caused significant stiffness asymmetry.

A major extension to the present analysis and computer code, would be to include three dimensional rotor elements to account for vibration modes of the rotor 'wheels'. It may be possible to incorporate the axisymmetric element developed by Eckert [89] into this present model for the rotor wheels only.

No data was presented here for the case of both internal damping and stiffness asymmetry. However a few computer runs of such cases were made and they suggest that the internal damping may stabilize the instabilities caused by stiffness asymmetry. This is reasonable because the internal damping is destabilizing for forward precessing modes at speeds above the frequencies of those modes and conversely, stabilizing to backward precessing modes. This would be an interesting avenue to pursue but probably of little practical use.

Although the results presented here extend what has been shown analytically for simpler models, it would be most desirable to carry out some experimental work to verify the findings and the limitations of this analysis. The present test rigs and instrumentation in the Department could be modified to carry out such a programme.

The bearing analyses and computer codes also offer scope for further work. On a purely practical level we have the means of producing design curves and dynamic coefficients for various bearing designs which could be used for design optimization. Although the bearing analyses appear to work well, the damping coefficients particularly are a little suspect for low speed operation. We know that at high eccentricities, plain bearings experience recirculation. It would be desirable to know if this is also the case for tilting pad bearings. Therefore the fluid mechanics assumptions could be investigated analytically and / or experimentally.

References

[1] H.H. Jeffcott 'The lateral Vibration of Loaded Shafts in the Neighbourhood of a Whirling Speed - The Effect of Want of Balance' *Phil. Mag. and J. of Sc.* **37***1919* pp. 304 -314.

[2] J.C. Wachel 'Rotordynamic Instability Field Problems' *N.A.S.A.- C.P. 2250 Texas A and M May 10-12 1982*

[3] A.G. Taylor, Unpublished Consulting Report *Bently Nevada Canada Ltd.*

[4] R.L. Bisplinghoff, H. Ashley, R.L. Halfman 'Aeroelasticity' *Addison - Wesley 1955*

[5] T. Theodorsen 'General Theory of Aerodynamic Instability and the Mechanism of Flutter' *N.A.C.A. Rpt. No. 496 1935*

[6] B.L. Newkirk, H.D. Taylor 'Shaft Whipping Due To Oil Action in Journal Bearings' *General Electric Review* **XXVIII** *No 8 Aug. 1925*

[7] A. Muszynska 'Whirl and Whip - Rotor / Bearing Instability Problems' *Journal of Sound and Vibration* **110***(3) 1986 pp. 443 - 462*

[8] A.G. Taylor 'Computer - Aided Diagnosis of Machinery Instability Problems - Several Case Histories' *Ninth Machinery Dynamics Seminar, National Research Council of Canada, Montréal 1986*

[9] C. Jackson 'The Practical Vibration Primer' *Gulf Publishing Co. 1985*

[10] A. Muszynska 'Multi - Mode Whirl and Whip in Rotor/Bearing Systems' *The Second International Symposium on Transport Phenomena, Dynamics, and Design of Rotating Machinery, Honolulu, Hawaii, April 1988*

[11] D. Robertson 'Whirling of a Journal in a Sleeve Bearing' *Phil. Mag. S.7***06***Jan. 1933 P.113*

[12] B.L. Newkirk, J.F. Lewis 'Oil Film Whirl - An Investigation of Disturbances Due to Oil Films in Journal Bearings' *Trans. ASME Jan. 1956 pp. 21 -27*

[13] J.W. Lund 'Stability and Damped Critical Speeds of a Flexible Rotor in Fluid - Film Bearings' *J. Eng. for Ind. May 1974*

[14] E.J. Gunter 'Dynamic Stability of Rotor - Bearing Systems' *N.A.S.A. Sp.- 113 1966*

[15] 'Special-Purpose Steam Turbines For Refinery Services - API Standard 612' *American Petroleum Institute, 2101 L Street, Washington, D.C. 20037.*

[16] 'International Standard ISO-3945, Mechanical vibration of large rotating machines with speed range from 10 to 200 rev/s. Measurement and evaluation of vibration severity *in situ*'. *International Organization For Standardization.*

[17] A.G. Taylor, Unpublished Consulting Report *Bently Nevada Canada Ltd.*

[18] Edward H. Miller, G.E. Co. 'Rotor Stabilizing Labyrinth Seal for Steam Turbines' *U.S. Pat. 4,420,161 Dec. 13, 1983*

[19] Hagg A.C., 'The Influence of Oil-Film Journal Bearings on the Stability of Rotating Machines'*J.of App. Mechs. Sept. 1946*

[20] Hagg A.C., Warner P.C. 'Oil Whip of Flexible Rotors'*Trans. ASME Oct. 1953*

[21] S.J. Needs 'Effects of Side Leakage in 120 - Degree Centrally Supported Journal Bearings' *Trans. A.S.M.E. APM - 56-16 pp. 721-732*

[22] A.C. Hagg, G.O. Sankey 'Some Dynamic Properties of Oil Film Journal Bearings With Reference to the Unbalance Vibration of Rotors' *J. of App. Mechs. June 1956*

[23] G.I. Taylor 'Stability of a Viscous Liquid Contained Between Two Rotating Cylinders.'*Phil. Trans. Royal . Soc.* **CCXXIII** *(223) Ser. A Feb. 8, 1923*

[24] A. Cameron 'The Principles of Lubrication' *Longmans 1966*

[25] H. Schlichting 'Boundary Layer Theory' *Mc Graw Hill 7th. edition 1979*

[26] B.Sternlicht 'Elastic and Damping Properties of Cylindrical Journal Bearings' *J. Bas. Eng. June 1957 p. 101*

[27] J.W. Lund, B. Sternlicht 'Rotor-Bearing Dynamics with Emphasis on Attenuation' *J. Bas. Eng. Dec. 1962 p. 491*

[28] J.W. Lund 'Spring and Damping Coefficients for the Tilting-Pad Journal Bearing' *A.S.L.E. Trans.* **7***pp. 342- 353 (1964)*

[29] N.O. Myklestad 'A New Method of Calculating Natural Modes of Uncoupled Bending Vibration of Airplane Wings and Other Types of Beams' *J. of Aero. Sc. Apr. 1944*

[30] M.A. Prohl 'A General Method for Calculating Critical Speeds of Flexible Rotors' *J. of App. Mech. Sept. 1945*

[31] J.W. Lund, F.K. Orcutt 'Calculations and Experiments on the Unbalance Response of a Flexible Rotor' *J. of Eng. for Ind. Nov. 1967 pp. 785 - 796*

[32] J.W. Lund, E. Saibel 'Oil Whip Whirl Orbits of a Rotor in Sleeve Bearings' *J. of Eng. for Ind. Nov. 1967*

[33] N.N. Boboliubov, Y.A. Mitropolsky 'Asymptotic Methods in the Theory of Non-Linear Oscillations' *Gordon and Breach Science Publishers / Hindustan Publishing Corpn. India (translation from the russian) 1961*

[34] J.W. Lund 'Modal Response of a Flexible Rotor in Fluid - Film Bearings' *J. of Eng. for Ind. May 1974 pp. 525 - 533*

[35] J. Boyd, A.A. Raimondi 'An Analysis of the Pivoted-Pad Journal Bearing' *Mechanical Engineering. May 1953 pp. 380-386*

[36] J. Boyd, A.A. Raimondi 'Clearance Considerations in Pivoted Pad Journal Bearings' *A.S.L.E. Trans.* **5** *1962 pp. 418-426*

[37] C.M.McC. Ettles 'The Analysis and Performance of Pivoted Pad Journal Bearings Considering Thermal and Elastic Effects' *J. Lub. Tech.* **102** *April 1980 pp. 182-192*

[38] K.E. Rouch 'Dynamics of Pivoted Pad Journal Bearings, Including Pad Translation and Rotation Effects *A.S.L.E. Trans.* **26**,*1 pp. 102-109*

[39] J.W. Lund, L.B. Pedersen 'The Influence of Pad Flexibility on the Dynamic Coefficients of a Tilting Pad Journal Bearing' *J. Trib.* **109** *Jan. 1987 pp. 65-70*

[40] L.L. Earles, A.B. Palazzolo, R.W. Armentrout 'A Finite Element Approach to Pad Flexibility Effects in Tilt Pad Journal Bearings: Part i - Single Pad Analysis' *J. Trib.* **112** *April 1990 pp.169-177*

[41] L.L. Earles, A.B. Palazzolo, R.W. Armentrout 'A Finite Element Approach to Pad Flexibility Effects in Tilt Pad Journal Bearings: Part ii - Assembled Bearing and System Analysis' *Trans. A.S.M.E.* **112** *April 1990 pp. 178-182*

[42] J.D. Knight, L.E. Barrett 'Analysis of Tilting Pad Journal Bearings With Heat Transfer Effects' *Trans. A.S.M.E.* **110** *Jan. 1988 pp. 128-133*

[43] K.W. Kim, C.M. Rodkiewicz 'On the Thermal Effects in the Design of Tilting-Pad Bearings Subjected to Inlet Pressure Build-Up' *Trans. A.S.M.E.* **113** *July 1991*

[44] J.F. Booker, K.H. Huebner 'Application of Finite Element Methods to Lubrication: An Engineering Approach' *J. Lub. Tech. Trans. ASME Oct. 1972 pp.313-323*

[45] K.H. Huebner, E.A. Thornton 'The Finite Element Method for Engineers' *Wiley 1983*

[46] P.E. Allaire, J.C. Nicholas, E.J. Gunter 'Systems of Finite Elements for Finite Bearings' *J. Lub. Tech. Trans. ASME April 1977*

[47] C.W. Ng, C.H.T. Pan 'A Linearized Turbulent Lubrication Theory' *J. Bas. Eng. Sept. 65 p.675*

[48] F.K. Orcutt 'The Steady - State and Dynamic Characteristics of the Tiltpad Journal Bearing in Laminar and Turbulent Flow Regimes' *J. Lub. Tech. Trans. A.S.M.E. July 1967*

[49] Y. Yamada 'Resistance of a Flow Through an Annulus with an Inner Rotating Cylinder' *Bul. Jap. Soc. Mech. Eng.* **18** *May 1962*

[50] F.W. White 'Viscous Fluid Flow' *Mc Graw Hill 1974*

[51] H.F. Black 'Empirical Treatment of Hydrodynamic Journal Bearing Performance in the Super - Laminar Régime' *J. Mech. Eng. Sc.* **12***(2) 1970*

[52] H.F. Black 'Effects of Hydraulic Forces in Annular Pressure Seals on the Vibration of Centrifugal Pump Rotors' *J. Mech. Eng. Sc.* **11***(2) 1969*

[53] H.F. Black, D.N. Jensen 'Dynamic Hybrid Bearing Characteristics of Annular Controlled Leakage Seals' *Proc. Inst. Mech. Engrs. 1969-1970* **184** *Pt3N pp. 92-100*

[54] A.L. Kimball 'Internal Friction Theory of Shaft Whirling' *General Electric Review Vol. XXVII No. 4 April 1924*

[55] A.L. Kimball 'Measurement of Internal Friction in a Revolving Deflected Shaft' *General Electric Review Vol. XXVIII N0. 8 Aug.1925*

[56] F.F. Ehrich 'Shaft Whirl Induced by Rotor Internal Damping' *J. App. Mechs. June 1964 pp. 279 - 282*

[57] A. Tondl 'Some Problems of Rotor Dynamics' *Publishing House of the Czechoslovak Academy of Sciences, Prague - Chapman & Hall London*

[58] D.W. Childs 'Simulation models for flexible spinning bodies' *Simulation, June 1969 pp. 291 - 296*

[59] D.W. Childs 'A Simulation Model for Flexible Rotating Equipment' *J. of Eng. for Ind. Feb.1972 pp.201 - 209*

[60] D.W. Childs 'A Rotor Fixed Modal Simulation Model for Flexible Rotating Equipment'*J. of Eng. for Ind. May 1973 pp. 659 - 669*

[61] D.W. Childs'SSME Turbopump Technology Improvement via Transient Rotordynamic Analysis - Final Report'*NASA - CR - 144165 Dec. 1975*

[62] D.W. Childs 'The Space Shuttle Main Engine High - Pressure Fuel Turbopump Rotordynamic Instability Problem'*J. of Eng. for Power Trans. ASME* **100***Jan. 1978*

[63] D.E. Bently 'Forced Subrotative Speed Dynamic Action of Rotating Machinery'*ASME Petroleum Mech. Eng. Conf. Dallas, Texas Sept. 1974*

[64] J. S. Alford 'Protecting Turbomachinery From Self Excited Rotor Whirl '*J. Eng. for Power Oct. 1965*

[65] D.W. Childs 'Rotordynamic Analysis for the HPFTP (High Pressure Fuel Turbopump) of the SSME (Space Shuttle Main Engine) - Final Report'*NASA - CR - 161620 July 1980*

[66] G.G. Hirs 'A Bulk Theory for Turbulence in Lubricant Films'*J. Lub. Tech. Apr. 1973*

[67] D.W. Childs 'Dynamic Analysis of Turbulent Angular Seals Based on Hirs' Lubrication Equation'*NASA - CR - 161620 July 1980*

[68] D.W. Childs 'Transient Rotordynamic Analysis for the Space - Shuttle Main Engine High Pressure Oxygen Turbopump' *NASA - CR - 140455 N74 34003. also synopsis in J. Spacecraft and Rockets* **12** *No.1 Jan. 1975*

[69] D.W. Childs, D.S. Moyer 'Vibration Characteristics of the HPOTP (High - Pressure Oxygen Turbopump) of the SSME (Space Shuttle Main Engine)'*J. Eng. for Gas Turbines for Power* **107** *Jan. 1985*

[70] Chang-Ho Kim, D.W. Childs 'Analysis for Rotordynamic Coefficients of Helically - Grooved Turbulent Annular Seals'*J. Trib. Trans. ASME Jan. 1987* **109** *p.136*

[71] D.W. Childs, Chang-Ho Kim 'Analysis and Testing for Rotordynamic Coefficients of Turbulent Annular Seals With Different, Directionally - Homogeneous Surface - Roughness Treatment for Rotor and Stator Elements'*J. Trib. July 1985 Trans. ASME* **107** *p.296*

[72] D. Childs, F. Garcia'Test Results for Sawtooth- Pattern Damper Seals: Leakage and Rotordynamic Coefficients'*J. Trib. Trans. ASME* **109** *Jan. 1987*

[73] P.J. Brosens, 'Whirling of Unsymmetrical Rotors' *D.Sc. Thesis, M.I.T. 1959*

[74] C.W. Stammers, 'On The Stability of Some Vibrating Systems Governed by Linear Equations with Periodic Coefficients' *Ph.D. Thesis, University of Southampton, 1968*

[75] J.H. Wilkinson, 'The Algebraic Eigenvalue Problem' *Clarendon Press 1988*

[76] P.J. Brosens and S.H. Crandall Sept. 1961. Whirling of Unsymmetrical Rotors. *Journal of Applied Mechanics 355 - 362.*

[77] R.E.D. Bishop and A.G. Parkinson 1965. Second Order Vibration of Flexible Shafts. *Philosophical Transactions of the Royal Society.* **259** *pp. 1-31.*

[78] A. Muszynska Oct. 1982. Shaft Crack Detection. *Seventh Machinery Dynamics Seminar, N.R.C. Canada, Edmonton, Alberta, Canada.*

[79] A.J. Baker 1983. Finite Element Computational Fluid Mechanics. *Hemisphere Publishing Corpn.*

[80] R. Davis, R.D. Henshell and G.B. Warburton 1972. A Timoshenko Beam Element. *Journal of Sound and Vibration.* **22***(4) 475-487.*

[81] S. Wolfram et al. 1988. Mathematica 2nd. Ed. *Wolfram Research, Addison-Wesley.*

[82] R.E.D. Bishop and D.C. Johnson 1958. On damped free vibration with particular reference to systems having nearly-equal natural frequencies. *The Aeronautical Quarterly.* **9** *pp. 71-95.*

[83] G.M.L. Gladwell and C.W. Stammers 1966. On the Stability of an Unsymmetrical Rigid Rotor Supported in Unsymmetrical Bearings. *Journal of Sound and Vibration.* **3***(3) pp. 221-232.*

[84] T. Someya (editor) et al. 1989 Journal Bearing Databook. *Springer - Verlag.*

[85] A. Cameron 1976. Basic Lubrication Theory. *Ellis-Horwood.*

[86] O. Pinkus and B. Sternlicht 1961. Theory of Hydrodynamic Lubrication. McGraw-Hil.

[87] P.R. Trumpler 1966. Design of Film Bearings. *MacMillan.*

[88] A.G. Taylor and A. Craggs 1993. A Finite Element Model for a Flexible Non-Symmetric Rotor On Distributed Bearings - A Stability Study. *Journal of Sound and Vibration.* Accepted for publication.

[89] W.F.Eckert 1992 The Application of Finite Element Models to the Analysis and System Identification of Flexible Rotors. *Ph. D. Thesis, University of Alberta.*

Appendix A

Analytical Methods

A.1 Complex Eigenvalues and Eigenvectors

A.1.1 Eigenvalues

Equation 3.21 can be written in abbreviated form:

$$[\delta_1]\left\{\ddot{\phi}\right\} + [G]\left\{\dot{\phi}\right\} + [\delta_2]\left\{\dot{\phi}\right\} + [\omega][\epsilon]\{\phi\} + [C][\nu_1]\{\phi\} + [C][\nu_2]\left\{\dot{\phi}\right\} = \{u\} \tag{A.1}$$

i.e.

$$[\delta_1]\left\{\ddot{\phi}\right\} + [[G] + [C][\nu_2]]\left\{\dot{\phi}\right\} + [[\delta_2] + [\omega][\epsilon] + [C][\nu_1]]\{\phi\} = \{u\} \tag{A.2}$$

To investigate the stability of the solution of the equations of motion we consider the case where there is no imbalance vector i.e. $\{u\} = \{0\}$. Then letting $\{\psi\} = \left\{\dot{\phi}\right\}$ we can write:

$$\left\{ \begin{array}{c} \dot{\psi} \\ \dot{\phi} \end{array} \right\} = \left[\begin{array}{cc} \left(-[\delta_1]^{-1}[[G] + [C][\nu_2]]\right) & \left(-[\delta_1]^{-1}[[\delta_2] + [\omega][\epsilon] + [C][\nu_1]]\right) \\ [I] & [0] \end{array} \right] \left\{ \begin{array}{c} \psi \\ \phi \end{array} \right\} \tag{A.3}$$

This represents eight equations. If we assume a solution of the form:

$$\left\{ \begin{array}{c} \psi \\ \phi \end{array} \right\} = \left\{ \begin{array}{c} \psi_0 \\ \phi_0 \end{array} \right\} e^{\lambda_n \tau}$$

then this reduces to the standard eigenvalue form:

$$\lambda_n \left\{ \begin{array}{c} \psi_0 \\ \phi_0 \end{array} \right\} = \left[A \right] \left\{ \begin{array}{c} \psi_0 \\ \phi_0 \end{array} \right\} \tag{A.4}$$

or,

$$[[A] - \lambda_n [I]] \{\Phi\} = 0 \tag{A.5}$$

In this equation the $[A]$ matrix is not symmetrical and the eigenvalues and eigenvectors are, in general complex. To solve this set of equations for the eigenvalues, the 'QR' method [75] was used. Then to derive the corresponding eigenvectors, a modification to the gaussian elimination method was made as described below to handle complex eigenvectors.

A.1.2 Eigenvectors

Having found the complex eigenvalues for the matrix of double the original characteristic equation, back substitution is not immediately possible for the complex eigenvectors because this matrix has redundances. One half of each eigenvector is the derivative of the other half.

The method used was to return to the original matrix equation and partition it into real and imaginary parts, as follows so that the complex eigenvalues could then be substituted back in to solve for the corresponding complex eigenvector by gaussian elimination.

$$[\Re[A] + i\Im[A]] \{\Re\{\Phi\} + i\Im\{\Phi\}\} = \{0\} \tag{A.6}$$

If we normalize the vector with respect to the last, (nth) complex element, i.e. divide through the vector by $(\Re\phi_n + i\Im\phi_n)$ then:

$$[\Re[A] + i\Im[A]] \begin{Bmatrix} \Re\phi'_1 + i\Im\phi'_1 \\ \vdots \\ \Re\phi'_n + i\Im\phi'_n \\ 1.0 + i0.0 \end{Bmatrix} = \{0\} \tag{A.7}$$

Partitioning and rearranging:

$$\begin{bmatrix} \Re[A] & -\Im[A] \\ \Im[A] & \Im[A] \end{bmatrix} \begin{Bmatrix} \{\Re\{\Phi'\}\} \\ \{\Im\{\Phi'\}\} \end{Bmatrix} = \{0\} \tag{A.8}$$

where the vector,

$$\left\{ \begin{array}{c} \{\Re\{\Phi'\}\} \\ \{\Im\{\Phi'\}\} \end{array} \right\} = \left\{ \begin{array}{c} \Re\phi'_1 \\ \Re\phi'_2 \\ \vdots \\ 1.0 \\ \Im\phi'_1 \\ \Im\phi'_2 \\ \vdots \\ 0 \end{array} \right\}$$

Interchanging rows and columns in pairs:

$$\left[\begin{array}{c} \\ [A^*] \\ \\ \\ \\ \\ \\ \\ \\ \end{array} \right] \left\{ \begin{array}{c} \Re\phi'_1 \\ \Im\phi'_1 \\ \Re\phi'_2 \\ \Im\phi'_2 \\ \vdots \\ \Re\phi'_{n-1} \\ \Im\phi'_{n-1} \\ 1.0 \\ 0 \end{array} \right\} = \left\{ \begin{array}{c} 0 \\ 0 \\ 0 \\ 0 \\ \vdots \\ 0 \\ 0 \\ 0 \\ 0 \end{array} \right\} \tag{A.9}$$

where the $[A^*]$ is the square matrix of Equation A.8 rearranged by interchanging the rows and columns in pairs.

We can now drop the 2n'th row and column and partition the remaining matrices to give a $2(n-1) \times 2(n-1)$ problem:

$$\left[\begin{array}{c} \\ [A^{*R}] \\ \\ \\ \\ \end{array} \right] \left\{ \begin{array}{c} \Re\phi'_1 \\ \Im\phi'_1 \\ \vdots \\ \Re\phi'_{n-1} \\ \Im\phi'_{n-1} \end{array} \right\} = - \left\{ \begin{array}{c} A^*(1, 2n-1) \\ \vdots \\ \vdots \\ \vdots \\ A^*(2(n-1), (2n-1)) \end{array} \right\} \tag{A.10}$$

This is now in the normal form for application of the gaussian elimination method (and other methods) for solving a set of linear algebraïc equations with real coefficients. We are in effect, using the last degree of freedom as the phase reference for all the other degrees of freedom.

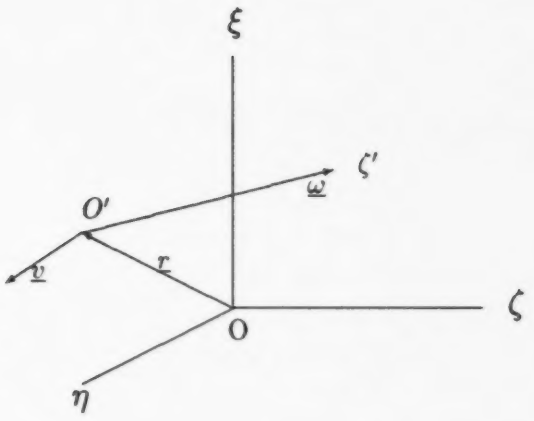

Figure A.1: Determination of Direction of Precession. $\underline{r}$ and $\underline{v}$ are the position and precessional velocity of a point on the shaft centre - line $O' - \zeta'$, i.e. the deflected axis of the rotor.

A.2 Direction of Precession and Orbit Shape

A.2.1 Precession

In the work of Stammers [74] and Brosens [73], as there was no damping in the system and only the two angular degrees of freedom, determining the direction of precession for the modes was straightforward. In terms of the present analysis, one component ϕ_η was purely real and the other, ϕ_ξ, purely 'imaginary' (or 'in quadrature'). Then the sign of ϕ_η/ϕ_ξ determined the direction of precession.

In the system of this study, the amplitudes of all four degrees of freedom are, in general complex. Therefore, the determination of the direction of precession for each mode requires a little more analysis.

The direction of precession can be defined in terms of the precessional angular momentum vector of a point on the deflected shaft centre - line about the axis of rotation in the rotating reference frame. For a precessional angular momentum vector $\underline{\mu}_n$.

$$\underline{\mu}_n = \underline{v} \times \underline{r} \tag{A.11}$$

where $\underline{r}$ is the position vector and $\underline{v}$ is the velocity vector of the shaft centre - line point in a plane normal to the rotor axis, $(\dot{\zeta})$ is negligible.

$$\underline{\mu}_n = (\xi\dot{\eta} - \eta\dot{\xi})\underline{e}_\zeta \tag{A.12}$$

where $\underline{e}_\zeta$ is a unit vector along O-ζ. The $\underline{\mu}_n$ vector has the same direction as the rotation vector $\underline{\omega} \simeq \omega\underline{e}_\zeta$ for forward precession and the opposite sign for backward precession.

In the general case:

$$\xi \equiv \Re\xi + i\Im\xi \quad \rightarrow \quad \xi = |A|\cos(\omega_n t + \theta_\xi)e^{\alpha_n t}$$

$$\eta \equiv \Re\eta + i\Im\eta \quad \rightarrow \quad \eta = |B|\cos(\omega_n t + \theta_\eta)e^{\alpha_n t}$$

where:

$$A = ((\Re\xi)^2 + (\Im\xi)^2)^{0.5} \qquad B = ((\Re\eta)^2 + (\Im\eta)^2)^{0.5}$$

and

$$\theta_\xi = \arctan \Im\xi/\Re\xi \qquad \theta_\eta = \arctan \Im\eta/\Re\eta$$

Thus evaluating the cross-product:

$$\underline{\mu}_n = e^{2\alpha_n}|A||B|\sin(\theta_\xi - \theta_\eta)\underline{e}_\zeta \tag{A.13}$$

Therefore, with $\underline{\mu}_n = \mu_n\underline{e}_\zeta$, $\sin(\theta_\xi - \theta_\eta)$ has the same sign as μ_n for forward precession and opposite for backward precession.

Note that the above condition for the direction of precession does not apply to the inertial reference frame case. This can be shown by performing a coordinate transformation to the inertial coordinate frame.

Given the condition for foreward precession:

$$\dot{\xi}\eta - \dot{\eta}\xi < 0 \text{ for positive } \omega \tag{A.14}$$

Transforming this inequality to the inertial coordinate frame we get:

$$\dot{x}y - \dot{y}x + \omega(x^2 + y^2) < 0 \tag{A.15}$$

The additional term $\omega\ (x^2 + y^2)$ or ωr^2 represents the angular momentum of a unit mass due to the rotation of the reference frame. This expression does not lead to a simple, programmable rule. However, this is generally unnecessary for the inertial frame analyses as the eigenvalues with negative imaginary parts can be immediately discarded as non - physical solutions, leaving pairs of roots which are easily distinguished.

A.2.2 Orbits

Consider one of the components of the eigenvectors, the angular motion about the O-x axis (inertial frame):

$$\phi_x^n(t) = \phi_{x_0}^n e^{\lambda_n t} \tag{A.16}$$

where n is the mode number, λ_n is the n'th eigenvalue and $\phi_{x_0}^n$ is the eigenvector component which is complex in general.

Letting $\lambda_n = \alpha_n + i\omega_n$:

$$\phi_x^n(t) = \phi_{x_0}^n e^{\alpha t} e^{i\omega t}$$

which is equivalent to:

$$\phi_x^n(t) = e^{\alpha t}|\phi_{x_0}|\cos(\omega_n t + \theta_{\phi_x})$$

where:

$$|\phi_{x_0}| = \sqrt{(\Re\phi_{x_0})^2 + (\Im\phi_{x_0})^2} \quad \text{and} \quad \tan\theta_{\phi_x} = \Im\phi_{x_0}/\Re\phi_{x_0}$$

Similarly:

$$\phi_y^n(t) = e^{\alpha t}|\phi_{y_0}|\cos(\omega_n t + \theta_{\phi_y})$$

$$\frac{x_{c.g.}}{l}(t) = e^{\alpha t}\left|\frac{x_{c.g.}}{l}\right|\cos(\omega_n t + \theta_x)$$

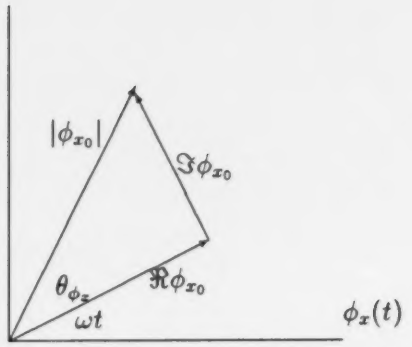

Figure A.2: Equivalence of Complex and Amplitude / Phase Representations.

$$\frac{y_{c.g.}}{l}(t) = e^{\alpha t}|\frac{y_{c.g.}}{l}|\cos(\omega_n t + \theta_y)$$

The motion at the forward (+ve z) end of the rotor is an orbit defined by its displacements from the undisturbed axis of rotation, $x_2/l, y_2/l$, where:

$$\frac{x_2}{l} = \frac{x_{c.g.}}{l} + \phi_y(1+\frac{s}{l}) \tag{A.17}$$

$$\frac{y_2}{l} = \frac{y_{c.g.}}{l} - \phi_y(1+\frac{s}{l}) \tag{A.18}$$

Therefore, substituting the above expressions we get:

$$\frac{x_2}{l} = e^{\alpha_n t}\left[\left|\frac{x_0}{l}\right|\cos(\omega_n t + \theta_x) + |\phi_{y_0}|(1+\frac{s}{l})\cos(\omega_n t + \theta_{\phi_y})\right] \tag{A.19}$$

$$\frac{y_2}{l} = e^{\alpha_n t}\left[\left|\frac{y_0}{l}\right|\cos(\omega_n t + \theta_y) - |\phi_{x_0}|(1+\frac{s}{l})\cos(\omega_n t + \theta_{\phi_x})\right] \tag{A.20}$$

These expressions are parametric equations of two superposed ellipses which are exponentially growing ($\alpha > 0$), exponentially decaying ($\alpha < 0$) or steady state ($\alpha = 0$).

The superposition of the two ellipses with different amplitudes and phase angles results in another ellipse as long as the cyclic frequency is the same. The proof of this is as follows:

The cyclically varying part of the parametric expressions are in the form:

$$x = a\cos(\omega t + \phi_1) + b\cos(\omega t + \phi_2)$$

$$x = a[\cos\omega t \cos\phi_1 - \sin\omega t \sin\phi_1] + b[\cos\omega t \cos\phi_2 - \sin\omega t \sin\phi_2]$$

$$x = \cos\omega t[a\cos\phi_1 + b\cos\phi_2] - \sin\omega t[a\sin\phi_1 + b\sin\phi_2]$$

$$\text{or} \quad x = C\cos\omega t - D\sin\omega t$$

let $C = A\cos\phi_3$ and $D = A\sin\phi_3$ then:

$$x = A\cos\phi_3\cos\omega t - A\sin\phi_3\sin\omega t = A\cos(\omega t + \phi_3)$$

where:

$$A^2 = C^2 + D^2 = (a\cos\phi_1 + b\cos\phi_2)^2 + (a\sin\phi_1 + b\sin\phi_2)^2$$

and

$$\tan\phi_3 = \frac{D}{C} = \frac{(a\sin\phi_1 + b\sin\phi_2)}{(a\cos\phi_1 + b\cos\phi_2)}$$

and similarly for the 'y' component. So the resulting ellipse has component amplitudes and phase which are functions of the four amplitude and phase values of the components of the original two ellipses.

Appendix B

Finite Element Analysis - Coefficient Matrices

The coefficient matrices referred to in Chapter 4 are set out below in detail. In the case of the stiffness matrices, additional details of the derivation prior to integration over the element length is also given.

B.1 Mass Terms

The element mass matrix $[M^e]$, which is symmetric, is given by:

$$[M^e] = \text{Diag}\left\{\frac{\rho Al}{(1+\phi_\eta)^2}\ \frac{\rho Al}{(1+\phi_\xi)^2}\ \frac{\rho Al}{(1+\phi_\xi)^2}\ \frac{\rho Al}{(1+\phi_\eta)^2}\right.$$

$$\left.\frac{\rho Al}{(1+\phi_\eta)^2}\ \frac{\rho Al}{(1+\phi_\xi)^2}\ \frac{\rho Al}{(1+\phi_\xi)^2}\ \frac{\rho Al}{(1+\phi_\eta)^2}\right\} \times$$

$$\begin{bmatrix} Mm11 & Mm12 \\ Mm21 & Mm22 \end{bmatrix} + \text{Diag}\left\{\frac{\rho J_\eta}{l(1+\phi_\eta)^2}\ \frac{\rho J_\xi}{l(1+\phi_\xi)^2}\ \frac{\rho J_\xi}{l(1+\phi_\xi)^2}\ \frac{\rho J_\eta}{l(1+\phi_\eta)^2}\right.$$

$$\left.\frac{\rho J_\eta}{l(1+\phi_\eta)^2}\ \frac{\rho J_\xi}{l(1+\phi_\xi)^2}\ \frac{\rho J_\xi}{l(1+\phi_\xi)^2}\ \frac{\rho J_\eta}{l(1+\phi_\eta)^2}\right\} \times \begin{bmatrix} Mi11 & Mi12 \\ Mi21 & Mi22 \end{bmatrix}.$$

where:

$$\phi_\eta = \frac{12\beta_\eta}{l^2} \quad \phi_\xi = \frac{12\beta_\xi}{l^2} \text{ and}$$

$$[Mm11] =$$

$$\begin{bmatrix} \left(\frac{13}{35} + \frac{7}{10}\phi_\eta + \frac{1}{3}\phi_\eta^2\right) & 0 & 0 & l\left(\frac{11}{210} + \frac{11}{120}\phi_\eta + \frac{1}{24}\phi_\eta^2\right) \\ 0 & \left(\frac{13}{35} + \frac{7}{10}\phi_\xi + \frac{1}{3}\phi_\xi^2\right) & l\left(\frac{11}{210} + \frac{11}{120}\phi_\xi + \frac{1}{24}\phi_\xi^2\right) & 0 \\ 0 & l\left(\frac{11}{210} + \frac{11}{120}\phi_\xi + \frac{1}{24}\phi_\xi^2\right) & l^2\left(\frac{1}{105} + \frac{1}{60}\phi_\xi + \frac{1}{120}\phi_\xi^2\right) & 0 \\ l\left(\frac{11}{210} + \frac{11}{120}\phi_\eta + \frac{1}{24}\phi_\eta^2\right) & 0 & 0 & l^2\left(\frac{1}{105} + \frac{1}{60}\phi_\eta + \frac{1}{120}\phi_\eta^2\right) \end{bmatrix}$$

$$[Mm12] =$$

$$\begin{bmatrix} \left(\frac{9}{70} + \frac{3}{10}\phi_\eta + \frac{1}{6}\phi_\eta^2\right) & 0 & 0 & l\left(-\frac{13}{420} - \frac{3}{40}\phi_\eta - \frac{1}{24}\phi_\eta^2\right) \\ 0 & \left(\frac{9}{70} + \frac{3}{10}\phi_\xi + \frac{1}{6}\phi_\xi^2\right) & l\left(-\frac{13}{420} - \frac{3}{40}\phi_\xi - \frac{1}{24}\phi_\xi^2\right) & 0 \\ 0 & l\left(\frac{13}{420} + \frac{3}{40}\phi_\xi + \frac{1}{24}\phi_\xi^2\right) & l^2\left(-\frac{1}{140} - \frac{1}{60}\phi_\xi - \frac{1}{120}\phi_\xi^2\right) & 0 \\ l\left(\frac{13}{420} + \frac{3}{40}\phi_\eta + \frac{1}{24}\phi_\eta^2\right) & 0 & 0 & l^2\left(-\frac{1}{140} - \frac{1}{60}\phi_\eta - \frac{1}{120}\phi_\eta^2\right) \end{bmatrix}$$

$$[Mm22] =$$

$$\begin{bmatrix} \left(\frac{13}{35}+\frac{7}{10}\phi_\eta+\frac{1}{3}\phi_\eta^2\right) & 0 & 0 & l\left(-\frac{11}{210}-\frac{11}{120}\phi_\eta-\frac{1}{24}\phi_\eta^2\right) \\ 0 & \left(\frac{13}{35}+\frac{7}{10}\phi_\xi+\frac{1}{3}\phi_\xi^2\right) & l\left(-\frac{11}{210}-\frac{11}{120}\phi_\xi-\frac{1}{24}\phi_\xi^2\right) & 0 \\ 0 & l\left(-\frac{11}{210}-\frac{11}{120}\phi_\xi-\frac{1}{24}\phi_\xi^2\right) & l^2\left(\frac{1}{105}+\frac{1}{60}\phi_\xi+\frac{1}{120}\phi_\xi^2\right) & 0 \\ l\left(-\frac{11}{210}-\frac{11}{120}\phi_\eta-\frac{1}{24}\phi_\eta^2\right) & 0 & 0 & l^2\left(\frac{1}{105}+\frac{1}{60}\phi_\eta+\frac{1}{120}\phi_\eta^2\right) \end{bmatrix}$$

$$[Mi11] =$$

$$\begin{bmatrix} \frac{6}{5} & 0 & 0 & l(\frac{1}{10}-\frac{1}{2}\phi_\eta) \\ 0 & \frac{6}{5} & l(\frac{1}{10}-\frac{1}{2}\phi_\xi) & 0 \\ 0 & l(\frac{1}{10}-\frac{1}{2}\phi_\xi) & l^2\left(\frac{2}{15}+\frac{1}{6}\phi_\xi+\frac{1}{3}\phi_\xi^2\right) & 0 \\ l(\frac{1}{10}-\frac{1}{2}\phi_\eta) & 0 & 0 & l^2\left(\frac{2}{15}+\frac{1}{6}\phi_\eta+\frac{1}{3}\phi_\eta^2\right) \end{bmatrix}$$

$$[Mi12] =$$

$$\begin{bmatrix} -\frac{6}{5} & 0 & 0 & l(\frac{1}{10}-\frac{1}{2}\phi_\eta) \\ 0 & -\frac{6}{5} & l(\frac{1}{10}-\frac{1}{2}\phi_\xi) & 0 \\ 0 & l(-\frac{1}{10}+\frac{1}{2}\phi_\xi) & l^2(-\frac{1}{30}-\frac{1}{6}\phi_\xi+\frac{1}{6}\phi_\xi^2) & 0 \\ l(-\frac{1}{10}+\frac{1}{2}\phi_\eta) & 0 & 0 & l^2(-\frac{1}{30}-\frac{1}{6}\phi_\eta+\frac{1}{6}\phi_\eta^2) \end{bmatrix}$$

$$[Mi22] =$$

$$\begin{bmatrix} \frac{6}{5} & 0 & 0 & l(-\frac{1}{10}+\frac{1}{2}\phi_\eta) \\ 0 & \frac{6}{5} & l(-\frac{1}{10}+\frac{1}{2}\phi_\xi) & 0 \\ 0 & l(-\frac{1}{10}+\frac{1}{2}\phi_\xi) & l^2\left(\frac{2}{15}+\frac{1}{6}\phi_\xi+\frac{1}{3}\phi_\xi^2\right) & 0 \\ l(-\frac{1}{10}+\frac{1}{2}\phi_\eta) & 0 & 0 & l^2\left(\frac{2}{15}+\frac{1}{6}\phi_\eta+\frac{1}{3}\phi_\eta^2\right) \end{bmatrix}$$

The element gyroscopic / coriolis matrix $[G^e]$ is given by;

$$[G^e] = 1/2[[G^{e*}] - [G^{e*}]^T]$$

Carrying out the integrations for $[G^{e*}]$ and $[G^{e*}]^T$ we obtain the following :

$$[G^e] = \text{Diag}\left\{\frac{\rho l^{-6}}{(1+\phi_\eta)^2}\ \frac{\rho l^{-6}}{(1+\phi_\xi)^2}\ \frac{\rho l^{-6}}{(1+\phi_\xi)^2}\ \frac{\rho l^{-6}}{(1+\phi_\eta)^2}\right.$$

$$\left.\frac{\rho l^{-6}}{(1+\phi_\eta)^2}\ \frac{\rho l^{-6}}{(1+\phi_\xi)^2}\ \frac{\rho l^{-6}}{(1+\phi_\xi)^2}\ \frac{\rho l^{-6}}{(1+\phi_\eta)^2}\right\} \times [G]$$

where,

$G_{1,1} = 0.$

$$G_{1,2} = -144\,\beta_\eta^2\,J_\eta\,l + 288\,\beta_\eta\,\beta_\xi\,J_\eta\,l - 144\,\beta_\xi^2\,J_\eta\,l - 144\,\beta_\eta^2\,J_\xi\,l + 288\,\beta_\eta\,\beta_\xi\,J_\xi\,l - 144\,\beta_\xi^2\,J_\xi\,l + 144\,\beta_\eta^2\,J_\zeta\,l - 288\,\beta_\eta\,\beta_\xi\,J_\zeta\,l + 144\,\beta_\xi^2\,J_\zeta\,l - 96\,A\,\beta_\eta\,\beta_\xi\,l^3 - (42\,A\,\beta_\eta\,l^5)/5 - (42\,A\,\beta_\xi\,l^5)/5 + (6\,J_\eta\,l^5)/5 + (6\,J_\xi\,l^5)/5 - (6\,J_\zeta\,l^5)/5 - (26\,A\,l^7)/35$$

$$G_{1,3} = -72\,\beta_\eta^2\,J_\eta\,l^2 + 72\,\beta_\eta\,\beta_\xi\,J_\eta\,l^2 - 72\,\beta_\eta^2\,J_\xi\,l^2 + 72\,\beta_\eta\,\beta_\xi\,J_\xi\,l^2 + 72\,\beta_\eta^2\,J_\zeta\,l^2 - 72\,\beta_\eta\,\beta_\xi\,J_\zeta\,l^2 - 12\,A\,\beta_\eta\,\beta_\xi\,l^4 - 6\,\beta_\eta\,J_\eta\,l^4 - 6\,\beta_\eta\,J_\xi\,l^4 + 6\,\beta_\eta\,J_\zeta\,l^4 - (6\,A\,\beta_\eta\,l^6)/5 - A\,\beta_\xi\,l^6 + (J_\eta\,l^6)/10 + (J_\xi\,l^6)/10 - (J_\zeta\,l^6)/10 - (11\,A\,l^8)/105$$

$$G_{1,4} = 0.$$

$$G_{1,5} = 0.$$

$$G_{1,6} = 144\,\beta_\eta^2\,J_\eta\,l - 288\,\beta_\eta\,\beta_\xi\,J_\eta\,l + 144\,\beta_\xi^2\,J_\eta\,l + 144\,\beta_\eta^2\,J_\xi\,l - 288\,\beta_\eta\,\beta_\xi\,J_\xi\,l + 144\,\beta_\xi^2\,J_\xi\,l - 144\,\beta_\eta^2\,J_\zeta\,l + 288\,\beta_\eta\,\beta_\xi\,J_\zeta\,l - 144\,\beta_\xi^2\,J_\zeta\,l - 48\,A\,\beta_\eta\,\beta_\xi\,l^3 - (18\,A\,\beta_\eta\,l^5)/5 - (18\,A\,\beta_\xi\,l^5)/5 - (6\,J_\eta\,l^5)/5 - (6\,J_\xi\,l^5)/5 + (6\,J_\zeta\,l^5)/5 - (9\,A\,l^7)/35$$

$$G_{1,7} = -72\,\beta_\eta^2\,J_\eta\,l^2 + 72\,\beta_\eta\,\beta_\xi\,J_\eta\,l^2 - 72\,\beta_\eta^2\,J_\xi\,l^2 + 72\,\beta_\eta\,\beta_\xi\,J_\xi\,l^2 + 72\,\beta_\eta^2\,J_\zeta\,l^2 - 72\,\beta_\eta\,\beta_\xi\,J_\zeta\,l^2 + 12\,A\,\beta_\eta\,\beta_\xi\,l^4 - 6\,\beta_\eta\,J_\eta\,l^4 - 6\,\beta_\eta\,J_\xi\,l^4 + 6\,\beta_\eta\,J_\zeta\,l^4 + (4\,A\,\beta_\eta\,l^6)/5 + A\,\beta_\xi\,l^6 + (J_\eta\,l^6)/10 + (J_\xi\,l^6)/10 - (J_\zeta\,l^6)/10 + (13\,A\,l^8)/210$$

$$G_{1,8} = 0.$$

$$G_{2,1} = 144\,\beta_\eta^2\,J_\eta\,l - 288\,\beta_\eta\,\beta_\xi\,J_\eta\,l + 144\,\beta_\xi^2\,J_\eta\,l + 144\,\beta_\eta^2\,J_\xi\,l - 288\,\beta_\eta\,\beta_\xi\,J_\xi\,l + 144\,\beta_\xi^2\,J_\xi\,l - 144\,\beta_\eta^2\,J_\zeta\,l + 288\,\beta_\eta\,\beta_\xi\,J_\zeta\,l - 144\,\beta_\xi^2\,J_\zeta\,l + 96\,A\,\beta_\eta\,\beta_\xi\,l^3 + (42\,A\,\beta_\eta\,l^5)/5 + (42\,A\,\beta_\xi\,l^5)/5 - (6\,J_\eta\,l^5)/5 - (6\,J_\xi\,l^5)/5 + (6\,J_\zeta\,l^5)/5 + (26\,A\,l^7)/35$$

$$G_{2,2} = 0.$$

$$G_{2,3} = 0.$$

$$G_{2,4} = -72\,\beta_\eta\,\beta_\xi\,J_\eta\,l^2 + 72\,\beta_\xi^2\,J_\eta\,l^2 - 72\,\beta_\eta\,\beta_\xi\,J_\xi\,l^2 + 72\,\beta_\xi^2\,J_\xi\,l^2 + 72\,\beta_\eta\,\beta_\xi\,J_\zeta\,l^2 - 72\,\beta_\xi^2\,J_\zeta\,l^2 + 12\,A\,\beta_\eta\,\beta_\xi\,l^4 + 6\,\beta_\xi\,J_\eta\,l^4 + 6\,\beta_\xi\,J_\xi\,l^4 - 6\,\beta_\xi\,J_\zeta\,l^4 + A\,\beta_\eta\,l^6 + (6\,A\,\beta_\xi\,l^6)/5 - (J_\eta\,l^6)/10 - (J_\xi\,l^6)/10 + (J_\zeta\,l^6)/10 + (11\,A\,l^8)/105$$

$$G_{2,5} = -144\,\beta_\eta^2\,J_\eta\,l + 288\,\beta_\eta\,\beta_\xi\,J_\eta\,l - 144\,\beta_\xi^2\,J_\eta\,l - 144\,\beta_\eta^2\,J_\xi\,l + 288\,\beta_\eta\,\beta_\xi\,J_\xi\,l - 144\,\beta_\xi^2\,J_\xi\,l + 144\,\beta_\eta^2\,J_\zeta\,l - 288\,\beta_\eta\,\beta_\xi\,J_\zeta\,l + 144\,\beta_\xi^2\,J_\zeta\,l + 48\,A\,\beta_\eta\,\beta_\xi\,l^3 + (18\,A\,\beta_\eta\,l^5)/5 + (18\,A\,\beta_\xi\,l^5)/5 + (6\,J_\eta\,l^5)/5 + (6\,J_\xi\,l^5)/5 - (6\,J_\zeta\,l^5)/5 + (9\,A\,l^7)/35$$

$$G_{2,6} = 0.$$

$$G_{2,7} = 0.$$

$$G_{2,8} = -72\,\beta_\eta\,\beta_\xi\,J_\eta\,l^2 + 72\,\beta_\xi^2\,J_\eta\,l^2 - 72\,\beta_\eta\,\beta_\xi\,J_\xi\,l^2 + 72\,\beta_\xi^2\,J_\xi\,l^2 + 72\,\beta_\eta\,\beta_\xi\,J_\zeta\,l^2 - 72\,\beta_\xi^2\,J_\zeta\,l^2 - 12\,A\,\beta_\eta\,\beta_\xi\,l^4 + 6\,\beta_\xi\,J_\eta\,l^4 + 6\,\beta_\xi\,J_\xi\,l^4 - 6\,\beta_\xi\,J_\zeta\,l^4 - A\,\beta_\eta\,l^6 - (4\,A\,\beta_\xi\,l^6)/5 - (J_\eta\,l^6)/10 - (J_\xi\,l^6)/10 + (J_\zeta\,l^6)/10 - (13\,A\,l^8)/210$$

$$G_{3,1} = 0. + 72\,\beta_\eta^2\,J_\eta\,l^2 - 72\,\beta_\eta\,\beta_\xi\,J_\eta\,l^2 + 72\,\beta_\eta^2\,J_\xi\,l^2 - 72\,\beta_\eta\,\beta_\xi\,J_\xi\,l^2 - 72\,\beta_\eta^2\,J_\zeta\,l^2 + 72\,\beta_\eta\,\beta_\xi\,J_\zeta\,l^2 + 12\,A\,\beta_\eta\,\beta_\xi\,l^4 + 6\,\beta_\eta\,J_\eta\,l^4 + 6\,\beta_\eta\,J_\xi\,l^4 - 6\,\beta_\eta\,J_\zeta\,l^4 + (6\,A\,\beta_\eta\,l^6)/5 + A\,\beta_\xi\,l^6 - (J_\eta\,l^6)/10 - (J_\xi\,l^6)/10 + (J_\zeta\,l^6)/10 + (11\,A\,l^8)/105$$

$$G_{3,2} = 0.$$

$$G_{3,3} = 0.$$

$$G_{3,4} = -48\,\beta_\eta\,\beta_\xi\,J_\eta\,l^3 - 48\,\beta_\eta\,\beta_\xi\,J_\xi\,l^3 + 48\,\beta_\eta\,\beta_\xi\,J_\zeta\,l^3 + (12\,A\,\beta_\eta\,\beta_\xi\,l^5)/5 - \beta_\eta\,J_\eta\,l^5 - \beta_\xi\,J_\eta\,l^5 - \beta_\eta\,J_\xi\,l^5 - \beta_\xi\,J_\xi\,l^5 + \beta_\eta\,J_\zeta\,l^5 + \beta_\xi\,J_\zeta\,l^5 + (A\,\beta_\eta\,l^7)/5 + (A\,\beta_\xi\,l^7)/5 - (2\,J_\eta\,l^7)/15 - (2\,J_\xi\,l^7)/15 + (2\,J_\zeta\,l^7)/15 + (2\,A\,l^9)/105$$

$$G_{3,5} = -72\,\beta_\eta^2\,J_\eta\,l^2 + 72\,\beta_\eta\,\beta_\xi\,J_\eta\,l^2 - 72\,\beta_\eta^2\,J_\xi\,l^2 + 72\,\beta_\eta\,\beta_\xi\,J_\xi\,l^2 + 72\,\beta_\eta^2\,J_\zeta\,l^2 - 72\,\beta_\eta\,\beta_\xi\,J_\zeta\,l^2 + 12\,A\,\beta_\eta\,\beta_\xi\,l^4 - 6\,\beta_\eta\,J_\eta\,l^4 - 6\,\beta_\eta\,J_\xi\,l^4 + 6\,\beta_\eta\,J_\zeta\,l^4 + (4\,A\,\beta_\eta\,l^6)/5 + A\,\beta_\xi\,l^6 + (J_\eta\,l^6)/10 + (J_\xi\,l^6)/10 - (J_\zeta\,l^6)/10 + (13\,A\,l^8)/210$$

$$G_{3,6} = 0.$$

$$G_{3,7} = 0.$$

$$G_{3,8} = -24\,\beta_\eta\,\beta_\xi\,J_\eta\,l^3 - 24\,\beta_\eta\,\beta_\xi\,J_\xi\,l^3 + 24\,\beta_\eta\,\beta_\xi\,J_\zeta\,l^3 - (12\,A\,\beta_\eta\,\beta_\xi\,l^5)/5 + \beta_\eta\,J_\eta\,l^5 + \beta_\xi\,J_\eta\,l^5 + \beta_\eta\,J_\xi\,l^5 + \beta_\xi\,J_\xi\,l^5 - \beta_\eta\,J_\zeta\,l^5 - \beta_\xi\,J_\zeta\,l^5 - (A\,\beta_\eta\,l^7)/5 - (A\,\beta_\xi\,l^7)/5 + (J_\eta\,l^7)/30 + (J_\xi\,l^7)/30 - (J_\zeta\,l^7)/30 - (A\,l^9)/70$$

$$G_{4,1} = 0.$$

$$G_{4,2} = 0. + 72\,\beta_\eta\,\beta_\xi\,J_\eta\,l^2 - 72\,\beta_\xi^2\,J_\eta\,l^2 + 72\,\beta_\eta\,\beta_\xi\,J_\xi\,l^2 - 72\,\beta_\xi^2\,J_\xi\,l^2 - 72\,\beta_\eta\,\beta_\xi\,J_\zeta\,l^2 + 72\,\beta_\xi^2\,J_\zeta\,l^2 - 12\,A\,\beta_\eta\,\beta_\xi\,l^4 - 6\,\beta_\xi\,J_\eta\,l^4 - 6\,\beta_\xi\,J_\xi\,l^4 + 6\,\beta_\xi\,J_\zeta\,l^4 - A\,\beta_\eta\,l^6 - (6\,A\,\beta_\xi\,l^6)/5 + (J_\eta\,l^6)/10 + (J_\xi\,l^6)/10 - (J_\zeta\,l^6)/10 - (11\,A\,l^8)/105$$

$$G_{4,3} = 48\,\beta_\eta\,\beta_\xi\,J_\eta\,l^3 + 48\,\beta_\eta\,\beta_\xi\,J_\xi\,l^3 - 48\,\beta_\eta\,\beta_\xi\,J_\zeta\,l^3 - (12\,A\,\beta_\eta\,\beta_\xi\,l^5)/5 + \beta_\eta\,J_\eta\,l^5 + \beta_\xi\,J_\eta\,l^5 + \beta_\eta\,J_\xi\,l^5 + \beta_\xi\,J_\xi\,l^5 - \beta_\eta\,J_\zeta\,l^5 - \beta_\xi\,J_\zeta\,l^5 - (A\,\beta_\eta\,l^7)/5 - (A\,\beta_\xi\,l^7)/5 + (2\,J_\eta\,l^7)/15 + (2\,J_\xi\,l^7)/15 - (2\,J_\zeta\,l^7)/15 - (2\,A\,l^9)/105$$

$$G_{4,4} = 0.$$

$$G_{4,5} = 0.$$

$$G_{4,6} = -72\,\beta_\eta\,\beta_\xi\,J_\eta\,l^2 + 72\,\beta_\xi^2\,J_\eta\,l^2 - 72\,\beta_\eta\,\beta_\xi\,J_\xi\,l^2 + 72\,\beta_\xi^2\,J_\xi\,l^2 + 72\,\beta_\eta\,\beta_\xi\,J_\zeta\,l^2 - 72\,\beta_\xi^2\,J_\zeta\,l^2 - 12\,A\,\beta_\eta\,\beta_\xi\,l^4 + 6\,\beta_\xi\,J_\eta\,l^4 + 6\,\beta_\xi\,J_\xi\,l^4 - 6\,\beta_\xi\,J_\zeta\,l^4 - A\,\beta_\eta\,l^6 - (4\,A\,\beta_\xi\,l^6)/5 - (J_\eta\,l^6)/10 - (J_\xi\,l^6)/10 + (J_\zeta\,l^6)/10 - (13\,A\,l^8)/210$$

$$G_{4,7} = 24\,\beta_\eta\,\beta_\xi\,J_\eta\,l^3 + 24\,\beta_\eta\,\beta_\xi\,J_\xi\,l^3 - 24\,\beta_\eta\,\beta_\xi\,J_\zeta\,l^3 + (12\,A\,\beta_\eta\,\beta_\xi\,l^5)/5 - \beta_\eta\,J_\eta\,l^5 - \beta_\xi\,J_\eta\,l^5 - \beta_\eta\,J_\xi\,l^5 - \beta_\xi\,J_\xi\,l^5 + \beta_\eta\,J_\zeta\,l^5 + \beta_\xi\,J_\zeta\,l^5 + (A\,\beta_\eta\,l^7)/5 + (A\,\beta_\xi\,l^7)/5 - (J_\eta\,l^7)/30 - (J_\xi\,l^7)/30 + (J_\zeta\,l^7)/30 + (A\,l^9)/70$$

$$G_{4,8} = 0.$$

$$G_{5,1} = 0.$$

$$G_{5,2} = 144\,\beta_\eta^2\,J_\eta\,l - 288\,\beta_\eta\,\beta_\xi\,J_\eta\,l + 144\,\beta_\xi^2\,J_\eta\,l + 144\,\beta_\eta^2\,J_\xi\,l - 288\,\beta_\eta\,\beta_\xi\,J_\xi\,l + 144\,\beta_\xi^2\,J_\xi\,l - 144\,\beta_\eta^2\,J_\zeta\,l + 288\,\beta_\eta\,\beta_\xi\,J_\zeta\,l - 144\,\beta_\xi^2\,J_\zeta\,l - 48\,A\,\beta_\eta\,\beta_\xi\,l^3 - (18\,A\,\beta_\eta\,l^5)/5 - (18\,A\,\beta_\xi\,l^5)/5 - (6\,J_\eta\,l^5)/5 - (6\,J_\xi\,l^5)/5 + (6\,J_\zeta\,l^5)/5 - (9\,A\,l^7)/35$$

$$G_{5,3} = 0. + 72\,\beta_\eta^2\,J_\eta\,l^2 - 72\,\beta_\eta\,\beta_\xi\,J_\eta\,l^2 + 72\,\beta_\eta^2\,J_\xi\,l^2 - 72\,\beta_\eta\,\beta_\xi\,J_\xi\,l^2 - 72\,\beta_\eta^2\,J_\zeta\,l^2 + 72\,\beta_\eta\,\beta_\xi\,J_\zeta\,l^2 - 12\,A\,\beta_\eta\,\beta_\xi\,l^4 + 6\,\beta_\eta\,J_\eta\,l^4 + 6\,\beta_\eta\,J_\xi\,l^4 - 6\,\beta_\eta\,J_\zeta\,l^4 - (4\,A\,\beta_\eta\,l^6)/5 - A\,\beta_\xi\,l^6 - (J_\eta\,l^6)/10 - (J_\xi\,l^6)/10 + (J_\zeta\,l^6)/10 - (13\,A\,l^8)/210$$

$$G_{5,4} = 0.$$

$$G_{5,5} = 0.$$

$$G_{5,6} = -144\,\beta_\eta^2\,J_\eta\,l + 288\,\beta_\eta\,\beta_\xi\,J_\eta\,l - 144\,\beta_\xi^2\,J_\eta\,l - 144\,\beta_\eta^2\,J_\xi\,l + 288\,\beta_\eta\,\beta_\xi\,J_\xi\,l - 144\,\beta_\xi^2\,J_\xi\,l + 144\,\beta_\eta^2\,J_\zeta\,l - 288\,\beta_\eta\,\beta_\xi\,J_\zeta\,l + 144\,\beta_\xi^2\,J_\zeta\,l - 96\,A\,\beta_\eta\,\beta_\xi\,l^3 - (42\,A\,\beta_\eta\,l^5)/5 - (42\,A\,\beta_\xi\,l^5)/5 + (6\,J_\eta\,l^5)/5 + (6\,J_\xi\,l^5)/5 - (6\,J_\zeta\,l^5)/5 - (26\,A\,l^7)/35$$

$$G_{5,7} = 72\,\beta_\eta^2\,J_\eta\,l^2 - 72\,\beta_\eta\,\beta_\xi\,J_\eta\,l^2 + 72\,\beta_\eta^2\,J_\xi\,l^2 - 72\,\beta_\eta\,\beta_\xi\,J_\xi\,l^2 - 72\,\beta_\eta^2\,J_\zeta\,l^2 + 72\,\beta_\eta\,\beta_\xi\,J_\zeta\,l^2 + 12\,A\,\beta_\eta\,\beta_\xi\,l^4 + 6\,\beta_\eta\,J_\eta\,l^4 + 6\,\beta_\eta\,J_\xi\,l^4 - 6\,\beta_\eta\,J_\zeta\,l^4 + (6\,A\,\beta_\eta\,l^6)/5 + A\,\beta_\xi\,l^6 - (J_\eta\,l^6)/10 - (J_\xi\,l^6)/10 + (J_\zeta\,l^6)/10 + (11\,A\,l^8)/105$$

$$G_{5,8} = 0.$$

$$G_{6,1} = -144\,\beta_\eta^2\,J_\eta\,l + 288\,\beta_\eta\,\beta_\xi\,J_\eta\,l - 144\,\beta_\xi^2\,J_\eta\,l - 144\,\beta_\eta^2\,J_\xi\,l + 288\,\beta_\eta\,\beta_\xi\,J_\xi\,l - 144\,\beta_\xi^2\,J_\xi\,l + 144\,\beta_\eta^2\,J_\zeta\,l - 288\,\beta_\eta\,\beta_\xi\,J_\zeta\,l + 144\,\beta_\xi^2\,J_\zeta\,l + 48\,A\,\beta_\eta\,\beta_\xi\,l^3 + (18\,A\,\beta_\eta\,l^5)/5 + (18\,A\,\beta_\xi\,l^5)/5 + (6\,J_\eta\,l^5)/5 + (6\,J_\xi\,l^5)/5 - (6\,J_\zeta\,l^5)/5 + (9\,A\,l^7)/35$$

$$G_{6,2} = 0.$$

$$G_{6,3} = 0.$$

$$G_{6,4} = 72\,\beta_\eta\,\beta_\xi\,J_\eta\,l^2 - 72\,\beta_\xi^2\,J_\eta\,l^2 + 72\,\beta_\eta\,\beta_\xi\,J_\xi\,l^2 - 72\,\beta_\xi^2\,J_\xi\,l^2 - 72\,\beta_\eta\,\beta_\xi\,J_\zeta\,l^2 + 72\,\beta_\xi^2\,J_\zeta\,l^2 + 12\,A\,\beta_\eta\,\beta_\xi\,l^4 - 6\,\beta_\xi\,J_\eta\,l^4 - 6\,\beta_\xi\,J_\xi\,l^4 + 6\,\beta_\xi\,J_\zeta\,l^4 + A\,\beta_\eta\,l^6 + (4\,A\,\beta_\xi\,l^6)/5 + (J_\eta\,l^6)/10 + (J_\xi\,l^6)/10 - (J_\zeta\,l^6)/10 + (13\,A\,l^8)/210$$

$$G_{6,5} = 144\,\beta_\eta^2\,J_\eta\,l - 288\,\beta_\eta\,\beta_\xi\,J_\eta\,l + 144\,\beta_\xi^2\,J_\eta\,l + 144\,\beta_\eta^2\,J_\xi\,l - 288\,\beta_\eta\,\beta_\xi\,J_\xi\,l + 144\,\beta_\xi^2\,J_\xi\,l - 144\,\beta_\eta^2\,J_\zeta\,l + 288\,\beta_\eta\,\beta_\xi\,J_\zeta\,l - 144\,\beta_\xi^2\,J_\zeta\,l + 96\,A\,\beta_\eta\,\beta_\xi\,l^3 + (42\,A\,\beta_\eta\,l^5)/5 + (42\,A\,\beta_\xi\,l^5)/5 - (6\,J_\eta\,l^5)/5 - (6\,J_\xi\,l^5)/5 + (6\,J_\zeta\,l^5)/5 + (26\,A\,l^7)/35$$

$$G_{6,6} = 0.$$

$$G_{6,7} = 0.$$

$$G_{6,8} = 72\,\beta_\eta\,\beta_\xi\,J_\eta\,l^2 - 72\,\beta_\xi^2\,J_\eta\,l^2 + 72\,\beta_\eta\,\beta_\xi\,J_\xi\,l^2 - 72\,\beta_\xi^2\,J_\xi\,l^2 - 72\,\beta_\eta\,\beta_\xi\,J_\zeta\,l^2 + 72\,\beta_\xi^2\,J_\zeta\,l^2 - 12\,A\,\beta_\eta\,\beta_\xi\,l^4 - 6\,\beta_\xi\,J_\eta\,l^4 - 6\,\beta_\xi\,J_\xi\,l^4 + 6\,\beta_\xi\,J_\zeta\,l^4 - A\,\beta_\eta\,l^6 - (6\,A\,\beta_\xi\,l^6)/5 + (J_\eta\,l^6)/10 + (J_\xi\,l^6)/10 - (J_\zeta\,l^6)/10 - (11\,A\,l^8)/105$$

$$G_{7,1} = 72\,\beta_\eta^2\,J_\eta\,l^2 - 72\,\beta_\eta\,\beta_\xi\,J_\eta\,l^2 + 72\,\beta_\eta^2\,J_\xi\,l^2 - 72\,\beta_\eta\,\beta_\xi\,J_\xi\,l^2 - 72\,\beta_\eta^2\,J_\zeta\,l^2 + 72\,\beta_\eta\,\beta_\xi\,J_\zeta\,l^2 - 12\,A\,\beta_\eta\,\beta_\xi\,l^4 + 6\,\beta_\eta\,J_\eta\,l^4 + 6\,\beta_\eta\,J_\xi\,l^4 - 6\,\beta_\eta\,J_\zeta\,l^4 - (4\,A\,\beta_\eta\,l^6)/5 - A\,\beta_\xi\,l^6 - (J_\eta\,l^6)/10 - (J_\xi\,l^6)/10 + (J_\zeta\,l^6)/10 - (13\,A\,l^8)/210$$

$$G_{7,2} = 0.$$

$$G_{7,3} = 0.$$

$$G_{7,4} = -24\,\beta_\eta\,\beta_\xi\,J_\eta\,l^3 - 24\,\beta_\eta\,\beta_\xi\,J_\xi\,l^3 + 24\,\beta_\eta\,\beta_\xi\,J_\zeta\,l^3 - (12\,A\,\beta_\eta\,\beta_\xi\,l^5)/5 + \beta_\eta\,J_\eta\,l^5 + \beta_\xi\,J_\eta\,l^5 + \beta_\eta\,J_\xi\,l^5 + \beta_\xi\,J_\xi\,l^5 - \beta_\eta\,J_\zeta\,l^5 - \beta_\xi\,J_\zeta\,l^5 - (A\,\beta_\eta\,l^7)/5 - (A\,\beta_\xi\,l^7)/5 + (J_\eta\,l^7)/30 + (J_\xi\,l^7)/30 - (J_\zeta\,l^7)/30 - (A\,l^9)/70$$

$$G_{7,5} = -72\,\beta_\eta^2\,J_\eta\,l^2 + 72\,\beta_\eta\,\beta_\xi\,J_\eta\,l^2 - 72\,\beta_\eta^2\,J_\xi\,l^2 + 72\,\beta_\eta\,\beta_\xi\,J_\xi\,l^2 + 72\,\beta_\eta^2\,J_\zeta\,l^2 - 72\,\beta_\eta\,\beta_\xi\,J_\zeta\,l^2 - 12\,A\,\beta_\eta\,\beta_\xi\,l^4 - 6\,\beta_\eta\,J_\eta\,l^4 - 6\,\beta_\eta\,J_\xi\,l^4 + 6\,\beta_\eta\,J_\zeta\,l^4 - (6\,A\,\beta_\eta\,l^6)/5 - A\,\beta_\xi\,l^6 + (J_\eta\,l^6)/10 + (J_\xi\,l^6)/10 - (J_\zeta\,l^6)/10 - (11\,A\,l^8)/105$$

$$G_{7,6} = 0.$$

$$G_{7,7} = 0.$$

$$G_{7,8} = -48\,\beta_\eta\,\beta_\xi\,J_\eta\,l^3 - 48\,\beta_\eta\,\beta_\xi\,J_\xi\,l^3 + 48\,\beta_\eta\,\beta_\xi\,J_\zeta\,l^3 + (12\,A\,\beta_\eta\,\beta_\xi\,l^5)/5 - \beta_\eta\,J_\eta\,l^5 - \beta_\xi\,J_\eta\,l^5 - \beta_\eta\,J_\xi\,l^5 - \beta_\xi\,J_\xi\,l^5 + \beta_\eta\,J_\zeta\,l^5 + \beta_\xi\,J_\zeta\,l^5 + (A\,\beta_\eta\,l^7)/5 + (A\,\beta_\xi\,l^7)/5 - (2\,J_\eta\,l^7)/15 - (2\,J_\xi\,l^7)/15 + (2\,J_\zeta\,l^7)/15 + (2\,A\,l^9)/105$$

$$G_{8,1} = 0.$$

$$G_{8,2} = 72\,\beta_\eta\,\beta_\xi\,J_\eta\,l^2 - 72\,\beta_\xi^2\,J_\eta\,l^2 + 72\,\beta_\eta\,\beta_\xi\,J_\xi\,l^2 - 72\,\beta_\xi^2\,J_\xi\,l^2 - 72\,\beta_\eta\,\beta_\xi\,J_\zeta\,l^2 + 72\,\beta_\xi^2\,J_\zeta\,l^2 + 12\,A\,\beta_\eta\,\beta_\xi\,l^4 - 6\,\beta_\xi\,J_\eta\,l^4 - 6\,\beta_\xi\,J_\xi\,l^4 + 6\,\beta_\xi\,J_\zeta\,l^4 + A\,\beta_\eta\,l^6 + (4\,A\,\beta_\xi\,l^6)/5 + (J_\eta\,l^6)/10 + (J_\xi\,l^6)/10 - (J_\zeta\,l^6)/10 + (13\,A\,l^8)/210$$

$$G_{8,3} = 24\,\beta_\eta\,\beta_\xi\,J_\eta\,l^3 + 24\,\beta_\eta\,\beta_\xi\,J_\xi\,l^3 - 24\,\beta_\eta\,\beta_\xi\,J_\zeta\,l^3 + (12\,A\,\beta_\eta\,\beta_\xi\,l^5)/5 - \beta_\eta\,J_\eta\,l^5 - \beta_\xi\,J_\eta\,l^5 - \beta_\eta\,J_\xi\,l^5 - \beta_\xi\,J_\xi\,l^5 + \beta_\eta\,J_\zeta\,l^5 + \beta_\xi\,J_\zeta\,l^5 + (A\,\beta_\eta\,l^7)/5 + (A\,\beta_\xi\,l^7)/5 - (J_\eta\,l^7)/30 - (J_\xi\,l^7)/30 + (J_\zeta\,l^7)/30 + (A\,l^9)/70$$

$$G_{8,4} = 0.$$

$$G_{8,5} = 0.$$

$$G_{8,6} = -72\,\beta_\eta\,\beta_\xi\,J_\eta\,l^2 + 72\,\beta_\xi^2\,J_\eta\,l^2 - 72\,\beta_\eta\,\beta_\xi\,J_\xi\,l^2 + 72\,\beta_\xi^2\,J_\xi\,l^2 + 72\,\beta_\eta\,\beta_\xi\,J_\zeta\,l^2 - 72\,\beta_\xi^2\,J_\zeta\,l^2 + 12\,A\,\beta_\eta\,\beta_\xi\,l^4 + 6\,\beta_\xi\,J_\eta\,l^4 + 6\,\beta_\xi\,J_\xi\,l^4 - 6\,\beta_\xi\,J_\zeta\,l^4 + A\,\beta_\eta\,l^6 + (6\,A\,\beta_\xi\,l^6)/5 - (J_\eta\,l^6)/10 - (J_\xi\,l^6)/10 + (J_\zeta\,l^6)/10 + (11\,A\,l^8)/105$$

$$G_{8,7} = 48\,\beta_\eta\,\beta_\xi\,J_\eta\,l^3 + 48\,\beta_\eta\,\beta_\xi\,J_\xi\,l^3 - 48\,\beta_\eta\,\beta_\xi\,J_\zeta\,l^3 - (12\,A\,\beta_\eta\,\beta_\xi\,l^5)/5 + \beta_\eta\,J_\eta\,l^5 + \beta_\xi\,J_\eta\,l^5 + \beta_\eta\,J_\xi\,l^5 + \beta_\xi\,J_\xi\,l^5 - \beta_\eta\,J_\zeta\,l^5 - \beta_\xi\,J_\zeta\,l^5 - (A\,\beta_\eta\,l^7)/5 - (A\,\beta_\xi\,l^7)/5 + (2\,J_\eta\,l^7)/15 + (2\,J_\xi\,l^7)/15 - (2\,J_\zeta\,l^7)/15 - (2\,A\,l^9)/105$$

$$G_{8,8} = 0.$$

The element 'centrifugal' matrix $[Y^e]$ is given by:

$$[Y^e] = \text{Diag}\left\{\frac{\rho}{(1+\phi_\eta)^2}\ \frac{\rho}{(1+\phi_\xi)^2}\ \frac{\rho}{(1+\phi_\xi)^2}\ \frac{\rho}{(1+\phi_\eta)^2}\right.$$

$$\left.\frac{\rho}{(1+\phi_\eta)^2}\ \frac{\rho}{(1+\phi_\xi)^2}\ \frac{\rho}{(1+\phi_\xi)^2}\ \frac{\rho}{(1+\phi_\eta)^2}\right\} \times [Y]$$

where:

$$Y(1,1) = (6J_\xi)/(5l) - (6J_\zeta)/(5l) + (2J_\xi\phi_\eta)/l - (2J_\zeta\phi_\eta)/l + (J_\xi\phi_\eta^2)/l - (J_\zeta\phi_\eta^2)/l - (2J_\xi\phi_\xi)/l + (2J_\zeta\phi_\xi)/l - (2J_\xi\phi_\eta\phi_\xi)/l + (2J_\zeta\phi_\eta\phi_\xi)/l + (J_\xi\phi_\xi^2)/l - (J_\zeta\phi_\xi^2)/l + (13Al)/35 + (7A\phi_\eta l)/10 + (A\phi_\eta^2 l)/3$$

$$Y(1,2) = 0.$$

$$Y(1,3) = 0.$$

$$Y(1,4) = J_\xi/10 - J_\zeta/10 - (J_\xi\phi_\xi)/2 + (J_\zeta\phi_\xi)/2 - (J_\xi\phi_\eta\phi_\xi)/2 + (J_\zeta\phi_\eta\phi_\xi)/2 + (J_\xi\phi_\xi^2)/2 - (J_\zeta\phi_\xi^2)/2 + (11Al^2)/210 + (11A\phi_\eta l^2)/120 + (A\phi_\eta^2 l^2)/24$$

$$Y(1,5) = -(6J_\xi)/(5l) + (6J_\zeta)/(5l) - (2J_\xi\phi_\eta)/l + (2J_\zeta\phi_\eta)/l - (J_\xi\phi_\eta^2)/l + (J_\zeta\phi_\eta^2)/l + (2J_\xi\phi_\xi)/l - (2J_\zeta\phi_\xi)/l + (2J_\xi\phi_\eta\phi_\xi)/l - (2J_\zeta\phi_\eta\phi_\xi)/l - (J_\xi\phi_\xi^2)/l + (J_\zeta\phi_\xi^2)/l + (9Al)/70 + (3A\phi_\eta l)/10 + (A\phi_\eta^2 l)/6$$

$$Y(1,6) = 0.$$

$$Y(1,7) = 0.$$

$$Y(1,8) = J_\xi/10 - J_\zeta/10 - (J_\xi\phi_\xi)/2 + (J_\zeta\phi_\xi)/2 - (J_\xi\phi_\eta\phi_\xi)/2 + (J_\zeta\phi_\eta\phi_\xi)/2 + (J_\xi\phi_\xi^2)/2 - (J_\zeta\phi_\xi^2)/2 - (13Al^2)/420 - (3A\phi_\eta l^2)/40 - (A\phi_\eta^2 l^2)/24$$

$$Y(2,1) = 0.$$

$$Y(2,2) = (6J_\eta)/(5l) - (6J_\zeta)/(5l) - (2J_\eta\phi_\eta)/l + (2J_\zeta\phi_\eta)/l + (J_\eta\phi_\eta^2)/l - (J_\zeta\phi_\eta^2)/l + (2J_\eta\phi_\xi)/l - (2J_\zeta\phi_\xi)/l - (2J_\eta\phi_\eta\phi_\xi)/l + (2J_\zeta\phi_\eta\phi_\xi)/l + (J_\eta\phi_\xi^2)/l - (J_\zeta\phi_\xi^2)/l + (13Al)/35 + (7A\phi_\xi l)/10 + (A\phi_\xi^2 l)/3$$

$$Y(2,3) = J_\eta/10 - J_\zeta/10 - (J_\eta\phi_\eta)/2 + (J_\zeta\phi_\eta)/2 + (J_\eta\phi_\eta^2)/2 - (J_\zeta\phi_\eta^2)/2 - (J_\eta\phi_\eta\phi_\xi)/2 + (J_\zeta\phi_\eta\phi_\xi)/2 + (11Al^2)/210 + (11A\phi_\xi l^2)/120 + (A\phi_\xi^2 l^2)/24$$

$$Y(2,4) = 0.$$

$$Y(2,5) = 0.$$

$$Y(2,6) = -(6J_\eta)/(5l) + (6J_\zeta)/(5l) + (2J_\eta\phi_\eta)/l - (2J_\zeta\phi_\eta)/l - (J_\eta\phi_\eta^2)/l + (J_\zeta\phi_\eta^2)/l - (2J_\eta\phi_\xi)/l + (2J_\zeta\phi_\xi)/l + (2J_\eta\phi_\eta\phi_\xi)/l - (2J_\zeta\phi_\eta\phi_\xi)/l - (J_\eta\phi_\xi^2)/l + (J_\zeta\phi_\xi^2)/l + (9Al)/70 + (3A\phi_\xi l)/10 + (A\phi_\xi^2 l)/6$$

$$Y(2,7) = J_\eta/10 - J_\zeta/10 - (J_\eta\phi_\eta)/2 + (J_\zeta\phi_\eta)/2 + (J_\eta\phi_\eta^2)/2 - (J_\zeta\phi_\eta^2)/2 - (J_\eta\phi_\eta\phi_\xi)/2 + (J_\zeta\phi_\eta\phi_\xi)/2 - (13Al^2)/420 - (3A\phi_\xi l^2)/40 - (A\phi_\xi^2 l^2)/24$$

$$Y(2,8) = 0.$$

$$Y(3,1) = 0.$$

$$Y(3,2) = J_\eta/10 - J_\zeta/10 - (J_\eta\phi_\eta)/2 + (J_\zeta\phi_\eta)/2 + (J_\eta\phi_\eta^2)/2 - (J_\zeta\phi_\eta^2)/2 - (J_\eta\phi_\eta\phi_\xi)/2 + (J_\zeta\phi_\eta\phi_\xi)/2 + (11Al^2)/210 + (11A\phi_\xi l^2)/120 + (A\phi_\xi^2 l^2)/24$$

$$Y(3,3) = (2J_\eta l)/15 - (2J_\zeta l)/15 + (J_\eta\phi_\eta^2 l)/4 - (J_\zeta\phi_\eta^2 l)/4 + (J_\eta\phi_\xi l)/6 - (J_\zeta\phi_\xi l)/6 + (J_\eta\phi_\xi^2 l)/12 - (J_\zeta\phi_\xi^2 l)/12 + (Al^3)/105 + (A\phi_\xi l^3)/60 + (A\phi_\xi^2 l^3)/120$$

$$Y(3,4) = 0.$$

$$Y(3,5) = 0.$$

$$Y(3,6) = -J_\eta/10 + J_\zeta/10 + (J_\eta\phi_\eta)/2 - (J_\zeta\phi_\eta)/2 - (J_\eta\phi_\eta^2)/2 + (J_\zeta\phi_\eta^2)/2 + (J_\eta\phi_\eta\phi_\xi)/2 - (J_\zeta\phi_\eta\phi_\xi)/2 + (13Al^2)/420 + (3A\phi_\xi l^2)/40 + (A\phi_\xi^2 l^2)/24$$

$$Y(3,7) = -(J_\eta l)/30 + (J_\zeta l)/30 + (J_\eta\phi_\eta^2 l)/4 - (J_\zeta\phi_\eta^2 l)/4 - (J_\eta\phi_\xi l)/6 + (J_\zeta\phi_\xi l)/6 - (J_\eta\phi_\xi^2 l)/12 + (J_\zeta\phi_\xi^2 l)/12 - (Al^3)/140 - (A\phi_\xi l^3)/60 - (A\phi_\xi^2 l^3)/120$$

$$Y(3,8) = 0.$$

$$Y(4,1) = J_\xi/10 - J_\zeta/10 - (J_\xi\phi_\xi)/2 + (J_\zeta\phi_\xi)/2 - (J_\xi\phi_\eta\phi_\xi)/2 + (J_\zeta\phi_\eta\phi_\xi)/2 + (J_\xi\phi_\xi^2)/2 - (J_\zeta\phi_\xi^2)/2 + (11Al^2)/210 + (11A\phi_\eta l^2)/120 + (A\phi_\eta^2 l^2)/24$$

$$Y(4,2) = 0.$$

$$Y(4,3) = 0.$$

$$Y(4,4) = (2J_\xi l)/15 - (2J_\zeta l)/15 + (J_\xi\phi_\eta l)/6 - (J_\zeta\phi_\eta l)/6 + (J_\xi\phi_\eta^2 l)/12 - (J_\zeta\phi_\eta^2 l)/12 + (J_\xi\phi_\xi^2 l)/4 - (J_\zeta\phi_\xi^2 l)/4 + (Al^3)/105 + (A\phi_\eta l^3)/60 + (A\phi_\eta^2 l^3)/120$$

$$Y(4,5) = -J_\xi/10 + J_\zeta/10 + (J_\xi\phi_\xi)/2 - (J_\zeta\phi_\xi)/2 + (J_\xi\phi_\eta\phi_\xi)/2 - (J_\zeta\phi_\eta\phi_\xi)/2 - (J_\xi\phi_\xi^2)/2 + (J_\zeta\phi_\xi^2)/2 + (13Al^2)/420 + (3A\phi_\eta l^2)/40 + (A\phi_\eta^2 l^2)/24$$

$$Y(4,6) = 0.$$

$$Y(4,7) = 0.$$

$$Y(4,8) = -(J_\xi l)/30 + (J_\zeta l)/30 - (J_\xi\phi_\eta l)/6 + (J_\zeta\phi_\eta l)/6 - (J_\xi\phi_\eta^2 l)/12 + (J_\zeta\phi_\eta^2 l)/12 + (J_\xi\phi_\xi^2 l)/4 - (J_\zeta\phi_\xi^2 l)/4 - (Al^3)/140 - (A\phi_\eta l^3)/60 - (A\phi_\eta^2 l^3)/120$$

$$Y(5,1) = -(6J_\xi)/(5l) + (6J_\zeta)/(5l) - (2J_\xi\phi_\eta)/l + (2J_\zeta\phi_\eta)/l - (J_\xi\phi_\eta^2)/l + (J_\zeta\phi_\eta^2)/l + (2J_\xi\phi_\xi)/l - (2J_\zeta\phi_\xi)/l + (2J_\xi\phi_\eta\phi_\xi)/l - (2J_\zeta\phi_\eta\phi_\xi)/l - (J_\xi\phi_\xi^2)/l + (J_\zeta\phi_\xi^2)/l + (9Al)/70 + (3A\phi_\eta l)/10 + (A\phi_\eta^2 l)/6$$

$$Y(5,2) = 0.$$

$$Y(5,3) = 0.$$

$$Y(5,4) = -J_\xi/10 + J_\zeta/10 + (J_\xi\phi_\xi)/2 - (J_\zeta\phi_\xi)/2 + (J_\xi\phi_\eta\phi_\xi)/2 - (J_\zeta\phi_\eta\phi_\xi)/2 - (J_\xi\phi_\xi^2)/2 + (J_\zeta\phi_\xi^2)/2 + (13Al^2)/420 + (3A\phi_\eta l^2)/40 + (A\phi_\eta^2 l^2)/24$$

$$Y(5,5) = (6J_\xi)/(5l) - (6J_\zeta)/(5l) + (2J_\xi\phi_\eta)/l - (2J_\zeta\phi_\eta)/l + (J_\xi\phi_\eta^2)/l - (J_\zeta\phi_\eta^2)/l - (2J_\xi\phi_\xi)/l + (2J_\zeta\phi_\xi)/l - (2J_\xi\phi_\eta\phi_\xi)/l + (2J_\zeta\phi_\eta\phi_\xi)/l + (J_\xi\phi_\xi^2)/l - (J_\zeta\phi_\xi^2)/l + (13Al)/35 + (7A\phi_\eta l)/10 + (A\phi_\eta^2 l)/3$$

$$Y(5,6) = 0.$$

$$Y(5,7) = 0.$$

$$Y(5,8) = -J_\xi/10 + J_\zeta/10 + (J_\xi\phi_\xi)/2 - (J_\zeta\phi_\xi)/2 + (J_\xi\phi_\eta\phi_\xi)/2 - (J_\zeta\phi_\eta\phi_\xi)/2 - (J_\xi\phi_\xi^2)/2 + (J_\zeta\phi_\xi^2)/2 - (11Al^2)/210 - (11A\phi_\eta l^2)/120 - (A\phi_\eta^2 l^2)/24$$

$$Y(6,1) = 0.$$

$$Y(6,2) = -(6J_\eta)/(5l) + (6J_\zeta)/(5l) + (2J_\eta\phi_\eta)/l - (2J_\zeta\phi_\eta)/l - (J_\eta\phi_\eta^2)/l + (J_\zeta\phi_\eta^2)/l - (2J_\eta\phi_\xi)/l + (2J_\zeta\phi_\xi)/l + (2J_\eta\phi_\eta\phi_\xi)/l - (2J_\zeta\phi_\eta\phi_\xi)/l - (J_\eta\phi_\xi^2)/l + (J_\zeta\phi_\xi^2)/l + (9Al)/70 + (3A\phi_\xi l)/10 + (A\phi_\xi^2 l)/6$$

$$Y(6,3) = -J_\eta/10 + J_\zeta/10 + (J_\eta\phi_\eta)/2 - (J_\zeta\phi_\eta)/2 - (J_\eta\phi_\eta^2)/2 + (J_\zeta\phi_\eta^2)/2 + (J_\eta\phi_\eta\phi_\xi)/2 - (J_\zeta\phi_\eta\phi_\xi)/2 + (13Al^2)/420 + (3A\phi_\xi l^2)/40 + (A\phi_\xi^2 l^2)/24$$

$$Y(6,4) = 0.$$

$$Y(6,5) = 0.$$

$$Y(6,6) = (6J_\eta)/(5l) - (6J_\zeta)/(5l) - (2J_\eta\phi_\eta)/l + (2J_\zeta\phi_\eta)/l + (J_\eta\phi_\eta^2)/l - (J_\zeta\phi_\eta^2)/l + (2J_\eta\phi_\xi)/l - (2J_\zeta\phi_\xi)/l - (2J_\eta\phi_\eta\phi_\xi)/l + (2J_\zeta\phi_\eta\phi_\xi)/l + (J_\eta\phi_\xi^2)/l - (J_\zeta\phi_\xi^2)/l + (13Al)/35 + (7A\phi_\xi l)/10 + (A\phi_\xi^2 l)/3$$

$$Y(6,7) = -J_\eta/10 + J_\zeta/10 + (J_\eta\phi_\eta)/2 - (J_\zeta\phi_\eta)/2 - (J_\eta\phi_\eta^2)/2 + (J_\zeta\phi_\eta^2)/2 + (J_\eta\phi_\eta\phi_\xi)/2 - (J_\zeta\phi_\eta\phi_\xi)/2 - (11Al^2)/210 - (11A\phi_\xi l^2)/120 - (A\phi_\xi^2 l^2)/24$$

$$Y(6,8) = 0.$$

$$Y(7,1) = 0.$$

$$Y(7,2) = J_\eta/10 - J_\zeta/10 - (J_\eta\phi_\eta)/2 + (J_\zeta\phi_\eta)/2 + (J_\eta\phi_\eta^2)/2 - (J_\zeta\phi_\eta^2)/2 - (J_\eta\phi_\eta\phi_\xi)/2 + (J_\zeta\phi_\eta\phi_\xi)/2 - (13Al^2)/420 - (3A\phi_\xi l^2)/40 - (A\phi_\xi^2 l^2)/24$$

$$Y(7,3) = -(J_\eta l)/30 + (J_\zeta l)/30 + (J_\eta\phi_\eta^2 l)/4 - (J_\zeta\phi_\eta^2 l)/4 - (J_\eta\phi_\xi l)/6 + (J_\zeta\phi_\xi l)/6 - (J_\eta\phi_\xi^2 l)/12 + (J_\zeta\phi_\xi^2 l)/12 - (Al^3)/140 - (A\phi_\xi l^3)/60 - (A\phi_\xi^2 l^3)/120$$

$$Y(7,4) = 0.$$

$$Y(7,5) = 0.$$

$$Y(7,6) = -J_\eta/10 + J_\zeta/10 + (J_\eta\phi_\eta)/2 - (J_\zeta\phi_\eta)/2 - (J_\eta\phi_\eta^2)/2 + (J_\zeta\phi_\eta^2)/2 + (J_\eta\phi_\eta\phi_\xi)/2 - (J_\zeta\phi_\eta\phi_\xi)/2 - (11Al^2)/210 - (11A\phi_\xi l^2)/120 - (A\phi_\xi^2 l^2)/24$$

$$Y(7,7) = (2J_\eta l)/15 - (2J_\zeta l)/15 + (J_\eta\phi_\eta^2 l)/4 - (J_\zeta\phi_\eta^2 l)/4 + (J_\eta\phi_\xi l)/6 - (J_\zeta\phi_\xi l)/6 + (J_\eta\phi_\xi^2 l)/12 - (J_\zeta\phi_\xi^2 l)/12 + (Al^3)/105 + (A\phi_\xi l^3)/60 + (A\phi_\xi^2 l^3)/120$$

$$Y(7,8) = 0.$$

$$Y(8,1) = J_\xi/10 - J_\zeta/10 - (J_\xi\phi_\xi)/2 + (J_\zeta\phi_\xi)/2 - (J_\xi\phi_\eta\phi_\xi)/2 + (J_\zeta\phi_\eta\phi_\xi)/2 + (J_\xi\phi_\xi^2)/2 - (J_\zeta\phi_\xi^2)/2 - (13Al^2)/420 - (3A\phi_\eta l^2)/40 - (A\phi_\eta^2 l^2)/24$$

$$Y(8,2) = 0.$$

$$Y(8,3) = 0.$$

$$Y(8,4) = -(J_\xi l)/30 + (J_\zeta l)/30 - (J_\xi\phi_\eta l)/6 + (J_\zeta\phi_\eta l)/6 - (J_\xi\phi_\eta^2 l)/12 + (J_\zeta\phi_\eta^2 l)/12 + (J_\xi\phi_\xi^2 l)/4 - (J_\zeta\phi_\xi^2 l)/4 - (Al^3)/140 - (A\phi_\eta l^3)/60 - (A\phi_\eta^2 l^3)/120$$

$Y(8,5) = -J_\xi/10 + J_\zeta/10 + (J_\xi\phi_\xi)/2 - (J_\zeta\phi_\xi)/2 + (J_\xi\phi_\eta\phi_\xi)/2 - (J_\zeta\phi_\eta\phi_\xi)/2 - (J_\xi\phi_\xi^2)/2 + (J_\zeta\phi_\xi^2)/2 - (11Al^2)/210 - (11A\phi_\eta l^2)/120 - (A\phi_\eta^2 l^2)/24$

$Y(8,6) = 0.$

$Y(8,7) = 0.$

$Y(8,8) = (2J_\xi l)/15 - (2J_\zeta l)/15 + (J_\xi\phi_\eta l)/6 - (J_\zeta\phi_\eta l)/6 + (J_\xi\phi_\eta^2 l)/12 - (J_\zeta\phi_\eta^2 l)/12 + (J_\xi\phi_\xi^2 l)/4 - (J_\zeta\phi_\xi^2 l)/4 + (Al^3)/105 + (A\phi_\eta l^3)/60 + (A\phi_\eta^2 l^3)/120$

B.2 Strain Energy

The element stiffness matrix, $[K^e]$ due to bending is given by :

$$[K_b^e] = \int_0^l E\,[T]^T\,[B'']\,[i]\,[B'']^T\,[T]\,d\zeta$$

$= \int_0^l E$ Diag $\{l^2(l^2+12\beta_\eta)^2,\ l^2(l^2+12\beta_\xi)^2, l^2(l^2+12\beta_\eta)^2, l^2(l^2+12\beta_\eta)^2, l^2(l^2+12\beta_\eta)^2, l^2(l^2+12\beta_\xi)^2, l^2(l^2+12\beta_\xi)^2, l^2(l^2+12\beta_\eta)^2\}^{-1}$

$$
\times \begin{bmatrix}
12J_\eta l^3 & 0. & 0. & 6J_\eta l^4 & -12J_\eta l^3 & 0. & 0. & 6J_\eta l^4 \\
0. & 12J_\xi l^3 & 6J_\xi l^4 & 0. & 0. & -12J_\xi l^3 & 6J_\xi l^4 & 0. \\
0. & 6J_\xi l^4 & (144\beta_\xi^2 J_\xi l & 0. & 0. & -6J_\xi l^4 & (-144\beta_\xi^2 J_\xi l & 0. \\
 & & +24\beta_\xi J_\xi l^3 & & & & -24\beta_\xi J_\xi l^3 & \\
 & & +4J_\xi l^5) & & & & +2J_\xi l^5) & \\
6J_\eta l^4 & 0. & 0. & (144\beta_\eta^2 J_\eta l & -6J_\eta l^4 & 0. & 0. & (-144\beta_\eta^2 J_\eta l \\
 & & & +24\beta_\eta J_\eta l^3 & & & & -24\beta_\eta J_\eta l^3 \\
 & & & +4J_\eta l^5) & & & & +2J_\eta l^5) \\
-12J_\eta l^3 & 0. & 0. & -6J_\eta l^4 & 12J_\eta l^3 & 0. & 0. & -6J_\eta l^4 \\
0. & -12J_\xi l^3 & -6J_\xi l^4 & 0. & 0. & 12J_\xi l^3 & -6J_\xi l^4 & 0. \\
0. & 6J_\xi l^4 & (-144\beta_\xi^2 J_\xi l & 0. & 0. & -6J_\xi l^4 & (144\beta_\xi^2 J_\xi l & 0. \\
 & & -24\beta_\xi J_\xi l^3 & & & & +24\beta_\xi J_\xi l^3 & \\
 & & +2J_\xi l^5) & & & & +4J_\xi l^5) & \\
6J_\eta l^4 & 0. & 0. & (-144\beta_\eta^2 J_\eta l & -6J_\eta l^4 & 0. & 0. & (144\beta_\eta^2 J_\eta l \\
 & & & -24\beta_\eta J_\eta l^3 & & & & +24\beta_\eta J_\eta l^3 \\
 & & & +2J_\eta l^5) & & & & +4J_\eta l^5)
\end{bmatrix} d\zeta
$$

The stiffness matrix, $[K_s^e]$ due to shear is given by :

$$[K_s^e] = \int_0^l [T]^T [C][C]^T [T]\, d\zeta$$

$$= \int_0^l K G A \,\mathrm{Diag}\{l^2(l^2+12\beta_\eta)^2,\ l^2(l^2+12\beta_\xi)^2, l^2(l^2+12\beta_\xi)^2, l^2(l^2+12\beta_\eta)^2, l^2(l^2+12\beta_\eta)^2, l^2(l^2+12\beta_\xi)^2, l^2(l^2+12\beta_\xi)^2, l^2(l^2+12\beta_\eta)^2\}^{-1}$$

$$\times \begin{bmatrix}
144\beta_\eta^2 l & 0. & 0. & 72\beta_\eta^2 l^2 & -144\beta_\eta^2 l & 0. & 0. & 72\beta_\eta^2 l^2 \\
0. & 144\beta_\xi^2 l & 72\beta_\xi^2 l^2 & 0. & 0. & -144\beta_\xi^2 l & 72\beta_\xi^2 l^2 & 0. \\
0. & 72\beta_\xi^2 l^2 & 36\beta_\xi^2 l^3 & 0. & 0. & -72\beta_\xi^2 l^2 & 36\beta_\xi^2 l^3 & 0. \\
72\beta_\eta^2 l^2 & 0. & 0. & 36\beta_\eta^2 l^3 & -72\beta_\eta^2 l^2 & 0. & 0. & 36\beta_\eta^2 l^3 \\
-144\beta_\eta^2 l & 0. & 0. & -72\beta_\eta^2 l^2 & 144\beta_\eta^2 l & 0. & 0. & -72\beta_\eta^2 l^2 \\
0. & -144\beta_\xi^2 l & -72\beta_\xi^2 l^2 & 0. & 0. & 144\beta_\xi^2 l & -72\beta_\xi^2 l^2 & 0. \\
0. & 72\beta_\xi^2 l^2 & 36\beta_\xi^2 l^3 & 0. & 0. & -72\beta_\xi^2 l^2 & 36\beta_\xi^2 l^3 & 0. \\
72\beta_\eta^2 l^2 & 0. & 0. & 36\beta_\eta^2 l^3 & -72\beta_\eta^2 l^2 & 0. & 0. & 36\beta_\eta^2 l^3
\end{bmatrix} d\zeta$$

After some considerable manipulation, the total stiffness matrix $[K^e]$reduces to the surprisingly simple form:

$$[K^e] = E\,\mathrm{Diag}\left\{\frac{J_\eta}{l^3(1+\phi_\eta)}\ \frac{J_\xi}{l^3(1+\phi_\xi)}\ \frac{J_\xi}{l^3(1+\phi_\xi)}\ \frac{J_\eta}{l^3(1+\phi_\eta)}\right.$$

$$\left.\frac{J_\eta}{l^3(1+\phi_\eta)}\ \frac{J_\xi}{l^3(1+\phi_\xi)}\ \frac{J_\xi}{l^3(1+\phi_\xi)}\ \frac{J_\eta}{l^3(1+\phi_\eta)}\right\} \times$$

$$\begin{bmatrix}
12 & 0 & 0 & 6l & -12 & 0 & 0 & 6l \\
0 & 12 & 6l & 0 & 0 & -12 & 6l & 0 \\
0 & 6l & l^2(4+\phi_\xi) & 0 & 0 & -6l & l^2(2-\phi_\xi) & 0 \\
6l & 0 & 0 & l^2(4+\phi_\eta) & -6l & 0 & 0 & l^2(2-\phi_\eta) \\
-12 & 0 & 0 & -6l & 12 & 0 & 0 & -6l \\
0 & -12 & -6l & 0 & 0 & 12 & -6l & 0 \\
0 & 6l & l^2(2-\phi_\xi) & 0 & 0 & -6l & l^2(4+\phi_\xi) & 0 \\
6l & 0 & 0 & l^2(2-\phi_\eta) & -6l & 0 & 0 & l^2(4+\phi_\eta)
\end{bmatrix}$$

Appendix C

Plain Bearing Stiffness and Damping Coefficients

The following is a re-working of the derivation of the incremental fluid forces by Pinkus and Sternlicht [86]. In Trumpler's form of Reynold's equation, Equation 5.1, the term $(\omega_j/2 - \omega_c)$ occurs, where ω_j is the journal angular velocity and $\omega_c = \dot{\psi}$ is the angular velocity of the line of centres. For the calculation of the pressure profile and the journal forces, we have taken ω_c to be zero.

For the purpose of examining the behaviour of small perturbations about the equilibrium position (ε_o, ψ_o), we can include $\dot{\psi}$ in order to allow a small perturbation $\delta\psi$ and $\delta\dot{\psi}$ about $\psi = \psi_o$, $\dot{\psi} = \dot{\psi}_o = 0$. As the $\delta\dot{\psi}$ is, by definition small, and $\dot{\psi}_o = 0$, we can assume the pressure profile to be unchanged by $\dot{\psi}$.

In the development of the finite element model, we had the relationship between dimensional and non-dimensional fluid forces as,

$$F_r = \mu \left(\frac{R}{c}\right)^2 N D L \overline{F}_r \tag{C.1}$$

and

$$F_t = \mu \left(\frac{R}{c}\right)^2 N D L \overline{F}_t \tag{C.2}$$

Note that [86] has opposite signs for dimensional and non - dimensional radial fluid forces.

Now,

$$\frac{\omega_j}{2} - \omega_c = \frac{\omega_j}{2}\left(1 - 2\frac{\omega_c}{\omega_j}\right) = \frac{\omega_j}{2}\left(1 - 2\frac{\dot{\psi}}{\omega_j}\right).$$

Or in terms of revolutions per second,

$$\frac{N_j}{2} - N_c = \frac{N_j}{2}\left(1 - 2\frac{N_c}{N_j}\right) = \frac{N_j}{2}\left(1 - 2\frac{\dot{\psi}}{\omega_j}\right),$$

where N_c is the angular speed of the line of centres.

Therefore we can write,

$$F_r = \mu\left(\frac{R}{c}\right)^2 N\left(1 - 2\frac{\dot{\psi}}{\omega_j}\right) D L \overline{F}_r\left(\varepsilon, \dot{\varepsilon}', \dot{\psi}\right) \tag{C.3}$$

$$F_t = \mu\left(\frac{R}{c}\right)^2 N\left(1 - 2\frac{\dot{\psi}}{\omega_j}\right) D L \overline{F}_t\left(\varepsilon, \dot{\varepsilon}', \dot{\psi}\right) \tag{C.4}$$

Substituting the Sommerfeld number we then have,

$$F_r = S^{-1} W\left(1 - 2\frac{\dot{\psi}}{\omega_j}\right) D L \overline{F}_r\left(\varepsilon, \dot{\varepsilon}', \dot{\psi}\right) \tag{C.5}$$

$$F_t = S^{-1} W\left(1 - 2\frac{\dot{\psi}}{\omega_j}\right) D L \overline{F}_t\left(\varepsilon, \dot{\varepsilon}', \dot{\psi}\right) \tag{C.6}$$

where W is the steady - state bearing load.

For small perturbations,

$$dF_r = \frac{\partial F_r}{\partial \dot{\psi}} d\dot{\psi} + \frac{\partial F_r}{\partial \varepsilon} d\varepsilon + \frac{\partial F_r}{\partial \dot{\varepsilon}'} d\dot{\varepsilon}' - F_t \sin d\psi \tag{C.7}$$

$$dF_t = \frac{\partial F_t}{\partial \dot{\psi}} d\dot{\psi} + \frac{\partial F_t}{\partial \varepsilon} d\varepsilon + \frac{\partial F_t}{\partial \dot{\varepsilon}'} d\dot{\varepsilon}' + F_t \sin d\psi \tag{C.8}$$

Thus for small deflections,

$$dF_r = S^{-1} W\left[-2\frac{\overline{F}_r}{\omega_j} d\dot{\psi} + \frac{\partial \overline{F}_r}{\partial \varepsilon} d\varepsilon + \frac{\partial \overline{F}_r}{\partial \dot{\varepsilon}'} d\dot{\varepsilon}' - \overline{F}_t d\psi\right] \tag{C.9}$$

$$dF_t = S^{-1} W\left[-2\frac{\overline{F}_t}{\omega_j} d\dot{\psi} + \frac{\partial \overline{F}_t}{\partial \varepsilon} d\varepsilon + \frac{\partial \overline{F}_t}{\partial \dot{\varepsilon}'} d\dot{\varepsilon}' - \overline{F}_r d\psi\right] \tag{C.10}$$

For small tangential and radial deflections ξ and η respectively, Figure C.1,

$$d\varepsilon = \frac{\eta}{c} \qquad d\psi = \frac{\xi}{\varepsilon_o c} \qquad d\dot{\psi} = \frac{\dot{\xi}}{\varepsilon_o c}$$

$$d\dot{\varepsilon}' = \frac{\dot{\varepsilon}}{\omega_j} = \frac{\dot{\eta}}{c\omega_j}$$

Therefore,

$$dF_r = S^{-1}W\left(-\frac{2\overline{F}_r\dot{\xi}}{\omega_j\varepsilon_o c} + \frac{\partial\overline{F}_r}{\partial\varepsilon}\frac{\eta}{c} + \frac{\partial\overline{F}_r}{\partial\dot{\varepsilon}'}\frac{\dot{\eta}}{c\omega_j} - \frac{\overline{F}_t\xi}{\varepsilon_o c}\right) \tag{C.11}$$

$$dF_t = S^{-1}W\left(-\frac{2\overline{F}_t\dot{\xi}}{\omega_j\varepsilon_o c} + \frac{\partial\overline{F}_t}{\partial\varepsilon}\frac{\eta}{c} + \frac{\partial\overline{F}_t}{\partial\dot{\varepsilon}'}\frac{\dot{\eta}}{c\omega_j} + \frac{\overline{F}_r\xi}{\varepsilon_o c}\right) \tag{C.12}$$

Then the bearing stiffness and damping coefficients along and parallel to the line of centres (radial and tangential), can be derived.

$$K_{\eta\eta} = -\frac{\partial F_r}{\partial\eta} = -\frac{S^{-1}W}{c}\frac{\partial\overline{F}_r}{\partial\varepsilon}$$

$$\frac{c}{W}K_{\eta\eta} = -S^{-1}\frac{\partial\overline{F}_r}{\partial\varepsilon} \tag{C.13}$$

$$K_{\eta\xi} = -\frac{\partial F_r}{\partial\xi} = S^{-1}W\frac{\overline{F}_t}{\varepsilon_o c}$$

$$\frac{c}{W}K_{\eta\xi} = S^{-1}\frac{\overline{F}_t}{\varepsilon_o} \tag{C.14}$$

$$K_{\xi\xi} = -\frac{\partial F_t}{\partial\xi} = -\frac{S^{-1}W}{c}\frac{\overline{F}_r}{\epsilon_o}$$

$$\frac{c}{W}K_{\xi\xi} = -S^{-1}\frac{\overline{F}_r}{\varepsilon_o} \tag{C.15}$$

$$K_{\xi\eta} = -\frac{\partial F_t}{\partial\eta} = -\frac{S^{-1}W}{c}\frac{\partial\overline{F}_t}{\partial\varepsilon}$$

$$\frac{c}{W}K_{\xi\eta} = -S^{-1}\frac{\partial\overline{F}_t}{\partial\varepsilon} \tag{C.16}$$

In summary, the stiffness matrix can be written,

$$\frac{c}{W}\begin{bmatrix} K_{\xi\xi} & K_{\xi\eta} \\ K_{\eta\xi} & K_{\eta\eta} \end{bmatrix} = S^{-1}\begin{bmatrix} -\frac{\overline{F}_r}{\varepsilon_o} & -\frac{\partial \overline{F}_t}{\partial \epsilon} \\ \frac{\overline{F}_t}{\varepsilon_o} & -\frac{\partial \overline{F}_r}{\partial \epsilon} \end{bmatrix}. \tag{C.17}$$

$$C_{\eta\eta} = -\frac{\partial F_r}{\partial \dot{\eta}} = -\frac{S^{-1}W}{c\omega_j}\frac{\partial \overline{F}_r}{\partial \dot{\epsilon}'}$$

$$\frac{c\omega_j}{W}C_{\eta\eta} = -S^{-1}\frac{\partial \overline{F}_r}{\partial \dot{\epsilon}'} \tag{C.18}$$

$$C_{\eta\xi} = -\frac{\partial F_r}{\partial \dot{\xi}} = S^{-1}W\frac{2\overline{F}_r}{\varepsilon_o c\omega_j}$$

$$\frac{c\omega_j}{W}C_{\eta\xi} = 2S^{-1}\frac{\overline{F}_r}{\varepsilon_o} \tag{C.19}$$

$$C_{\xi\xi} = -\frac{\partial F_t}{\partial \dot{\epsilon}} = \frac{S^{-1}W}{\omega_j c}\frac{2\overline{F}_t}{\varepsilon_o}$$

$$\frac{c\omega_j}{W}C_{\xi\xi} = S^{-1}\frac{2\overline{F}_t}{\varepsilon_o} \tag{C.20}$$

$$C_{\xi\eta} = -\frac{\partial F_t}{\partial \dot{\eta}} = -\frac{S^{-1}W}{\omega_j c}\frac{\partial F_t}{\partial \dot{\epsilon}'}$$

$$\frac{c\omega_j}{W}C_{\xi\eta} = -S^{-1}\frac{\partial F_t}{\partial \dot{\epsilon}'} \tag{C.21}$$

The damping coefficient matrix is then,

$$\frac{c\omega_j}{W}\begin{bmatrix} C_{\xi\xi} & C_{\xi\eta} \\ C_{\eta\xi} & C_{\eta\eta} \end{bmatrix} = S^{-1}\begin{bmatrix} \frac{2\overline{F}_t}{\varepsilon_o} & -\frac{\partial \overline{F}_t}{\partial \dot{\epsilon}'} \\ \frac{2\overline{F}_r}{\varepsilon_o} & -\frac{\partial \overline{F}_r}{\partial \dot{\epsilon}'} \end{bmatrix}. \tag{C.22}$$

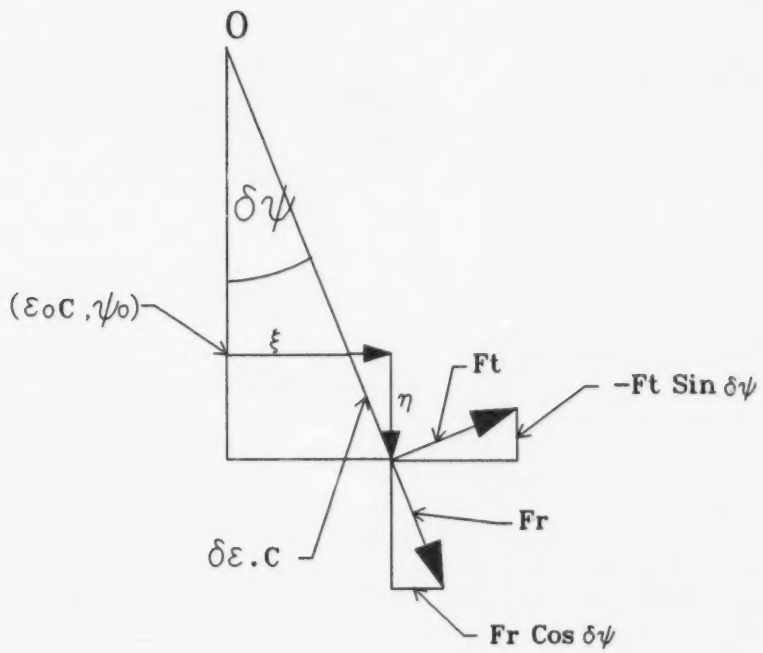

Figure C.1: Small Deflections of Journal Centre Parallel and Perpendicular to the Line of Centres (journal - bearing), Showing Contributions to the Incremental Forces due to Rotation of the Fluid Force Components.